THE FORMATION OF ACOUSTICAL FIELDS IN OCEANIC WAVEGUIDES

Coherence phenomena

Nizhny Novgorod
1997

Published on the decision of the Editorial-Board of IAP RAS

The influence of waveguide propagation on the acoustical signal processing was investigated in previous books of IAP RAS. As the result of investigations shown, the coherence phenomena limit the possibilities for acoustical reconstruction of the spatially-localized inhomogeneities parameters in oceanic environments. The results of investigation of decreasing the coherence of propagating and scattering acoustical waves in oceanic waveguides due to influence of random inhomogeneities as well as the possibilities for tomographical reconstuction are presented in this book.

The publishing of the book was made in the frames of Special Federal Programme "Integratsiya".

ISBN 5-201-09300-0

CONTENTS

Preface 4

E. Yu. Gorodetskaya, A. I. Malekhanov, A. G. Sazontov, V. I. Talanov, N. K. Vdovicheva. Acoustic coherence in a deep water: effects on array signal processing 5

A. I. Khil'ko, A. G. Sazontov and N. K. Vdovicheva. Diffraction of acoustic waves by an object in a random oceanic waveguide 48

I. P. Smirnov, J. W. Caruthers and A. I. Khil'ko. Multiscale coherence of the acoustic field of a noise source in randomly inhomogeneous ocean 71

A. V. Lebedev and B. M. Salin. Experimental method for determining the scattering characteristics of elongated objects 114

M. Yu. Galaktionov, V. V. Borodin, A. V. Mamayev. Numerical and experimental study of sound field forming in shallow water environments 134

V. V. Borodin and M. Yu. Galaktionov. New mathematical model of sound field fluctuations in shallow water environments with boundary and volume roughness 161

E. L. Borodina, A. A. Stromkov and A. I. Khil'ko. Coherent structure of broadband pulse signals in the shallow sea 186

A. A. Pokrovsky. Using regularities in the behavior of a two-frequency correlation function of acoustic field in monitoring of oceanic inhomogeneities 213

S. M. Grudskii, A. I. Khil'ko, S. S. Mikhalkovich. Propagation of low-frequency sound in a hydroacoustic waveguide with surface covered by a non-continuous ice layer 219

A. I. Belov and A. I. Khil'ko. Diffraction of acoustic waves by spatially-localized inhomogeneities in horizontally inhomogeneous shallow water oceanic waveguides 240

PREFACE

This book continues the series of collected papers. The books which can be united into series of books deal with various interrelated problems of synthesis and analysis of underwater acoustic signals. These books are: "The Formation of Acoustical Fields in Oceanic Waveguides" (in Russian), "The Formation of Acoustical Fields in Oceanic Waveguides. Reconstruction of Inhomogeneities" (in Russian), and "The Formation of Acoustical Fields in Oceanic Waveguides" (in English) issued in IAP RAS, Nizhny Novgorod, in 1991, 1994, and 1995, recpectively. The basic features of these problems are associated mainly with the properties of oceanic waveguides as the channels of long-range sound propagation. The corresponding calculations are often very difficult because of inherent inhomogeneities and instabilities of oceanic environments. Moreover, a full set of appropriate data on random inhomogeneities and their temporal characteristics are unknown in practice, so one has to use the approximate physical models and theoretical approaches. On the other hand, a particular problem arising here is to optimize the methods of reconstruction of the ocean inhomogeneities characteristics.

Many previous works in this field, our previous collected papers included, show that the influence of randomly distributed inhomogeneities of oceanic medium is very important for developing the schemes of ocean remote sounding and ocean acoustical tomography. In the context of long-range and/or large-array signal receiving/processing, a key point is, therefore, ocean acoustic coherence which is a central issue of this book.

We tried to collect here recent results on acoustic coherence in oceanic waveguides obtained by scientists not only from IAP RAS but also from other Russian research centres engaged in underwater sound. The most part of the papers is based on new experimental data which were effectively used for developing adequate calculations and empirical models of oceanic inhomogeneities. I do hope that the results presented allow a reader to estimate the state-of-the-art in this promising field and to be introduced in the current studies of the acoustic coherence and its effects on the tomographical reconstruction.

It is my sincere pleasure to thank all the authors who submitted their papers to be collected in this book.

Vitaly Zverev

ACOUSTIC COHERENCE IN A DEEP WATER: EFFECTS ON ARRAY SIGNAL PROCESSING

E. Yu. Gorodetskaya, A. I. Malekhanov, A. G. Sazontov, V. I. Talanov, and N. K. Vdovicheva

INTRODUCTION

Long–range acoustic signal propagation in underwater channels is known to lead to loss of the signal coherence in space, time and frequency, which results from multiple sound scattering by random inhomogeneities of the oceanic medium (see, e.g. [1, 2]). From an application point of view, the knowledge of the spatial–temporal mutual coherence function (MCF) of the registered acoustic field is of the uppermost importance to optimize the signal processing techniques and, therefore, to decrease a coherence–induced degradation of the processor performances.

Following the general idea of spatial–temporal processing factorization, we restrict ourselves to the study of coherence effects mainly in spatial domain, which is of a particular interest in large–array beamforming. Previously, the problem of array processing under the conditions of reduced signal coherence was studied by several authors [3–6] on the base of a general theory of random signal detection against the noise background [7, 8], but without invoking specific models for underwater sound coherence. On the other hand, the subjects of numerous works on the ocean acoustic coherence are restricted, as a rule, to the propagation problem itself.

In this paper, we present our recent results on combined consideration of the sound wavefield coherence and array signal processing in long–range deep–water environments. A distinctive feature of our study is incorporating realistic calculations of the signal MCF of space [9–11] to predict the coherence effects on the array beampattern and gain for several types of processors, optimal ones included [12–14].

A specific scheme of our study is as follows. To calculate the ocean acoustic MCF, we develop a technique of the radiation transport equation (RTE) and derive in a closed form an useful approximate solution for the multimodal MCF. In our analysis of array processors, we exploit, as a basic approach, the eigenvalue–eigenvector decomposition of the signal covariance matrices. Generally, this approach can be effectively used for various detection criteria, the maximum likelihood (ML) and signal–to–noise (SNR) ones included. Our particular interest concerns here the small–signal asymptotics

of the ML detection performance, which is a reasonable choice for long–range underwater acoustics.

The body of this paper reflects the scheme summarized above. Section 1 reviews the wave–theoretical model of acoustic transmission in a random–inhomogeneous oceanic waveguide. It contains a brief discussion of the RTE technique that has been developed to calculate the ocean acoustic MCF for long–range multimode propagation. Section 2 gives the most significant aspects of large–array processing of partially coherent signals with emphasis on comparative analysis of linear and quadratic beamformers. Next, Sec. 3 addresses the numerical simulation of acoustic signal propagation and array processing for realistic deep–water environments from the North–West Pacific. Calculations of the expected acoustic coherence in the special cases of internal–wave medium fluctuations and fully developed wind seas are employed to show in detail the acoustic coherence effects on the array beampattern and gain for several types of beamformers including both horizontal and vertical array configurations. Finally, Sec. 4 summarizes the results obtained and gives the most essential conclusions from this study.

1. OCEAN ACOUSTIC COHERENCE: WAVE–THEORETICAL DESCRIPTION

The acoustic propagation problem in a random ocean is of a great interest for various applications concerned with underwater detection, communication, and the ocean acoustic tomography. The significant unusual characteristics of the ocean medium are the presence of an underwater sound channel and the anisotropy and inhomogeneity of the sound–speed fluctuations. Thus, the study of the combined effects of anisotropic scattering and regular refraction on acoustic coherence is of great importance in understanding statistical behavior of oceanic sound transmission. From the theoretical point of view analysis of this problem reduces to evaluating the MCF of space, time and frequency. The MCF contains important statistical properties of the acoustic field that has traversed a medium with random fluctuations. For example, the coherence time and coherence lengths that determine the maximum effective integration times and array lengths that can be utilized in sonar systems are contained in the MCF. The MCF of frequency controls the coherent bandwidth and also describes the behavior of the ensemble–averaged pulse for a pulse–transmission experiment.

1.1. Preliminaries

Recently, the systematic investigations examining the propagation of the MCF in a refractive oceanic waveguide containing random inhomogeneities have been carried out in the framework of a ray oriented approach using the path integral formalism. The predictions of acoustic coherence from the path integral theory and its comparisons with single–receiver measurements are fairly well summarized in the book by Flatte *et al.* [1]. It should be noted that a solution for MCF equivalent to that obtained by path integral methods can be derived as the first approximation of the second moment equation when only one path of multipath configuration is treated [15, 16].

For low–frequency long–range propagation the ray theory is not adequate and the wave–theoretical description like the normal–mode method is more suitable. The use of this approach introduces the effect of sound–speed profile in a direct and systematic way. Applied to ocean acoustics the modal treatment has been developed in a series of publications (see, e. g. [17–32]). The statistical description of a stochastic waveguide propagation usually deals with a set of differential equations for the self–modal and cross–modal coherence functions, which predict the evolution in range of both the energy and correlation characteristics of an underwater acoustic field. These equations can be solved at least with the aid of a computer. For low–frequency regime a general computer program has been developed by Dozier and Tappert [21] and Beilis and Tappert [22] to evaluate the effects of volume and rough surface scattering on the transmission loss as a function of range and depth in a canonical–model random ocean. However, when a large number of propagating modes is present, the numerical integration becomes rather cumbersome and, hence, there is a need to develop approximate analytical methods. Most of the research to date using a normal mode decomposition has been restricted primarily to the average wavefield intensity evolution which was obtained by means of a diffusion approach [17, 20, 27, 28] when a discrete set of guided modes is regarded as a continuum. The analytical works concerning the correlation characteristics of a miltimode signal have also been tried by use of a matrix analog of the Rytov approximation, although their results are applicable only to the case of short propagating distances [26, 30, 32].

A considerable progress in theoretical study of acoustic coherence for a large class of scattering models in long–range ocean environments has been recently achieved by Sazontov [9, 10], who proposed an efficient method for solving the RTE for multimodal propagation. Below, we present an useful approximate wave–theoretical expression for the total MCF which is valid for a wide range of refractive index profiles and types of scattering irregularities. It is important to have such a solution since it enables one

to study acoustic propagation and loss of coherence in realistic underwater environments.

1.2. Volume scattering in a deep oceanic channel. Problem formulation

Consider an underwater sound channel of depth H, in which the refractive index is the sum of the deterministic background profile $n_0(z)$ depending on vertical coordinate z and the stochastic field $\mu(\mathbf{r}, z, t)$ modeling the acoustic medium fluctuations. Here, $\mathbf{r} = (x, y)$ is the horizontal two-dimensional position vector and t is the time. The coordinate system is chosen with the z-axis downwards. The perturbation μ is assumed to be a Gaussian random variable with zero mean, and can be described by its autocorrelation function

$$< \mu(\mathbf{r}_1, z_1, t_1)\mu(\mathbf{r}_2, z_2, t_2) >= B_\mu(|\mathbf{r}_1 - \mathbf{r}_2|, z_1, z_2, t_1 - t_2).$$

The angular brackets $< \cdots >$ indicate ensemble averaging.

Let a nondirectional acoustic source be located at coordinates $(0, z_0)$ and emit a signal having time dependence $g(t) = s(t)\exp(-i\omega_0 t)$, where $\omega_0 = 2\pi f_0$ denotes the radian carrier frequency. In terms of normal modes the complex envelope of the acoustic pressure field $P(\mathbf{r}, z, t)$ in an irregular oceanic channel far enough from a source can be formally represented by

$$P(\mathbf{r}, z, t) = \int_{-\infty}^{\infty} d\omega\, g(\omega)\, e^{-i\omega t} \sum_{n=1}^{M(\omega)} \frac{1}{\sqrt{\kappa_n}}\, p_n(\mathbf{r}, \omega, t)\, \varphi_n(z, \omega). \qquad (1)$$

Here, $g(\omega)$ is the frequency spectrum of the transmitted signal, $\varphi_n(z, \omega)$ denotes the n-th vertical eigenfunction of the deterministic background medium associated with the eigenvalue $\kappa_n^2(\omega)$, M is the number of propagating modes, and $p_n(\mathbf{r}, \omega, t)$ are the random normal mode amplitudes. In writing (1) we ignored the farfield contribution from the modes of continuous spectrum. The normal mode functions $\varphi_n(z, \omega)$ satisfy the eigenvalue problem

$$\frac{d^2}{dz^2}\varphi_n(z, \omega) + \left[k^2 n_0^2(z) - \kappa_n^2(\omega)\right]\varphi_n(z, \omega) = 0, \quad n = 1, 2, \ldots, M \qquad (2)$$

together with appropriate boundary conditions and an orthonormality relation, i. e., $\int_0^H dz\, \varphi_n(z, \omega)\varphi_m(z, \omega) = \delta_{nm}$. Here, $k = \omega/c_0$, where c_0 is some reference sound speed.

In a waveguide with large scale (compared to the wavelength) inhomogeneities, the expansion coefficients $p_n(\mathbf{r},\omega,t)$ obey the coupled parabolic wave equations:

$$\left(\frac{\partial}{\partial x} - i\kappa_n(\omega) - \frac{i}{2\kappa_n(\omega)}\frac{\partial^2}{\partial y^2}\right) p_n(\mathbf{r},\omega,t) = i\sum_m V_{nm}(\mathbf{r},\omega,t)\, p_m(\mathbf{r},\omega,t), \tag{3}$$

where x-axis is taken in the main direction of wave propagation, and $V_{nm}(\mathbf{r},t)$ is the matrix coupling coefficient (depending on t as a parameter) defined according to:

$$V_{nm}(\mathbf{r},\omega,t) = \frac{k^2}{\sqrt{\kappa_n(\omega)\kappa_m(\omega)}}\,\mu_{nm}(\mathbf{r},\omega,t),$$

$$\mu_{nm}(\mathbf{r},\omega,t) = \int_0^H dz\, n_0(z)\mu(\mathbf{r},z,t)\varphi_n(z,\omega)\varphi_m(z,\omega). \tag{4}$$

Note, that parabolic approximation consists of considering solutions in which waves are traveling only at small angles to a particular direction; in the ocean this direction is in the horizontal, labeled here by x.

The important correlation properties of an acoustic wave that has traversed a random oceanic waveguide are described by the second moment of the pressure field

$$B_p(\mathbf{r}_1,z_1,t_1|\mathbf{r}_2,z_2,t_2) = <P(\mathbf{r}_1,z_1,t_1)\,P^*(\mathbf{r}_2,z_2,t_2)>, \tag{5}$$

where the asterisk denotes complex conjugate. Inserting the field expansion from Eq. (1) into Eq. (5), one finds that

$$B_p(\mathbf{r}_1,z_1,t_1|\mathbf{r}_2,z_2,t_2) = \int_{-\infty}^{\infty} d\omega_1 \int_{-\infty}^{\infty} d\omega_2\, g(\omega_1)g^*(\omega_2)\Gamma(\cdot|\cdot)e^{-i\omega_1 t_1 + i\omega_2 t_2}, \tag{6}$$

where $\Gamma(\mathbf{r}_1,z_1,\omega_1,t_1|\mathbf{r}_2,z_2,\omega_2,t_2)$ is the total MCF defined as

$$\Gamma(\mathbf{r}_1,z_1,\omega_1,t_1|\mathbf{r}_2,z_2,\omega_2,t_2) = \sum_{n,m}\frac{\varphi_n(z_1,\omega_1)\varphi_m(z_2,\omega_2)}{\sqrt{\kappa_n(\omega_1)\kappa_m(\omega_2)}}\,\Gamma_{nm}(1,2) \tag{7}$$

$$\Gamma_{nm}(1,2) = <p_n(1)\,p_m^*(2)>.$$

The labels 1 and 2 refer to two different horizontal position points, times and frequencies. Thus, the evaluation of the total MCF applied to the stochastic

waveguide propagation requires the knowledge of the cross-modal coherence functions $\Gamma_{nm}(1,2)$.

In Ref. [32] the basic RTE for the cross-modal MCF $\Gamma_{nm}(1,2)$ taken at two horizontal position points $\mathbf{r_1} = (x, y_1)$, $\mathbf{r_2} = (x, y_2)$ in the same x plane, at two different times and frequencies has been derived from Eq. (3) under the Markov approximation:

$$\left[\frac{\partial}{\partial x} - i\kappa_{nm}^{-} - i\xi_{nm}^{+}\frac{\partial^2}{\partial\rho\partial R} - \frac{i}{2}\xi_{nm}^{-}\left(\frac{\partial^2}{\partial\rho^2} + \frac{1}{4}\frac{\partial^2}{\partial R^2}\right)\right]\Gamma_{nm} =$$

$$= -\frac{1}{2}\left[\sum_{n'} A_{nn'}(1,1)\,\Gamma_{n'm} + \sum_{m'} A_{m'm}(2,2)\,\Gamma_{nm'}\right] + \sum_{n',m'} A_{nn'}^{mm'}(1,2)\,\Gamma_{n'm'} \tag{8}$$

with the definitions $\rho = y_1 - y_2$, $R = 0.5(y_1 + y_2)$, $\tau = t_1 - t_2$, $\kappa_{nm}^{-} = \kappa_n(\omega_1) - \kappa_m(\omega_2)$, $\xi_{nm}^{+} = 0.5\left[\kappa_n^{-1}(\omega_1) + \kappa_m^{-1}(\omega_2)\right]$, $\xi_{nm}^{-} = \kappa_n^{-1}(\omega_1) - \kappa_m^{-1}(\omega_2)$, $A_{nn'}(1,1) = \sum_{m'} A_{nm'}^{n'm'}(1,1)$, and the coupling matrix $A_{nn'}^{mm'}(1,2)$ is given by

$$A_{nn'}^{mm'}(1,2) = \int_{-\infty}^{\infty} d\eta\, B_{nn'}^{mm'}(1,2;\eta)\, e^{\,i(\kappa_{nm}^{+} - \kappa_{n'm'}^{+})\,\eta},$$

$$B_{nn'}^{mm'}(1,2;\eta) = < V_{nn'}(x + \frac{1}{2}\eta, y_1, \omega_1, t_1) V_{mm'}(x - \frac{1}{2}\eta, y_2, \omega_2, t_2) >,$$

where $\kappa_{nm}^{+} = 0.5\left(\kappa_n(\omega_1) + \kappa_m(\omega_2)\right)$. As a consequence of Eq. (8), we obtain the conservation relation

$$\frac{d}{dx}\sum_{n=1}^{M}\int_{-\infty}^{\infty}\Gamma_{nn}(x, \rho = 0, R, \tau = 0, \omega, \omega)\, dR = 0.$$

1.3. Asymptotic expression for the cross-modal MCF

The set of coupled integrodifferential equations (8) is very hard to solve exactly and numerical simulations are needed. If M becomes too large, the numerical integration of these equations becomes impractical. However, in the quasi-classical approximation, when the WKB formulae are valid for $\varphi_n(z, \omega)$, it is possible to construct the analytical solution for $\Gamma_{nm}(1,2)$ and to obtain an useful, approximate representation for the total MCF [9, 10].

The approach employed uses the well-known properties of the quasi-classical elements V_{nm}, Eq. (4), according to which the corresponding coupling matrix is a function mainly of difference indices of interacting modes [33, 34]:

$$\mu_{nn'}(\mathbf{r},\omega,t)=\frac{2}{\Lambda_n}\int\limits_0^{\Lambda_n/2}dx' n_0[z_n(x')]\mu(\mathbf{r},z_n(x'),t)\cos\Big(\frac{2\pi}{\Lambda_n}(n-n')x'\Big),$$

where $\Lambda_n(\omega)$ is the mode cycle distance, $z_n(x)$ is the modal ray trajectory satisfying the equation

$$\frac{d^2z_n(x)}{dx^2}=\frac{1}{2a_n}\frac{d}{dz}n_0^2[z_n(x)],\quad a_n=\frac{\kappa_n(\omega)}{k}$$

with

$$\frac{dz_n(x)}{dx}=\frac{1}{a_n}\sqrt{n_0^2(z)-a_n^2}\equiv \mathrm{tg}\,\chi_n(x)\ ;\ n_0[z_n(x)]\cos\chi_n(x)=a_n,$$

and $\chi_n(x)$ is the angle the modal ray makes with the horizontal at the point x.

As a result, Eq. (8) can be regarded as a discrete convolution type equation. This circumstance together with the generating function technique allow us to reduce Eq. (8) to the equation which coincides formally with the equation governing the propagation of the MCF in free space. Then, the solution for the generating function can be found analytically. This has the advantage of offering the possibility of obtaining solution in a closed form for the cross-modal MCF by the Fourier inversion of the generating function to give:

$$\begin{aligned}\Gamma_{nm}(1,2)&=\Gamma^{\perp}_{nm}(1,2)\,e^{\,i(\kappa_n-\kappa_m)x},\\ \Gamma^{\perp}_{nm}(1,2)&=\frac{1}{(2\pi)^2}\sum_{\nu,\lambda}\int\limits_0^{2\pi}d\alpha\,e^{\,-i(n-\nu)\alpha}\int\limits_0^{2\pi}d\beta\,e^{\,i(m-\lambda)\beta}\,\Gamma^{\alpha\beta}_{\nu\lambda}(1,2).\end{aligned}\qquad(9)$$

Here, $\Gamma^{\alpha\beta}_{\nu\lambda}(1,2)$ is defined according to

$$\Gamma^{\alpha\beta}_{\nu\lambda}(1,2)=\Gamma^{0}_{\nu\lambda}(1,2)\exp\Big[-\frac{1}{2}D^{\alpha\beta}_{\nu\lambda}(1,2)\Big],\qquad(10)$$

where

$$\Gamma^{0}_{\nu\lambda}(1,2)=\frac{1}{8\pi x}\,\varphi_\nu(z_0,\omega_1)\,\varphi_\lambda(z_0,\omega_2)\exp\left[\frac{i\rho R}{\xi^{+}_{\nu\lambda}x}-\frac{i\xi^{-}_{\nu\lambda}}{2\xi^{+}_{\nu\lambda}x}\Big(R^2+\frac{1}{4}\rho^2\Big)\right]$$

is the solution of the transport equation in the absence of random inhomogeneities for a point source situated at coordinates $(0, z_0)$, and the quantity $D^{\alpha\beta}_{\nu\lambda}$ describing the loss of wavefield coherence has the form:

$$D^{\alpha\beta}_{\nu\lambda}(1,2) = \int_0^x dx' \Big[d^{\alpha\alpha}_{\nu\nu}(x, 1|x', 1) + d^{\beta\beta}_{\lambda\lambda}(x, 2|x', 2) - 2d^{\alpha\beta}_{\nu\lambda}(x, 1|x', 2) \Big]; \tag{11}$$

$$d^{\alpha\beta}_{\nu\lambda}(x, 1|x', 2) = 2\pi k_1 k_2 \int_{-\infty}^{\infty} d\Omega \iint_{-\infty}^{\infty} d\text{æ}_y d\text{æ}_z \frac{\Phi_\mu\Big(\text{æ}_{\nu\lambda}(x'), \Omega, z^{\alpha\beta}_{\nu\lambda}(x')\Big)}{\cos\chi_\nu(x')\cos\chi_\lambda(x')} \times$$

$$\times \cos\Big(\text{æ}_y \rho \frac{x'}{x}\Big) \cos\Big(\text{æ}_z \varsigma^{\alpha\beta}_{\nu\lambda}(x')\Big) \cos(\Omega\tau).$$

In writing Eq. (11) the following notation is used: $\Phi_\mu(\text{æ}, \Omega, z)$ is the local spectrum of the sound-speed fluctuations taken at $\text{æ} = \text{æ}^{\alpha\beta}_{\nu\lambda}(x)$, where the wave number $\text{æ}^{\alpha\beta}_{\nu\lambda}(x)$ has components

$$\text{æ}^{\alpha\beta}_{\nu\lambda}(x) = \Big(-0.5\big(\mathrm{tg}\,\chi^\alpha_\nu(x) + \mathrm{tg}\,\chi^\beta_\lambda(x)\big)\text{æ}_z, \text{æ}_y, \text{æ}_z\Big),$$

$\mathrm{tg}\,\chi^\alpha_\nu(x) = dz^\alpha_\nu(x)/dx$ is the inclination of a modal ray with the path $z^\alpha_\nu(x) \equiv z_\nu(x - \alpha\Lambda_\nu/2\pi)$, $z^{\alpha\beta}_{\nu\lambda}(x) = 0.5\big(z^\alpha_\nu(x) + z^\beta_\lambda(x)\big)$, and $\xi^{\alpha\beta}_{\nu\lambda}(x) = z^\alpha_\nu(x) - z^\beta_\lambda(x)$.

The expression for $D^{\alpha\beta}_{\nu\lambda}(1,2)$, Eq. (11), is immediately recognized as the phase-structure function (PSF) with the only difference that the integral in Eq. (11) is taken along a modal ray instead of a usual geometric ray. The combination $d^{\alpha\alpha}_{\nu\nu}(x, 1|x', 1) + d^{\beta\beta}_{\lambda\lambda}(x, 2|x', 2) - 2d^{\alpha\beta}_{\nu\lambda}(x, 1|x', 2)$ can now be regarded as a density of the PSF. Such a ray-modal analogy allows one to use in the calculation of coherence the well-known results for PSF obtained in the framework of the ray theory. [1]

Equations (6), (7), (9)-(11) present in a closed form an useful approximate solution to the problem of interest. For a given sound speed profile and spectrum of the volume medium fluctuations they give explicit rules for calculating both the correlation function and the wavefield intensity in a random oceanic waveguide. The restrictions on the theory are detailed in Refs. [9, 10].

[1] The methods for evaluating the PSF from a general internal-wave model [35] were presented by Esswein and Flatte [36].

1.4. Rough surface scattering effects on the MCF

Equation (3) describes the coupling between the normal mode amplitudes due to random volume irregularities of refractive index. In certain circumstances, for example, when the propagation takes place in an upper sound channel, surface interactions play a predominant role in acoustic signal fluctuations. The formalism developed in Refs. [9, 10] may be extended to the analysis of acoustic coherence after long range multiple surface scatterings. This can be done as follows.

In the presence of a soft boundary $z = \eta(\mathbf{r}, t)$, where η represents random displacements of the ocean surface, in addition to the wave equation the following condition on the acoustic pressure field is imposed

$$P(\mathbf{r}, \eta(\mathbf{r}, t), t) = 0.$$

Concerning the statistics of $\eta(\mathbf{r}, t)$ we assume that $\eta(\mathbf{r}, t)$ is a Gaussian homogeneous and stationary field with zero mean and is characterized by the spatial-temporal correlation function B_η:

$$B_\eta(\rho, \tau) = < \eta(\mathbf{r}, t)\, \eta(\mathbf{r} + \rho, t + \tau) > .$$

For a small Rayleigh parameter, the explicit boundary condition can be expanded at the mean ocean surface $z = 0$ in powers of η to give

$$P(\mathbf{r}, 0, t) = -\eta \left. \frac{\partial P(\mathbf{r}, z, t)}{\partial z} \right|_{z=0} .$$

In the case considered, it is straightforward to derive that the normal mode amplitudes $p_n(\mathbf{r}, t)$ in the representation (1) formally obey the set of stochastic equations (3) in which the coupling coefficients V_{nm} are now defined according to Ref. [17]

$$V_{nm}(\mathbf{r}, t) = \frac{\varphi_n'(0, \omega_1)\varphi_m'(0, \omega_2)}{2\sqrt{\kappa_n(\omega_1)\kappa_m(\omega_2)}}\, \eta(\mathbf{r}, t),$$

where the prime denotes differentiation with respect to depth z.

Hence, rough surface and volume scattering effects can be formally described in the framework of united approach and the particular scattering mechanism specifies the concrete form of the coupling elements V_{nm}. Therefore, the equations governing the propagation of the MCF in a waveguide with a rough surface are thus the same as before except that the coupling matrix $A_{nn'}^{mm'}(1,2)$ must be replaced by

$$A_{nn'}^{mm'}(1,2) = \frac{\pi}{2} \frac{\left[\varphi_n'(0, \omega_1)\varphi_{n'}'(0, \omega_1)\varphi_m'(0, \omega_2)\varphi_{m'}'(0, \omega_2)\right]}{\left[\kappa_n(\omega_1)\kappa_{n'}(\omega_1)\kappa_m(\omega_2)\kappa_{m'}(\omega_2)\right]^{1/2}} \times$$

$$\times \int_{-\infty}^{\infty} d\Omega\, e^{-i\Omega\tau} \int_{-\infty}^{\infty} d\text{æ}_y\, e^{i\text{æ}_y\rho} F_\eta(\kappa_{nm}^{+} - \kappa_{n'm'}^{+}, \text{æ}_y, \Omega),$$

where $F_\eta(\text{æ}, \Omega)$ is the Fourier transform of the surface autocorrelation function $B_\zeta(\rho, \tau)$ with respect to ρ and τ.

A considerable simplification occurs for waveguides having a nonequidistant spectrum of wavenumbers κ_n. In this case the diagonal elements of the matrix $\Gamma_{nm}(1,2)$ decouple from the off-diagonal elements in Eq. (8). As a consequence, for Γ_{nm} at $n \neq m$ we have approximately [37]

$$\Gamma_{nm}(1,2) = < \mathrm{p}_n(1) > < \mathrm{p}_m^*(2) > T_{nm}(1,2), \quad n \neq m, \tag{12}$$

where

$$< \mathrm{p}_n(\mathbf{r}, \omega, t) > = \frac{-i\varphi_n(z_0, \omega)}{\sqrt{8\pi x}} \exp\left(i\kappa_n(\omega)|\mathbf{r}| - \frac{1}{2}\sigma_n(\omega) - i\frac{\pi}{4}\right)$$

is the coherent field of the n-th mode, $\sigma_n(\omega) = A_{nn}(1,1)$ is the scattering coefficient, and

$$T_{nm}(1,2) = \exp\left\{\int_0^x dx' A_{nm}^{nm}\left(\rho\frac{x}{x'}, \tau, \omega_1, \omega_2\right)\right\}.$$

For most oceanic applications the characteristic correlation length l_η of surface irregularities is much less than the typical mode cycle distance, i.e. $l_\eta \ll \Lambda_n$. In this case, elementary acts of scattering occur at statistically independent ensembles of the surface, and the formula (12) reduces to a simpler form [18]:

$$\Gamma_{nm}(1,2) = < \mathrm{p}_n(1) > < \mathrm{p}_m^*(2) >, \quad n \neq m. \tag{13}$$

For the diagonal elements $\Gamma_{nn}^{\perp}(1,2)$, a formal procedure similar to that given in obtaining Eq. (9) leads to the expression [37]:

$$\Gamma_{nn}^{\perp}(1,2) = \frac{1}{2\pi} \sum_{m=1}^{M} \Gamma_{mm}^{0}(1,2) \int_0^{2\pi} d\alpha\, e^{-i(n-m)\alpha - \frac{1}{2} D_m^{\alpha}(1,2)}, \tag{14}$$

where $\Gamma_{mm}^{0}(1,2)$ are the self-modal functions in the absence of random scattering, and

$$D_m^{\alpha}(1,2) = \frac{\pi}{2} \frac{\varphi_m'(0,\omega_1)\varphi_m'(0,\omega_2)}{\sqrt{\kappa_m(\omega_1)\kappa_m(\omega_2)}} \sum_{q=1}^{M} \frac{\varphi_q'(0,\omega_1)\varphi_q'(0,\omega_2)}{\sqrt{\kappa_q(\omega_1)\kappa_q(\omega_2)}} \times$$

$$\times \int_0^x dx' \int_{-\infty}^{\infty} d\Omega \int_{-\infty}^{\infty} d\text{æ}_y F_\eta(\kappa_m - \kappa_q, \text{æ}_y, \Omega) \left[1 - \cos\left(\text{æ}_y \rho \frac{x'}{x}\right) \cos(\Omega\tau) e^{i(q-m)\alpha}\right].$$

Equations (13) and (14) together with Eq. (7) allow for estimation of the key correlation characteristics of the acoustic signal in an upper–sound channel where the rough surface scattering effects are important.

2. SIGNAL COHERENCE EFFECTS ON LARGE–ARRAY BEAMFORMING

In this section, we give a short introduction to array processing of coherence–reduced signals, which is then supported (see Sec. 3) by the numerical results on array beamforming in realistic deep–water environments from the North–West Pacific. Our analysis is aimed at the array gain and its coherence–induced loss for several types of beamformers, linear and quadratic ones included.

2.1. Background

Generally, the problem of array signal processing is to detect a signal source and/or to estimate unknown source or transmission parameters. In both cases, one possible strategy is to optimally process the outputs of array elements (sensors) according to a predetermined statistical criterion. In this respect, the ML processor is well known to be of fundamental importance because it is optimal for a variety of detection and estimation criteria [7, 8].

Conventional array beamformers such as those used for plane–wave source detection or bearing estimation in radar [39, 40] are derived under the key assumptions of time–invariant and spatially homogeneous transmission channel between the source and sensors. In long–range sonar applications, however, such model assumptions are generally unrealistic. Therefore, two principal issues arise, which are (i) the effects of signal propagation in a deterministically inhomogeneous channel and (ii) the effects of random inhomogeneities which perturb a regular wavefield and cause its coherence loss.

The survey of literature reveals that several important developments have been made in these directions. First, a technique of matched–field processing (MFP) was proposed [41] and studied as an effective generalization of plane–wave beamforming (PWBF) with applications to the source localization in underwater channels and ocean acoustic tomography (for recent reviews, see Refs. [42–44]). Second, a general theory of array signal

processing in regular multimode/multipath channels was developed with applications to underwater acoustics [45]. Third, the coherence effects on the array beampattern [46, 47] and the detection performance [3–6] were examined by the use of some models of the plane–wave signal coherence. Finally, more relevant models of the multimode signal coherence were used to predict the array beampattern degradation [48] and to compare SNR loss for several linear and quadratic beamformers, optimal ones included [49, 50, 12–14].

Thus, the theoretical background of our study concerned with large–array beamforming is recent developments of array signal processing in random–inhomogeneous multimode channels with emphasis on the signal coherence effects.

2.2. Preliminary formulations

The problem of array signal processing under the conditions of reduced signal coherence was clearly formulated and studied by Cox [3], and then was elaborated by other authors [4–6, 51, 52] on the base of a general theory of random signal detection [7, 8]. Following these works, we outline here an effective approach to large–array processing of partially coherent signals.

The signal of interest and noise background are both assumed to be zero–mean, mutually uncorrelated and Gaussian random processes. The detection problem is formulated as a two–hypothesis alternative:

$$\mathbf{x} = \mathbf{s} + \mathbf{n}, \quad or \quad \mathbf{x} = \mathbf{n},$$

where $\mathbf{s}$ and $\mathbf{n}$ are, respectively, the N–dimensional signal and noise vectors of the Fourier–transformed data vector $\mathbf{x}$ received by the N–element array. In the numerical simulations following in Sec. 3, the components of the signal vector are exactly the acoustic pressures from Eq. (1), i. e. $s_j = P(\mathbf{r}_j, z_j, t)$, $j = 1, 2, \ldots, N$.

In general, the data vector $\mathbf{x}$ can be processed in quadratic form to obtain the detection statistic d by

$$d = \mathbf{x}^{+}\mathbf{A}\mathbf{x}, \tag{15}$$

where $\mathbf{A}$ is an arbitrary $(N \times N)$ matrix, and the superscript $^{+}$ denotes conjugate transpose. For the ML criterion, the optimal matrix $\mathbf{A}_{opt}$ is expressed by

$$\mathbf{A}_{opt} = \mathbf{M}_n^{-1} - (\mathbf{M}_s + \mathbf{M}_n)^{-1}.$$

Here, $\mathbf{M}_s$ and $\mathbf{M}_n$ are the spatial covariance matrices of the signal and noise, respectively, which are defined as $\mathbf{M}_x = < \mathbf{x}^{*}\mathbf{x}^{T} >$ (the supercript ^{T} denotes transpose).

Under the small–signal condition which is a reasonable assumption for long–range underwater acoustics and will be used in further analysis, the detection performance can be characterized by the deflection q of the detection statistic d. The deflection, also known as the detection index or generalized SNR, is given by

$$q = \frac{< d(\mathbf{s}+\mathbf{n}) > - < d(\mathbf{n}) >}{(< d(\mathbf{n})^2 > - < d(\mathbf{n}) >^2)^{1/2}} \,. \tag{16}$$

The components of this equation vary with the signal and noise power (since q itself depends quadratically on the components s_j and n_j, $j = 1, 2, \ldots, N$). Therefore, the deflection q (16) can be used directly to compare the SNR gain G and the gain loss δ for different beamformers. The gain is defined as the deflection normalized to the input SNR q_0, and the gain loss, as the gain normalized to the number of array elements, by

$$G = \frac{q}{q_0} \,, \quad q_0 = \frac{\mathrm{Tr}(\mathbf{M}_s)}{\mathrm{Tr}(\mathbf{M}_n)}, \quad \delta = \frac{G}{N} \tag{17}$$

(the symbol $\mathrm{Tr}(\cdot)$ denotes the matrix trace). Concerning the array gain definition, we point out that the input SNR q_0 is defined here to be the ratio of the signal and noise intensities which are spatially averaged over the array length.

The optimal small–signal matrix $\mathbf{A}_{opt}$ and deflection q_{opt} are given, respectively, by

$$\mathbf{A}_{opt} = \mathbf{M}_n^{-1} \mathbf{M}_s \mathbf{M}_n^{-1}, \tag{18}$$

$$q_{opt} = \left[\mathrm{Tr} \left(\mathbf{M}_n^{-1} \mathbf{M}_s \right)^2 \right]^{1/2}. \tag{19}$$

An important point is the fact that Eqs. (18), (19) can be alternatively derived by directly maximizing the deflection q (16) for an arbitrary signal statistics. Therefore, the choice of the maximum deflection criterion is quite reasonable in the situation of weak unknown (non–Gaussian) signals in Gaussian noise background, when the ML criterion is generally not applicable to give the optimal processor.

2.3. Array beamformers

A general structure of quadratic beamformer (QBF), the structure of the optimal QBF from Eqs. (18), (19) included, can be clearly described using the matrix $\mathbf{A}$ (15) in factorized form, $\mathbf{A} = \mathbf{W}^* \mathbf{W}^T$, where $\mathbf{W}$ is an $(N \times r)$ weight matrix consisting of vector–rows $\mathbf{w}_p$ $(p = 1, 2, \ldots, r,\ 1 \leq r \leq N)$.

This structure consists, therefore, of the matrix filter $\mathbf{W}$ followed by r–channel quadratic processor. Its weight–square–sum output y_{QBF} is obtained directly as a quadratic function of the input vector $\mathbf{x}$ by

$$y_{QBF} = d = |\mathbf{W}^T\mathbf{x}|^2 = \sum_{p=1}^{r} |\mathbf{w}_p^T\mathbf{x}|^2. \tag{20}$$

The output SNR q_{QBF} is given from Eq. (16) by the following ratio:

$$q_{QBF} = \frac{\mathrm{Tr}(\mathbf{W}\mathbf{W}^+\mathbf{M}_s)}{[\mathrm{Tr}(\mathbf{W}\mathbf{W}^+\mathbf{M}_n)^2]^{1/2}}. \tag{21}$$

Each partial channel of the quadratic scheme (characterized by the corresponding weight vector $\mathbf{w}_p$) is seen to be a linear beamformer (LBF). According to this well–known scheme, LBF weights the output of each array element and then sums the weighted outputs. As distinct from QBF, its weight–sum output y_{LBF} is obtained as a linear function of the input vector $\mathbf{x}$, and the detection statistic d, as a squared y_{LBF} by

$$y_{LBF} = \mathbf{w}^T\mathbf{x}, \qquad d = |\mathbf{w}^T\mathbf{x}|^2, \tag{22}$$

where $\mathbf{w}$ is an arbitrary $(N \times 1)$ weight vector. The output SNR q_{LBF} is given by the following ratio:

$$q_{LBF} = \frac{\mathbf{w}^+\mathbf{M}_s\mathbf{w}}{\mathbf{w}^+\mathbf{M}_n\mathbf{w}}. \tag{23}$$

Thus, the LBF structure gives a vector filter $\mathbf{w}$ followed by a single–channel quadratic detector.

General structures of LBF and QBF, as they follow directly from respective Eqs. (22), (20), are shown in Fig. 1. Comparing these structures, we conclude that the QBF scheme is an incoherent (squared) combination of r partial LBFs and reduces to the linear scheme in the particular case of $r = 1$.

A choice of the weight vector $\mathbf{w}$ and matrix $\mathbf{W}$ in the LBF and QBF schemes, respectively, determines directly the output processor performances for given signal and noise covariance matrices.

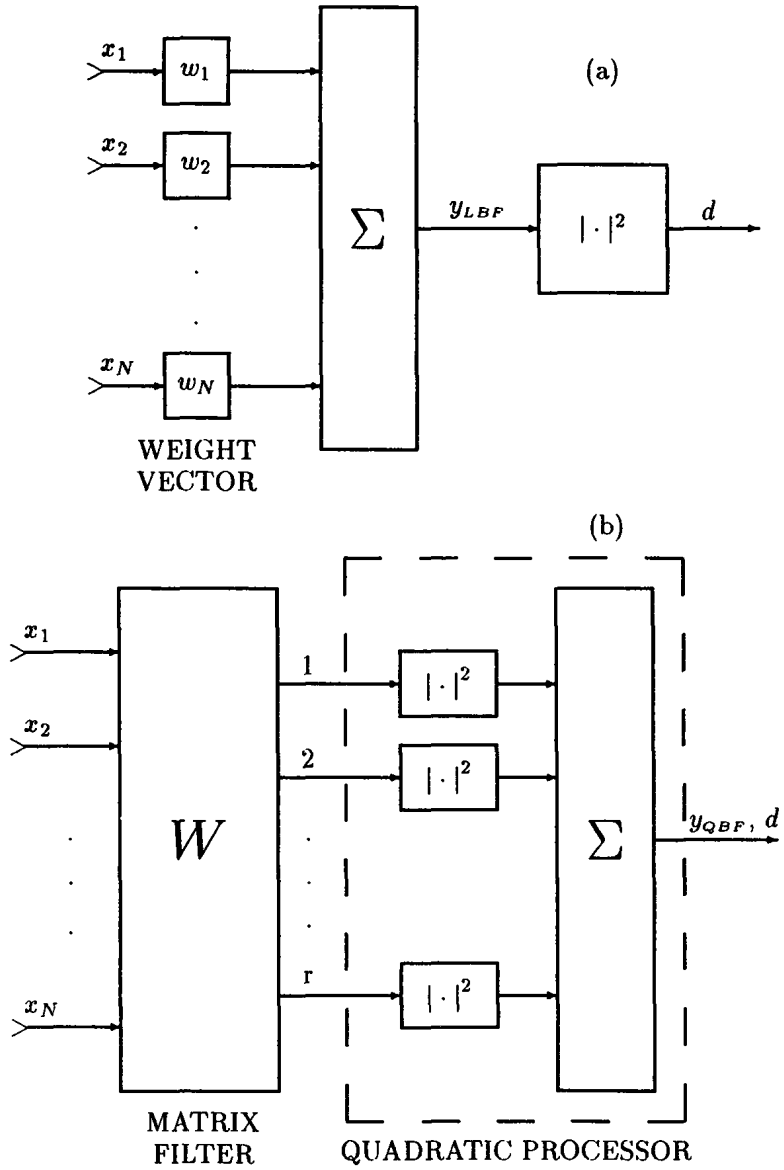

Fig. 1. A general structure of linear (a) and quadratic (b) beamformer

We turn now to the optimal solutions which are then used in Sec. 3 to examine numerically the array beamformers in deep–water environments.

For the optimal QBF derived from Eqs. (18)–(20), the partial weight vectors $\mathbf{w}_p$ and SNR q_{opt} are given by

$$\mathbf{w}_p = \lambda_p^{1/2}\mathbf{M}_n^{-1}\mathbf{m}_p, \qquad q_{opt} = \left\{\sum_{p=1}^{r} q_p^2\right\}^{1/2}. \tag{24}$$

Here, the values λ_p and vectors $\mathbf{m}_p$ are the eigenvalues and eigenvectors of the signal matrix $\mathbf{M}_s$, respectively, and the values q_p are determined below. The eigenvalues λ_p are assumed to be ordered and normalized by

$$\lambda_1 \geq \lambda_2 \geq \ldots \lambda_r > 0, \quad r = \mathrm{rank}(\mathbf{M}_s), \quad \sum_{p=1}^{N} \lambda_p = 1. \tag{25}$$

As follows from Eq. (24), the number r of partial LBFs in the optimal QBF is exactly the signal rank. Therefore, the linear structure can be optimal if and only if the signal matrix $\mathbf{M}_s$ is the rank–one matrix, or the signal is perfectly coherent. This conclusion is extremely important for our study because the signal coherence and the signal rank are intrinsically interrelated: the rank r increases with the array length N as compared to the signal coherence length N_c, i. e. with the increase of the N/N_c ratio.

Of particular interest is also the optimal linear processor which exhibits the ultimate coherence–induced limitation for all possible LBFs (in other words, for all possible vectors $\mathbf{w}$ in Eqs. (22), (23)). Its weight vector and SNR are given by the following eigenvalue–eigenvector problem:

$$q_p\mathbf{v}_p = \mathbf{M}_n^{-1}\mathbf{M}_s\mathbf{v}_p, \quad p = 1, 2, \ldots, r = \mathrm{rank}(\mathbf{M}_s). \tag{26}$$

The largest eigenvalue q_1 is the maximum SNR q_{LBF} (23), and the corresponding eigenvector $\mathbf{v}_1$ is the optimal weight vector. Moreover, the eigenvalues q_p from Eq. (26) give the optimal SNR q_{opt} (19), (24).

It follows straightforward from Eqs. (24), (26) that in the case of rank–one signal matrix emphasized above, both the optimal QBF and optimal LBF reduce to the steady–state adaptive beamformer which is, therefore, the optimal scheme to process the perfectly coherent signal against the noise interference [39, 40]. Its weight vector is given by

$$\mathbf{w} = \mathbf{M}_n^{-1}\mathbf{s}^*. \tag{27}$$

This well–known equation derives the noise prewhitening beamformer followed by the matched–signal filter.

Completing our short introduction to optimal array processing, we point out, for the purpose of emphasizing the signal coherence effect, a particular case of spatially white noise. In this case, the optimal QBF scheme is the incoherent λ_p–weighted combination of the partial filters matched to the signal eigencomponents $(\lambda_p, \mathbf{m}_p)$ from Eq. (24), while the optimal LBF matches the first (most powerful) eigencomponent $(\lambda_1, \mathbf{m}_1)$. Therefore, an additional gain Q of the optimal QBF over the optimal LBF is determined only by the signal eigenvalues:

$$Q = \frac{G_{QBF}}{G_{LBF}} = \frac{\left(\sum_{p=1}^{r} \lambda_p^2 \right)^{1/2}}{\lambda_1}, \quad 1 \leq Q \leq r^{1/2}. \tag{28}$$

In practice, only the largest eigenvalues and an "effective" rank r_{eff} (defined as their number) are of real importance for estimation of the quadratic processor performance, while contribution of the high–order eigenvalues λ_p (with the numbers $p > r_{eff}$) can be ignored.

Thus, the following characteristics of the received signal are of the greatest importance with application to the optimal large–array processors: the first (largest) eigenvalue λ_1, the effective rank r_{eff}, and the quadratic gain Q from Eqs. (24)–(28). All of them are determined by the signal eigenvalues and, therefore, are intrinsically interrelated. A physical parameter related to the signal eigenspace is the ratio N_c/N which can be estimated by direct measurements using the array. For the case of coherence–degraded signal, $N_c/N \ll 1$, the following estimates are of interest:

$$\lambda_1 \sim \frac{N_c}{N}, \quad r_{eff} \sim \frac{N}{N_c}, \quad Q \sim r_{eff}^{1/2} \sim \left(\frac{N}{N_c} \right)^{1/2}. \tag{29}$$

The general formulations outlined above have been effectively exploited by several authors to simulate the optimal processors and to consider suboptimal (quadratic and linear) techniques by the use of exponential–type models for the signal coherence [3–6, 51]. In our more recent papers [52, 49, 50], the theory has been developed by incorporating a model of multimode signal coherence and simulations of the modal covariance effects on array beamforming. Two intrinsic factors, the modal covariances and the mode orthogonality, were shown to affect mutually optimal array beamforming and the detection performance. For example, the signal rank r is considerable, $r \sim M$, if the signal–carrying modes (M is their number) are weakly correlated and the array length is sufficient for their spatial orthogonality, or resolution.

Simulated beamformers

In this paper, the effects of ocean acoustic coherence on the array gain are compared for the following four beamforming techniques.

The first (simplest) beamformer is a conventional PWBF of the steered array. The entries of its weight vector $\mathbf{w}_{PW}$ are given by

$$w_{PW}(j) = \exp[-ikd(j-1)\sin\beta], \quad j = 1, 2, \ldots, N, \tag{30}$$

where β is the steering angle (arbitrary).

The second one is PWBF with noise interference prewhitening, or adaptive PWBF [39, 40]. Its weight vector $\mathbf{w}_{APW}$ (see also Eq. (27)) is given by

$$\mathbf{w}_{APW} = \mathbf{M}_n^{-1}\mathbf{w}_{PW}. \tag{31}$$

The third one is the optimal LBF given above:

$$\mathbf{w}_{LBF} = \mathbf{v}_1, \qquad q_{LBF} = q_1, \tag{32}$$

where q_1 and $\mathbf{v}_1$ are, respectively, the largest eigenvalue and the corresponding eigenvector from Eq. (26).

Finally, the fourth one is the full-optimal QBF from Eqs. (18), (19), (24):

$$\mathbf{W}_{QBF}^{*}\mathbf{W}_{QBF}^{T} = \mathbf{A}_{opt}, \qquad q_{QBF} = q_{opt}. \tag{33}$$

Obviously, the first three techniques follow from the linear structure in Fig. 1a, and the last technique, from the quadratic structure in Fig. 1b.

3. PREDICTIONS OF THE ACOUSTIC MCF WITH APPLICATION TO LARGE-ARRAY PERFORMANCE DEGRADATION

In this section, we give some illustrative examples to exhibit numerical predictions of (i) the acoustic MCF for a given sound-speed profile and spectum of oceanic inhomogeneities, and (ii) the coherence-induced effects on the array beampattern and SNR gain for both horizontal and vertical array configurations.

The two sound-speed profiles chosen for our calculations are shown in Fig. 2. They represent summer and winter seasonal averages and buoyancy frequency in the North-West Pacific at latitude 45°N. The sound scattering in the summer channel is caused mainly by volume fluctuations in the index of refraction, and in the winter channel, by contrast, by a stochastically

rough surface. To illustrate the corresponding effects of random volume and surface scattering on acoustic transmission we exploit the Garrett–Munk spectrum [35] for internal waves and the Pierson–Moskowitz spectrum [38] for surface wind waves.

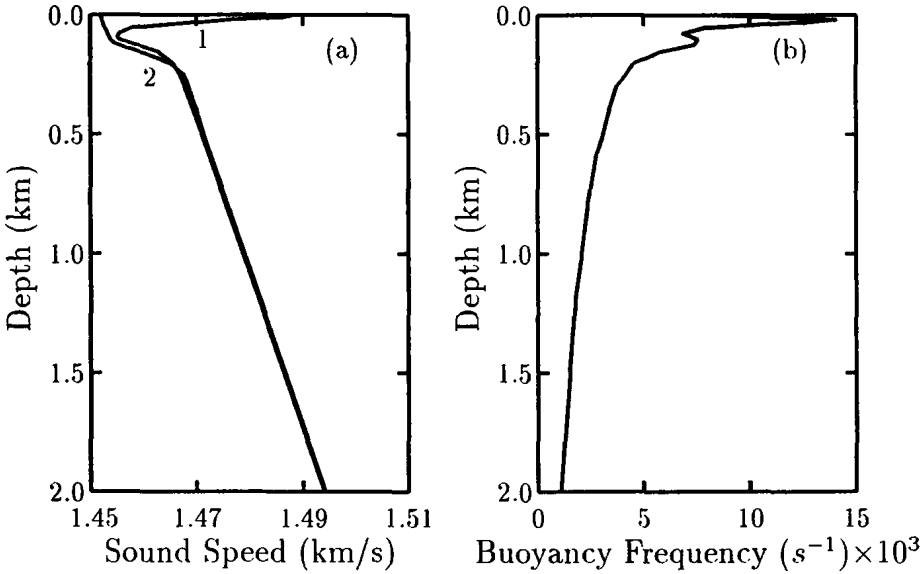

Fig. 2. Upper parts of sound speed profiles (a) and buoyancy distribution (b) from the North–West Pacific. The profiles are: summer (1) and winter (2)

3.1. Evaluations of the acoustic MCF

We begin with observing the effect of medium fluctuations on the sound wavefield coherence.

The coherence degree of the received signal is characterized by the correlation coefficient:

$$C(\mathbf{r_1}, z_1, \omega_1, t_1|\mathbf{r_2}, z_2, \omega_2, t_2) = \tag{34}$$

$$= \frac{\Gamma(\mathbf{r_1}, z_1, \omega_1, t_1|\mathbf{r_2}, z_2, \omega_2, t_2)}{\sqrt{\Gamma(\mathbf{r_1}, z_1, \omega_1, t_1|\mathbf{r_1}, z_1, \omega_1, t_1)\Gamma(\mathbf{r_2}, z_2, \omega_2, t_2|\mathbf{r_2}, z_2, \omega_2, t_2)}}.$$

This function is fully determined by solutions of the eigenvalue problem, Eq. (2), and the RTE, Eq. (8).

Volume scattering by random internal waves

In Fig. 3 we plot the magnitude of the correlation coefficient from Eq. (34) in the case of transverse horizontal and vertical separations. Figure 4 shows the behavior of the normalized MCF as a function of time and acoustic frequency.

Calculations were carried out for the summer profile from the North–West Pacific (curve 1 in Fig. 2), for the source frequency of 250 Hz and the source depth of 50 m. The theoretical curves in Figs. 3 and 4 were plotted using the results of the work of Esswein and Flatte [36] for the phase–structure density from internal waves. It is evident from these figures that the characteristic coherence time and coherence lengths decrease as the range increases.

Rough surface scattering by fully developed seas

As mentioned previously, when the propagation takes place in an upper sound channel, surface interactions play a predominant role in acoustic signal fluctuations. For example, in the North Pacific such situations exist perhaps 50% of the time in the winter.

For the case considered the corresponding graphs for correlation functions are presented in Figs. 5 and 6. There is an additional parameter of the ocean environments simulation, the wind speed v, which varies here from 10 m/s to 15 m/s. Obviously, the increase of the wind speed leads to the increase of the rough surface scattering and coherence loss.

For moderate v ($v < 13$ m/s) the MCF behaves in an oscillatory fashion which indicates that the scattering is weak, so that there can be a high degree of signal coherence even at relatively large separation of the observation points. It should be emphasized that the normalized MCF tends asymptotically to the coherence parameter $I_c = |< P(\mathbf{r}, z, t) >|^2 / < |P(\mathbf{r}, z, t)|^2 >$. The characteristic coherence length, time and coherent bandwidth which are determined by the half–power decay of the correlation coefficient in the case studied depend on wind speed and are approximately 10 m, 2 s and 0.3 Hz, respectively, for $v = 10$ m/s.

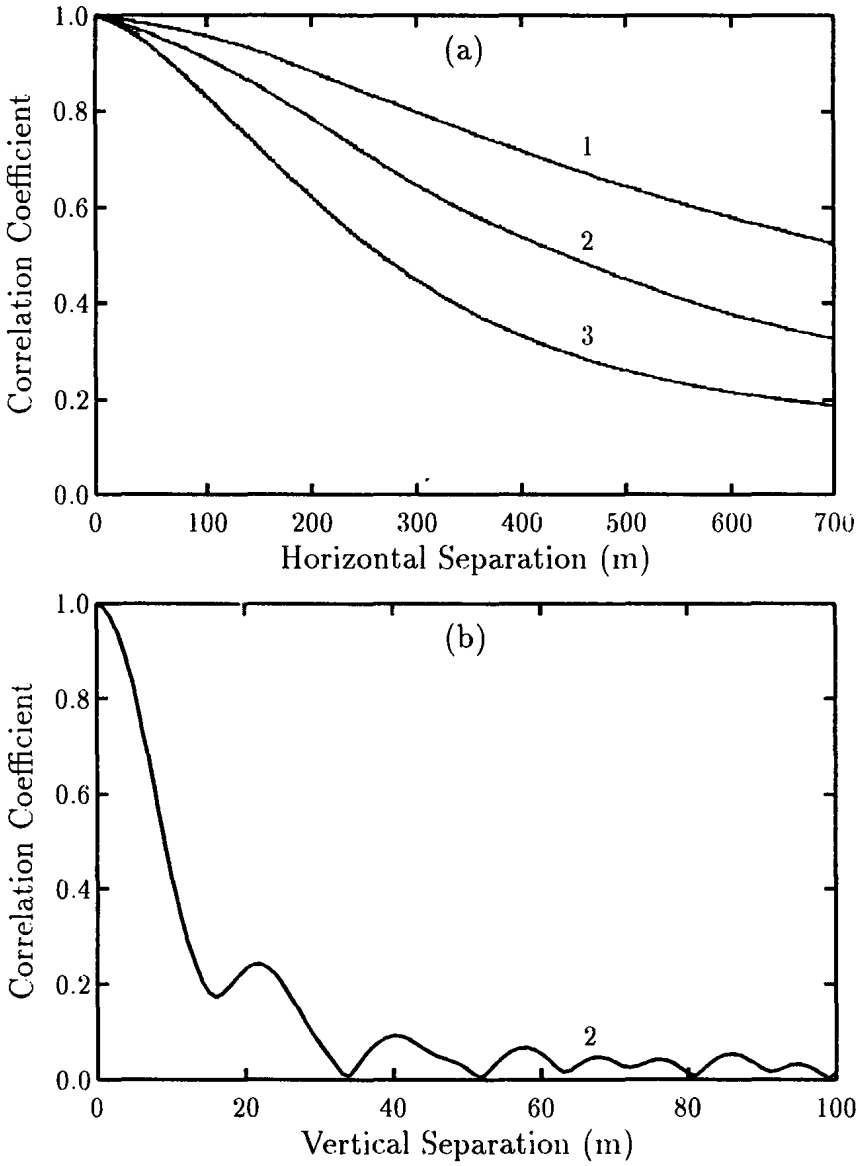

Fig. 3. The normalized MCF of horizontal (a) and vertical separation (b) for summer environments at various ranges: 1 - 250 km, 2 - 500 km, 3 - 1000 km. Source frequency is 250 Hz, source depth is 50 m, depth of the horizontal array (a) and the 1st element of vertical array (b) is 300 m

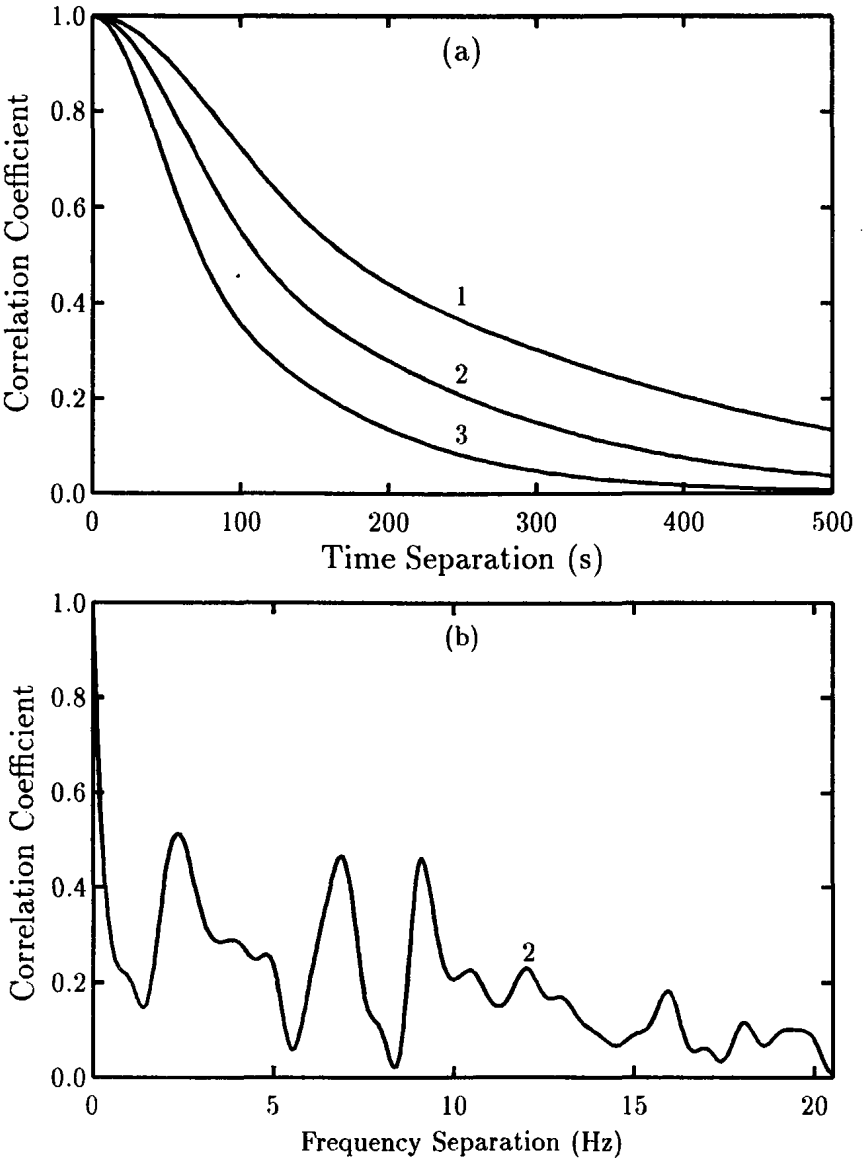

Fig. 4. The normalized MCF of time (a) and frequency separation (b) for summer environments at various ranges: 1 — 250 km, 2 — 500 km, 3 — 1000 km. Source frequency is 250 Hz, source depth is 50 m, and receiver depth is 300 m

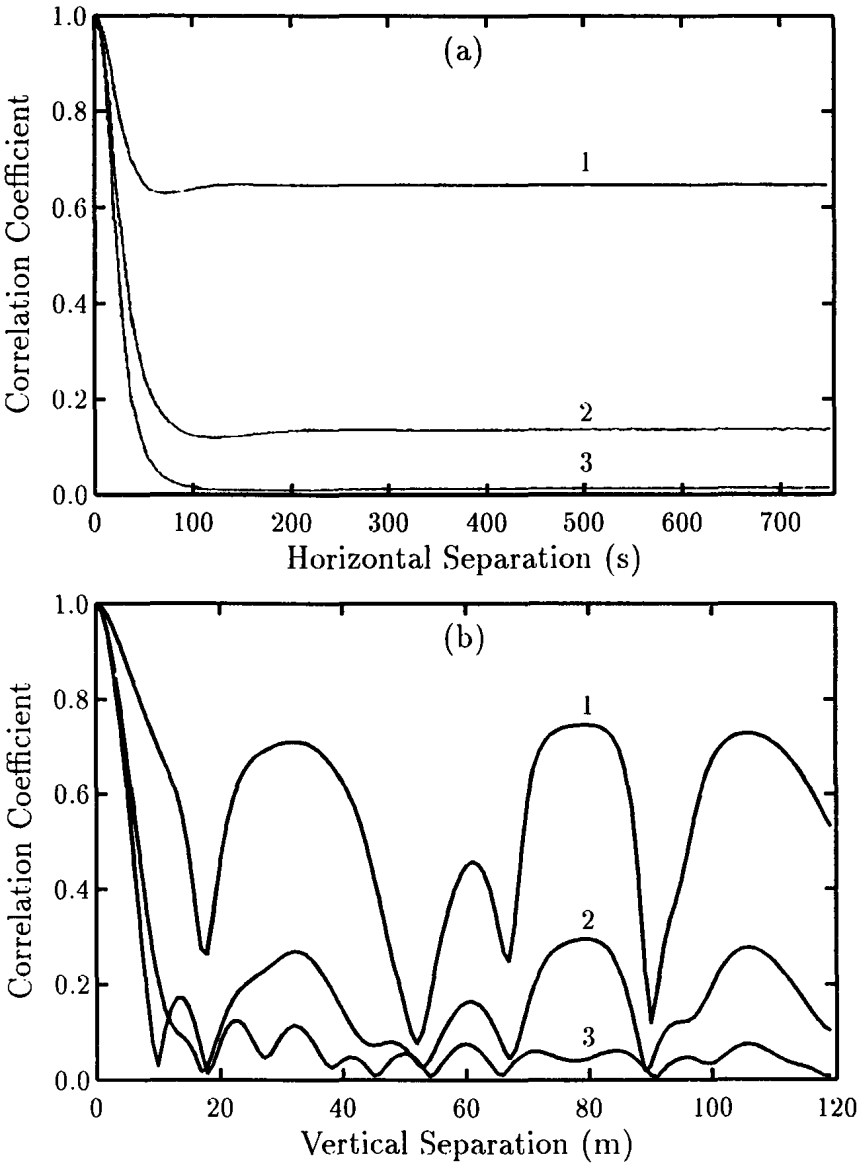

Fig. 5. The normalized MCF of horizontal (a) and vertical separation (b) for winter environments at the range of 500 km and various surface roughness: 1 — $v = 10$ m/s, 2 — $v = 13$ m/s, 3 — $v = 15$ m/s. Source frequency is 250 Hz, source depth is 100 m, depth of the horizontal array (a) and the 1st element of vertical array (b) is 300 m

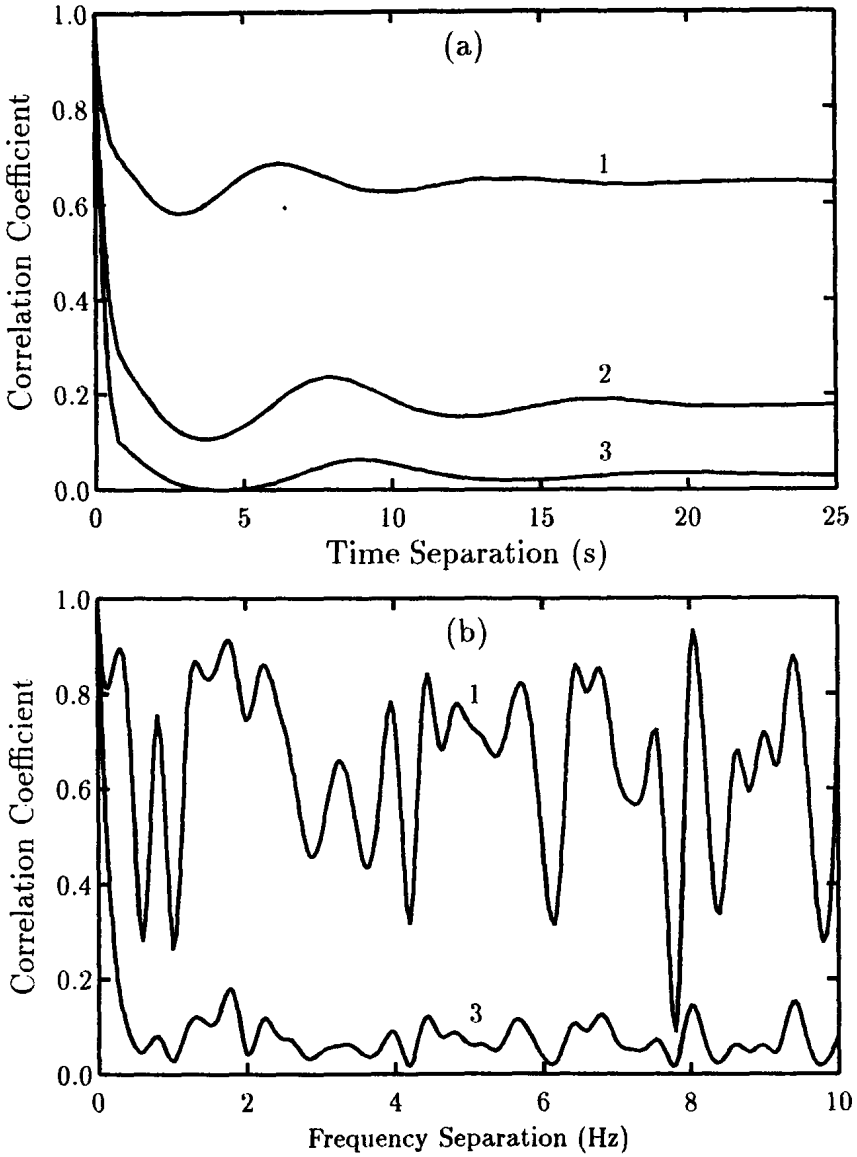

Fig. 6. The normalized MCF of time (a) and frequency separation (b) for winter environments at the range of 500 km and various surface roughness: 1 — $v = 10$ m/s, 2 — $v = 13$ m/s, 3 — $v = 15$ m/s. Source frequency is 250 Hz, source depth is 100 m, and receiver depth is 300 m

Concluding this subsection, we emphasize that the results on the MCF is a base to examine the signal processing schemes (discussed in Sec. 2) in the same ocean environments.

3.2. Horizontal array gain limitations

Now we turn to the numerical predictions of the coherence–induced loss of the array processor performances including the beampattern and gain. First, we give the results for the horizontal array configuration.

For the main purpose of evaluating the signal coherence effects, the simulation is focused on the situation of spatially white noise background, i. e. $\mathbf{M}_n = \mathbf{I}$ in the equations from Sec. 2 ($\mathbf{I}$ is the identity matrix). To calculate the signal matrix $\mathbf{M}_s$ we exploit the relative MCFs from Figs. 3a and 5a.

Figure 7 shows the mean beampattern of the 256–element phased array as a function of the steering angle β for the source direction $\alpha = 30°$ in the summer (a) and winter (b) channels, respectively (curves 1 in both cases correspond to a regular channel, or perfectly correlated modes). Signal coherence loss is seen to lead to considerable degradation of the beampattern. This fact is generally well known [46, 47] but the pronounced feature is shown to be the main lobe angular displacement caused by multimode broadening of the signal angular spectrum. Therefore, an adaptive correction of the main lobe direction is required to adjust the PWBF steering angle to the angular response maximum.

Figure 8 shows the gain loss δ, Eq. (17), as a function of the number N of the array elements in the summer channel for the source direction $\alpha = 30°$. A considerable degradation of the PWBF gain (for $\beta = \alpha$, see curve 4) is caused primarily by the main lobe displacement emphasized above. It is worthy of notice that the steep increase of the gain loss $\delta(N)$ for $N \gtrsim 50$ corresponds to the decreasing gain $G(N)$. The latter function achieves the maximum value $G \simeq 15$ dB for $N \simeq 50$ and shows a gradual decrease of the gain for larger arrays. The angular correction required for such array lengths is seen to lead to the significant gain increase up to $\sim 5 - 10$ dB and to achieve near–optimal LBF performance (see curves 2 and 3). On the other hand, this angular correction of PWBF does not entail any increase in computational complexity and has the essential advantage of environmental robustness.

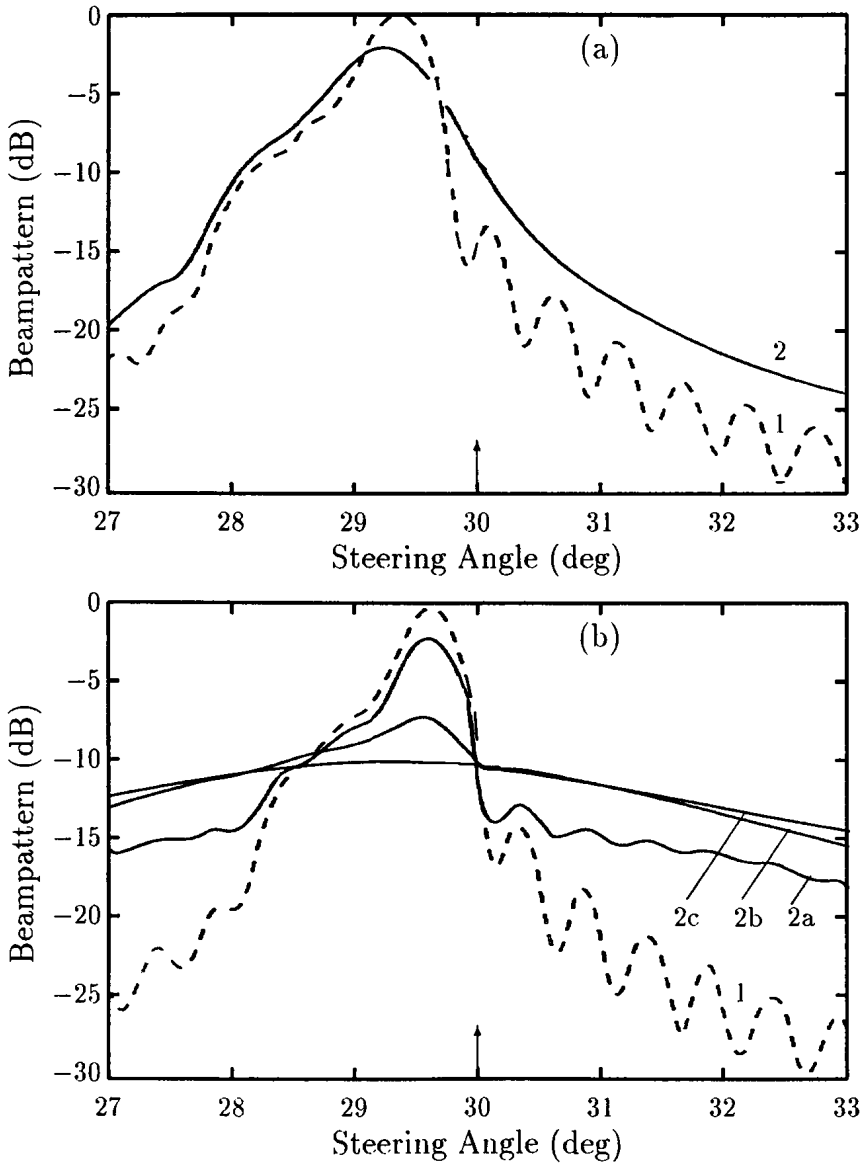

Fig. 7. Beampattern of the horizontal 256–element array for the summer (a) and the winter (b) environments in the absence (1) and in the presence (2) of random inhomogeneities: 2a — $v = 10$ m/s, 2b — $v = 13$ m/s, 2c — $v = 15$ m/s. Arrow indicates the angle of arrival

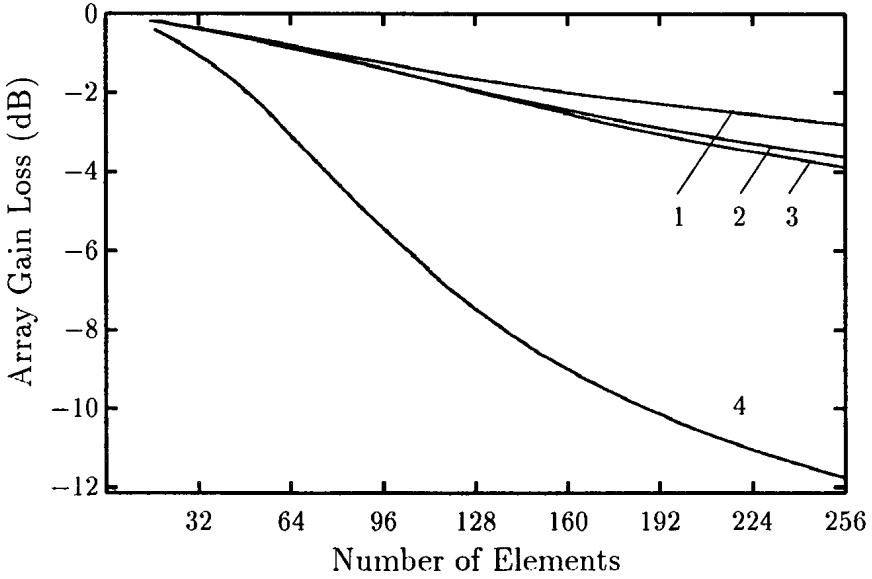

Fig. 8. Horizontal array gain loss in the summer environments as a function of the number of array elements: 1 — optimal QBF, 2 — optimal LBF, 3 — PWBF with angular correction, 4 — conventional PWBF

Figure 9 shows the same function $\delta(N)$ in the winter channel for the same angle $\alpha = 30°$ and two values of the wind speed $v = 10$ m/s (a) and $v = 15$ m/s (b). The curves in Fig. 9a are generally similar to those in Fig. 8 and illustrate, in particular, the angular dependence of the PWBF efficiency that amounts up to ~ 10 dB. From Fig. 9b, however, two essential conclusions concerned with fully developed wind waves follow. First, all the linear beamformers, the optimal LBF included, degrade in comparison with the optimal QBF with the increase of the speed v: the additional quadratic gain Q, Eq. (28), is about 3 dB for the array length $N \sim 100$ and increases gradually with N. Second, the angular correction of PWBF does not entail a significant effect on the array gain. A physical reason is rather clear, namely, the coherence length N_c is small as compared to the array length N, $N_c/N \ll 1$ (see Fig. 5a). This leads to (i) an increase of the signal rank r and, therefore, to an increase of the "gap" between the optimal LBF and QBF performances according to Eqs. (28), (29) and to (ii) full degradation of the large-array beampattern (see Fig. 7b) and to consequent vanishing of the angular dependence of the PWBF performance.

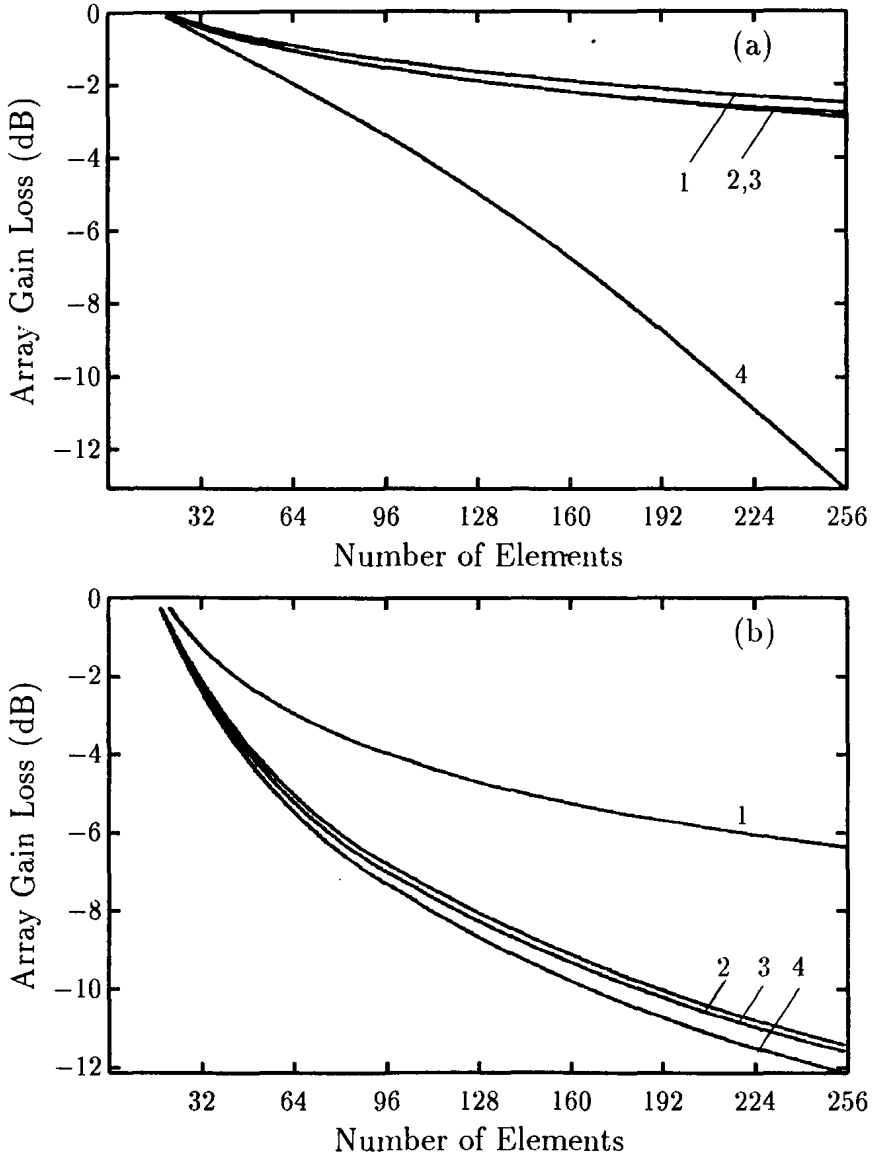

Fig. 9. Horizontal array gain loss in the winter environments as a function of the number of array elements for $v = 10$ m/s (a) and $v = 15$ m/s (b): 1 — optimal QBF, 2 — optimal LBF, 3 — PWBF with angular correction, 4 — conventional PWBF

To clarify the difference between the summer and winter conditions in more detail, we show in Fig. 10 the largest eigenvalues (25) of the covariance matrix $\mathbf{M}_s$ for $N = 256$ and $\alpha = 30°$.

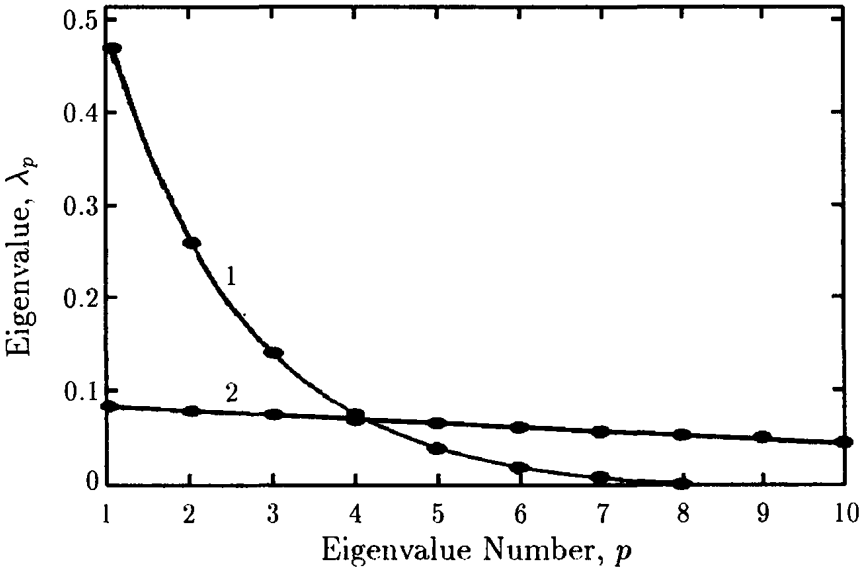

Fig. 10. Eigenvalues of simulated signal correlation matrix $\mathbf{M}_s$ for the 256–element horizontal array in the summer (1) and the winter (2) (at $v = 15$ m/s) environments

In the summer channel, the signal eigenvalues are seen to decrease rapidly with the number p, and $r_{eff} \sim 3$. In the winter channel, on the contrary, the eigenvalue spectrum for $v = 15$ m/s is nearly uniform for the first numbers, and $r_{eff} \sim 15$.

It is also of interest to compare the amplitude–and–phase array weights $w(j)$ for the PWBF with the angular correction and for the optimal LBF. These beamforming techniques, as is seen from Figs. 8 and 9, achieve almost the same gain performance. The reason is that the phase distribution of the first signal eigenvector $\mathbf{m}_1$ (which gives the weight vector for optimal LBF, Eq. (26)), is very close to the phase distribution of the corrected PWBF array:

$$\arg(m_1(j)) \simeq -kd(j-1)\sin\beta_{max} \ ,$$

where β_{max} is the direction of maximum angular response from Fig. 7. These weight coefficients differ only by their magnitudes, or by the shapes

of the spatial windows. For example, Fig. 11 shows the weight magnitudes for the 256-element array in the winter channel for three values of the speed v. These non-uniform windowing shapes entail some broadening of the optimal beampattern main lobe in comparison with the PWBF main lobe, which is caused by fluctuations of the modal angles of arrival.

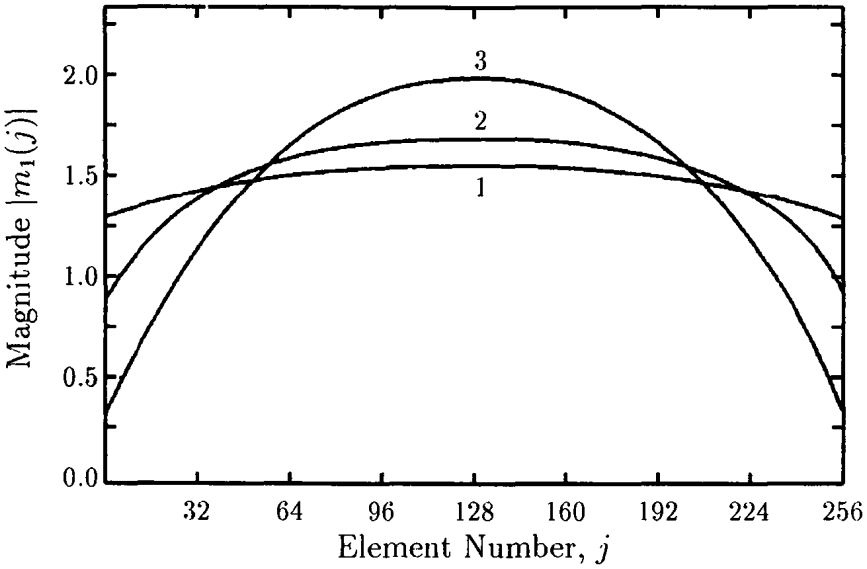

Fig. 11. Weight magnitudes for the 256-element horizontal array in the winter environments: 1 — $v = 10$ m/s, 2 — $v = 13$ m/s, 3 — $v = 15$ m/s

Thus, the coherence-induced effects on the horizontal array beampattern and gain are shown to be significant, especially in the winter environments of fully developed wind seas, and to depend essentially on the beamforming technique used.

3.3. Vertical array gain limitations

To take into account the well-known vertical directionality of the ocean ambinient noise, the examination of vertical array processors includes also modeling the noise covariance matrix $\mathbf{M}_n$. We assume the noise to be the sum of spatially white noise and partially coherent ambient noise of the ocean:

$$\mathbf{M}_n = \sigma \mathbf{I} + \mathbf{M}_{an} \ , \tag{35}$$

where $\mathbf{I}$ is the identity matrix, $\mathbf{M}_{an}$ is the covariance matrix of ambient noise, and σ is the white noise level. We calculate the "vertical" matrix $\mathbf{M}_{an}$ by exploiting a widely used model of the ocean surface–generated noise [45, 53], according to which the noise is generated by uncorrelated sources with homogeneous spatial distribution on the ocean surface. The treatment is also based on the normal mode approach, so we interprete the ambient noise in Eq. (35) as the modal noise. As was previously estimated in Ref. [54], the modal noise effect on the vertical array gain depends inherently on "overlapping" of the signal and noise modal spectra.

To calculate the signal matrix $\mathbf{M}_s$ we exploit the relative MCFs from Figs. 3b and 5b.

We examine here the array gain G (17) instead of the gain loss δ. The reason is that modal noise prewhitening by the use of special techniques of matrix inversion, Eqs. (24), (26), (31), leads to some additional gain. This additional "noise" gain may be essential only if the modal noise is much more intensive in comparison with the white noise background. That is the case of our particular interest, so we suppose $\sigma = -20$ dB in Eq. (35).

Figure 12 shows the 64–element array beampatterns in the summer (a) and winter (b) channels. For both figures, the beampatterns are plotted to be compared for regular and random–inhomogeneous channels (curves 1 correspond to a regular channel). The signal coherence loss is seen to lead to a considerable degradation of the array beampattern, similarly to the case of a large horizontal array (see Fig. 7). In both channels, however, the maximum angular response corresponds to transverse propagation because the signal modal spectrum has a maximum in the low–order modes (see also curves 1 in the following Fig. 13).

Figure 13 shows the modal spectra of the received signal and the ocean noise in the summer (a) and winter (b) channels. Comparison of these two cases shows that they differ essentially. In the summer channel, the noise power spectrum has a smooth maximum in the high–order ($m \gtrsim 100$) modes, so the signal and noise are localized mainly in different groups of modes. This fact leads to a general possibility of highly efficient modal noise suppression, which obviously corresponds to the particular case of transverse signal reception and modal interference reception in the sidelobe domain. An opposite situation is seen to be realized in the winter channel owing to the noise power localization in the lower–order modes. This difference leads to a dramatic effect on the array gain [54], which is illustrated below.

Figure 14 shows the array gain function $G(N)$ in the summer channel for the white noise (a) and modal noise (b) background. Since the main lobe is not displaced from the transverse direction ($\beta_{max} = 0°$), we plot only three gain functions in Fig. 14a.

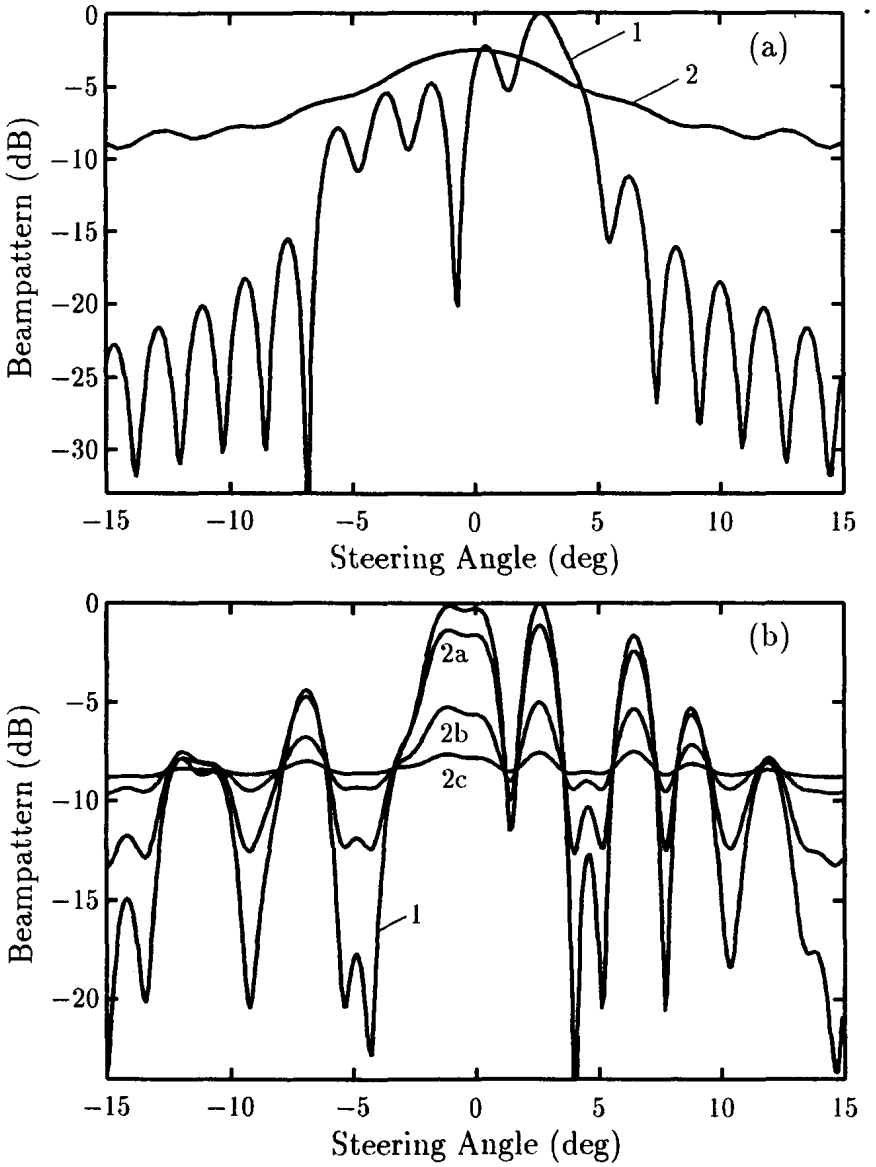

Fig. 12. Beampattern of the vertical 64–element array for the summer (a) and the winter (b) environments in the absence (1) and in the presence (2) of random inhomogeneities: 2a — $v = 10$ m/s, 2b — $v = 13$ m/s, 2c — $v = 15$ m/s

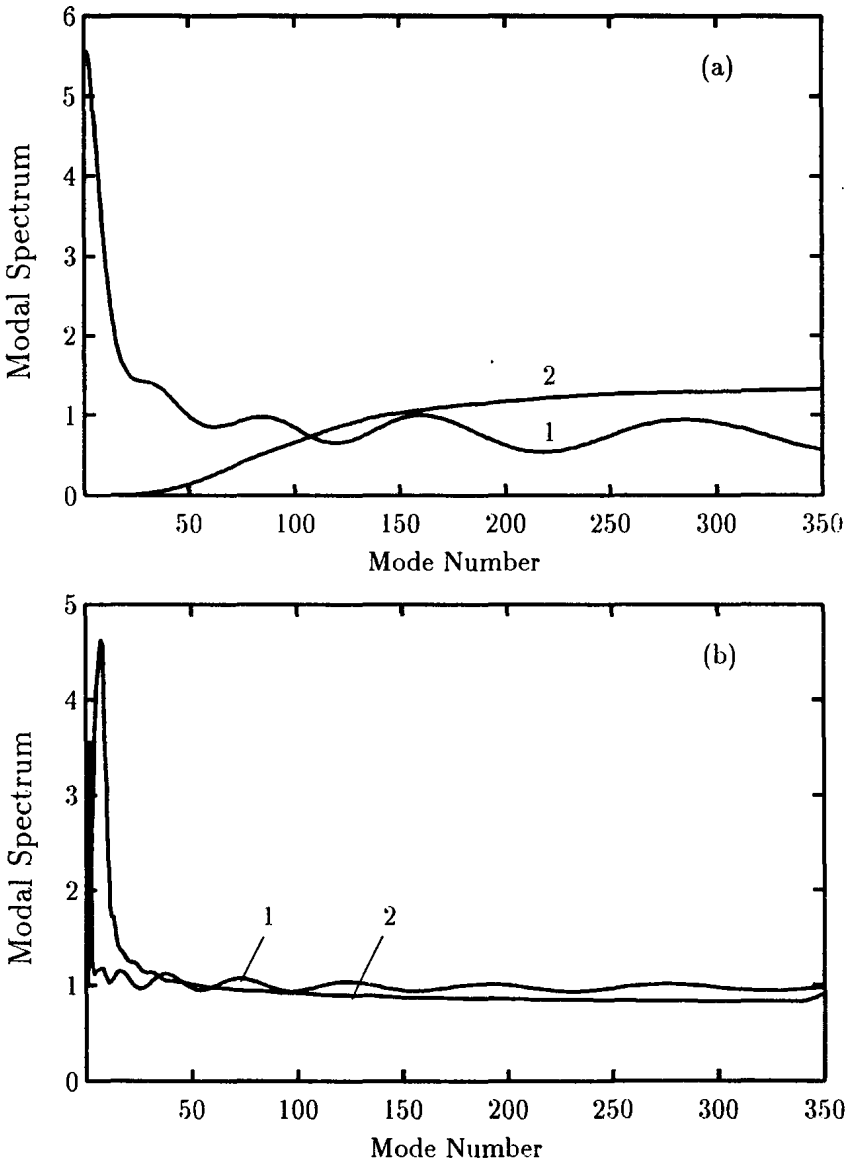

Fig. 13. Modal spectra of the signal (1) and ambient noise (2) for the summer (a) and winter (b) (at $v = 15$ m/s) environments. Modal spectra have been normalized to the area under their respective curves

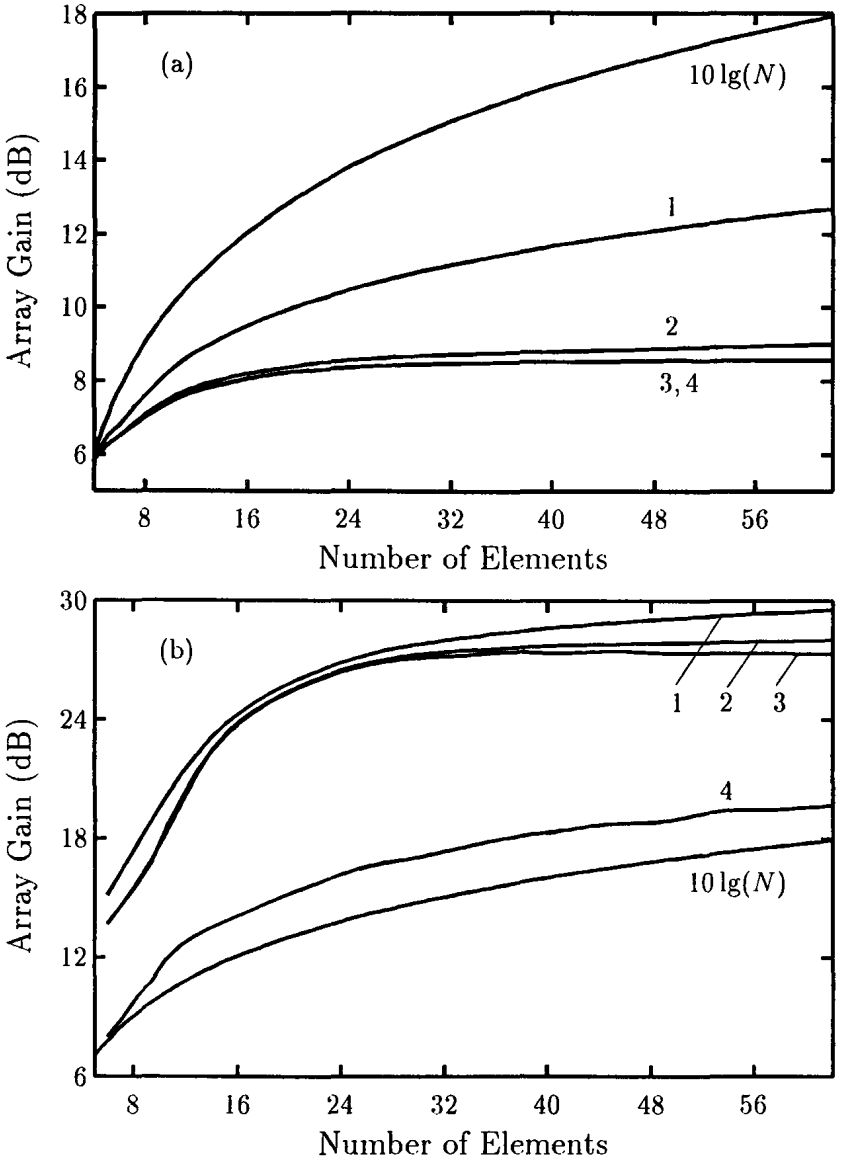

Fig. 14. Vertical array gain in the summer environments as a function of the number of array elements for white noise (a) and modal noise (b): 1 — optimal QBF, 2 — optimal LBF, 3 — adaptive PWBF, 4 — PWBF

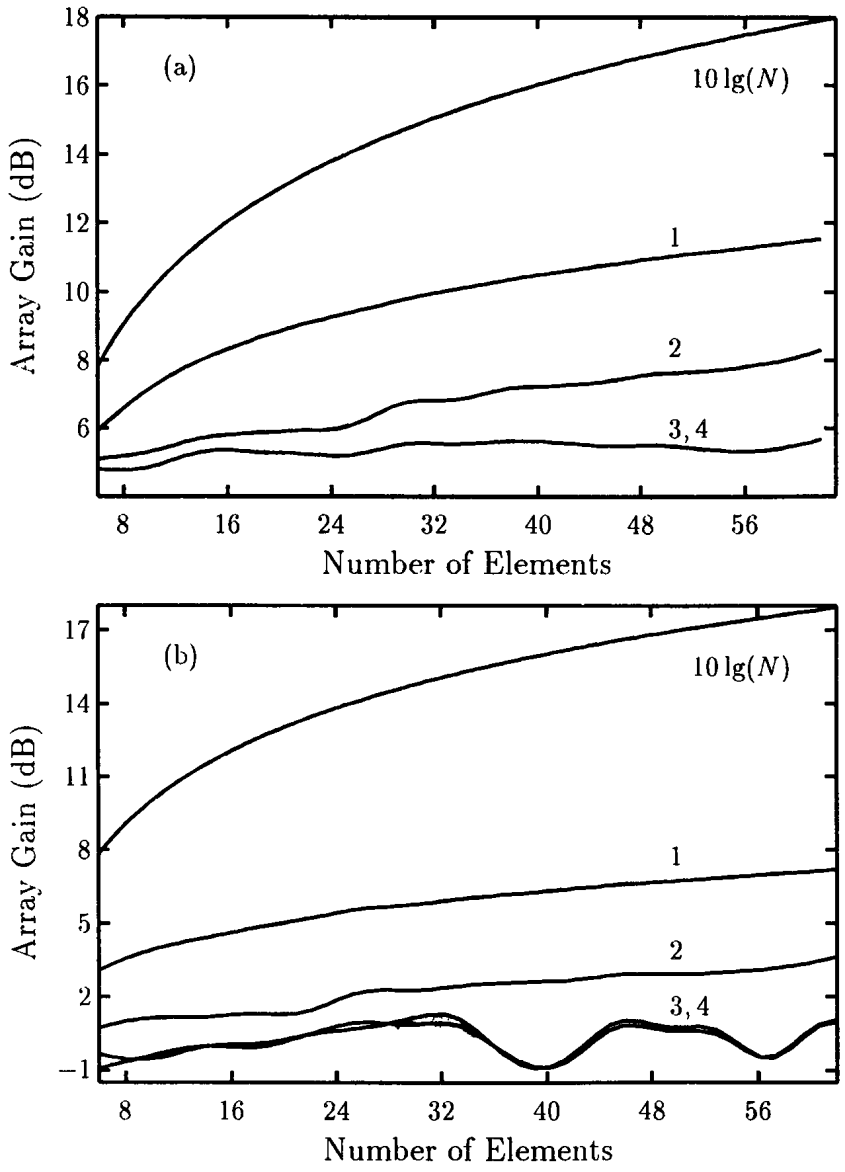

Fig. 15. Vertical array gain in the winter (at $v = 15$ m/s) environments as a function of the number of array elements for white noise (a) and modal noise (b): 1 — optimal QBF, 2 — optimal LBF, 3 — adaptive PWBF, 4 — PWBF

The considerable increase of the gain in the case of modal noise as compared to the case of white noise is shown to be about $10-20$ dB for all the beamformers. The most significant increase is seen to be achievable for the beamforming techniques which prewhite the modal noise. The gain increase for conventional PWBF is, however, also significant due to angular selection of the received fields by narrowing the beampattern main lobe with increasing the number of array elements.

Figure 15 shows the array gain function $G(N)$ in the winter channel for the wind speed $v = 15$ m/s and the same cases of the noise background. For the modal noise, the gain is seen to decrease (down to about -5 dB) for all the beamformers owing to similarity of the signal and noise modal spectra, which was emphasized above (see Fig. 13b). Only the optimal large–array QBF achieves in this case a significant value of gain $G \sim 5-7$ dB. Moreover, PWBF does not achieve any practical gain for all array lengths, so the PWBF array is concluded to be ineffective under these input conditions.

Thus, the estimates of vertical array gain vary essentially depending not only on the signal coherence loss but on the ambient noise modal spectrum as it is proved above. Moreover, the last dependence can be even more essential and may lead to a dramatic effect, especially in the case of similar modal (angular) spectra of the signal and ambient noise.

4. SUMMARY AND CONCLUSIONS

In this section, we conclude our study on the coherence effects on large–array signal processing in long–range deep–water environments and summarize the key results obtained.

The MCF is of great importance for understanding statistical behavior of ocean acoustic transmission. It was shown how to efficiently derive an asymptotic expression for the MCF in terms of modal structure of the acoustic pressure field using the RTE. The method for solving the corresponding matrix equation is based on combined use of the WKB approximation and generating function technique. The procedure elaborated allows one to reduce the problem of the wavefield coherence calculation in a refractive sound channel with random volume inhomogeneities to the analogous problem in free space. The method employed was also extended to include rough surface scattering effects. The application is illustrated by numerical computation of the expected acoustic coherence for deep water ocean environments under the assumption that the random field of either internal waves or fully developed seas is the dominant source of transmission fluctuations.

Rough surface scattering was established to cause the most significant effects on ocean acoustic coherence. In particular, as observed in the results

of Sec. 3, for a source of 250 Hz, at a range of 500 km and wind speed of 15 m/s, the characteristic horizontal coherence length and coherence time have an order of magnitude of 50 m and of 2 s, respectively. For comparison, the corresponding scales computed from the Garrett–Munk spectrum and summer profile in Fig. 2 are of order 400 m and 200 s.

We emphasize that the underlying assumption of the dominance of internal–waves or fully developed wind seas has been previously tested in ample detail against data for time behavior of the MCF. In particular, the experiments performed by researchers of the Institute of Applied Physics RAS in the North–West Pacific at the sound frequency of 250 Hz and at ranges up to 1000 km demonstrate that the signal fluctuations have the correlation time of a few hundred seconds in the summer environment, and of a few seconds in the winter one [55]. Our respective calculations are in a good agreement with these experimental results.

Measurements of horizontal and vertical coherence have also been carried out in many experiments. The available data have been collected in the book by Stefanick [56]. The majority of the data indicate that typical measures of coherence lengths are 10 to 100 wavelengths for horizontal separations and less than 10 wavelengths for vertical separations. Again, the order–of–magnitude is consistent with our numerical predictions.

Thus, we can conclude from this study that the RTE technique is a powerful tool for calculating acoustic propagation in a medium where random scattering effects are important. It is clear, however, that more accurate oceanographic measurements taken simultaneously with acoustic measurements will be required to compare with our theoretical expressions.

The effect of oceanic fluctuations on the received signal coherence was shown to be of the most importance with application to large–array beamforming. The following three factors were shown distinctly to be the key points, namely, (i) multimode spreading of the received signal angular spectrum; (ii) multimode signal coherence degradation; and (iii) ambient noise directionality. The particular effects of these factors depend intrinsically on the array configuration in a channel and the array length. Moreover, the beamforming techniques were shown to be very different from the point of view of environmental robustness.

The PWBF technique was shown to be the most "sensitive" to the factors (i)–(iii). This means that the PWBF gain can dramatically vary as a function of environmental parameters. Of the greatest importance is the fact that adaptive correction of the steering angle can lead to an essential improvement of the performance, for example, up to $\sim$ 10 dB for the horizontal array lengths $L \sim 100\lambda$. However, the possibility to maintain the PWBF efficiency is firmly restricted by the cases of "residual" signal coher-

ence over the full array length, and partial separation of the modal spectra of the received signal and noise background. These two cases are generally independent of each other but affect mutually the large–array PWBF gain.

An obvious advantage of the PWBF techniques is their comparative simplicity. They do not require a preprocessing procedure to estimate the signal eigenspace, and their performance can easily be controlled by reforming the beampattern, including adaptive angular correction of the main lobe.

As distinct from PWBF, the optimal processing techniques require the eigenvalue–eigenvector analysis of the desired signal. To synthesize the optimal LBF and QBF schemes, one needs, therefore, to estimate the signal eigenspace in the noise background. The full–optimal QBF reduces significantly the coherence–induced array gain loss, however, at a cost of increased processor complexity: the number of partial weight–sum channels is equal to the number of the largest signal eigenvalues, as compared to the linear beamformers which require to synthesize only one weight–sum channel. The reason to follow such a complicated scheme is only the long–range signal coherence degradation, namely, the small values of the ratio $N_c/N \ll 1$, or, in other words, the case of $r_{eff} \gg 1$. Under these conditions, the additional quadratic gain Q (28) is considerable, $Q \sim r_{eff}^{1/2}$, and its value was shown to be $\sim 3 - 6$ dB. The most essential and pronounced feature of the optimal QBF is the increase of the gain function $G(N)$ for all array lengths without a "saturation" plateau. The latter, in turn, is an intrinsic feature of the optimal LBF.

We point out that the eigenvalue–eigenvector approach to the optimal processing techniques can be also developed in the temporal and frequency domains by the use of the results on respective MCFs of time and frequency from deep–water environments (see Figs. 4 and 6).

In conclusion, we summarize that (i) the large–array gain performance in long–range ocean environments is inherently limited by the spatial coherence of multimode acoustic signal, and (ii) the full potential of large arrays will not be realized unless the coherence characteristics are known in detail and incorporated into signal processing.

ACKNOWLEDGEMENTS

This work was supported by the Russian Foundation for Basic Research under Grants No 96–02–19462 and No 96–02–19460.

References

1. *Flatte S. M. et al.*, Sound Transmission Through a Fluctuating Ocean, edited by S. M. Flatte (Cambridge U. P., New York, 1979).

2. *Brekhovskikh L. M. and Lysanov Yu. P.*, Fundamentals of Ocean Acoustics (Springer–Verlag, Berlin, New York, 1982).

3. *Cox H.*, Line array performance when the signal coherence is spatially dependent // J. Acoust. Soc. Am., 1973, vol. 54(6), pp. 1743–1746.

4. *Vural A. M.*, Effects of perturbations on the performance of optimum/adaptive arrays // IEEE Trans. AES, 1979, vol. 15(1), pp. 76–87.

5. *Laval R. and Labasque Y.*, Medium inhomogeneities and instabilities: effects on spatial and temporal signal processing // In: Underwater Acoustics and Signal Processing, edited by L. Bjørno (Reidel, Dordrecht, Holland, 1981), pp. 41–70.

6. *Morgan D. R. and Smith T. M.*, Coherence effects on the detection performance of quadratic array processors, with application to large–array matched–field beamforming // J. Acoust. Soc. Am., 1990, vol. 87(2), pp. 737–747.

7. *Van Trees H. L.*, Detection, Estimation and Modulation Theory, Part I (Wiley, New York, 1968).

8. *Baker C. R.*, Optimum quadratic detection of a random vector in Gaussian noise // IEEE Trans. Commun., 1966, vol. 14(6), pp. 802–805.

9. *Sazontov A. G.*, Acoustics coherence in a deep random oceanic waveguide // In: Formation of Acoustical Fields in Oceanic Waveguides, edited by V. I. Talanov and V. A. Zverev (IAP RAS, Nizhny Novgorod, 1995), pp. 37–62.

10. *Sazontov A. G.*, Quasi–classical solution of radiation transport equation in a scattering medium with regular refraction // Akust. Zhur., 1996, vol. 42(4), pp. 551–559 [in Russian].

11. *Sazontov A. G. and Vdovicheva N. K.*, Modelling low–frequency sound scattering in a random oceanic waveguide using a modal formulation // Proc. 3rd Europ. Conf. on Underwater Acoustics, edited by J. S. Papadakis (Heraklion, Greece, 1996), vol. 1, pp. 133–138.

12. *Gorodetskaya E. Yu., Malekhanov A. I., Sazontov A. G., and Farfel' V. A.*, Effects of long–range propagation of sound in a random inhomogeneous ocean on the gain loss of a horizontal antenna array // Akust. Zhur., 1996, vol. 42(5), pp. 615–622 [in Russian].

13. *Gorodetskaya E. Yu., Malekhanov A. I., Sazontov A. G., and Vdovicheva N. K.*, Large–array gain limitations in a random oceanic waveguide with application to the North Pacific // Proc. 3rd Europ. Conf. on Underwater Acoustics, edited by J. S. Papadakis (Heraklion, Greece, 1996), vol. 1, pp. 507–512.

14. *Gorodetskaya E. Yu., Malekhanov A. I., Sazontov A. G., and Vdovicheva N. K.*, Vertical array gain in a random–inhomogeneous oceanic waveguide // Akust. Zhur., 1997, vol. 43(6) (to be published) [in Russian].

15. *Macaskill C. C. and Uscinski B. J.*, Propagation in waveguides containing random irregularities: The second moment equation // Proc. R. Soc. Lond., 1981, vol. A377, pp. 73–98.

16. *Beran M. J., Whitman A. M., and Frankenthal S.*, Scattering calculations using the characteristic rays of the coherence function // J. Acoust. Soc. Am., 1982, vol. 71(5), pp. 1124–1130.

17. *Bass F. G. and Fuks I. M.*, Wave Scattering From Statistically Rough Surface (Pergamon, Oxford, U.K., 1979).

18. *Kudryashov B. M.*, On the evaluation of acoustic fields in waveguides with statistically rough surface // In: Mathematical Problems of Geophysics (Nauka, Novosibirsk, 1973), vol. 4, pp. 256–272 [in Russian].

19. *Kryazhev F. I., Kudryashov B. M., and Petrov N. A.*, Propagation of low–frequency sound waves in a waveguide with irregular boundaries // Sov. Phys. Acoust., 1976, vol. 22(3), pp. 21–24.

20. *Kohler W. E. and Papanicolaou G. C.*, Wave propagation in a random–inhomogeneous ocean // In: Lecture Notes in Physics, vol. 70. Wave Propagation and Underwater Acoustics, edited by J. B. Keller and J. S. Papadakis (Springer–Verlag, Berlin, 1977), pp. 153–223.

21. *Dozier L. B. and Tappert F. D.*, Statistics of normal–mode amplitudes in a random ocean. I. Theory, and II. Computations // J. Acoust. Soc. Am., 1978, vol. 63(2), pp. 353–365 and 1978, vol. 64(2), pp. 533–547.

22. *Beilis A. and Tappert F. D.*, Coupled mode analysis of multiple rough surface // Ibid., 1979, vol. 66(3), pp. 811–826.

23. *Sutton G. R. and McCoy J. J.*, Spatial coherence of acoustic signals in randomly inhomogeneous waveguides — a multiple-scatter theory // J. Math. Phys., 1977, vol. 18(12), pp. 1052–1057.

24. *Sutton G. R.*, Application of a stochastic waveguide propagation model to ocean acoustics // J. Math. Phys., 1981, vol. 22(12), pp. 974–976.

25. *Dolin L. S. and Nechaev A. G.*, Mode description of the acoustic field interference structure in a waveguide with statistically rough wall // Izv. VUZov, Radiofizika, 1981, vol. 24(11), pp. 1337–1344 [in Russian].

26. *Moiseev A. A.*, On the evaluation of field coherence function in a randomly inhomogeneous waveguide // Dokl. Akad. Nauk SSSR, 1984, vol. 279(6), pp. 1339–1344 [in Russian].

27. *Sazontov A. G. and Farfel' V. A.*, On the calculation of low-frequency sound attenuation in the ocean due to scattering by internal waves // Akust. Zhur., 1986, vol. 32(4), pp. 492–498 [in Russian].

28. *Artel'nyi V. V., Kukushkin V. D., and Raevskii M. A.*, On the energy and correlation characteristics of low-frequency acoustic waves in underwater sound channels // Ibid., pp. 591–597 [in Russian].

29. *Nechaev A. G.*, Decay of the interference structure of the sound field in an ocean with random inhomogeneities // Sov. Phys. Acoust., 1987, vol. 33(3), pp. 312–314.

30. *Virovlyansky A. L., Kostern A. G., and Malakhov A. N.*, Modal fluctuations in a canonical underwater sound channel // Akust. Zhur., 1989, vol. 35(2), pp. 229–236 [in Russian].

31. *Beran M. J. and Frankenthal S.*, Volume scattering in a shallow channel // J. Acoust. Soc. Am., 1992, vol. 91(6), pp. 3203–3211.

32. *Sazontov A. G.*, Calculation of the two-frequency coherence function of the field and the temporal integral characteristics of a pulse signal in a randomly inhomogeneous ocean // Sov. Phys. Acoust., 1989, vol. 35(5), pp. 526–531.

33. *Landau L. D. and Lifshitz E. M.*, Theoretical Physics. Vol. III. Quantum Mechanics (Nauka, Moscow, 1989) [in Russian].

34. *Migdal A. B.*, Qualitative Methods in Quantum Theory (Nauka, Moscow, 1975) [in Russian].

35. *Garrett C. and Munk W. H.*, Space-time scales of internal waves: A progress report // J. Geophys. Res., 1975, vol. 80(3), pp. 291–297.

36. *Esswein R. and Flatte S. M.*, Calculation of the phase-structure function density from oceanic waves // J. Acoust. Soc. Am., 1981, vol. 70(5), pp. 1387–1396.

37. *Sazontov A. G. and Farfel' V. A.*, Calculation of the degree of coherence and form of a pulse sound signal in an oceanic waveguide with a rough surface // Acoust. Phys., 1995, vol. 41(1), pp. 109–113.

38. *Pierson W. J. and Moskowitz L.*, A proposed spectral form for fully developed wind seas based on the similarity theory of S. A. Kitaigorodskii // J. Geophys. Res., 1964, vol. 69(24), pp. 5181–5190.

39. *Shirman Ya. D. and Manzhos V. N.*, Theory and Techniques of Signal Processing in Radar (Radio i Svyaz', Moscow, 1981) [in Russian].

40. *Monzingo R. A. and Miller T. W.*, Introduction to Adaptive Arrays (Wiley, New York, 1980).

41. *Bucker H. P.*, Use of calculated sound fields and matched-field detection to locate sound in shallow water // J. Acoust. Soc. Am., 1976, vol. 59(1), pp. 368–373.

42. *Tolstoy A.*, Matched Field Processing for Underwater Acoustics (World Scientific, Singapore, 1993).

43. *Sullivan E. J.* (Editor), Special Issue on Matched Field Processing // IEEE J. Ocean Eng. (November 1993).

44. *Zuikova N. V. and Svet V. D.*, Matched-field processing of signals in ocean waveguides (review) // Akust. Zhur., 1993, vol. 39(3), pp. 389–403 [in Russian].

45. *Il'ichev V. I., Kalyuzhnyi A. Ya., Krasnyi L. G., and Lapii V. Yu.*, Statistical Theory of Hydroacoustic Signal Detection (Nauka, Moscow, 1992) [in Russian].

46. *Shifrin Ya. S.*, Problems of Statistical Array Theory (Sovetskoje Radio, Moscow, 1970) [in Russian].

47. *Uscinski B. J. and Reeve D. E.*, The effect of ocean inhomogeneities on array output // J. Acoust. Soc. Am., 1990, vol. 87(6), pp. 2527–2534.

48. *Sazontov A. G. and Farfel' V. A.*, Operation of a horizontal discrete array in a randomly inhomogeneous ocean // Sov. Phys. Acoust., 1990, vol. 36(1), pp. 71–74.

49. *Gorodetskaya E. Yu., Malekhanov A. I., and Talanov V. I.*, Modeling of the optimal array signal processing in underwater sound channels // Sov. Phys. Acoust., 1992, vol. 38(6), pp. 571–575.

50. *Gorodetskaya E. Yu. and Malekhanov A. I.*, The theoretical gain limitations of array signal processing in underwater sound channels // Proc. 2nd Europ. Conf. on Underwater Acoustics, edited by L. Bjørno (Luxemburg, 1994), pp. 665–670.

51. *Knapp C. H.*, Signal detectors for deformable hydrophone arrays // IEEE Trans. ASSP, 1989, vol. 37(1), pp. 1–7.

52. *Malekhanov A. I. and Talanov V. I.*, Optimal signal reception in multimode waveguides // Sov. Phys. Acoust., 1990, vol. 36(5), pp. 496–499.

53. *Kuperman W. A. and Ingenito F.*, Spatial correlation of surface generated noise in a stratified ocean // J. Acoust. Soc. Am., 1980, vol. 67(6), pp. 1988–1996.

54. *Malekhanov A. I.*, Incoherent spatial mode filtering in randomly inhomogeneous ocean waveguides // Sov. Phys. Acoust., 1992, vol. 38(5), pp. 489–493.

55. *Artel'nyi V. V. et al*, Statistical model of low–frequency acoustic field in surface waveguides in deep sea // In: The Formation of Acoustic Fields in Oceanic Waveguides, edited by V. A. Zverev (IAP RAS, Nizhny Novgorog, 1991), pp. 149–173 [in Russian].

56. *Stefanick T.*, Strategic Antisubmarine Warfare and Naval Strategy (Institute for Defence & Disarmament Studies, Lexington Books, Massachusetts/Toronto, 1987).

DIFFRACTION OF ACOUSTIC WAVES BY AN OBJECT IN A RANDOM OCEANIC WAVEGUIDE

A. I. Khilko, A. G. Sazontov, and N. K. Vdovicheva

Introduction

A problem of interest in underwater acoustics is the multimode diffraction of acoustic waves in oceanic waveguides. Most of the previous works examining this problem have been carried out under the basic assumption that the multimode signal is the coherent superposition of normal modes [1–5]. In real channels, however, in addition to deterministic background environments there are random inhomogeneities that can change significantly the transmission of acoustic fields in waveguides. Thus, a combination of the effects of regular refraction and multiple scattering is the basic factor determining the potentialities of underwater acoustic systems whose purpose is the diagnostic of scatterers in the ocean. [1]

The aim of this paper is to develop wave–theoretical expressions for energy and correlation characteristics of an acoustic field scattered by an object in a random oceanic waveguide, that allow for simple physical interpretations. A derivation of the quantities of interest is given for the case of both source and receiver far from the target. The method presented is based on the combined use of the Kirchhoff diffraction model and the radiation transport equation governing the evolution of the mutual coherence function (MCF) for multimode propagation. The major approximation made is the neglect of multiple scattering from an object.

The body of this article is organized as follows. The Kirchhoff formulation of the diffraction problem is briefly discussed in Sec. 1. Section 2 derives the mutual coherence function (MCF) of a cw signal scattered by an object. Next, Sec. 3 addresses the effects of stochastic waveguide propagation on the target strength. In Sec. 4 some numerical examples are given. Finally, Sec. 5 summarizes the key results of this work.

1. Problem formulation

Consider an underwater sound channel of depth H, in which the refractive index is the sum of the deterministic background profile $n_0(z)$ depending on vertical coordinate z and the stochastic field $\mu(\mathrm{r}, z, t)$ modeling

[1] In the absence of regular refraction, the influence of large scale medium fluctuations on the diffraction process has been analyzed in Ref. [6].

the acoustic medium fluctuations, where $\mathbf{r} = (x, y)$ is the horizontal two-dimensional position vector and t is the time. (The coordinate system is chosen with the z-axis downwards.) The perturbation μ is assumed to be Gaussian random variable with zero mean, and can be described by its autocorrelation function

$$<\mu(\mathbf{r}_1, z_1, t_1)\,\mu(\mathbf{r}_2, z_2, t_2)>= B_\mu(|\mathbf{r}_1 - \mathbf{r}_2|, z_1, z_2, t_1 - t_2).$$

The angular brackets $< \cdots >$ indicate ensemble averaging. In the subsequent analysis we shall assume that the scale of oceanic inhomogeneities is much greater than acoustic wavelength and the characteristic frequencies of B_μ are small compared with a carrier frequency of sound field.

Let a nondirectional source with acoustic power W be located at coordinates $(\mathbf{r}_0, z_0)$ and emit a CW signal of the carrier frequency ω_0. This signal passed trough a random oceanic channel is scattered by an object. The coordinates of the body center are $(0, z_s)$. The geometry of the problem is shown in Fig. 1.

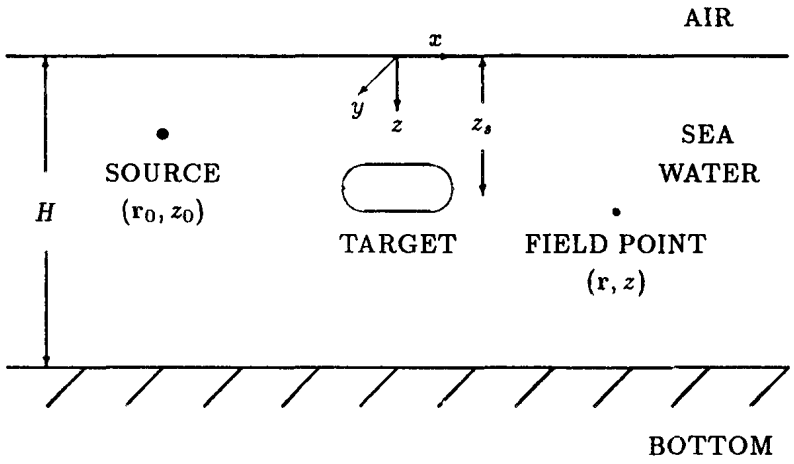

Fig. 1. The geometry of the problem showing deep-water channel of depth H containing source, target, and the coordinate system

As a result of scattering for the total acoustic pressure field $P(\mathbf{r}, z)$ we get

$$P(\mathbf{r}, z) = P_i(\mathbf{r}, z) + P_d(\mathbf{r}, z),$$

where $P_i(\mathbf{r}, z)$ is the incident field and $P_d(\mathbf{r}, z)$ is the diffracted field produced by the object.

It is well known that an exact investigation of diffraction processes is faced with essential mathematical difficulties. A considerable simplification in theoretical study of acoustic scattering from a target in oceanic waveguide occurs when multiple scattering effects between the target and boundaries may be neglected in order to avoid problems with evaluating the medium Green's function in the near field. This assumption is valid as long as the scatterer is sufficiently far from the water surface (see, e.g. [7, 8]). If, in addition to neglecting multiple scattering, the characteristic target sizes are large compared to the wavelength, then the diffracted wavefield may be derived from the Kirchhoff integral:

$$P_d(\mathbf{R}) = \iint\limits_{S_s} \left[P_d(\mathbf{R}_s) \frac{\partial}{\partial n_s} G(\mathbf{R},\mathbf{R}_s) - G(\mathbf{R},\mathbf{R}_s) \frac{\partial}{\partial n_s} P_d(\mathbf{R}_s) \right] dA_s, \qquad (1)$$

where $\mathbf{R} = (\mathrm{r}, z)$, dA_s is the area element, S_s is the surface of the scatterer, n_s is the outward normal to S_s, and $G(\mathbf{R},\mathbf{R}')$ is the medium Green's function which satisfies the Helmholtz equation together with appropriate boundary conditions at the ocean surface and bottom (but does not satisfy the boundary condition on the object's surface).

For concrete analysis we assume that the scattering object is acoustically rigid, and hence

$$\frac{\partial P_i(\mathbf{R}_s)}{\partial n_s} = -\frac{\partial P_d(\mathbf{R}_s)}{\partial n_s}, \qquad \mathbf{R}_s \in S_s. \qquad (2)$$

We will be interested in the behavior of the field scattered in the forward direction. In this case the integration in (1) can be extended only over the plane restricted by the shadow-forming line. Then, in the Kirchhoff approximation letting

$$P_d(\mathbf{R}_s) = \begin{cases} -P_i(\mathbf{R}_s), & \mathbf{R}_s \in S_s; \\ 0, & \mathbf{R}_s \notin S_s, \end{cases}$$

and using (2), for $P_d(\mathbf{R})$ we obtain

$$P_d(\mathbf{R}) = \iint\limits_{S} \left[G(\mathbf{R},\mathbf{R}'_s) \frac{\partial P_i(\mathbf{R}'_s)}{\partial n_s} - P_i(\mathbf{R}'_s) \frac{\partial G(\mathbf{R},\mathbf{R}'_s)}{\partial n_s} \right] d^2\mathbf{R}'_{\perp s}, \qquad (3)$$

where the integral is taken over the shadow-forming plane S.

In the farfield, the quantities $\partial P_i(\mathbf{R}_s)/\partial n_s$ and $\partial G(\mathbf{R},\mathbf{R}_s)/\partial n_s$ appearing in (3) can be approximated by

$$\frac{\partial P_i(\mathbf{R}_s)}{\partial n_s} \approx ik \cos\alpha_s \, P_i(\mathbf{R}_s), \qquad \frac{\partial G(\mathbf{R},\mathbf{R}_s)}{\partial n_s} \approx -ik \cos\alpha_s \, G(\mathbf{R},\mathbf{R}_s),$$

where α_i and α_s are the angle of incidence and the scattering angle, respectively, measured from the normal to the scattering plane, and $k = 2\pi/\lambda$ is some reference wavenumber. In the present treatment we shall be concerned only with the case $\alpha_i = \alpha_s$, $\alpha_s \ll 1$. Making this simplification and introducing the function

$$E(\mathbf{R}_{\perp s}) = \begin{cases} 1, & \mathbf{R}_{\perp s} \in S; \\ 0, & \mathbf{R}_{\perp s} \notin S, \end{cases}$$

from (3) we find

$$P_d(\mathbf{R}) = 2ik \int\int_{-\infty}^{\infty} E(\mathbf{R}'_{\perp s}) P_i(\mathbf{R}'_s) G(\mathbf{R},\mathbf{R}'_s)\, d\mathbf{R}'_{\perp s}. \qquad (4)$$

Equation (4) is the starting equation for the subsequent statistical analysis.

2. MCF of diffracted signal

The two-dimensional integral (4) contains the product of two random fields $P_i(\mathbf{R}_s)$ and $G(\mathbf{R}_s, \mathbf{R})$ describing the stochastic waveguide propagation between source and target, and target and receiver, respectively. Since we have already used the fact of forward scattering, the corresponding fields are statistically independent. This circumstance simplifies significantly the problem of finding a result for the coherence function of the diffracted field reducing it to the evaluation of the direct wavefield correlation characteristics over source–target and target–receiver distances. Taking it into account, for the spatial MCF of the diffracted signal defined as $\Gamma_d(\mathbf{R}_1, \mathbf{R}_2) = < P_d(\mathbf{R}_1)\, P_d^*(\mathbf{R}_2) >$ from Eq. (4) we get:

$$\Gamma_d(\mathbf{R}_1,\mathbf{R}_2) = 4k^2 \int\int_{-\infty}^{\infty} d\mathbf{R}'_{\perp s} E(\mathbf{R}'_{\perp s}) \times$$

$$\times \int\int_{-\infty}^{\infty} d\mathbf{R}''_{\perp s} E(\mathbf{R}''_{\perp s}) \Gamma_i(\mathbf{R}'_s,\mathbf{R}''_s)\, \Gamma_s(\mathbf{R}_1,\mathbf{R}_2|\mathbf{R}'_s,\mathbf{R}''_s), \qquad (5)$$

where

$$\Gamma_i(\mathbf{R}'_s,\mathbf{R}''_s) = < P_i(\mathbf{R}'_s)\, P_i^*(\mathbf{R}''_s) > \qquad (6)$$

is the MCF of the incident field, the asterisk denotes complex conjugate, and

$$\Gamma_s(\mathbf{R}_1,\mathbf{R}_2|\mathbf{R}'_s,\mathbf{R}''_s) = < G(\mathbf{R}_1,\mathbf{R}'_s)\, G^*(\mathbf{R}_2,\mathbf{R}''_s) > \qquad (7)$$

has the sense of the MCF generated by secondary sources placed on the surface of the scatterer and registered at two different position points in the plane of observation. Note, that the incident field $P_i(\mathbf{R}_s)$ can be expressed in terms of Green's function as follows

$$P_i(\mathbf{R}_s) = \sqrt{8\pi\rho_w c(z_0)W}\, G(\mathbf{R}_s,\mathbf{R}_0), \tag{8}$$

where ρ_w is the density of water, $c(z_0)$ is the speed of sound taken at the source depth. Hence, in order to calculate (5), it suffices to evaluate the second moment of the random Green's function (7).

2.1. Second–order statistics of the medium Green's function

The medium Green's function $G(\mathrm{R},\mathrm{R}')$ in an irregular oceanic waveguide can be formally represented by

$$G(\mathrm{R},\mathrm{R}') = \sum_{n,m}^{\mathrm{M}} \frac{1}{\sqrt{\kappa_n \kappa_m}}\, g_{nm}(\mathrm{r},\mathrm{r}')\, \varphi_n(z)\varphi_m(z'), \tag{9}$$

where, $\varphi_n(z)$ is the n-th vertical eigenfunction of a regular channel associated with the eigenvalue κ_n^2, M is the number of propagating modes, and $g_{nm}(\mathrm{r},\mathrm{r}')$ are the random expansion coefficients. In writing (9) we ignored the farfield contribution from the modes of continuous spectrum. The normal mode functions $\varphi_n(z)$ satisfy the eigenvalue problem

$$\frac{d^2}{dz^2}\,\varphi_n(z) + \left[k^2 n_0^2(z) - \kappa_n^2\right]\,\varphi_n(z) = 0, \quad n = 1, 2, \ldots, \mathrm{M} \tag{10}$$

together with appropriate boundary conditions and an orthonormality relation, i. e., $\int_0^{\mathrm{H}} dz\, \varphi_n(z)\varphi_m(z) = \delta_{nm}$. Here, H is the ocean depth, $n_0(z)$ is the regular part of the refractive index, and $k = \omega/c_0$, where c_0 is some reference sound speed.

In the case of large–scale (compared to the wavelength) medium inhomogeneities, when multiple scattering angles are small, the equation governing the change of $g_{nm}(\mathrm{r},\mathrm{r}')$ as a result of the scattering can be derived from the original Helmholtz equation, and in the parabolic approximation has the form:

$$\left(\frac{\partial}{\partial x} - i\kappa_n - \frac{i}{2\kappa_n}\,\frac{\partial^2}{\partial y^2}\right) g_{nm}(\mathrm{r},\mathrm{r}') = i\sum_{n'}^{\mathrm{M}} V_{nn'}(\mathrm{r},t)\, g_{n'm}(\mathrm{r},\mathrm{r}'), \tag{11}$$

where x-axis is taken in the main direction of wave propagation, $V_{nn'}(\mathbf{r},t)$ is the matrix coupling coefficient (depending on t as a parameter) defined according to [9]

$$V_{nn'}(\mathbf{r},t)=\frac{k^2}{\sqrt{\kappa_n\kappa_{n'}}}\int_0^H n_0(z)\,\mu(\mathbf{r},z,t)\varphi_n(z)\varphi_{n'}(z)\,dz. \tag{12}$$

With the use of Eq. (9), for the second moment (7) one finds:

$$\Gamma_s(\mathbf{R}_1,\mathbf{R}_2|\mathbf{R}',\mathbf{R}'')=\sum_{n,\nu}\sum_{m,\lambda} g_{n\nu}^{m\lambda}(\mathbf{r}_1,\mathbf{r}_2|\mathbf{r}',\mathbf{r}'')\,\frac{\varphi_n(z_1)\varphi_m(z_2)\varphi_\nu(z')\varphi_\lambda(z'')}{\sqrt{\kappa_n\kappa_m\kappa_\nu\kappa_\lambda}};$$
$$< g_{n\nu}^{m\lambda}(1,2|1',2')>=<g_{n\nu}(1,1')\,g_{m\lambda}^{*}(2,2')>, \tag{13}$$

where the labels 1, 2 and 1', 2' refer to two different horizontal position points $\mathbf{r}_1$, $\mathbf{r}_2$ and $\mathbf{r}'$, $\mathbf{r}''$, respectively.

In Refs. [10, 11] the basic transport equation for the matrix $g_{n\nu}^{m\lambda}(1,2|1',2')$ taken at two couples of the horizontal position points $\mathbf{r}_1=(x,y_1)$, $\mathbf{r}_2=(x,y_2)$, and $\mathbf{r}'=(x',y')$, $\mathbf{r}''=(x',y'')$ in the planes $x=\text{const}$ and $x'=\text{const}$ has been derived from (11) under the forward–scattering approximation:

$$\left[\frac{\partial}{\partial x}-i\kappa_{nm}^{-}-i\xi_{nm}^{+}\frac{\partial^2}{\partial\rho\partial R}-\frac{i}{2}\xi_{nm}^{-}\left(\frac{\partial^2}{\partial\rho^2}+\frac{1}{4}\frac{\partial^2}{\partial R^2}\right)\right] g_{n\nu}^{m\lambda}=$$
$$=-\frac{1}{2}\left[\sum_{n'}A_{nn'}(1,1)\,g_{n\nu}^{m\lambda}+\sum_{m'}A_{m'm}(2,2)\,g_{n\nu}^{m'\lambda}\right]+\sum_{n',m'}A_{nn'}^{mm'}(1,2)\,g_{n'\nu}^{m'\lambda}; \tag{14}$$

$$g_{n\nu}^{m\lambda}(1,2|1',2')\big|_{x=x'}=\frac{1}{4}\,\delta_{n\nu}\,\delta_{m\lambda}\,\delta(\rho-\rho')\,\delta(R-R').$$

In writing (14) the following notation is used:
$\rho=y_1-y_2$, $R=0.5(y_1+y_2)$, $\rho'=y'-y''$, $R'=0.5(y'+y'')$, $\kappa_{nm}^{-}=\kappa_n-\kappa_m$, $\xi_{nm}^{+}=0.5\left(\kappa_n^{-1}+\kappa_m^{-1}\right)$, $\xi_{nm}^{-}=\kappa_n^{-1}-\kappa_m^{-1}$, $A_{nn'}(1,1)=\sum_{m'}A_{nm'}^{nm'}(1,1)$, and the coupling matrix $A_{nn'}^{mm'}(1,2)$ is given by

$$A_{nn'}^{mm'}(1,2)=\int_{-\infty}^{\infty}d\eta\,B_{nn'}^{mm'}(\eta,\rho)\,e^{\,i\left(\kappa_{nm}^{+}-\kappa_{n'm'}^{+}\right)\eta},$$

$$B_{nn'}^{mm'}(\eta,\rho)=<V_{nn'}(x+\frac{1}{2}\eta,R+\frac{1}{2}\rho)V_{mm'}(x-\frac{1}{2}\eta,R-\frac{1}{2}\rho)>,$$

where $V_{nm}(\mathrm{r},t)$ is determined from Eq. (12) and $\kappa_{nm}^{+}=0.5\,(\kappa_n+\kappa_m)$.

A detailed analysis of coupled integrodifferential equations (14) is presented in Refs. [10, 11]. In what follows we employ the results obtained for the problem of interest. Under weak restrictions on the theory (specified in [10, 11]) the corresponding Green's matrix can be found analytically and has the form:

$$g_{n\nu}^{m\lambda}(1,2|1',2')=g_{\nu\lambda}^{0}(1,2|1',2')\,h_{n\nu}^{m\lambda}(1,2|1',2')e^{\,i(\kappa_n-\kappa_m)x-i(\kappa_\nu-\kappa_\lambda)x'}, \tag{15}$$

where

$$g_{\nu\lambda}^{0}(1,2|1',2')=\frac{u_\nu(1,1')u_\lambda^{*}(2,2')}{8\pi\xi_{\nu\lambda}^{+}(x-x')},\quad u_\nu(\mathrm{r}_1,\mathrm{r}_2)=\exp\left[i\kappa_\nu\frac{(y_1-y_2)^2}{2(x_1-x_2)}\right]$$

has the nature of a Green's function of the radiation transport equation in the absence of fluctuations and the matrix $h_{n\nu}^{m\lambda}(1,2|1',2')$ describing the influence of random oceanic inhomogeneities is given by

$$h_{n\nu}^{m\lambda}(1,2|1',2')=\frac{1}{(2\pi)^2}\int_0^{2\pi}\!\!\int d\alpha\,d\beta\,e^{-i(n-\nu)\alpha+i(m-\lambda)\beta-\frac{1}{2}D_{\nu\lambda}^{\alpha\beta}(1,2|1',2')}$$

with

$$D_{\nu\lambda}^{\alpha\beta}(1,2|1',2')=\int_{x'}^{x}d\xi\left[d_{\nu\nu}^{\alpha\alpha}(1,1|1',1';\xi)+d_{\lambda\lambda}^{\beta\beta}(2,2|2',2';\xi)-2d_{\nu\lambda}^{\alpha\beta}(1,2|1',2';\xi)\right]; \tag{16}$$

$$d_{\nu\lambda}^{\alpha\beta}(1,2|1',2';\xi)=2\pi k^2\int_{-\infty}^{\infty}\!\!\int\frac{d\text{æ}_y\,d\text{æ}_z\,\Phi_\mu\left(\text{æ}_{\nu\lambda}(\xi),z_{\nu\lambda}^{\alpha\beta}(\xi)\right)}{\cos\chi_\nu(\xi)\cos\chi_\lambda(\xi)}\times$$

$$\times\cos\left[\text{æ}_y\left(\rho\,\frac{\xi-x'}{x-x'}+\rho'\,\frac{x-\xi}{x-x'}\right)\right]\cos\left(\text{æ}_z\varsigma_{\nu\lambda}^{\alpha\beta}(\xi)\right).$$

In (16) the following notation is used: $\Phi_\mu(\text{æ},z)$ is the local spatial spectrum of the sound-speed fluctuations taken at $\text{æ}=\text{æ}_{\nu\lambda}^{\alpha\beta}(x)$, where the wavenumber $\text{æ}_{\nu\lambda}^{\alpha\beta}(x)$ has components

$$\text{æ}_{\nu\lambda}^{\alpha\beta}(x)=\left(-0.5\big(\mathrm{tg}\,\chi_\nu^{\alpha}(x)+\mathrm{tg}\,\chi_\lambda^{\beta}(x)\big)\text{æ}_z,\text{æ}_y,\text{æ}_z\right),$$

and $\chi_\nu^{\alpha}(x)$ is the angle the modal ray makes with the horizontal at the point x; $\mathrm{tg}\,\chi_\nu^{\alpha}(x)=dz_\nu^{\alpha}(x)/dx$ is the inclination of a modal ray with the

path $z_\nu^\alpha(x) \equiv z_\nu(x - \alpha\Lambda_\nu/2\pi)$ and the cycle distance Λ_n, where $z_\nu(x)$ obeys the equation

$$\frac{d^2 z_n(x)}{dx^2} = \frac{1}{2a_n}\frac{d}{dz}n_0^2[z_n(x)], \quad a_n = \frac{\kappa_n}{k},$$

$z_{\nu\lambda}^{\alpha\beta}(x) = 0.5\big(z_\nu^\alpha(x) + z_\lambda^\beta(x)\big)$; $\varsigma_{\nu\lambda}^{\alpha\beta}(x) = z_\nu^\alpha(x) - z_\lambda^\beta(x)$. The expression for $D_{\nu\lambda}^{\alpha\beta}(1,2)$, Eq. (16), is immediately recognized as the phase–structure function [13] with the only difference that the integral in (16) is taken along modal ray instead of usual geometric ray. Note also, that the combination $d_{\nu\nu}^{\alpha\alpha}(x,1|x',1) + d_{\lambda\lambda}^{\beta\beta}(x,2|x',2) - 2d_{\nu\lambda}^{\alpha\beta}(x,1|x',2)$ can be regarded as a density of the phase–structure function.

The knowledge of the matrix Green's function $g_{n\nu}^{m\lambda}(1,2|1',2')$ allows one to evaluate both the energy and correlation characteristics of the acoustic field produced by the sources of different types. In particular, for the MCF of the incident field, Eq. (6), from Eqs. (8), (15) it is easy to find

$$\Gamma_i(\mathbf{R}_s',\mathbf{R}_s'') = 8\pi\rho_w c(z_0) W \sum_{n,\,n'} \Gamma_{nn'}^i(\mathbf{r}_s',\mathbf{r}_s'')\, J_{nn'}(x_0)\varphi_n(z_s')\varphi_{n'}(z_s''), \quad (17)$$

$$\Gamma_{nn'}^i(\mathbf{r}_s',\mathbf{r}_s'') = \sum_{\nu,\,\nu'} u_\nu(\mathbf{r}_s',\mathbf{r}_0)u_{\nu'}^*(\mathbf{r}_s'',\mathbf{r}_0)h_{n\nu}^{n'\nu'}(\mathbf{r}_s',\mathbf{r}_s''|\mathbf{r}_0,\mathbf{r}_0)\varphi_\nu(z_0)\varphi_{\nu'}(z_0),$$

where

$$J_{nm}(x) = \frac{1}{8\pi\sqrt{\kappa_n\kappa_m}\,x}\exp\Big[i(\kappa_n - \kappa_m)x\Big].$$

With the aid of the expressions (13), (15)–(17) the MCF of the diffracted signal, Eq. (5), can be written in the form [12]:

$$\Gamma_d(\mathbf{R}_1,\mathbf{R}_2) = 8\pi\rho_w c(z_0) W \sum_{m,\,m'} \Gamma_{nm'}^d(\mathbf{r}_1,\mathbf{r}_2)\, J_{mm'}(x)\varphi_m(z_1)\varphi_{m'}(z_2). \quad (18)$$

Here

$$\Gamma_{nm'}^d(\mathbf{r}_1,\mathbf{r}_2) = \sum_{n,\,n'} S_{nn'}^{mm'}(\mathbf{r}_1,\mathbf{r}_2) J_{nn'}(x_0)\varphi_n(z_0)\varphi_{n'}(z_0), \quad (19)$$

with

$$S_{nn'}^{mm'}(\mathbf{r}_1,\mathbf{r}_2) = 4k^2 \sum_{\nu,\,\nu'}\sum_{\lambda,\,\lambda'} \int_{-\infty}^{\infty} dy_s'\, t_{\nu\lambda}(y_s')u_\nu(\mathbf{r}_s',\mathbf{r}_0)u_\lambda(\mathbf{r}_1,\mathbf{r}_s')\times$$

$$\times \int_{-\infty}^{\infty} dy_s''\, t_{\nu'\lambda'}^*(y_s'')u_{\nu'}^*(\mathbf{r}_s'',\mathbf{r}_0)u_{\lambda'}^*(\mathbf{r}_2,\mathbf{r}_s'')\, h_{\nu n}^{\nu' n'}(\mathbf{r}_s',\mathbf{r}_s''|\mathbf{r}_0,\mathbf{r}_0)h_{m\lambda}^{m'\lambda'}(\mathbf{r}_1,\mathbf{r}_2|\mathbf{r}_s',\mathbf{r}_s''), \quad (20)$$

where

$$t_{\nu\lambda}(y) = \int_{-\infty}^{\infty} dz'_s\, E(y, z'_s)\, \varphi_\nu(z'_s)\varphi_\lambda(z'_s).$$

Equations (18)–(20) constitute our central results. They give explicit rules for calculating both the correlation function and the wavefield intensity of the acoustic field scattered by an object in a random oceanic waveguide.

As it seen from Eqs. (18)–(20), the scatterer can be regarded as a redistributer of the modal content of an incident acoustic signal: each pair of modes n and n' of the primary field transforms their energy into diffracted modes m and m', and the strength of the interaction is determined by the matrix function $S_{nn'}^{mm'}$. It should be emphasized that the quantity $S_{nn'}^{mm'}$ contains a complete information about the refractive and reflective properties of a random oceanic waveguide and an object within the channel. Thus, the problem of finding an useful result for the MCF of the diffracted signal now reduces to evaluating the two-point correlation matrix $S_{nn'}^{mm'}(\mathbf{r}_1,\mathbf{r}_2)$.

2.2. Analysis of limiting cases

For an unspecified object, the integrals over y'_s and y''_s in (20) may be estimated in two limiting cases: for small and large sizes of the scatterer in comparison with the corresponding spatial correlation lengths of the incident and diffracted fields.

Consider first the case when the characteristic horizontal size of the scatterer, l_h, is much smaller than the characteristic scales of the variation of the functions $h_{\nu n}^{\nu' n'}(\cdot|\cdot)$ and $h_{m\lambda}^{m'\lambda'}(\cdot|\cdot)$ versus $\rho' = y'_s - y''_s$. In the system of interest, we can regard the corresponding structure functions describing the coherence loss of incident and scattered signals to be almost constant inside the shadow-forming plane in the region that is critical for integration over y'_s and y''_s. Consequently, we have

$$S_{nn'}^{mm'}(\mathbf{r}_1,\mathbf{r}_2) = 4k^2 \sum_{\nu,\,\lambda} \sum_{\nu',\,\lambda'} f_{\nu\lambda}(\mathbf{r}_1,\mathbf{r}_0)\, f^*_{\nu'\lambda'}(\mathbf{r}_2,\mathbf{r}_0) \times$$

$$\times\, h_{\nu n}^{\nu' n'}(0,0|\mathbf{r}_0,\mathbf{r}_0)\, h_{m\lambda}^{m'\lambda'}(\mathbf{r}_1,\mathbf{r}_2|0,0), \qquad (21)$$

where

$$f_{\nu\lambda}(\mathbf{r}_1,\mathbf{r}_2) = \int_{-\infty}^{\infty}\!\!\int dy'_s\, dz'_s\, E(y_s, z_s) u_\nu(\mathbf{r}_1,\mathbf{r}') u_\lambda(\mathbf{r}',\mathbf{r}_2)\, \varphi_\nu(z'_s)\varphi_\lambda(z'_s).$$

Physically, the quantity $f_{\nu\lambda}$ is a matrix amplitude of scattering that describes the regular diffraction field of the λ-th mode behind the object at normal incidence of the ν-th mode. In the case considered the effects of deterministic multimodal diffraction have been isolated in the first two factors, and the effects of the medium fluctuations in the last two.

As follows from (21), the correlation function of the diffracted field in the horizontal plane does not depend on the degree of spatial coherence of incident radiation. Instead, it is determined completely by the scattering properties of the propagation medium from the body to the plane of observation. This means that a random wave diffracted at a small body produces on it a spatially coherent field of secondary sources. The latter circumstance is well known from the general statistical theory of diffraction (see, e.g., [14]).

Consider now the second limiting case, when the horizontal size of the scatterer is much larger than the corresponding correlation length of incident and diffracted fields. For approximate calculation of the integral (20) we make a transformation to new variables $\rho' = y_s' - y_s''$ and $R' = (y_s' + y_s'')/2$ and designate the half-sum $(y_1 + y_2)/2$ through R and the difference $y_1 - y_2$ through ρ. It is not difficult to show that the main contribution to the double integral in (20) comes from the region when $|y_s' - y_s''| \ll l_h$. Therefore, the integration over ρ' may be extended to infinity without negligible error, and the function $E(R' \pm \rho'/2, z)$ may be replaced by $E(R', z)$. These give

$$S_{nn'}^{mm'}(\mathbf{r}_1,\mathbf{r}_2) = 4k^2 \sum_{\nu,\lambda}\sum_{\nu',\lambda'} e^{i\left(\frac{\kappa_{\lambda\lambda'}^{+} R\rho}{x}\right)} \int_{-\infty}^{\infty} dR' t_{\nu\lambda}(R') t_{\nu'\lambda'}(R') e^{-i\left(\frac{\kappa_{\lambda\lambda'}^{+} R'\rho}{x}\right)} \times$$

$$\times \int_{-\infty}^{\infty} d\rho'\, h_{\nu n}^{\nu' n'}(0,\rho'|x_0,0) h_{m\lambda}^{m'\lambda'}(x,\rho|0,\rho') \exp\left[-i\rho'\left(\frac{\kappa_{\lambda\lambda'}^{+} R}{x} + \frac{\kappa_{\nu\nu'}^{+} y_0}{|x_0|}\right)\right]. \tag{22}$$

The correlation matrix (22) as a function of transverse coordinate ρ has two characteristic scales. The first of them is associated with the finite length of spatial field coherence at the target–receiver distance and depends on the specific features of the function $h_{n\lambda}^{m'\lambda'}(x,\rho|0,\rho')$. The second one is determined by the characteristic width of the diffraction pattern of a multimode signal described by the integral over R' in (22). It is noteworthy that the field correlation length in a randomly inhomogeneous medium is a diminishing function of the distance passed by the wave, while the width of the diffraction lobe increases with increasing distance from the object. Therefore, the role of the effects of multiple scattering by medium fluctuations is

dominating in formation of the coherence function of a diffracted signal at long acoustic distances.

We have analyzed above the asymptotic behavior of the two-point matrix $S^{mm'}_{nn'}(\mathrm{r}_1,\mathrm{r}_2)$ determining the correlation properties of the registered field along the horizontal plane. As follows from (18), the behavior of the coherence function in the vertical plane depends on both the regular mode structure of the acoustic signal and the statistical propagation effects that lead to the decay of cross-modal correlation functions $\Gamma^d_{mm'}$ for $m \neq m'$ and to equipartition of energy among all mode intensities Γ^d_{mm}, similarly to the direct signals in multimode randomly inhomogeneous waveguides (see, e.g., [15, 16]).

3. Target strength of an object in a random oceanic waveguide

The total mean intensity of the diffracted field at the observation point is given by

$$I_d(\mathbf{R}) = < |P_d(\mathbf{R})|^2 > \equiv \Gamma_d(\mathbf{R},\mathbf{R}).$$

Setting $\mathbf{R}_1 = \mathbf{R}_2 = \mathbf{R}$ in Eq. (18), for $I_d(\mathbf{R})$ we get:

$$I_d(\mathbf{R}) = 8\pi\rho_w c(z_0) W \sum_{m,\,m'} \Gamma^d_{mm'}(\mathrm{r},\mathrm{r})\, J_{mm'}(x)\varphi_m(z)\varphi_{m'}(z); \qquad (23)$$

$$\Gamma^d_{mm'}(\mathrm{r},\mathrm{r}) = \sum_{n,\,n'} \sigma^{mn'}_{nn'}(\mathrm{r}) J_{nn'}(x_0)\varphi_n(z_0)\varphi_{n'}(z_0),$$

where $\sigma^{mn'}_{nn'}(\mathrm{r}) \equiv S^{mm'}_{nn'}(\mathrm{r},\mathrm{r})$ represents the partial scattering cross-section, which characterizes the efficiency of the energy exchange from modes n and n' of the incident field into modes m and m' of the diffracted field.

In what follows we will be interested in the behavior of the averaged (over interference pattern) energy characteristics of the diffracted signal. Then, the expression for smoothed intensity $\tilde{I}_d$ contains only a double sum equal to

$$\tilde{I}_d(\mathbf{R}) = \frac{\rho_w c(z_0) W}{8\pi|x_0|x} \sum_{n,\,m} \frac{1}{\kappa_n \kappa_m} \sigma^{mm}_{nn}(\mathrm{r})\, \varphi^2_n(z_0)\varphi^2_m(z). \qquad (24)$$

The reflection properties of an object are fully described by the scattering cross-section. Following Ref. [1] we define the quantity of interest

σ as a coefficient of proportionality between the intensities of incident and scattered waves taking into account the waveguiding type of propagation:

$$\sigma = 2\pi \lim_{|\mathbf{r}-\mathbf{r}_s|\to\infty} \left(\frac{\tilde{I}_d(\mathbf{R})}{\tilde{I}_i(\mathbf{R}_s)} |\mathbf{r}-\mathbf{r}_s| \, r^0(\mathbf{r}_s, z_s; \mathbf{r}, z) \right), \qquad (25)$$

where $\tilde{I}_i(\mathbf{R}_S)$ is the smoothed intensity of the incident field taken at the point of scatterer location:

$$\tilde{I}_i(\mathbf{R}_s) = \frac{\rho_w c(z_0) W}{|x_0|} \sum_{n,\nu} \frac{1}{\sqrt{\kappa_n \kappa_\nu}} \varphi_n^2(z_s) \varphi_\nu^2(z_0) h_{n\nu}(\mathbf{r}_s; \mathbf{r}_0); \qquad (26)$$

$$h_{n\nu}(\mathbf{r}_s; \mathbf{r}_0) \equiv h_{n\nu}^{n\nu}(\mathbf{r}_s, \mathbf{r}_s | \mathbf{r}_0, \mathbf{r}_0),$$

and $r^0(\mathbf{r}_s, z_s, \mathbf{r}, z)$ has the sense of the transition range (smoothed with respect to the interference pattern) from the omnidirectional point source at $(\mathbf{r}_s, z_s)$ to the observation plane:

$$\frac{1}{r_0(\mathbf{r}_s, z_s; \mathbf{r}, z)} = 2\pi \sum_{n,\nu} \frac{1}{\sqrt{\kappa_n \kappa_\nu}} h_{n\nu}(\mathbf{r}; \mathbf{r}_s) \, \varphi_n^2(z) \varphi_\nu^2(z_s).$$

Taking into account Eqs. (24) and (26), from Eq. (25) it is easy to obtain:

$$\sigma = \frac{1}{(4\pi)^2} \frac{\sum\limits_{n,m} \sigma_{nn}^{mm}(\mathbf{r}) \varphi_n^2(z_0) \varphi_m^2(z)}{\sum\limits_{n,\nu} \varphi_\nu^2(z_0) \varphi_n^2(z_s) h_{\nu n}(0; \mathbf{r}_0) \sum\limits_{m,\lambda} \varphi_\lambda^2(z_s) \varphi_m^2(z) h_{m\lambda}(\mathbf{r}; 0)}. \qquad (27)$$

In writing (27) we have used the fact that the grazing angles of the modes are small in most oceanic situations, so we have put $\kappa_n \approx \kappa_m \approx k$ in the amplitude factors.

In order to evaluate σ it is necessary to find a result for the matrix $\sigma_{nn}^{mm}(\mathbf{r})$ whose elements appear in the definition of σ according to (27).

The asymptotic forms of this matrix can be found in the limiting cases of small and large sizes of the object (in comparison with the corresponding correlation lengths of the incident and diffracted fields). According to (21), for coherent "illumination" (small-size scatterer) for $\sigma_{nn}^{mm}(\mathbf{r})$ we have

$$\sigma_{nn}^{mm}(\mathbf{r}) \equiv S_{nn}^{mm}(\mathbf{r}, \mathbf{r}) = 4k^2 \sum_{\nu,\lambda} |f_{\nu\lambda}(\mathbf{r}, \mathbf{r}_0)|^2 \, h_{\nu n}(0; \mathbf{r}_0) h_{m\lambda}(\mathbf{r}; 0). \qquad (28)$$

Let us estimate the matrix scattering amplitude $f_{\nu\lambda}$ entering into (28) for the case of both source and receiver far from the target (in the Fraunhofer zone relative to the horizontal size of the scatterer), supposing that

the WKB approximation is valid for the eigenfunctions $\varphi_n(z)$. In this approximation, simple calculations give the following result for $f_{\nu\lambda}$:

$$f_{\nu\lambda}(\mathbf{r},\mathbf{r}_0) = S\,Д_{\nu\lambda}(\mathbf{r},\mathbf{r}_0)\,\varphi_\nu(z_s)\varphi_\lambda(z_s),$$

$$Д_{\nu\lambda}(\mathbf{r},\mathbf{r}_0) \equiv Д\Big[\kappa_\lambda\,\frac{y}{x} + \kappa_\nu\,\frac{y_0}{|x_0|};\, q_\nu(z_s) - q_\lambda(z_s)\Big]. \qquad (29)$$

Here, S is the area of the shadow-forming plane, $q_\nu(z) = \sqrt{k^2 n_0^2(z) - \kappa_\nu^2}$ is the local vertical wavenumber of the ν-th mode, and

$$Д(x,y) = \frac{1}{S}\int\!\!\int_{-\infty}^{\infty} d\xi\,d\zeta\;E(\xi, z_s+\zeta)\,e^{\,i(\xi x + \zeta y)}$$

is the scattering function for the same scatterer in an unbounded homogeneous medium. The inequalities

$$\frac{1}{2}\left|\frac{dq_\nu(z_s)}{dz} - \frac{dq_\lambda(z_s)}{dz}\right| l_v^2 \ll 1, \qquad \left|\frac{d\gamma_\nu(z_s)}{dz}\right| l_v \ll 1, \qquad (30)$$

were supposed to be fulfilled in derivation of (29). Here, l_v is the characteristic vertical size of the scatterer, $\gamma_\nu(z_s) = q_\nu(z_s)/k$, and the fact that the depth of immersion of the body, z_s, is much larger than its size l_v, i.e. $z_s \gg l_v$ is taken into account. Thus, the total scattering cross-section (27) in the situation under consideration takes the form

$$\sigma = \sigma_0\,F(\mathbf{r}, z|\mathbf{r}_0, z_0; z_s). \qquad (31)$$

Here, $\sigma_0 = (S/\lambda)^2$ is the vacuum forward-scattering cross-section and the formfactor $F(\cdot)$ equal to

$$F = \frac{\sum\limits_{n,m}\sum\limits_{\nu,\lambda} |Д_{\nu\lambda}(\mathbf{r},\mathbf{r}_0)|^2 h_{\nu n}(0;\mathbf{r}_0) h_{m\lambda}(\mathbf{r};0)\varphi_n^2(z_0)\varphi_\nu^2(z_s)\varphi_\lambda^2(z_s)\varphi_m^2(z)}{\sum\limits_{n,\nu}\varphi_\nu^2(z_0)\varphi_n^2(z_s)h_{\nu n}(0;\mathbf{r}_0)\sum\limits_{m,\lambda}\varphi_\lambda^2(z_s)\varphi_m^2(z)h_{m\lambda}(\mathbf{r};0)}$$

describes mutual influence of the effects of regular diffraction and multiple scattering on the reflectivity of the body.

Note that, at relatively short acoustic distances when the exchange processes do not change substantially the energy structure of the field, so that $h_{\nu n}(\cdot) \approx \delta_{n\nu}$ and $h_{m\lambda}(\cdot) \approx \delta_{m\lambda}$, the formula (31) transforms to the well-known expression for the scattering cross-section in a smoothly inhomogeneous medium [1]. It should be emphasized that the inequalities (30)

impose definite restrictions on the vertical size of the body, under which the matrix scattering amplitude f_{nm} may be expressed in terms of plane-wave scattering function of the object corresponding to an infinite homogeneous space. Under these suppositions, the diffraction part of the problem is similar to that in free space, while account of the effects of multiple sound scattering by medium fluctuations reduces to investigation of cross-modal transformation of normal modes.

If the quantity l_v satisfies a more rigorous condition

$$\max |q_n(z_s) - q_m(z_s)|\, l_v \ll 1, \tag{32}$$

and the source and observation point are located at the axis $y = y_0 = 0$, then $J\!I_{nm} \approx 1$, provided that $F = 1$ and the formulas obtained immediately for a homogeneous medium are valid. By virtue of

$$\max |q_n(z_s) - q_m(z_s)| = k\sqrt{n_0^2(z_s) - \cos^2\theta_{cr}},$$

where θ_{cr} is the critical angle of the waveguide, the inequality (32) can be put into a more physically illustrative form

$$l_v \ll z_c(z_s),$$

where

$$z_c(z) = \frac{\lambda}{\sqrt{n_0^2(z) - \cos^2\theta_{cr}}}$$

has the sense of a vertical correlation length of the sound field excited by a spatially incoherent source [17]. The corresponding value has a local character, i.e., it depends on the location of the scatterer.

For an incoherent "illumination" (large-size scatterer), the quantity of interest $\sigma_{nn}^{mm}(\mathrm{r})$ may be expressed with the aid of Eq. (22) taken at $\mathrm{r}_1 = \mathrm{r}_2$, which for convenience is rewritten as

$$\sigma_{nn}^{mm}(\mathrm{r}) = 4k^2 \int_{-\infty}^{\infty} dR' \int_{-\infty}^{\infty} dz_s' dz_s'' E(R', z_s') E(R', z_s'') \times$$

$$\times \int_{-\infty}^{\infty} d\rho' R_n(\mathrm{r}_0, \rho', z_s', z_s'') R_m(\mathrm{r}, \rho', z_s', z_s''), \tag{33}$$

where

$$R_n(\mathrm{r}, \rho, z_1, z_2) = \sum_{\nu} \varphi_\nu(z_1)\varphi_\nu(z_2)\, h_{n\nu}(x, 0; 0, \rho)\, e^{-i\left(\frac{\kappa_\nu \rho y}{x}\right)}.$$

The simplest expression for σ_{nn}^{mm} is obtained for large vertical sizes of scatterer: $l_v \gg z_k(z_s)$. For approximate evaluation of the integrals over z_s' and z_s'' in (33) we pass to new variables $\xi' = z_s' - z_s''$ and $\eta' = (z_s' + z_s'')/2$. Under these approximations,

$$E(R', \eta' + \xi'/2)E(R', \eta' - \xi'/2) \approx E^2(R', \eta') = E(R', \eta')$$

and then we have

$$\sigma_{nn}^{mm}(\mathrm{r}) = 4k^2 \int\int_{-\infty}^{\infty} dR' d\eta' E(R', \eta') \int\int_{-\infty}^{\infty} d\rho' d\xi' R_n(\mathrm{r}_0, \rho', \eta', \xi') R_m(\mathrm{r}, \rho', \eta', \xi') \approx$$

$$\approx 4k^2 S \int\int_{-\infty}^{\infty} d\rho' d\xi' R_n(\mathrm{r}_0, \rho', z_s, \xi') R_m(\mathrm{r}, \rho', z_s, \xi'). \qquad (34)$$

Here, we again employed the fact that the vertical size of the body is much smaller than the depth of its immersion. The substitution of (34) into (27) yields

$$\sigma = \frac{S S_c}{\lambda^2}, \qquad (35)$$

where S_c designates the effective area of diffraction field coherence:

$$S_c = \frac{\sum\limits_{n,m} \int\int_{-\infty}^{\infty} d\rho' d\xi' R_n(\mathrm{r}_0, \rho', z_s, \xi') R_m(\mathrm{r}, \rho', z_s, \xi') \varphi_n^2(z_0) \varphi_m^2(z)}{\sum\limits_{n,\nu} \varphi_\nu^2(z_0) \varphi_n^2(z_s) h_{n\nu}(0; \mathrm{r}_0) \sum\limits_{m,\lambda} \varphi_\lambda^2(z_s) \varphi_m^2(z) h_{m\lambda}(\mathrm{r}; 0)}.$$

It is significant that S_c is a diminishing function of the sound frequency carrier and of the corresponding distances passed by the wave. Comparison of (35) and (31) shows that for large-size objects, the influence of multiple scattering processes on the reflectivity of the body is much weaker, which results in a S/S_c-fold decrease of the scattering cross-section as compared to the case of the coherent "illumination".

4. Illustrative examples

To illustrate the effects of random volume scattering on diffraction of acoustic signal by rigid object we consider the deep ocean environment from the North-West Pacific and assuming that fluctuation phenomena in this case are due to the presence of internal waves. The sound-speed and buoyancy profiles chosen for our calculations are shown in Fig. 2.

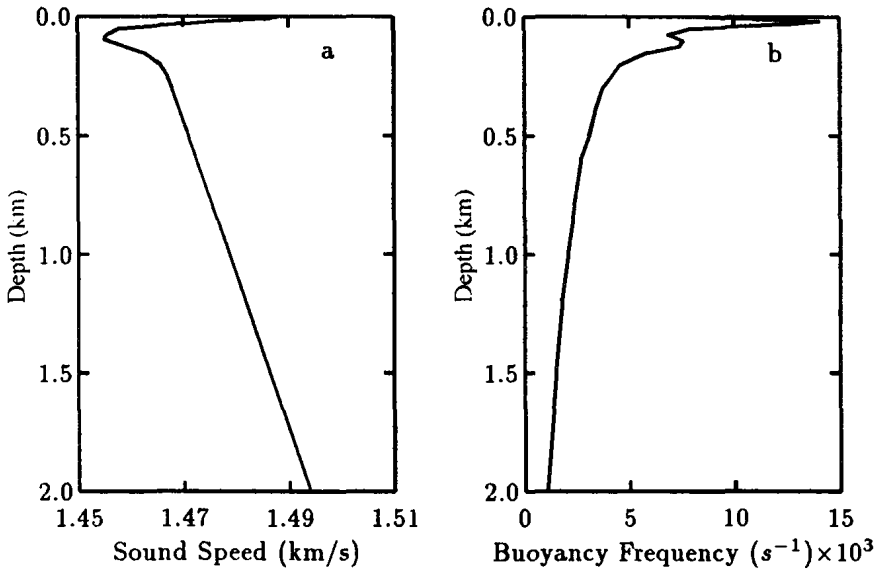

Fig. 2. Upper parts of sound speed profile (a) and buoyancy distribution (b) from the North–West Pacific at latitude $45^{\circ}N$.

The analysis is carried out under the supposition that the shadow-forming plane is shaped as a rectangle with the sides l_h and l_v. We restrict consideration to the case of practical interest, when the horizontal size of the scatterer l_h is much smaller than the corresponding correlation lengths of incident and diffracted fields. For simplicity, we take the source on the x-axis. In all cases, the source level is 200 dB.

We begin with observing the effect of internal wave scattering on the mean intensity of diffracted field assuming the Garrett–Munk spectrum for $\Phi_\mu(æ, z)$. The function of interest is given by Eq. (23). According to (23), to obtain a result for I_d it is necessary to calculate the modal content $\Gamma^d_{nm}(\mathrm{r})$ of the registered signal. For the case considered, the partial scattering cross-section $\sigma^{nm m'}_{nn'}(\mathrm{r})$ appearing in the definition of $\Gamma^d_{nm}(\mathrm{r})$ with the use of Eq. (21) can be expressed as

$$\sigma^{nm m'}_{nn'}(\mathrm{r}) = 4k^2 \sum_{\nu,\lambda} \sum_{\nu',\lambda'} f_{\nu\lambda}(\mathrm{r},\mathrm{r}_0)\, f^{*}_{\nu'\lambda'}(\mathrm{r},\mathrm{r}_0) h^{\nu'n'}_{\nu n}(0,0|\mathrm{r}_0,\mathrm{r}_0)\, h^{m'\lambda'}_{m\lambda}(\mathrm{r},\mathrm{r}|0,0),$$

where

$$f_{\nu\lambda}(\mathrm{r},\mathrm{r}_0) = S \frac{\sin\left[(\kappa_\nu y/x + \kappa_\lambda y_0/x_0)\, l_h/2\right]}{(\kappa_\nu y/x + \kappa_\lambda y_0/x_0)\, l_h/2} \frac{1}{l_v} \int_{-l_v/2}^{l_v/2} dz'_s\, \varphi_\nu(z_s+z'_s)\, \varphi_\lambda(z_s+z'_s).$$

As was mentioned above, the diagonal elements $\Gamma_{nn}(\mathbf{r})$ (having the sense of modal intensities) play a dominant role in modeling the asymptotic behavior of the MCF for long ranges. Figure 3 shows how the initial modal intensities (curve 1) decay to equilibrium. For long ranges, the random scattering effects lead to equipartition of energy among all diffracted modes.

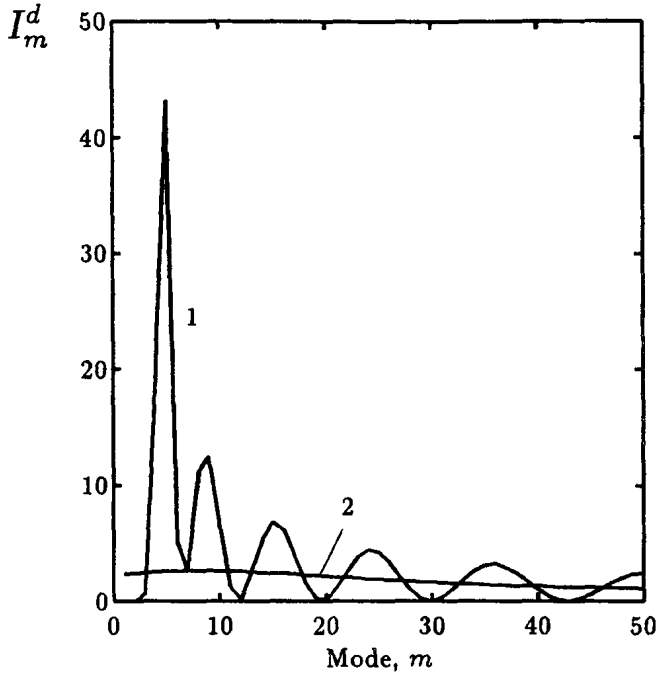

Fig. 3. Behavior of modal intensities versus m in the absence (1) and in the presence (2) of random inhomogeneities. Source frequency of 200 Hz, source depth of 50 m, target depth of 100 m, and receiver depth of 300 m. The distance between source and target is 500 km and the target–receiver distance is 1000 km. Modal intensities have been normalized to the area under the corresponding curve

An intrinsic consequence of this evolution is the redistribution of the total intensity of diffracted signal. Figure 4 shows the behavior of wavefield intensity, Eq. (23), as a function of depth z and horizontal position y of the receiver.

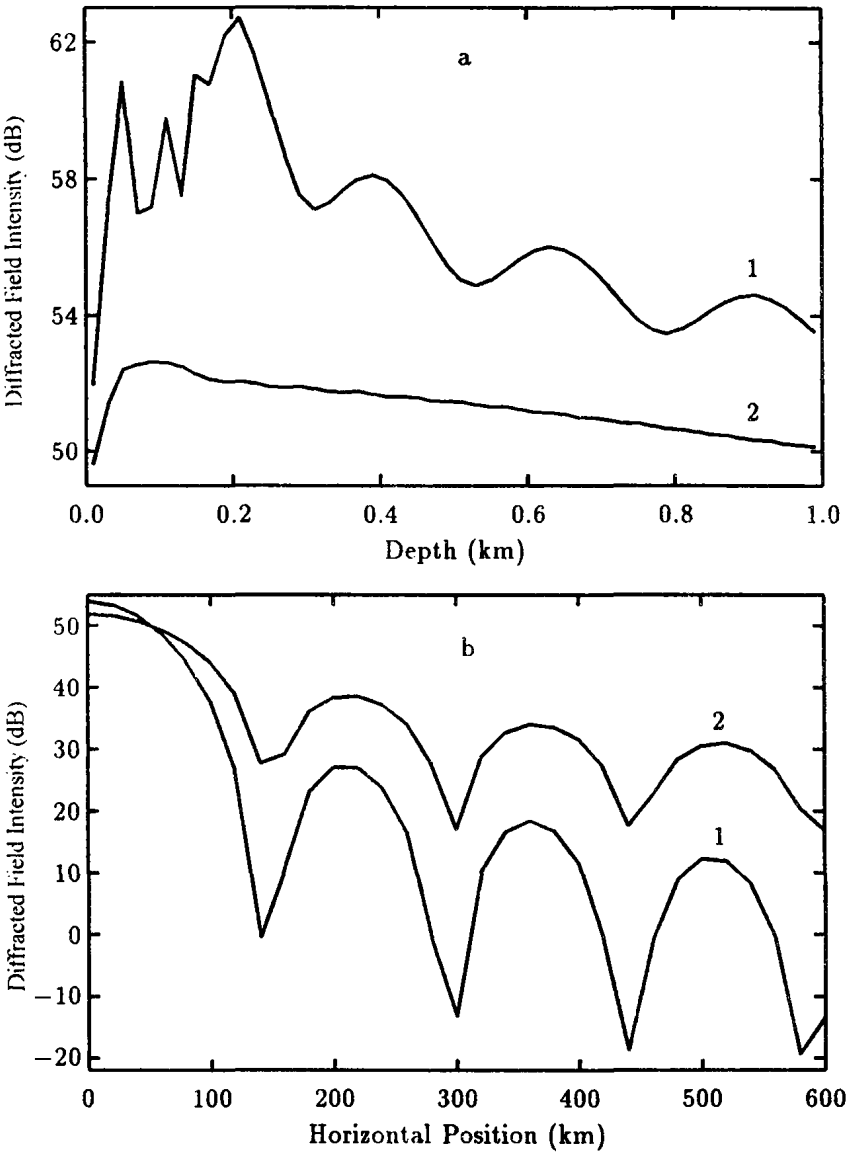

Fig. 4. Total diffracted field intensity as a function of depth (a) and horizontal position (b) in the absence (1) and in the presence (2) of random inhomogeneities. Source frequency of 200 Hz, source depth of 50 m, target depth of 100 m, and receiver depth of 300 m. The distance between source and target is 500 km and the target–receiver distance is 1000 km

In Fig. 4a we plot the function $I_d(\mathbf{R})$ (in decibel notation) for fixed y ($y = 0$) and variable z. The calculations were carried out for the sound speed profile in Fig. 2 at $f_0 = 200$ Hz, $z_0 = 100$ m, $x_0 = 500$ km, $x = 1000$ km, $l_h = 50$ m, $l_v = 10$ m, in the absence (curve 1) and in the presence (curve 2) of random surface scattering. It is seen from this figure that volume scattering effects are responsible for redistribution the initial intensity distribution.

The results of numerical calculations of the diffracted field intensity versus horizontal position of the receiver y are presented in Fig. 4b (curve 1 corresponds to the regular channel). In this example, $y_0 = 0$ and the receiver is located at the depth $z = 300$ m. The most striking feature in Fig. 4b is the fact that the random scattering leads to considerable degradation of the diffraction pattern.

However, of the most importance is the effect of oceanic fluctuations on the diffracted signal coherence loss which increase with the carrier frequency and propagation distance. In Fig. 5 we plot the mutual coherence function of vertical separation for two carrier frequencies of 100 Hz and 200 Hz.

For the case considered the characteristic vertical coherence length has an order of magnitude of several tens of meters.

The theoretical curves in Fig. 5 were plotted using the results of the work of Esswein and Flatte [18] for the phase–structure density from internal waves. It is clear that as the frequency increases, the rate of coherence loss increases too. This fact, of course, indicates that high frequency scattering occurs at a more rapid rate.

5. Summary and conclusions

The objective of this article has been to develop wave–theoretical expressions for the energy and correlation characteristics of the acoustic signal diffracted by an object in a refractive oceanic waveguide containing random inhomogeneities. The method presented is based on the combined use of the Kirchhoff approximation and the small angle radiation transport equation for the second moment of the medium Green's function. In the framework of the approach proposed the problem of finding a result for the diffracted field reduces to the evaluation of the Kirchhoff integral containing the product of two random Green's functions describing the stochastic waveguide propagation between source and target, and target and receiver, respectively. In the case of forward scattering the corresponding Green's functions are statistically independent and, hence, the correlation properties of diffracted wave can be entirely expressed in terms of the mutual coherence functions (MCF) for the incident and scattered field.

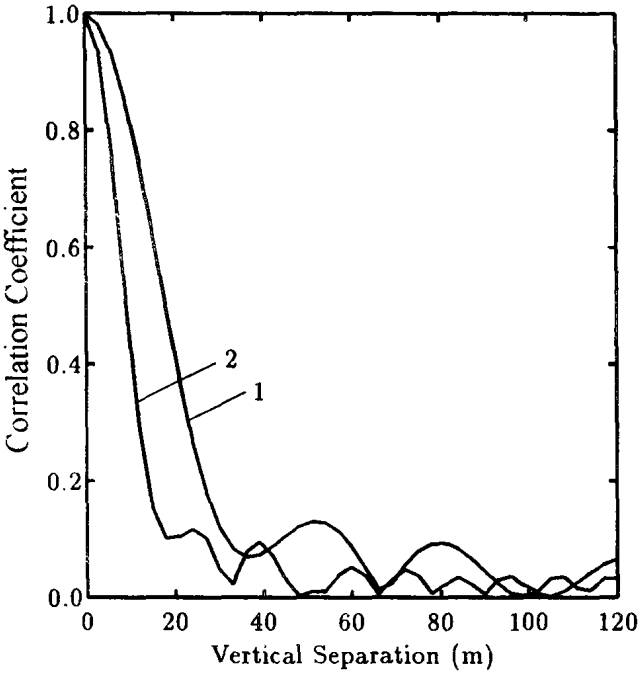

Fig. 5. Normalized mutual coherence function of vertical separation for frequencies 100 Hz (1) and 200 Hz (2). Source depth of 50 m, target depth of 100 m, and receiver depth of 300 m. The distance between source and target is 500 km and the target–receiver distance is 1000 km

For the MCF of interest we formulated the matrix radiation transport equation and presented its approximate analytical solution. The results for the acoustic MCF have been then employed to the statistical analysis of diffraction phenomena. The general formulae for the mean intensity and spatial coherence function of a diffracted field produced by a rigid object have been derived and analyzed in two limiting cases, when the body sizes are significantly large or small compared with corresponding coherence lengths of incident radiation. The scattering cross–section of the body has been evaluated as well. The major limitation made is the neglect of multiple scattering from an object. The application is illustrated by computation of effects considered for realistic deep–water environments from the North–West Pacific under the assumption that the random field of internal waves is the dominant source of transmission fluctuations.

Several conclusions may be drawn from the above analysis. The presence of random volume scattering results in modal coupling with continual energy

exchange between the modes. This "mixing" of energy leads to essential transformation of the modal spectrum of the registered signal.

An intrinsic consequence of this transformation is the evolution of acoustic field intensity that leads to redistribution the initial intensity as a function of depth. After sufficiently long range, the initial intensity peaks at the depth corresponding to the target depth and are difficult to distinguish relative to other intensity levels.

However, of the most importance is the effect of oceanic fluctuations on the received signal coherence loss which increases with the carrier frequency and distance from a source. In particular, as observed in the results of Sec. 4, for a source of 200 Hz, at a range of 1000 km the characteristic vertical coherence length has an order of magnitude of few tens of meters.

It has been established that the target strength at the diffraction from a sufficiently small object is independent of the incident signal coherence degree and depends mainly on the geometric characteristics of a scatterer and regular refractive properties of an oceanic waveguide. In the other limiting case of incoherent "illumination", the medium fluctuations produce a significant effect on the target strength leading to reduction of the scattering cross-section by $(S/S_c)^2$ times.

Acknowledgments

This work was supported by Russian Foundation for Basic Research under Grants No 97-02-17536 and No 97-02-17555.

References

1. *Yu. A. Kravtsov, V. M. Kuz'kin, and V. G. Petnikov.* Wave diffraction from regular scatterers in multimode waveguides // Sov. Phys. Acoust., 1984, vol. 30, pp. 199–202.

2. *F. Ingenito.* Scattering from an object in a stratified medium // J. Acoust. Soc. Amer., 1987, vol. 82(6), pp. 2051–2059.

3. *S. M. Gorsky, V. A. Zverev* et.al.. Short–wave diffraction in a multimode layered waveguide // Sov. Phys. Acoust., 1988, vol. 34(1), pp. 55–59 (in Russian).

4. *Ye. L. Borodina,* et.al.. Potentialities of shadow methods in the study of diffracted wave fields in waveguides // In: Formation of Acoustic Fields in Oceanic Waveguides, Ed. by V. A. Zverev (IAP RAS, Nizhny Novgorod, 1991), pp. 174–200 (in Russian).

5. *S. M. Gorskii, V. A. Zverev, and A. I. Khilko.* Sound scattering by spatial–localized inhomogeneities in oceanic waveguides: calculation and measurement methods // In: Formation of Acoustic Fields in Oceanic Waveguides, Ed. by V. I. Talanov and V. A. Zverev (IAP RAS, Nizhny Novgorod, 1995), pp. 63–80.

6. *A. A. Fraiman.* Diffraction of fluctuating radiation // Izv. Vuzov, Radiofizika, 1972, vol. 15(9), pp. 1362–1366 (in Russian).

7. *A. A. Kleshchev.* Sound scattering from a spheroidal object located near the interface // Sov. Phys. Acoust., 1979, vol. 25(3), pp. 143–145 (in Russian).

8. *N. K. Uzunoguli and J. G. Fikioris.* Scattering from an inhomogeneity inside a dielectric–slad waveguide // J. Opt. Soc. Amer., 1982, vol. 72(5), pp. 628–637.

9. *W. E. Kohler and G. C. Papanicolaou.* Wave propagation in a random–inhomogeneous ocean // In: Lecture Notes in Physics, vol. 70, Wave Propagation and Underwater Acoustics, Ed. by J. B. Keller and J. S. Papadakis (Springer–Verlag, Berlin, 1977), pp. 153–223.

10. *A. G. Sazontov.* Acoustic coherence in a deep random oceanic waveguide // In: The Formation of Acoustical Fields in Oceanic Waveguides, Ed. by V. I. Talanov and V. A. Zverev (Institute of Applied Physics RAS, Nizhny Novgorod, 1995), pp. 37–62.

11. *A. G. Sazontov.* Quasi-classical solution of radiation transport equation in a scattering medium with regular refraction // Akust. Zhur., 1996, vol. 42(4), pp. 551–559 (in Russian).

12. *N. K. Vdovicheva, A. G. Sazontov, and A. I. Khilko.* Diffraction of acoustic field by an object immersed into a randomly inhomogeneous oceanic waveguide // Preprint No 393, (Institute of Applied Physics RAS, Nizhny Novgorod, 1996).

13. *S. M. Flatte, R. Dashen, W. H. Munk, K. M. Watson, and F. Zachariasen.* Sound Transmission Through a Fluctuating Ocean, Ed. by S. M. Flatte (Cambridge U. P., New York, 1979.)

14. *S. M. Rytov, Y. A. Kravtsov, and V. I. Tatarskii.* Principles of Statistical Radiophysics, (Springer–Verlag, Berlin, 1988), Vols. 1–4.

15. *L. B. Dozier and F. D. Tappert.* Statistics of normal–mode amplitudes in a random ocean. I. Theory, and II. Computations // J. Acoust. Soc. Amer., 1978, vol. 63(2), pp. 353–365 and 1978, vol. 64(2), pp. 533–547.

16. *A. Beilis and F. D. Tappert.* Coupled mode analysis of multiple rough surface // Ibid., 1979, vol. 66(3), pp. 811–826.

17. *S. S. Abdullaev and B. A. Niyazov.* Spatial coherence and field intensity distribution in an underwater sound channel // Sov. Phys. Acoust., 1985, vol. 31(4), pp. 417–422 (in Russian).

18. *R. Esswein and S. M. Flatte,* Calculation of the phase–structure function density from oceanic internal waves // J. Acoust. Soc. Amer., 1981, vol. 70(5), pp. 1387–1396.

MULTISCALE COHERENCE OF THE ACOUSTIC FIELD OF A NOISE SOURCE IN RANDOMLY INHOMOGENEOUS OCEAN

I.P. Smirnov, J.W. Caruthers, and A.I. Khil'ko

INTRODUCTION

The field intensity of an acoustic source in refractive oceanic waveguides has a complex space-time structure, characterized by shadow zones, zones of convergence, bundles etc. All these features are due to propagation of acoustic fields in non-uniform environment such as layered refractive waveguides. Similar features exist in space-time distributions of other field characteristics, in particular, those which are used to describe signals of noise and non-stationary sources, such as the coherence, pulse duration and others. The purpose of this paper is study of space-time distributions of the fields of noise sources in refractive oceanic waveguides.

Multipath modes, as well as the randomly distributed inhomogeneities in oceanic environment, result in significant interference noise in the excitation of waveguide waves by a coherence point source of sound [1, 2, 3]. Physically, this phenomenon is close to speckle noise in optics and radiophysics when an electromagnetic field propagates in randomly inhomogeneous environment or is scattered by rough objects [4, 5].

Unlike in free space, in the ocean the acoustic field at each point is formed by a set of partial waves, for example, modes. Partially coherent field of noise source propagats along an acoustical paths assoiciated with partial waves. The resultant field at the point of observation is the sum of partially coherent fields. Hence, the result coherence decreases. The field fluctuations arising therein impede the solution of various, in particular, inverse problems associated with the remote diagnostics of inhomogeneities. One of the methods for elimination of this factor consists in decreasing the coherence of the illuminating field, which results in a partial suppression of interferometric noise [6, 7]. Similar ideas are developed in the acoustics of the ocean, where the noise of ships and noisy port zones or explosions are considered as sources of partially coherent illuminating field for acoustic monitoring [8, 9, 10, 11]. The analysis of noise structure, radiated by partially coherent acoustic sources is also important for

the solution of the space-time structure of a bubble clouds using the radiated noise measured at a distance [12]. The restoration of the source characteristics by measuring the radiation is a classical inverse problem in the optics and radiophysics [4, 5]. It is known that the solution of such a problem is reduced to the solution of the Fredholm integral equation of the first type. The difficulties of solution of such equations are accosiated with the impossibility of restoration of non propagating fields in the far zone due to their weakness and the influence of additive noise [13]. Oceanic medium, being inhomogeneous, introduces additional features in this solution, which are stipulated by the multiwave propagation and geometrical dispersion, the occurrence of shadow zones and focusing. To solve the reconstruction problem of the source characteristics in this case, it is necessary to regularize the measured data by use of prior information about oceanic environment. More effective method of regularization of this problem is the use of a model of a source of the partially coherent field in oceanic waveguide, i.e. the use of the solution of a direct problem.

The mentioned lines of research define the interest in the analysis of partially coherent acoustic source field distribution in layered oceanic waveguides.

In this connection, it is necessary to mention the study of the statistical and interferometrical structures of noise fields, associated with distant shipping [14]. There is known examination of acoustic systems for inhomogeneities visualization using as the illumination the surface noise [9, 10], and also the systems of diagnostics of bottom structure, based on the mesurements of the correlation characteristics of the acoustic noise of the ship [15]. The transformation of the space-time coherence of the acoustic field from an extended noise source in refractive oceanic waveguides is investigated in [11]. Finally, the features of partially coherent acoustic field difraction by bodies in layered oceanic waveguides are considered in the series of works for the case, where the illuminating field became partially coherent due to the noise nature of radiated acoustic source, as well as due to the influence of the randomly distributed perturbations of oceanic waveguide [16, 17].

At the same time, the space-time transformation of the destribution of coherence structure in refractive oceanic waveguides as for stationary, and, in greater degree, for non-stationary noise sources have not been investigated in sufficient detail. The examples are the multiscale space-time distributions of acoustic field coherence in ocean, associated with existing of the bundles of rays [16]. In the present paper these phenomena are investigated in detail. In particular, the parameters of bundles are studied for an extended noise

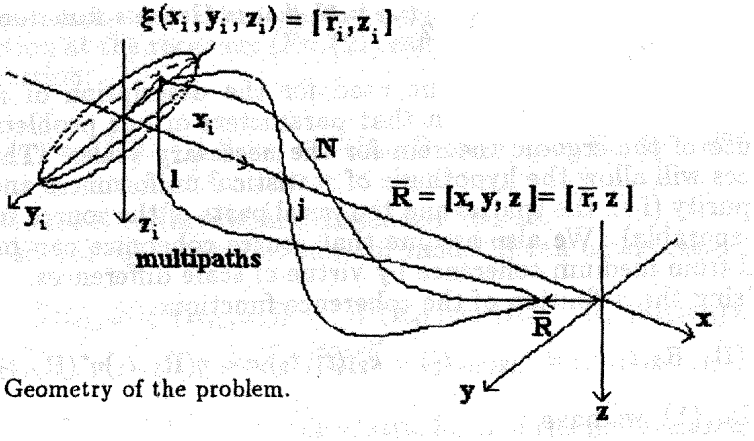

Fig. 1. Geometry of the problem.

acoustic source in the presence of volume-distributed random inhomogeneities.

1 PARTIALLY COHERENT ACOUSTIC WAVES FROM A NOISE SOURCE IN OCEANIC WAVEGUIDES

1.1 Basic Expressions

The physical problem formulated in the introduction can be presented as a stochastic problem for the excitation of partially coherent (PC) space-time waves by spatially localized noise sources $\xi(\mathbf{R}_i, \omega)$, where $\mathbf{R}_i = [x_i, y_i, z_i] = [\mathbf{r}_i, y_i]$ is a point in the distribution of a noise source in a layered refractive waveguide with a sound speed profile $c(\mathbf{r}) = c(z)$ and ω is the angular frequency. (The geometry of the problem is shown in Fig. 1.) To solve this problem, physical models of spatially localized noise sources, as well as models of the layered waveguide, will be introduced.

The particle velocity potential, $\eta(\mathbf{R}, t)$, where $\mathbf{R} = [x, y, z] = [\mathbf{r}, y]$ is a field point in the waveguide, can be expressed as a sum of partial waves from each point element of the noise source with complex amplitude $\xi(\mathbf{R}_i, \omega)$. Then,

$$\eta(\mathbf{R}, t) = \iint_{-\infty}^{\infty} \xi(\mathbf{R}_i, \omega) e^{-i\omega t} G(\mathbf{R}_i, \mathbf{R}, \omega) d\mathbf{R}_i d\omega, \qquad (1)$$

where $G(\mathbf{R}_i, \mathbf{R}, \omega) = G_{\mathbf{R_i R}_{1,2}}(\omega) = G_{12}(\omega)$ is Green's function for an inhomogeneous medium.

Correlation theory will be used for the description of random waves under the assumption that parameters of our problem allow the use of the ergodic theorem for the necessary scales. The noise sources will allow the hypothesis of statistical uniformness and spectral purity (i.e., the spatial and temporal parts of the source function are separable). We also assume that source coherence can be separated from medium coherence by virtue of scale differences.

Using the definition of the coherence function:

$$k_\eta(\mathbf{R}_1, \mathbf{R}_2, t_1, t_2) = k_{12}(t_1, t_2) = k_{21}(t_1, t_2) = < \eta(\mathbf{R}_1, t_1)\eta^*(\mathbf{R}_2, t_2) >,$$

and Eq. (1), we have

$$k_{12}(t_1, t_2) = \int_{-\infty}^{+\infty}\int\int < \xi(\mathbf{R}_{i1}, \omega_1)\xi^*(\mathbf{R}_{i2}, \omega_2) > e^{-i(\omega_1 t_1 - \omega_2 t_2)} \times$$

$$\times < G(\mathbf{R}_{i1}, \mathbf{R}_1, \omega_1)G^*(\mathbf{R}_{i2}, \mathbf{R}_2, \omega_2) > d\mathbf{R}_{i1} d\mathbf{R}_{i2} d\omega_1 d\omega_2, \qquad (2)$$

where $< \ldots >$ represents ensemble averaging for either the source or the medium and $\mathbf{R}_{i1,2}$ are the different points of source. When we actually use Eq. (2), we further assume stationarity with $\tau = t_2 - t_1$.

1.2 Noise Source Models

For a more detailed analysis of PC waves in the ocean, specific source function models, $< \xi(\mathbf{R}_{i1}, \omega_1)\xi^*(\mathbf{R}_{i2}, \omega_2) >$, must be introduced. Appropriately simplified source models can help simplify the coherence function in Eq. (2). It is important that these models represent real ship noise sources, since such sources may prove useful for the acoustic probing of oceanic inhomogeneities. In some cases narrowband spectral components that are present in the ship noise can be singled out as quasiharmonic signals by a receiver [14].

Model A – Broadband Point Source.
For model A, we use a noise signal given by $\xi(\mathbf{R}_i, \omega) = A_0(\mathbf{R}_{i0})\sqrt{\mathrm{S}_\xi(\omega)}$, where $\mathrm{S}_\xi(\omega)$ is the energy spectrum and $\mathbf{R}_{i0} = \mathbf{R}_{i1}$ is a single point. The source coherence function for this model becomes

$$< \xi(\mathbf{R}_{i0}, \omega)\xi^*(\mathbf{R}_{i2}, \omega_2) >= A_0^2(\mathbf{R}_{i0})\delta(\mathbf{R}_{i0} - \mathbf{R}_{i2})\mathrm{S}_\xi(\omega)\delta(\omega - \omega_2) \qquad (3)$$

where δ denotes the Dirac delta function. Using Eq. (3), the coherence function at the receivers (Eq. (2)) can be represented by the following expression:

$$k_{12}(\tau) = A_0^2(\mathbf{R}_{i0}) \int \mathbf{S}_\xi(\omega) < G(\mathbf{R}_{i0}, \mathbf{R}_1, \omega) G^*(\mathbf{R}_{i0}, \mathbf{R}_2, \omega) > e^{i\omega\tau} d\omega. \quad (4)$$

Model B – Narrowband Extended Source.
The source coherence function for model B can be expressed as

$$\begin{aligned} \langle \xi(\mathbf{R}_{i1}, \omega_1) \xi^*(\mathbf{R}_{i2}, \omega_2) \rangle &= A^2(\mathbf{R}_{i1}) \operatorname{sinc}(\mathbf{R}_{i1} - \mathbf{R}_{i2}) \mathbf{S}_{\xi 0}(\omega_0) \times \\ &\times e^{-\frac{(\omega-\omega_0)^2}{\Delta\omega^2}} \delta(\omega_1 - \omega_2), \end{aligned} \quad (5)$$

where $A^2(\mathbf{R}_i)$ determines the spatial form of the noise source, $\mathbf{S}_{\xi 0}(\omega_0)$ specifies a narrowband spectrum centered at ω_0, and $\operatorname{sinc} x = \sin x / x$. Substituting Eq. (5) into Eq. (2), and assuming that the coherence scale in space is small, we obtain the coherence function

$$k_{12}(\tau) = \mathbf{S}_{\xi 0}(\omega_0) e^{i\omega_0\tau} \int A^2(\mathbf{R}_i) < G(\mathbf{R}_i, \mathbf{R}_1, \omega_0) G^*(\mathbf{R}_i, \mathbf{R}_2, \omega_0) > d\mathbf{R}_i. \quad (6)$$

Model C – Horizontally Moving, Narrowband Point Source.
Let model C be a noncoherent,narrowband point source which moves along the y_i axis a distance L at a depth z_{i0} and the receiver is a vertical array on the line $\mathbf{R} = [a, 0, z]$ with hydrophones at depths z_1 and z_2 (see Fig. 1). If the averaging time of the receiver is more than the characteristic time of movement, then the source function is

$$\begin{aligned} \langle \xi(\mathbf{R}_{i1}, \omega_1) \xi^*(\mathbf{R}_{i2}, \omega_2) \rangle &= A^2(y_i) \delta(x_i - 0) \delta(z_i - z_{i0}) \mathbf{S}_{\xi 0}(\omega_0) \times \\ &\times e^{-\frac{(\omega-\omega_0)^2}{\delta\omega^2}} \delta(\omega_1 - \omega_2), \end{aligned} \quad (7)$$

where $A^2(y_i) = (1, y_i \le L; 0, y_i > L)$. The coherence function is

$$\begin{aligned} k_{12}(\tau) &= \mathbf{S}_{\xi 0}(\omega_0) e^{i\omega_0\tau} \int A^2(y_i) \langle G(y_i, z_{i0}, a, z_1, \omega_0) \times \\ &\times G^*(y_i, z_{i0}, a, z_2, \omega_0) \rangle \, dy_i. \end{aligned} \quad (8)$$

Note that we have chosen such noise source models that in one case (model A) the source is localized in space (point source) and in another case (model B) it is localized in frequency (narrowband). The final case (model C) is a combination of A and B, where the narrowband source point is moving. The resulting coherence functions (Eqs. (4), (6), and (8)) have similar forms. They show smoothing of

the space-time interference structure of $k_{12}(\tau)$ due to the influence of the source size, $A^2(\mathbf{R}_i)$, and bandwidth, $S_\xi(\omega)$.

1.3 Propagation in the Waveguide

A propagation signal in an inhomogeneous waveguide can take various paths (see Fig. 1). Such propagation can be represented as a sum of terms $j = 1, 2, \ldots N$ associated with the partial waves in an unperturbed oceanic waveguide:

$$G(\mathbf{R}_i, \mathbf{R}, \omega) = \sum_{j=1}^{N} G_j(\mathbf{R}_i, \mathbf{R}, \omega). \tag{9}$$

Such partial waves can be described using the mode approximation [11]:

$$G_j(\mathbf{R}_i, \mathbf{R}, \omega) = \varphi_j(z_i)\varphi_j(z) \exp[i|\mathbf{r}_i - \mathbf{r}|h_j - \pi/4](|\mathbf{r}_i - \mathbf{r}|h_j)^{-1/2},$$

where φ_j and h_j denote the eigenfunctions and eigennumbers of the unperturbed waveguide, respectively, or by using the ray approximation [1]:

$$G_j(\omega) = A_j e^{ikS_j},$$
$$S_j \equiv \int_{C_j} n(\mathbf{r})\, dl,\ n(\mathbf{r}) \equiv \tfrac{c_0}{c(\mathbf{r})}.$$

Here, A_j is the amplitude of the wave intensity by the ray of number j along arc C_j connecting the corresponding points ξ and R, S_j are the optical length of the ray, $k \equiv \omega/c_0$, c_0 is the typical value of the speed in the waveguide, $c(\mathbf{r})$ is the sound speed profile, and $n(\mathbf{r})$ is the refractive index. (It should be noted that both representations describe the real wave field and can be transformed one into another [1].)

1.4 Analysis of the structures of partially coherent acoustic waves in a waveguide

Using Eq.(9) in either of its two forms in Eq.(2) (or in the subsequent forms, Eq. (4), (6), or (8)) would lead to the possibility of splitting the coherence function into two terms:

$$k_{12}(\tau) = k_{12}^E(\tau) + k_{12}^I(\tau).$$

The first term is the energy sum for similar paths or modes (i.e., $E : m = n$) of all partial waves in the expansion of $< G(.)G^*(.) >$ and the second term is the interference between paths or modes (i.e., $I : m \neq n$).

Inspection of these equations shows that, for the scales which are associated with the interaction of partial waves with large differences between term indices, increasing the size or frequency bandwidth of the noise source smooths the space-time variations of the acoustic field. In the limiting case, where all variations are eliminated, the size of the source and noise frequency bandwidth must be larger than all variation scales of $< G(.)G^*(.) >$ in the space and frequency domains. Such fields can be seen as noncoherent acoustical fields. But to introduce more exact definitions for coherent and noncoherent acoustical fields in the ocean, the properties of oceanic waveguides as a space and frequency filter have to be taken into account.

To illustrate these concepts by specific exampl and to provide a basis for further development, we examine two cases:

Case 1 – Application of the ray representation to model A: The straightforward substitution of ray representation into Eq. (9), then into Eq. (4) gives

$$k_{12}(\tau) = A_0^2(\mathrm{R}_i) \sum_{mn} \int \mathbf{S}_\xi(\omega) a_m a_n^* e^{ik(S_m - S_n) - i\omega\tau} d\omega.$$

Case 2 – Application of the mode representation to model C: Assuming the small-angle approach, we obtain the coherence function by the substitution of mode representation to Eq. (8):

$$k_{12}(\tau) = \mathbf{S}_{\xi 0}(\omega_0) e^{i\omega_0 \tau} \sum_{mn} \varphi_m(z_1)\varphi_n^*(z_2) \times$$

$$\times \int A^2(y_i) \exp\left[i \left| y_i - \sqrt{a^2 + z_1^2} \right| h_m - i \left| y_i - \sqrt{a^2 + z_2^2} \right| h_n \right] \times$$

$$\times \left[\left| y_i - \sqrt{a^2 + z_1^2} \right| h_m \right]^{1/2} \left[\left| y_i - \sqrt{a^2 + z_2^2} \right| h_n \right]^{1/2} dy_i .$$

The integral in the last equation determines interference noise elimination for different space scales. If $L \ll a$, then this equation can be reduced further.

For the specific examples cited later, we will use a bilinear sound speed profile in the $(x, z) - plane$ defined by $[z_i(m), c_i(m/s)] = [0, 1500]$; $[200, 1470]$; $[3000, 1550]$, and a typical undersurface channel, which can be seen in North Pacific (Fig. 2).

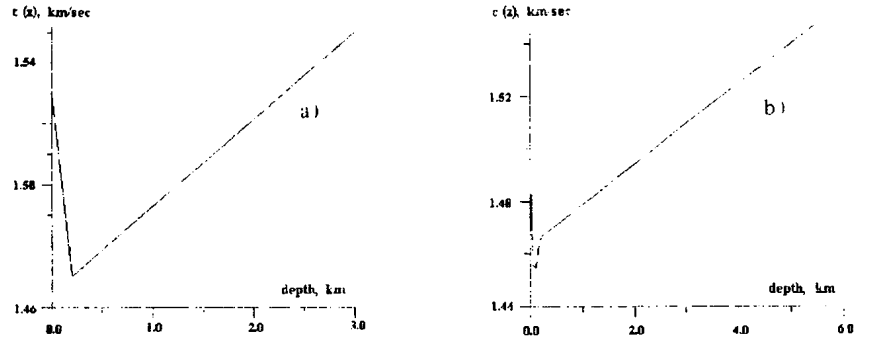

Fig. 2. The bilinear (a), and typical under surface (b) oceanic channels.

According to preceeding sections' analytical results, acoustic waves in oceanic waveguides can have significant partially coherent interference noise due to the interaction among partial waves in the waveguide (additional source of interference flactuations is interaction of partial waves with inhomogeneities in the waveguide). This is in contrast to optical and ultrasonic imaging, where waveguide interference is no problem. For short scales, the interference structure in the space-time domain can be imaged as random patterns and described statistically.

1.5 Coherence transfer properties

In this section we analyse the interference structures suggested by the partitions in equation for $k_{12}(\tau)$. To simplify discussion, we introduce the term Coherence Transfer Property (CTP), which we use to suggest a property of the space-time coherence function of the source transferred to the field points in the waveguide [18, 19]. That is, the properties associated with Eq. (2).

Coefficient of Vision for Interference Structures

The high-frequency space-time interference structure, which is produced by many partial waves characterized by very different parameters among the various indices, can be defined as interference noise. Coherence cannot be maintained for long distances due to the high dispersion of parameters among those indices. To describe the space-time interference structure, we introduce the quantity $\beta(\mathbf{R}) = \overline{k_{11}^I / k_{11}^E}$, which is the single-receiver, time-averaged interference part of the coherence function divided by the energy part. This quantity is a special ratio of CTPs which we call the Vision Coefficient

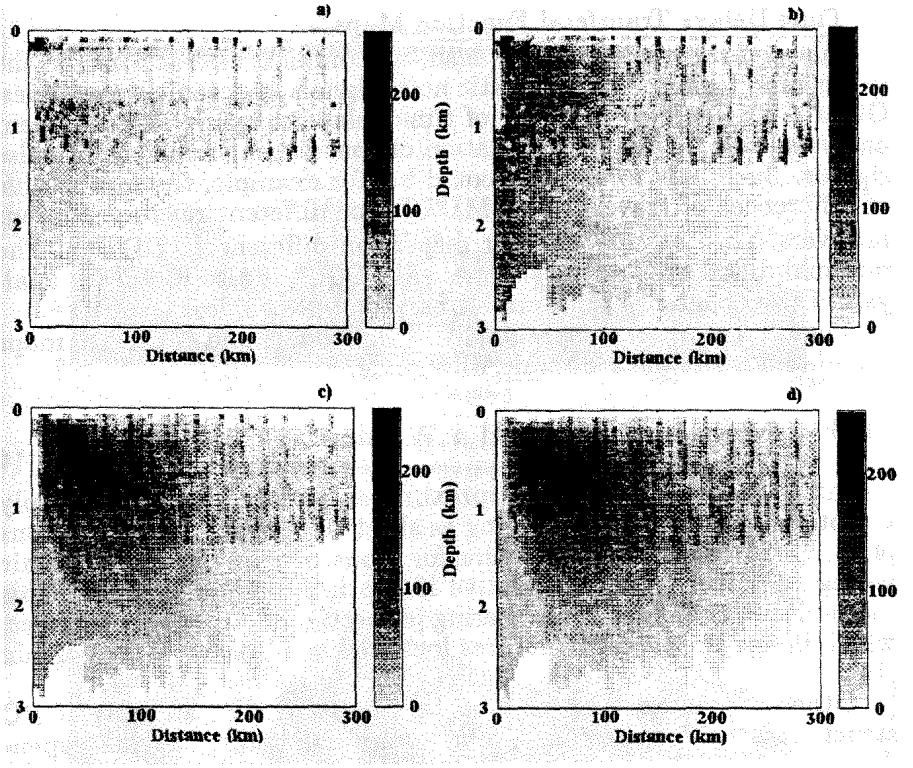

Fig. 3. Spatial distributions of VC for bilinear oceanic channel and different values of the bandwidths (τ = 0.1 sec (a), 1 (b), 100 (c), 1000 sec (d), $\sigma = 0.001, \epsilon_0 = 0.01$).

(VC) of the interference structure. Figure 3 shows VC maps in the $(x, z) - plane$ for noise signals with different bandwidths.

Close analysis of the energy and interference terms, leading to the spatial distributions of VC seen in Fig. 3, suggests that a diversity in paths, coupled with strong random phase dispersions among those paths, lead to strong interference and rapid decorrelation with distance. On the other hand, in regions where the energy terms dominate, coherence lasts for greater distances.

These results suggest a method for the analysis of such wave structures involving isolating terms in $k_{12}(\tau)$ corresponding to the interference of rays (i.e., $I : (m \neq n)$). The energy part of $k_{12}(\tau)$ (i.e., $E : (m = n)$) has a broadband spatial spectrum, including large-scale interference, which can be smoothed by using large-size noise sources.

Time Delays Transferal Function Maps

Inhomogeneous structures lead to complex interactions of the space-time variations for acoustic noise signals in oceanic waveguides. Other CTPs defined in terms of time delays can provide convenient analysis tools for the interpretation of space-time variations of noise signals. Such aids to analysis could be, for example, the mean value of differences of travel times (MDTT) for different rays at different receivers $\overline{\Delta\tau_{mn}}$ as well as their dispersion differences (DDTT). The minimal difference for travel times (MinDTT) is also useful for analysis of the coherence structure of noise in waveguides.

Fugure 4 shows examples of MDTT, DDTT, and MinDTT maps calculated for bilinear oceanic waveguide.

1.6 Multi-scaleness and a Window of Coherence

Interference noise can be approximately isolated relatively simply in optical and ultrasonic imaging as short scale space-time variations [4, 5]. But a comparable operation for acoustic noise signals in oceanic waveguides will be more effective if another method is used. This method uses the space-time filtering properties of oceanic waveguides, which image the signal structures localized in the space-time domain [16].

Other characteristics can also be imaged in the analysis of PC structures in the waveguides. For example, Fig. 5 shows the dependences of ray cycle lengths at the initial path angles $D(\alpha_j)$ for the bilinear and undersurface oceanic waveguides. As the analysis shows, these dependencies have relatively smooth local extrema, which determine the formation of ray bundles (or, more generally, partial wave bundles) [20, 21].

Because, within a bundle or beam partial wave, parameters differ only slightly, coherence in the bundle is maintained for propagation to long distances. Another situation is for rays or waves outside the bundle. They lose coherence with the bundle very rapidly due to large differences in their parameters from those in the bundle. Thus, the effective method for isolation of interference noise for oceanic waveguides is the representation of the coherence function as coherent sums of partial waves within the bundles and as diffuse sums between them:

$$k_{12}(\tau) = \sum_{mn}^{\Delta_k} k_{12}^{mnk}(\tau) + \sum_{mn \neq \Delta_k} k_{12}^{mnk}(\tau).$$

Here, $\Delta_k (k = 1 \ldots s)$ denotes the localized bundles, and each bundle is formed by a set of coherent partial waves. On this basis, we

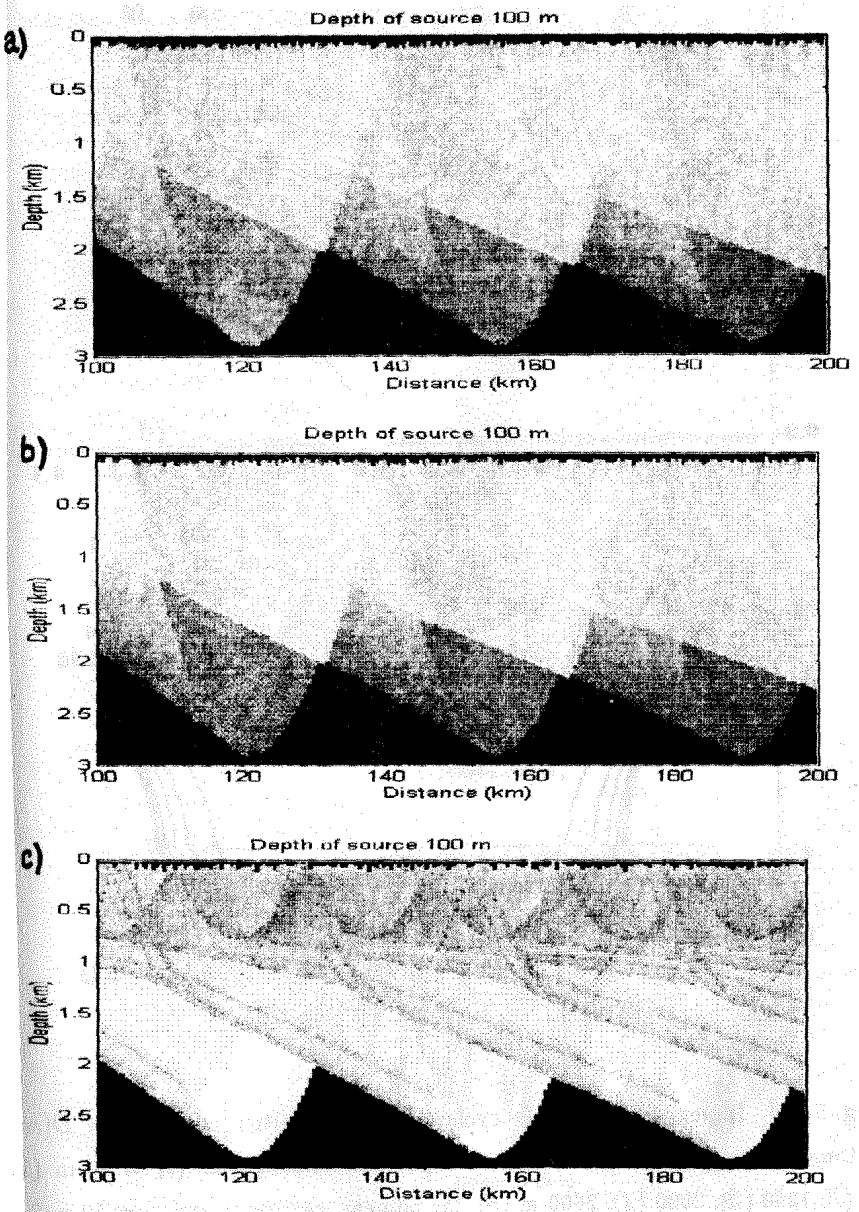

Fig. 4. Examples of MDTT (*a*), DDTT (*b*), and MinDTT (*c*) maps calculated for the bilinear oceanic waveguides.

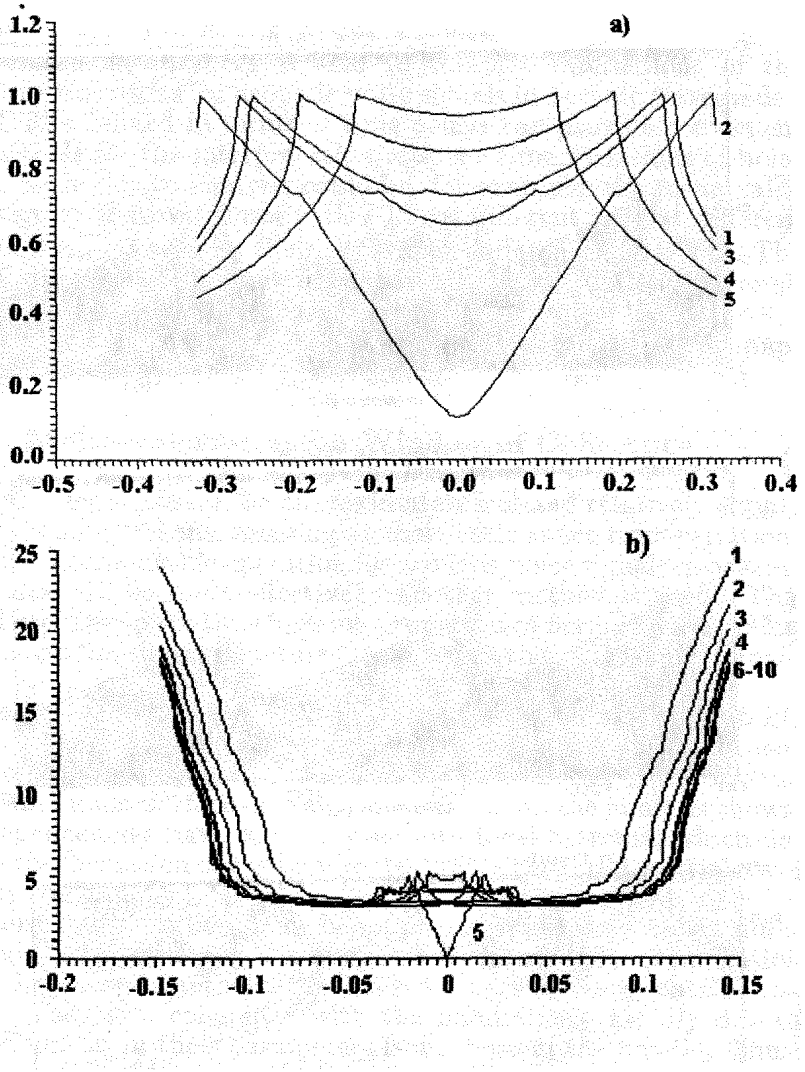

Fig. 5. Dependencies of ray cycle lengths on initial path angles $D(\alpha_j)$ for the bilinear (*a*) and under surface (*b*) oceanic waveguides (z_i = 50 m (*1*), 190 (*2*),1260 (*3*), 2000 (*4*), 2600 m (*5*); for bilinear waveguide and z_i = 50 m (*1*), 58 (*2*), 66 (*3*), 74 (*4*), 80 (*5*), 88 (*6*), 96 (*7*), 106 (*8*), 120 (*9*), 128 m (*10*); for under surface one).

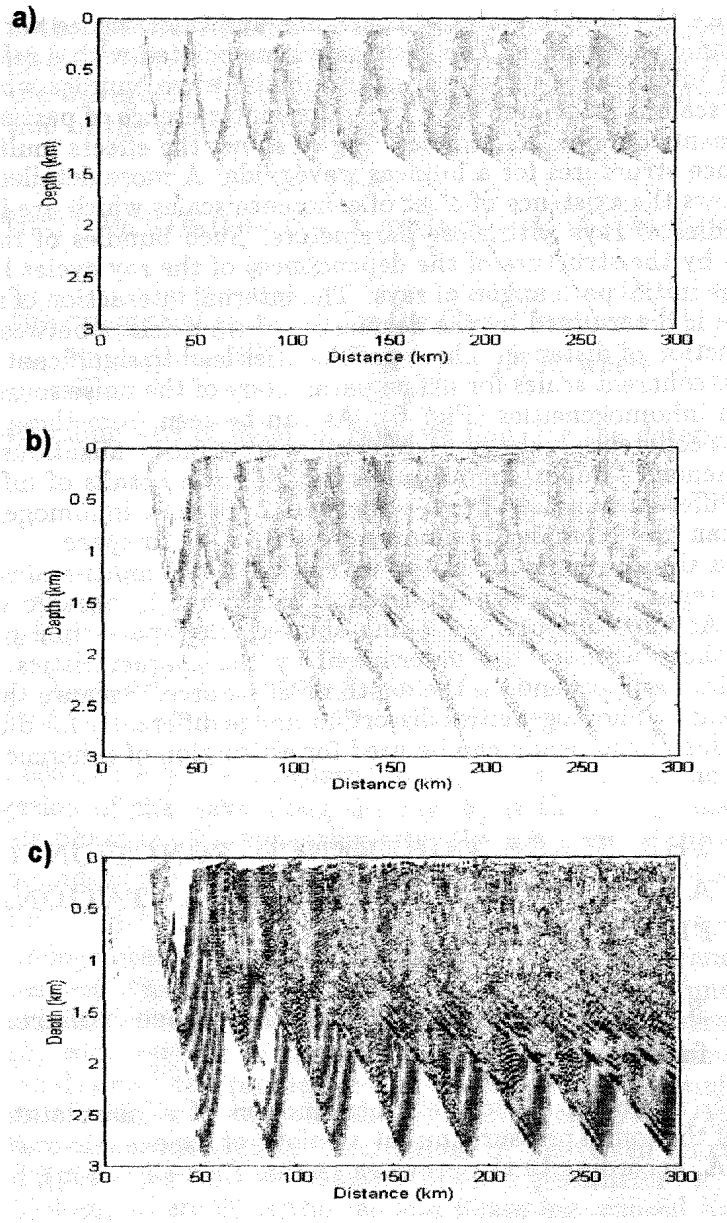

Fig. 6. Spatial distribution of VC for a bilinear oceanic waveguide, for different dispersians of fluctuation (τ_0 =0.001 sec. (*a*), 0.01 (*b*), 1 sec. (*c*); $\sigma = 0.01$, $\epsilon_0 = 0.01$).

introduce the double scales of coherence and interference variations for oceanic waveguides. The first scale is associated with a relatively smooth interference structure within partial wave bundles while the second scale is associated with the diffuse interference of partial wave components outside the bundles. Fig. 6 shows the effects multi-scale coherence structures for a bilinear waveguide. A more detailed analysis shows the existence of a set of coherence scales which are formed by bundles of rays with close parameters. Such bundles of rays are defined by the structure of the dependences of the ray cycles lengths from the initial path angles of rays. The internal interaction of rays in bundele is determined by the decreasing of time delays between rays as a function of distance. These paculiarities lead to significant differences in coherent scales for define parameters of the noise source and random inhomogeneities (Fig. 6). As can be seen from these maps, different coherence scales have different space-time localizations. This phenomenon is important for understanding the details of influence of the different bundles of rays with random oceanic inhomogeneities which can have complex nonuniform distribution in space.

For a simple physical picture, we can view this multi-scaleness as the existence of space-time coherence "windows" in oceanic waveguides. As the computer modeling showed, the space-time properties of these windows are determined by the characteristics of the waveguides and depend on the depth of the source. Because the random oceanic inhomogeneities distort an image differently for different scales, this phenomenon can be used for estimation of coherence windows.

2 THE SPACE COHERENCE FUNCTION OF A STATIONARY SOURCE IN A STATIONARY FLUCTUATING OCEAN

2.1 Ray-optical approach for the space coherence function

Let $k_\xi(\tau)$ be an autocorrelation function of a noise stationary source of the sound pressure, put at a point ξ of the oceanic waveguide (model A, according to the previous section's classification),

$$k_\xi(\tau) = \langle \xi(t)\xi^*(t+\tau) \rangle = \int_{-\infty}^{+\infty} \exp(i\omega\tau)\, d\mathrm{S}_\xi(\omega),$$

where $\mathbf{S}_\xi$ is the spectral function of the signal $\xi(t)$, $d\mathbf{S}_\xi(\omega) = \mathbf{S}_\xi(\omega)d\omega$.

Let $\eta_{(1,2)}(t) \equiv \eta\left(t, R_{(1,2)}\right)$ be signals received at the given points R_1, R_2 of the waveguide. In a nonrandom medium the mutual coherence function of the signals according to (4) is

$$k_\eta(R_1, R_2; \tau) = \langle \eta_1(t)\, \eta_2^*(t+\tau) \rangle = \int_{-\infty}^{+\infty} \exp(i\omega\tau)\, G_1(\omega)\, G_2^*(\omega)\, d\mathbf{S}_\xi(\omega)\,.$$

Using the ray-optical approach for the Green functions [1] $G_{(1,2)}(i\omega) = \sum_{j \in J_{(1,2)}} A_j^{(1,2)} e^{ikS_j^{(1,2)}}$, $S_j^{(1,2)} \equiv \int_{C_j^{(1,2)}} n(\mathbf{r})\, dl$, where $J_{(1,2)}$ are the corresponding sets of index of rays, we find, for the determined ocean,

$$\begin{aligned} & k_\eta(R_1, R_2; \tau) = \\ & = \sum_{j \in J_1} \sum_{j' \in J_2} A_j^{(1)} A_{j'}^{(2)} \int_{-\infty}^{+\infty} \exp\left(i\omega\tau + ik\left(S_j^{(1)} - S_{j'}^{(2)}\right)\right) d\mathbf{S}_\xi(\omega) = \\ & = \sum_{j \in J_1} \sum_{j' \in J_2} A_j^{(1)} A_{j'}^{(2)} \exp(i\Psi_{jj'}) \int_{-\infty}^{+\infty} \exp\left(i\omega\left(\tau + \tau_{jj'}\right)\right) d\mathbf{S}_\xi(\omega), \end{aligned} \tag{10}$$

where the eikonals $kS_j^{(1,2)}$ are replaced by $\omega\tau_j^{(1,2)} + \Psi_j^{(1,2)}$, τ_j is the time of propagation of the wave along the ray, Ψ_j is the supplementary determinate phase lag Ψ_j, appearing after the reflection of the wave from the bounds of the media and from the caustics, $\Psi_{jj'} \equiv \Psi_j^{(1)} - \Psi_{j'}^{(2)}$, and $\tau_{jj'} \equiv \tau_j^{(1)} - \tau_{j'}^{(2)}$.

In a random ocean the Green functions $G_{(1,2)}$ are also random, and independent from the $\xi(t)$. The mutual coherence function $k_\eta(R_1, R_2; \tau)$ in this case can be obtained by additional averaging of eq. (10) with respect to the statistics of the Green functions. Rigorous analysis of the problem requires taking into account the fluctuations of number of rays and the parameters of rays A_j, τ_j, Ψ_j [2, 22]. We can assume that the fluctuations of the Green functions are caused by independent fluctuations of their parameters A_j and $kS_j = \langle kS_j \rangle + \psi_j$, where ψ_j is the random phase lag, caused by the stochastic fluctuations of the refractive index. We consider the number of rays and their trajectories corresponding to the average profile of the waveguide.

For such an approach after complementary averaging, we obtain for the coherence function of the stationary noise source in the stationary fluctuating waveguide the following expression

$$k_\eta(R_1, R_2; \tau) = \sum_{j \in J_1} \sum_{j' \in J_2} \left\langle A_j^{(1)} A_{j'}^{(2)} \right\rangle \exp(i\Psi_{jj'}) \times \\ \times \int_{-\infty}^{+\infty} \exp(i\omega(\tau + \tau_{jj'})) \langle \exp(i\psi_{jj'}) \rangle \, d\mathbf{S}_\xi(\omega), \tag{11}$$

where $\psi_{jj'} \equiv \psi_j^{(1)} - \psi_{j'}^{(2)}$.

The statistical parts of the phases are

$$\psi_j^{(1,2)} = k \int_{C_j^{(1,2)}} \varepsilon(\mathbf{r}) \, dl, \tag{12}$$

where $\varepsilon(\mathbf{r})$ is the random fluctuations of the refractive index : $n(\mathbf{r}) = \langle n(\mathbf{r}) \rangle + \varepsilon(\mathbf{r})$. If the distribution of $\varepsilon(\mathbf{r})$ is of Gaussian form with the correlation function $\Phi(\mathbf{r}_1, \mathbf{r}_2) \equiv \langle \varepsilon(\mathbf{r}_1) \varepsilon(\mathbf{r}_2) \rangle$, then according to the central limit theorem the statistics of vectors $\left(\psi_1^{(1,2)} \ldots, \psi_n^{(1,2)}\right)$ is Gaussian too, with mean values $\left\langle \psi_j^{(1,2)} \right\rangle = 0$ and with the correlation matrix

$$\frac{1}{k^2} \left\langle \psi_j^{(i_1)} \psi_{j'}^{(i_2)} \right\rangle = \left\langle \int_{C_j^{(i_1)}} \varepsilon(\mathbf{r}) \, dl \int_{C_{j'}^{(i_2)}} \varepsilon(\mathbf{r}) \, dl \right\rangle = \\ = \int_0^{l_j^{(i_1)}} ds_1 \int_0^{l_{j'}^{(i_2)}} \left\langle \varepsilon\left(\mathbf{r}_j^{(i_1)}(s_1)\right) \varepsilon\left(\mathbf{r}_{j'}^{(i_2)}(s_2)\right) \right\rangle ds_2 = \\ = \int_0^{l_j^{(i_1)}} ds_1 \int_0^{l_{j'}^{(i_2)}} \Phi\left(\mathbf{r}_j^{(i_1)}(s_1), \mathbf{r}_{j'}^{(i_2)}(s_2)\right) ds_2 \equiv m_{jj'}^{(i_1 i_2)}, \tag{13}$$

where $i_1, i_2 = \overline{1,2}$, $\mathbf{r}_j^{(1,2)}(s)$ are the radius-vectors, $l_j^{(1,2)}$ are the lengths of the corresponding rays.

Using the properties of Gaussian distribution, we can find the mean values

$$\langle \exp(i\psi_{jj'}) \rangle = \exp\left(-\langle \psi_{jj'}^2 \rangle / 2\right) =$$
$$= \exp\left(\left\langle \psi_j^{(1)} \psi_{j'}^{(2)} \right\rangle - \left(\left\langle \left(\psi_j^{(1)}\right)^2 \right\rangle + \left\langle \left(\psi_{j'}^{(2)}\right)^2 \right\rangle\right)/2\right) =$$
$$= \exp\left(-\left(\frac{T_{jj'}\omega}{2}\right)^2\right),$$
$$T_{jj'}^2 \equiv \frac{4}{c_0^2}\left(\frac{m_{jj}^{(11)} + m_{j'j'}^{(22)}}{2} - m_{jj'}^{(12)}\right).$$

Putting this expressions into (11), we obtain the space coherence function in the form

$$k_\eta(R_1, R_2; \tau) = \sum_{j \in J_1} \sum_{j' \in J_2} \left\langle A_j^{(1)} A_{j'}^{(2)} \right\rangle \exp(i\Psi_{jj'})\, k_{jj'}(\tau + \tau_{jj'}), \qquad (14)$$

$$k_{jj'}(\tau) \equiv \int_{-\infty}^{+\infty} \exp\left(i\omega\tau - \left(\frac{T_{jj'}\omega}{2}\right)^2\right) d\mathbf{S}_\xi(\omega).$$

For example, for autocorrelation function of noise source

$$k_\xi(\tau) = k_\xi(0) \exp\left(-\left(\frac{\tau}{\tau_0}\right)^2 - i\omega_0\tau\right), \qquad (15)$$

where τ_0 is the time of coherence of the source noise, and ω_0 is the basic frequency, we have

$$k_{jj'}(\tau) \equiv k_\xi(0) \frac{\tau_0}{2\sqrt{\pi}} \int_{-\infty}^{+\infty} \exp\left(i\omega\tau - \frac{T_{jj'}^2\omega^2}{4} - \frac{(\omega+\omega_0)^2\tau_0^2}{4}\right) d\omega =$$
$$= k_\xi(0)\sqrt{q_{jj'}} \exp\left(-q_{jj'}\left(\left(\frac{\tau}{\tau_0}\right)^2 + \left(\frac{\omega_0 T_{jj'}}{2}\right)^2 + i\omega_0\tau\right)\right) = \qquad (16)$$
$$= k_{jj'}(0) \exp\left(-\frac{\tau^2}{\tau_0^2 + T_{jj'}^2}\right) \exp(-i\omega_0 q_{jj'}\tau),$$
$$q_{jj'} \equiv \frac{\tau_0^2}{T_{jj'}^2 + \tau_0^2} = \frac{1}{1 + (T_{jj'}/\tau_0)^2}.$$

By analysis of formulas (14, 16) we can see the important role of the values $T_{jj'}^2$ in the formation of functions $k_{jj'}(\tau)$ and, therefore, of the space coherence function $k_\eta(R_1, R_2; \tau)$. The terms with comparatively small values of $T_{jj'}^2$ $\left(T_{jj'}^2 \simeq \tau_0^2\right)$ give the main contribution to

the sum in eq. (14). The value $T_{jj'}$ has the measure of time. For given statistics of $\varepsilon(\mathbf{r})$ this value depends only on the mutual geometry of rays j and j' and tends to zero when the trajectories of rays tends to each other. In contrast to the *geometric difference of times* $\tau_{jj'}$ it may be called the *statistical difference of times* between the rays [22]. As it follows from expressions (14) and (16), the decrease of statistical differencies of times between the rays lead to the distortion of the coherence. If the dispersion of $T_{jj'}$ is determined, then the structure, formed by rays with large differencies of parameters, will lose coherence first. The beams due to the locally smooth extrema in angle distributions of rays, are formed by rays with slightly different parameters. Such beams will save the coherence.

Using the formulas outlined in the previous sections, we now study the influence of random inhomogeneities in the oceanic environment on coherence of radiated noise in detail. Let us define the physical model of random oceanic inhomogeneities and investigate the coherence of acoustical signals as the function of the characteristics of a noise acoustic source and parameters of random oceanic inhomogeneities.

In the next section we consider only the case of stratified ocean $c = c(z)$ with a spatially homogeneous distribution of random fluctuations of index $n(\mathbf{r})$ (when the autocorrelation function $\Phi(\mathbf{r}_1, \mathbf{r}_2)$ depends only on difference $\mathbf{r}_1 - \mathbf{r}_2$: $\Phi(\mathbf{r}_1, \mathbf{r}_2) \equiv \varphi(\mathbf{r}_1 - \mathbf{r}_2)$). To be exact, let us consider the following approach for the correlative function [1, 10, 23]:

$$\Phi(\mathbf{r}_1, \mathbf{r}_2) = \varepsilon_0^2 \exp\left(-\frac{1}{2}\left[\frac{(x_1 - x_2)^2}{\sigma_x^2} + \frac{(z_1 - z_2)^2}{\sigma_z^2}\right]\right). \qquad (17)$$

Here ε_0^2 is the dispersion of fluctuations, σ_x, σ_z are the horizontal and vertical scales of correlation, respectively.

In different practical situations, the physical model of oceanic inhomogeneities can give good results describing, for example, the thermohaline fine structure of perturbations of the sound velocity the in ocean [1]. Taking into account the aim of our investigation, we focus on the analysis of the influence of random inhomogeneities on the coherence of bundles and diffusion part of the acoustic field using this simple type of inhomogeneities in the analysis. As for other types of oceanic inhomogeneities, such as internal waves, turbulence pulsations, and so on, it will be the next spatial stage of research.

2.2 Dispersion of fluctuations $m_{jj}^{1,1}$

Let us estimate the dispersion of fluctuations of the phase in eq. (12) for the rays which are described by the equation $\mathbf{r} = \mathbf{r}(s)$, $s =$

$\overline{0,l}$. Generally, we find, from (13),

$$\frac{1}{k^2}\left\langle(\psi_{jj}^{1,1})^2\right\rangle = \int_0^l\int_0^l \Phi(\mathbf{r}(s_1),\mathbf{r}(s_2))\,ds_1 ds_2 = \\ = \int_0^l\int_0^l \varphi(\mathbf{r}(s_1)-\mathbf{r}(s_2))\,ds_1 ds_2. \tag{18}$$

It can be seen, that using model (17), the dispertion of fluctuations $m_{jj}^{1,1}$ is defined by the differencies of the ray trajectories. To continue analysis, let us discuss two limiting cases of fluctuations, in particular, the cases associated with very long and very short scales of inhomogeneities.

2.2.1 Fluctuations with large spatial scales

If the spatial scales of correlations of the refractive index σ_x, σ_z are large in comparison with the size of the waveguide, then, as is evident from (18),

$$m_{jj}^{1,1} = \langle\psi^2\rangle \simeq k^2\varepsilon_0^2 l^2 = \left(\frac{\omega\varepsilon_0 l}{c_0}\right)^2.$$

2.2.2 Fluctuations with large horizontal scales

For a more typical case where the horizontal scale σ_x essentially exceeds the lenth of acoustic path among the source and observation point we can, formally setting in (17) $\sigma_x = \infty$, consider $\varphi(\mathbf{r}_1-\mathbf{r}_2) \equiv \varphi(z_1-z_2)$. The expression (18) now can be transformed to the form

$$\frac{1}{k^2}\left\langle(\psi_{jj}^{11})^2\right\rangle = \int_0^l\int_0^l \varphi(z(s_1)-z(s_2))\,ds_1 ds_2 = \\ = \int_{z_<}^{z_>}\int_{z_<}^{z_>} \varphi(z_1-z_2)\,K(z_1)\beta(z_1)\,K(z_2)\beta(z_2)\,dz_1 dz_2 = \\ = \varepsilon_0^2 \int_{z_<}^{z_>}\int_{z_<}^{z_>} \exp\left(-\frac{(z_1-z_2)^2}{2\sigma_z^2}\right) d\mathcal{L}_1 d\mathcal{L}_2, \tag{19}$$

where $\beta(z) \equiv \sqrt{1+(x'(z))^2}$, $K(z)$ is the number of intersections by the ray of the horizon z, $z_<, z_>$ are the lower and upper horizons, respectively, of turning of the ray, $d\mathcal{L}(z) \equiv K(z)\beta(z)\,dz$ are the summarize length of all segments of the ray entering the horizontal window $(z, z+dz)$. The value of the last integral depends on the ratio of the vertical scales $\Delta Z \equiv z_> - z_<$ and σ_z.

- Case $\sigma_z/\Delta Z \gg 1$.

  In this case, the exponent under the integral (19) is approximately equal 1, as it was in the case with long fluctuations (see section 2.2.1)

- Case $\sigma_z/\Delta Z \ll 1$. A more interesting situation for description of real conditions in oceanic environment takes place in the case where the vertical sizes of inhomogeneities are smaller relative to ΔZ. Changing the variables $z \equiv (z_1 + z_2)/2$, $p \equiv z_1 - z_2$ in the double integral (19), we obtain the iterated integral

$$\int_{z_<}^{z_>} dz \int_{-p_1(z)}^{p_1(z)} \exp\left(-\frac{p^2}{2\sigma_z^2}\right) K(z+p/2) \times$$
$$\times \beta(z+p/2) K(z-p/2) \beta(z-p/2)\, dp,$$

  where

$$p_1(z) \equiv \begin{cases} 2(z - z_<), & z_< < z < (z_< + z_>)/2 \\ 2(z_> - z), & (z_< + z_>)/2 < z < z_>. \end{cases}$$

  Taking into account the high speed of variability of the exponent, we replace the finite limits of integration in the internal integral to the infinite limits. Replacing also the arguments of other slow functions to z, we find after integration with respect to the variable p and utilization of the Cauchy - Bounyakovsky integral inequality, the low estimation of the dispersion

$$\frac{1}{k^2}\left\langle (\psi_{jj}^{1,1})^2 \right\rangle \simeq \sqrt{2\pi}\varepsilon_0^2 \sigma_z \int_{z_<}^{z_>} K^2(z)\beta^2(z)\, dz \geq$$
$$\geq \sqrt{2\pi}\varepsilon_0^2 \frac{\sigma_z}{\Delta Z}\left(\int_{z_<}^{z_>} K(z)\beta(z)\, dz\right)^2 = \sqrt{2\pi}\varepsilon_0^2 \frac{\sigma_z}{\Delta Z} l^2.$$

  Although the connection with l^2 are saved, the fluctuations decreased by a factor of $\frac{\sigma_z}{\Delta Z}$.

2.2.3 Fluctuations of small spatial scales

Let the scales of fluctuations $\sigma_z \ll \Delta Z$, $\sigma_x \ll D$, where D is the horizontal cycle of the ray. Since for stratified medium any ray lies in

a vertical plane, it can be parametrized by the longitudinal coordinate x : $\mathbf{r} = \mathbf{r}(x)$, $0 \le x \le X$. So

$$\frac{1}{k^2}\left\langle (\psi_{jj}^{1,1})^2 \right\rangle = \int_0^X dx_1 \int_0^X \varphi(x_1 - x_2, z(x_1) - z(x_2))\,\alpha(x_1)\,\alpha(x_2)\,dx_2,$$

where $X \equiv |x_\xi - x_R|$ is the distance between points ξ and R in the horizontal plane and $\alpha(x) \equiv \sqrt{1 + (z'(x))^2}$.

Replacing the variables x_1, x_2 in the last double integral by new variables $x \equiv (x_1 + x_2)/2$, $\rho \equiv x_1 - x_2$ and taking into account the variability speeds of the corresponding functions , we find

$$\frac{1}{k^2}\left\langle (\psi_{jj}^{1,1})^2 \right\rangle = \int_0^X dx \int_{-\rho_1(x)}^{\rho_1(x)} \alpha\left(x + \frac{\rho}{2}\right)\alpha\left(x - \frac{\rho}{2}\right) \times$$
$$\times \varphi\left(\rho, z\left(x + \frac{\rho}{2}\right) - z\left(x - \frac{\rho}{2}\right)\right) d\rho \simeq$$

$$\simeq \varepsilon_0^2 \int_0^X \alpha^2(x) \int_{-\infty}^{+\infty} \exp\left(-\frac{\rho^2}{2}\left(\frac{1}{\sigma_x^2} + \frac{(z'(x))^2}{\sigma_z^2}\right)\right) dx =$$
$$= \sqrt{2\pi}\varepsilon_0^2 \int_0^X \frac{\alpha^2(x)}{\sqrt{\frac{1}{\sigma_x^2} + \frac{(z'(x))^2}{\sigma_z^2}}} dx = \lambda \int_0^X \sqrt{\frac{1 + (z'(x))^2}{\vartheta + \vartheta^{-1}(z'(x))^2}}\, dx,$$

where $\lambda \equiv \sqrt{2\pi}\varepsilon_0^2\sigma$, $\sigma \equiv \sqrt{\sigma_x \sigma_z}$, $\vartheta \equiv \sigma_z/\sigma_x$,

$$\rho_1(x) \equiv \begin{cases} 2x, & 0 < x < X/2 \\ 2(X - x), & X/2 < x < X. \end{cases}$$

The function

$$\sqrt{\frac{1+u}{\vartheta^2 + u}},$$

which is used in the last integral, decreases monotonically in the region $u \ge 0$ and lies in the interval $\left(1, \frac{1}{\vartheta}\right)$. Thus, we can do the following estimation of the integral

$$\int_C \sqrt{\frac{1 + (z'(x))^2}{\vartheta^2 + (z'(x))^2}}\, dl = \frac{\chi(\vartheta)}{\vartheta} l,$$

where $0 < \chi(\vartheta) \le 1$, $\chi(1) = 1$.

Thus, the dispersion is given by

$$\frac{1}{k^2}\left\langle \psi^2 \right\rangle \simeq \sqrt{2\pi}\varepsilon_0^2 \sigma \frac{\chi(\vartheta) l}{\sqrt{\vartheta}}.$$

Let us note, that in contrast to the previous cases, the dispersion increases proportionally to the length of a ray. It can be interpreted as the coherent and noncoherent summation of fluctuations along the acoustic paths of rays due to large or short scales of inhomogeneities, respectively.

2.3 Mutual correlation moment $m_{jj'}^{1,1}$

Let us estimate the mutual correlation moment of the phase fluctuations on the rays $\mathbf{r} = \mathbf{r}_1(s)$, $s = \overline{0, l_1}$ and $\mathbf{r} = \mathbf{r}_2(s)$, $s = \overline{0, l_2}$. In the general case, we have, from (13),

$$\begin{aligned} m_{jj'}^{12} \equiv \tfrac{1}{k^2}\left\langle \psi_j^1 \psi_{j'}^2 \right\rangle &= \int_0^{l_1}\int_0^{l_2} \Phi\left(\mathbf{r}_1(s_1), \mathbf{r}_2(s_2)\right) ds_1 ds_2 = \\ &= \int_0^{l_1}\int_0^{l_2} \varphi\left(\mathbf{r}_1(s_1) - \mathbf{r}_2(s_2)\right) ds_1 ds_2. \end{aligned} \tag{20}$$

2.3.1 Large space-scale fluctuations

If the space correlation scales of the refractive index σ_x, σ_z are large in comparison with the size of the waveguide, then from (20) we find

$$m_{jj'}^{12} \simeq \varepsilon_0^2 l_1 l_2.$$

Assume, as in section 2.2.2, that the horizontal scale of the fluctuations σ_x exceeds essentially the horizontal size of the waveguide. Then we set $\varphi(\mathbf{r}_1 - \mathbf{r}_2) \equiv \varphi(z_1 - z_2)$. The expression (20) transforms to

$$\begin{aligned} m_{jj'}^{12} &= \int_0^{l_1}\int_0^{l_2} \varphi\left(z_1(s_1) - z_2(s_2)\right) ds_1 ds_2 = \\ &= \int_{z_<^{(1)}}^{z_>^{(1)}}\int_{z_<^{(2)}}^{z_>^{(2)}} \varphi(z_1 - z_2) K_1(z_1) \beta_1(z_1) K_2(z_2) \beta_2(z_2) dz_1 dz_2 = \\ &= \varepsilon_0^2 \int_{z_<^{(1)}}^{z_>^{(1)}}\int_{z_<^{(2)}}^{z_>^{(2)}} \exp\left(-\tfrac{(z_1 - z_2)^2}{2\sigma_*^2}\right) d\mathcal{L}_1 d\mathcal{L}_2, \end{aligned}$$

where the parameters $z^{(1,2)}_{(<,>)}$, $K_{(1,2)}$, *and* $\beta_{(1,2)}$ are the same, as in section 2.2.2.

Let $z_< \equiv \max\left(z^{(1)}_<, z^{(2)}_<\right)$, $z_> \equiv \min\left(z^{(1)}_>, z^{(2)}_>\right)$, *and* $\Delta Z \equiv z_> - z_<$. In the limiting cases, as in the previouse section, the value $m^{12}_{jj'}$ can be estimated easily.

- Case $\sigma_z/\Delta Z \gg 1$.

  Here we have, similar to the case of a large scale

$$m^{12}_{jj'} = \varepsilon_0^2 l_1 l_2.$$

- Case $\sigma_z/\Delta Z \ll 1$.

  Taking into account the high speed of variability of the exponent in the integral, we find, by analogy with section 2.2.2, the upper estimate of the mutual statistical moment

$$m^{12}_{jj'} = \varepsilon_0^2 \int_{z^{(1)}_<}^{z^{(1)}_>} \int_{z^{(2)}_<}^{z^{(2)}_>} \exp\left(-\tfrac{(z_1-z_2)^2}{2\sigma_z^2}\right) d\mathcal{L}_1 d\mathcal{L}_2 \simeq$$

$$\simeq \varepsilon_0^2 \int_{z_<}^{z_>} \int_{z_<}^{z_>} \exp\left(-\tfrac{(z_1-z_2)^2}{2\sigma_z^2}\right) d\mathcal{L}_1 d\mathcal{L}_2 \simeq$$

$$\simeq \varepsilon_0^2 \int_{z_<}^{z_>} K_1(z)\,\beta_1(z)\,K_2(z)\,\beta_2(z)\,dz \int_{-\infty}^{\infty} \exp\left(-\tfrac{p^2}{2\sigma_z^2}\right) dp =$$

$$= \sqrt{2\pi}\varepsilon_0^2 \sigma_z \int_{z_<}^{z_>} K_1(z)\,\beta_1(z)\,K_2(z)\,\beta_2(z)\,dz \leq$$

$$\leq \sqrt{2\pi}\varepsilon_0^2 \tfrac{\sigma_z}{\Delta Z} \tilde{l}_1 \tilde{l}_2.$$

  Here $\tilde{l}_{(1,2)}$ are the summary lengths of arcs of rays, entering the vertical layer $z_< \leq z \leq z_>$. In the particular case where $z_< \equiv z^{(1)}_<$, $z_> \equiv z^{(1)}_>$, we have $\tilde{l}_1 = l_1$; if one of rays continues the other, then $\tilde{l}_{(1,2)} = l_{(1,2)}$.

2.3.2 Small space-scale fluctuations

Parametrizing the rays by the longitudinal coordinate x: $\mathbf{r} = \mathbf{r}_1(x)$, $x = \overline{0, X_1}$, $\mathbf{r} = \mathbf{r}_2(x)$, $x = \overline{0, X_2}$, we obtain, as in section 2.2.3,

$$m^{12}_{jj'} = \int_0^{X_1} \int_0^{X_2} \varphi(\mathbf{r}_1(x_1) - \mathbf{r}_2(x_2))\,\alpha_1(x_1)\,\alpha_2(x_2)\,dx_1 dx_2.$$

Replacing the variables x_1 and x_2 in this double integral by new variables x and ρ, we find the integral

$$\int_0^X dx \int_{-\rho_1(x)}^{\rho_2(x)} \alpha_1\left(x+\tfrac{\rho}{2}\right)\alpha_2\left(x-\tfrac{\rho}{2}\right)\times \\ \times\varphi\left(\rho, z_1\left(x+\tfrac{\rho}{2}\right)-z_2\left(x-\tfrac{\rho}{2}\right)\right)d\rho, \tag{21}$$

where $X \equiv (X_1+X_2)/2$,

$$\rho_i(x) \equiv \begin{cases} 2x, & 0<x<X_i/2 \\ 2(X_i-x), & X/2<x<X \end{cases}, \quad i=\overline{1,2}.$$

In respect to the similar assumptions made in the previouse section, let the values σ_x, σ_z be small in comparison with the variation scales of the functions $z_{1,2}$. In this case, we can change the corresponding expressions in (21) by their asymptotic forms:

$$z_1\left(x+\tfrac{\rho}{2}\right)-z_2\left(x-\tfrac{\rho}{2}\right) \simeq \Delta z_{12}(x)+\rho d_{12}(x), \\ \alpha_{1,2}\left(x\pm\tfrac{\rho}{2}\right) \simeq \alpha_{1,2}(x),$$

$$\Delta z_{12}(x) \equiv z_1(x)-z_2(x),\ d_{12}(x) \equiv \frac{z_1'(x)+z_2'(x)}{2}.$$

After such exchange and integrating with respect to ρ in infinite bounds, we have

$$m_{jj'}^{12} \simeq \epsilon_0^2 \int_0^{\tilde{X}} dx \alpha_1(x)\alpha_2(x)\exp\left(\tfrac{\Delta z_{12}^2(x)}{2\sigma_z^2}\right)\times \\ \times\int_{-\infty}^{+\infty}\exp\left(-\frac{\rho^2}{2}\left(\tfrac{1}{\sigma_x^2}+\tfrac{d_{12}^2(x)}{\sigma_z^2}\right)-\rho\tfrac{\Delta z_{12}(x)d_{12}(x)}{\sigma_z^2}\right)d\rho \equiv \lambda\delta_{12},$$

$$\delta_{12} \equiv \int_0^{\tilde{X}} \frac{\alpha_1(x)\alpha_2(x)}{\sqrt{\vartheta+\vartheta^{-1}d_{12}^2(x)}}\exp\left(-\frac{\Delta z_{12}^2(x)}{2\sigma^2(\vartheta+\vartheta^{-1}d_{12}^2(x))}\right)dx, \tag{22}$$

where $\tilde{X} \equiv \min\{X_1, X_2\}$.

To estimate the values δ_{12} let us select the next two cases.

- The case where the ray number 2 is the continuation of the ray number 1 or, in other words, points $R_{1,2}$ belong to one ray and $l_2 > l_1$.

Here, we have

$$\delta_{12} = \int_0^{\tilde{X}} \frac{(\alpha_1(x))^2}{\sqrt{\vartheta + \vartheta^{-1}\left(z_1'(x)\right)^2}} dx = \\ = \sqrt{\vartheta} \int_{C_1} \sqrt{\frac{1+\left(z_1'(x)\right)^2}{\vartheta^2+\left(z_1'(x)\right)^2}} dl.$$

In a manner similar to that used in section 2.2.3, we find

$$\delta_{12} = \frac{\chi_1(\vartheta)\, l_1}{\sqrt{\vartheta}},$$

where $0 < \chi_1(\vartheta) \leq 1,\ \chi_1(1) = 1$.

In the particular case where $\sigma_z = \sigma_x$ $(\vartheta = 1)$, we have

$$\delta_{12} = l_1.$$

- The case, where the points $R_{1,2}$ do not belong to one ray.

  In this case, the values δ_{12} tends to zero when $\sigma \to 0$. The neighborhoods of the points $(x_l, z(x_l))$ of intersection of rays do the main contribution to integral (22). To estimate δ_{12} let us approximate the functions z_1, z_2 in these neighborhoods by linear terms of the Taylor series. After integration we arrive at

$$\delta_{12} = \sigma \sum_l \nu_l \sqrt{\frac{\left(1+\left(z_1'(x_l)\right)^2\right)\left(1+\left(z_2'(x_l)\right)^2\right)}{\left(z_1'(x_l)-z_2'(x_l)\right)^2}} = \\ = \sigma \sum_l \frac{\nu_l}{\sin\left|\theta_l^1 - \theta_l^2\right|},$$

  where $\nu_l = \sqrt{\pi/2}$ for boundary points (source ξ and receiver R) and $\nu_l = \sqrt{2\pi}$ for other points of intersection, θ_l^j is the sliding angle of the ray with number j at the point of intersection $(x_l, z(x_l))$.

· The number of intersections of rays significantly decrease if the points of observation $R_{1,2}$ are close one to another. If the space duration among points of observation increases, the number of intersections can be small.

2.4 Statistic time-difference between rays

As the final result of the above investigations, we have the following formulas for the parameter $T_{jj'}^2$.

- In the case of short-scale fluctuations of the refractive index associated with the noncoherent summation of fluctuations (see sections 2.2.3 and 2.3.2)

$$T_{jj'}^2 \simeq 4\sqrt{2\pi}\frac{\varepsilon_0^2}{c_0^2}\sigma\left(\frac{\chi_j l_j + \chi_{j'} l_{j'}}{2\sqrt{\vartheta}} - \sigma\sum_l \frac{\nu_l}{\sin\left|\theta_l^j - \theta_l^{j'}\right|}\right),$$

if the rays j and j' do not continue each other, otherwise

$$T_{jj'}^2 \simeq 4\sqrt{\frac{2\pi}{\vartheta}}\frac{\varepsilon_0^2}{c_0^2}\sigma\left(\frac{\chi_j l_j + \chi_{j'} l_{j'}}{2} - \chi_{jj'}(\vartheta)\min\{l_j, l_{j'}\}\right),$$

When $\sigma_z = \sigma_x$ $(\vartheta = 1)$ these formulas are given by

$$T_{jj'}^2 \simeq 4\sqrt{2\pi}\frac{\varepsilon_0^2}{c_0^2}\sigma\left(\frac{l_j + l_{j'}}{2} - \sigma\sum_l \frac{\nu_l}{\sin\left|\theta_l^j - \theta_l^{j'}\right|}\right) \tag{23}$$

and

$$T_{jj'}^2 \simeq 2\sqrt{2\pi}\frac{\varepsilon_0^2}{c_0^2}\sigma\left|l_j - l_{j'}\right|, \tag{24}$$

respectively.

Let us discuss in detail the formula (23). If the initial sliding angles of the rays differ essentially $\left(\left|\theta_1^j - \theta_1^{j'}\right| \gg \sigma/\tilde{X}\right)$, then so do the sliding angles at other points of intersection. For such pairs of rays the sum $\sigma\sum_l \nu_l \sin^{-1}\left|\theta_l^j - \theta_l^{j'}\right|$ is small in comparison with $(l_j + l_{j'})/2$ and

$$T_{jj'}^2 \simeq 2\sqrt{2\pi}\frac{\varepsilon_0^2}{c_0^2}\sigma\left(l_j + l_{j'}\right).$$

On the contrary, for pairs of rays with closed initial angles their sliding angles at other points of intersection are closed too. Let us estimate the corresponding terms in the sum (23). According to Snell's law for a stratified medium

$$q_l \cos\theta_l = \cos\theta_1,$$

where $q_l \equiv n(z_l)/n_\xi$, $n_\xi \equiv n(z_\xi)$. Hence, for small values $\Delta\theta_1$

$$\left|q_l \sin(\theta_l)\,\Delta\theta_l\right| \simeq \left|\sin(\theta_1)\,\Delta\theta_1\right|,$$

$$\left|\frac{1}{\sin(\Delta\theta_l)}\right| \simeq \left|\frac{1}{\Delta\theta_l}\right| \simeq \left|\frac{q_l \sin(\theta_l)}{\sin(\theta_1)\Delta\theta_1}\right| =$$
$$= \left|\frac{q_l\sqrt{1-\cos^2(\theta_l)}}{\sin(\theta_1)\Delta\theta_1}\right| = \frac{1}{|\Delta\theta_1|}\sqrt{q_l^2 + (q_l^2-1)\,ctg^2(\theta_1)}.$$

As $q_l \simeq 1$, then for pairs of similar rays, which do not belong to the neighborhood of the singular ray $\theta_1 = 0$, we have

$$\sigma \sum_l \frac{\nu_l}{\sin\left|\theta_l^j - \theta_l^{j'}\right|} \simeq \frac{\sigma}{|\Delta\theta_1|}\sum_l \nu_l \sqrt{q_l^2 + (q_l^2-1)\,ctg^2(\theta_1)} \simeq$$
$$\simeq \frac{\sigma}{|\Delta\theta_1|}(k-1)\sqrt{2\pi},$$

where k is the total number of points of intersection of rays (including initial and final points ξ and R). Therefore, for such pairs of rays

$$T_{jj'}^2 \simeq 4\sqrt{2\pi}\frac{\varepsilon_0^2}{c_0^2}\sigma\left(\frac{l_j + l_{j'}}{2} - \frac{\sigma}{|\Delta\theta_1|}(k-1)\sqrt{2\pi}\right). \qquad (25)$$

- In the case of fluctuations of large horizontal scales (see section 2.2.2)

$$T_{jj'}^2 \geq 4\sqrt{2\pi}\frac{\varepsilon_0^2}{c_0^2}\frac{\sigma_z}{\Delta Z}\left(\frac{l_j^2 + l_{j'}^2}{2} - \tilde{l}_j\tilde{l}_{j'}\right) \qquad (26)$$

when $\sigma_z/\Delta Z \ll 1$, or

$$T_{jj'}^2 \simeq 2\frac{\varepsilon_0^2}{c_0^2}(l_j - l_{j'})^2. \qquad (27)$$

when $\sigma_z/\Delta Z \gg 1$.

- In the case of large-scale fluctuations (see sections 2.2.1 and 2.3.1)

$$T_{jj'}^2 \simeq 2\frac{\varepsilon_0^2}{c_0^2}(l_j - l_{j'})^2. \qquad (28)$$

As mentioned above, the terms corresponding to pairs of rays with minimal values of the parameter $T_{jj'}^2$ do the main contribution to the coherence function (14). The above formulas make it possible to study typical features of such pairs of rays and, therefore, estimate the possibility of their occurrence in different areas of the ocean.

In the case of large-scale fluctuations, small values of the parameter $T_{jj'}$ are typical for pairs with close geometrical lengths (see (28)).

The reason of it is as follows: fluctuations in different regions of the waveguide are similar, so the total random phase lag is simply proportional to the length of the ray. As $l_j^{(i)} \simeq c_0 \tau_j$, then $|T_{jj'}| \simeq \sqrt{2}\varepsilon_0 |\tau_{jj'}|$ and, therefore, for such pairs the parameter $\tau_{jj'}$ is also small. The existence of such pairs is probable for all far distances in an oceanic waveguide.

Conversely, for small-scaled fluctuations, the random phase lag depends not only on the length of the ray, but also on its location. In this case, small values of the parameter $T_{jj'}^2$ can be realized only for the pair of geometrically close rays, which transfer through the same small-scale local inhomogeneities. In particular, the parameter $T_{jj'}^2$ is small for rays that continue each other (see formula (24)), if only their lengths are close to each other.

For rays with different output angles the formula (25) makes it possible to do upper estimation for the difference of the output angles $\Delta\theta_1$, for which the parameter $T_{jj'}^2$ is less than the preset value, for example, τ_0^2. In particular, for rays entering one point, such estimation is

$$|\Delta\theta| \leq \frac{\sigma(k-1)\sqrt{2\pi}}{\bar{l} - \frac{l_0^2}{2\lambda}},$$

where $l_0 \equiv c_0\tau_0$, $\bar{l} \equiv (l_j + l_{j'})/2$. Since $\bar{l} \simeq (k-2)D$, then for waves with $l_0 \simeq \sigma \ll \bar{l}$ for the difference of the output angles the following rough estimation is valid

$$|\Delta\theta_1| \leq \frac{2\sigma(k-1)}{\bar{l}} \simeq \frac{2\sigma}{D}.$$

For example, for natural values of the parameters $\sigma \simeq 0.1$, $D \simeq 20\,(km)$ we have $|\Delta\theta_1| \leq 0.01$. Since the corresponding rays must enter one point, then it is possible only for rays, belonging to the so called *weakly diverging bundles (WDB)* [21, 22], for which $dD/d\theta \simeq 0$. Hence, we expect the localization of small values of the parameter $T_{jj'}^2$ in the neighborhoods of weakly diverging bundles. The differences of times $\tau_{jj'}$ in these neighborhoods are also small, which follows from the properties of WDB (see, for example, [21]). However, the last parameter, in principle, also can be small for pair of rays, which do not belong to WDB.

2.5 Coherence function of the received signal

Detailed analysis of the problem consists in the investigation of the space and time coherence structure, for example, scales of space

and time coherence, for receiving signals, propagating along acoustic path in oceanic waveguide as the function of noise parameters of acoustical source and parameters of volume (and surface, in general) inhomogeneities of oceanic environment, as well as the waveguide characteristics. Taking into account our aim associated with the investigation of the phenomena of multiscale coherence due to local extrema in dispersive connections of rays (partial waves, in general), we decrease our problems to study the vision of interference structure coefficients β. This value is defined by the coherence function of received signals, as was discussed in the previous section. In the case of random inhomogeneities they can give us the possibilities to characterize the decrease in the acoustic field coherence in an oceanic waveguide due to random inhomogeneities in the analysis of multiscale coherence phenomena.

Acording to this aim, putting $R_1 = R_2 = R$ to (14) we find the coherence function of the signal received at point R:

$$
\begin{aligned}
k_\eta(\tau) \equiv k_\eta(R, R; \tau) = \\
= \sum_{j \in J} \sum_{j' \in J} \langle A_j A_{j'} \rangle \exp(i\Psi_{jj'}) k_{jj'}(\tau + \tau_{jj'}) = \\
= \sum_{j \in J} \langle A_j^2 \rangle k_\xi(\tau) + \sum_{j \neq j'} \langle A_j A_{j'} \rangle \exp(i\Psi_{jj'}) k_{jj'}(\tau + \tau_{jj'}) = \\
= \sum_{j \in J} \langle A_j^2 \rangle \left(k_\xi(\tau) + \sum_{j > j'} p_{jj'} \times \right. \\
\left. \times (\exp(i\Psi_{jj'}) k_{jj'}(\tau + \tau_{jj'}) + \exp(-i\Psi_{jj'}) k_{jj'}(\tau - \tau_{jj'})) \right) = \\
= \sum_{j \in J} \langle A_j^2 \rangle \int_{-\infty}^{\infty} \exp(i\omega\tau) \left(1 + \sum_{j > j'} p_{jj'} \times \right. \\
\left. \times \cos(\Psi_{jj'} + \omega\tau_{jj'}) \exp\left(- \left(\frac{\omega T_{jj'}}{2} \right)^2 \right) \right) d\mathbf{S}_\xi(\omega),
\end{aligned}
\tag{29}
$$

where $p_{jj'} \equiv 2\langle A_j A_{j'} \rangle / \sum_j \langle A_j^2 \rangle$. The power spectrum density is then

$$
\begin{aligned}
\mathrm{s}_\eta(\omega) = \mathrm{s}_\xi(\omega) \sum_{j \in J} \langle A_j^2 \rangle \left(1 + \sum_{j > j'} p_{jj'} \times \right. \\
\left. \times \cos(\Psi_{jj'} + \omega\tau_{jj'}) \exp\left(- \left(\frac{\omega T_{jj'}}{2} \right)^2 \right) \right),
\end{aligned}
$$

where $\mathrm{s}_\xi(\omega)$ is the power spectral density of the signal $\xi(t)$.

2.6 Intensity of the received wave. Interference coefficient β

Assuming $\tau = 0$ in formula (29), we determine the signal intensity at point R

$$\begin{aligned} I_\eta \equiv \langle \eta^2(t) \rangle = \sum_j \langle A_j^2 \rangle k_\xi(0) + \\ + \sum_{j \neq j'} \langle A_j A_{j'} \rangle \exp(i\Psi_{jj'}) k_{jj'}(\tau_{jj'}) \equiv \\ \equiv I_0 \left(1 + \mathrm{Re} \sum_{j>j'} p_{jj'} \exp(i\Psi_{jj'}) R_{jj'}(\tau_{jj'}) \right), \end{aligned} \tag{30}$$

where $R_{jj'}(\tau) \equiv k_{jj'}(\tau)/k_\xi(0)$, $I_0 \equiv \sum_j \langle A_j^2 \rangle k_\xi(0)$ is the intensity of the signal with incoherent summation of partial waves that arrive along different trajectories.

The parameter

$$\beta \equiv \left| \mathrm{Re} \sum_{j>j'} p_{jj'} \exp(i\Psi_{jj'}) R_{jj'}(\tau_{jj'}) \right|, \tag{31}$$

the coefficient of vision of interference, describes the influence of the correlations between the partial waves on the intensity of the summary wave. In particular, for a coherence function of type (15), the interference coefficient is given by

$$\begin{aligned} \beta \equiv \Bigg| \sum_{j>j'} p_{jj'} \sqrt{q_{jj'}} \times \\ \times \exp\left(-q_{jj'} \left(\left(\frac{\tau_{jj'}}{\tau_0} \right)^2 + \left(\frac{\omega_0 T_{jj'}}{2} \right)^2 \right) \right) \cos(\omega_0 q_{jj'} \tau_{jj'} + \Psi_{jj'}) \Bigg|. \end{aligned} \tag{32}$$

Analysis of (32) shows two factors which tend to decrease field coherence in an oceanic waveguide, which manifests in the decreasing of the interferometrical variances of the acoustic field along the acoustic path. The first of them is the finiteness of the band width of the source noise (the boundedness of the time of coherence): if for a given pair of rays the geometrical time-difference $\tau_{jj'} \gg \tau_0$, then the waves arriving along these rays are not coherent at point R and $R_{jj'}(\tau_{jj'}) \simeq 0$. The second factor is the stochastic fluctuations of the refractive index: if the statistical time-difference $T_{jj'} \gg \tau_0$, then the stochastic phase lag between the waves is large and $q_{jj'} \simeq 0$. The

reason of this decorrelation of waves is in their passage through the regions with independent fluctuations of the refractive index. Exceptions to this are the pairs of rays with small value of the parameter $T_{jj'}$. As it was mentioned in section 2.4, for small scale of fluctuations of the refractive index the probability of the existence of such pairs is large only inside the weakly deverging bundles.

The numerical calculations of the distribution maps of the index β verify the results of analytical investigations. They were performed for a waveguide with the piecewise linear approximation of the $n^2(z)$ for the bi-linear and under surface profile.

The first set of patterns (see Fig. 7) represents the distribution of the parameter β in the given region $-2km \leq z \leq 0,\ 0 \leq x \leq 100km$ for fixed parameters of the under surface oceanic waveguide and inhomogeneities and different values of the time of coherence τ_0. For large values of τ_0 the form of the distribution of the parameter β is identical all over the waveguide, since the wave coherence is large everywhere. However, if the value τ_0 decreases step-by-step, the parameter β will also decrease everywhere in the waveguide. An exception of it are some well visible spatial structures, where the coefficient β remains big (as it was in a bilinear waveguide).

These periodical structures coincide with the localization regions of WDB. This can be easily verified by observation of the figure 7, in which weakly deverging bundles are represented by more bright color than other rays.

The regions located near the *singular WDB* with zero output angle are selected most distinctly. But the regions of localization of two other WDB (of the 2nd kind - see section 3) are selected too. By artificial damping of the WDB it's possible to amplify the effect of selection of the other scales coherence associated with diffuse part of the field, which are constructed by rays with significant differencies of D. As follows from these maps, the interference of these rays are neglected for $\tau_0 \ll 10^{-3}$, while the WDB can be seen very clearly for the same parameters of the current noise (see Fig. 8).

Note that the expansion of high interference regions in the direction from the source is most distinct for singular WDB.

The set of patterns in Fig. 9 represents the distribution of the coefficient β for given parameters of the source noise and different parameters of the random inhomogeneities destributed in the waveguide. It is well seen that the decrease of the spatial scale σ also tends to localization of high-lovel coherence in the regions associated with WDB.

According to the results of the analytical and numerical modelling of the acoustic noise signals propagating in randomly inhomogeneous oceanic waveguide, we can extract different scales of coherence as-

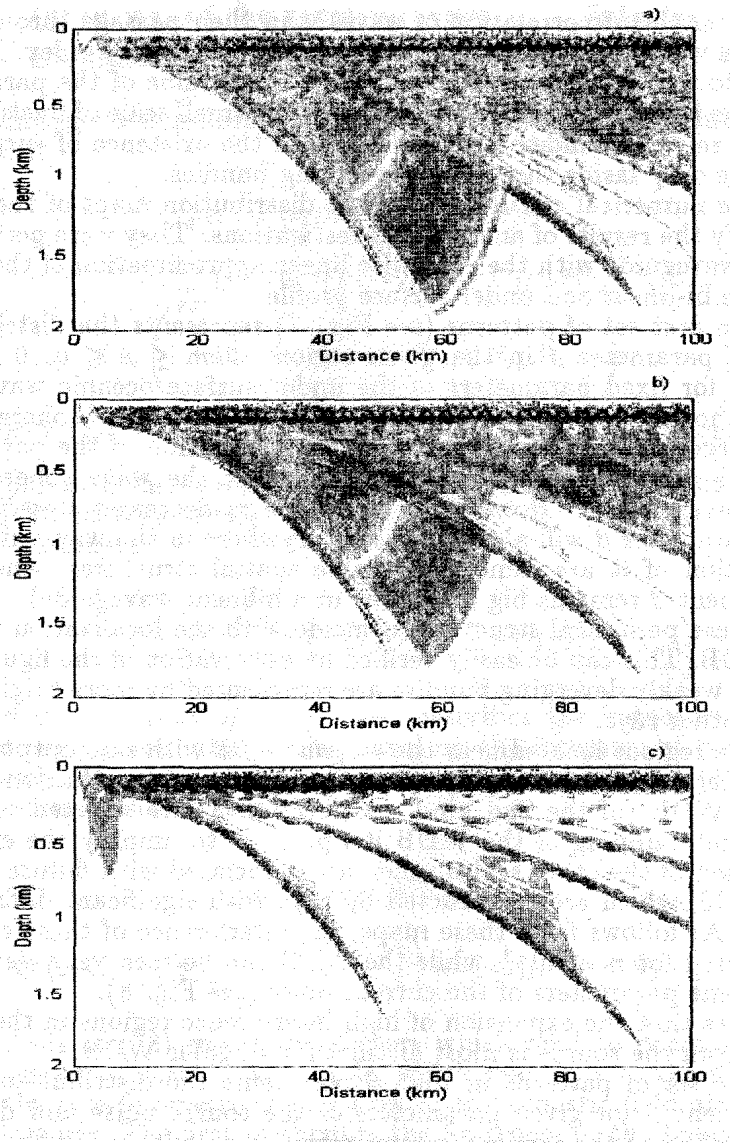

Fig. 7. Spatial distribution of VC for an undersurface oceanic channel for different bandwidths (τ_0 =1 sec. (*a*), 0.02 (*b*), 0.001 sec. (*c*); $\sigma = 0.2, \epsilon_0 = 0.01, z_i =$ 0.057 km).

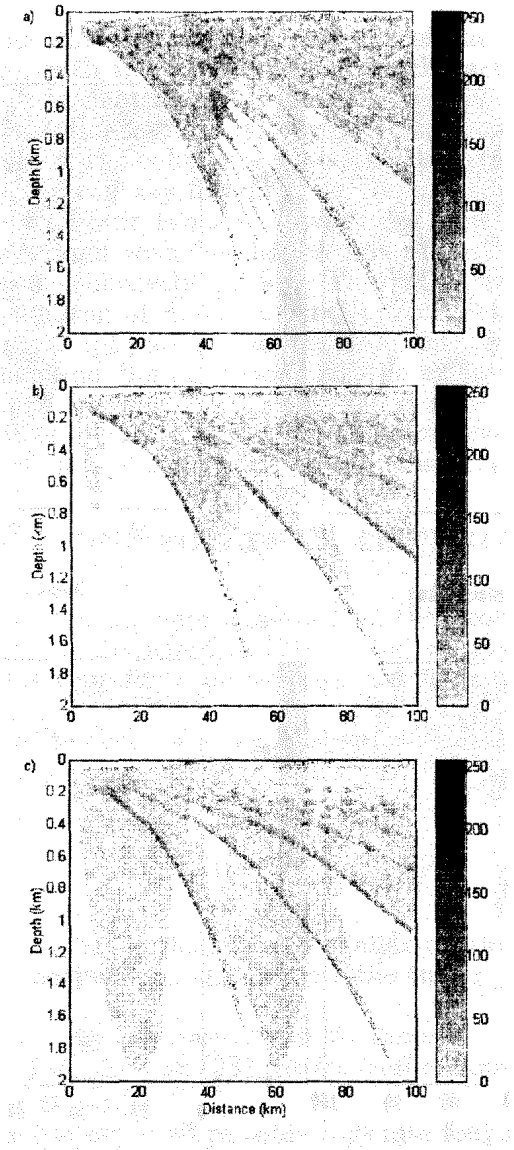

Fig. 8. Map of the parameter β with artifitial damping of the singular WDB for an undersurface waveguide: τ_0 =10 sec. (*a*), 0.005 (*b*), 0.001 sec. (*c*), $\sigma = 0.1$, $\epsilon_0 = 0.01$, $f_0 = 100$Hz.

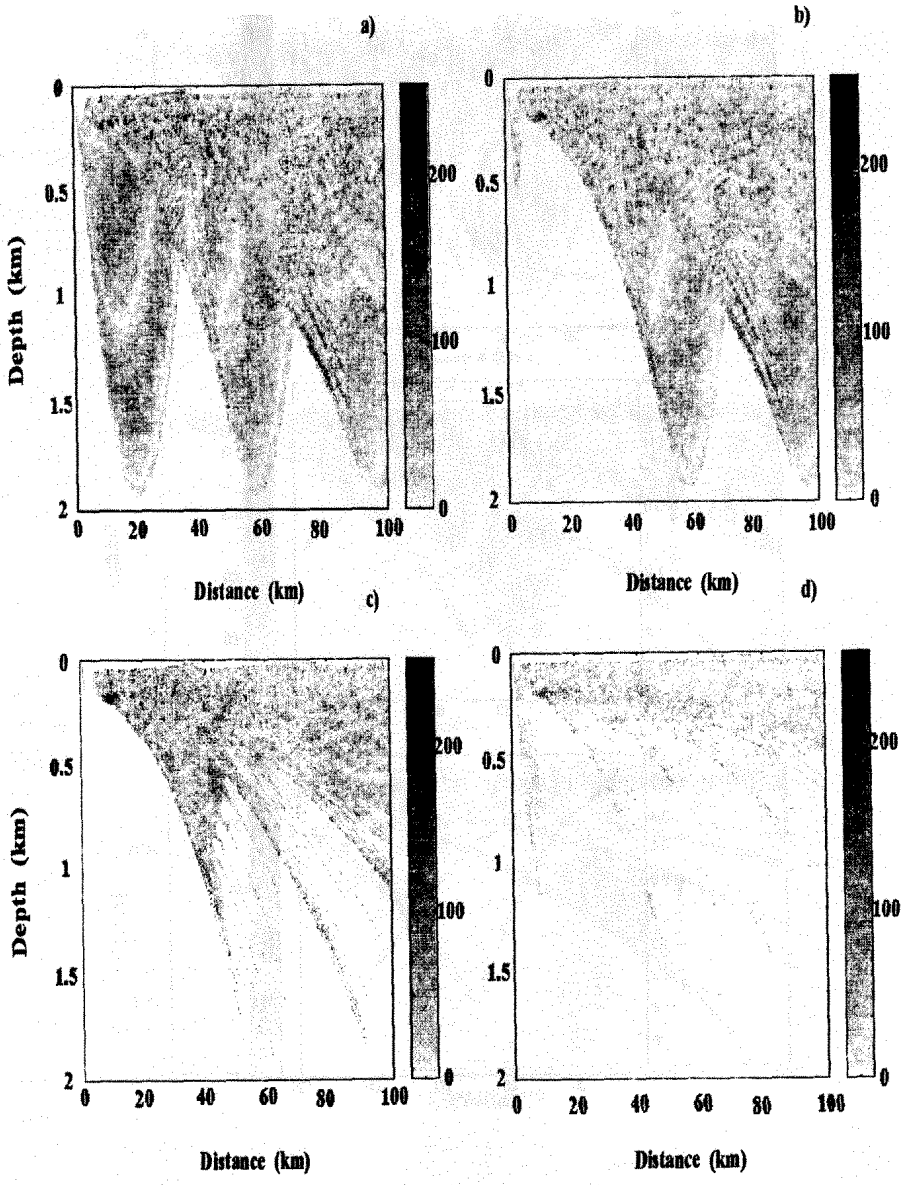

Fig. 9. The similar like in Fig.8 distributions for $\tau = 1$ sec., $z_i = 0.057$ km, σ=10 (*a*); 1 (*b*); 0.1 (*c*); 0.01 (*d*).

sociated with the existence of local extrema of the function $D(\alpha_j)$ and, on contrary, with the regions which are characterized by large derivatives D'_α. It is clear that it is possible to single out fine structure of coherence scales, especially, using information from the time duration structure of the coherence function. However, based on our research results, we can say for sure that at least WDB scales can exist for different oceanic types of waveguides as well as the scales of coherence associated with the diffuse part of partial waves which lose their coherence relatively quickly. The WDB structures can be very useful for solution of different practical problems, such as, for example, the tomographycal monitoring of ocean [28]. It is very important to understand the conditions for the existence of WDB in different regions of the world ocean. The next section is devoted to the development of methods for classification of oceanic waveguides from the point of view of conditions for the existence of WDB.

3 CONDITIONS FOR THE EXISTENCE OF WDB

For a piecewise linear approximation of the profile $c(z)$ the existence of WDB was discussed in [21]. Here, we give some further conditions of this type for a piecewise linear approximation of the profile $n^2(z)$.

For length of the cycle of a ray in a stratified ocean we have the formula [1]

$$D(a) = 2 \int_{z_<}^{z_>} \frac{a\, dz}{\sqrt{n^2(z) - a^2}}, \tag{33}$$

where $a = n_S \cos\theta_S$, n_S is the refractive index on the horizon of the source, θ_S is the output angle, $z_<$, $z_>$ are the turning horizons of the ray.

Definition. *The ray corresponding to the parameter* a, $0 < a < n_S$, *is called WDB ray, if the function* (33) *has the local extremum at the point* a *and the derivative* $D'(a) = 0$.[1]

Let us divide the set of all possible rays into four kinds according to their turning horizons $z_<$, $z_>$

[1] Also we consider the singular ray $\theta_S = 0$ as WDB ray (compare with [21]).

Kinds of the ray	$z_<$	$z_>$
1st	$> H$	< 0
2nd	$> H$	$= 0$
3rd	$= H$	< 0
4th	$= H$	$= 0$

Note (see also [21] that WDB ray cannot be of the 4th kind. Actually, for ray of 4th kind we have, from (33),

$$D'(a) = 2\left(\int_H^0 \frac{a\,dz}{\sqrt{n^2(z)-a^2}}\right)'_a = \\ = 2\int_H^0 \frac{n^2(z)\,dz}{(n^2(z)-a^2)^{3/2}} > 0,$$

so it is impossible for it to be WDB ray.

But WDB rays of 4th (and 3rd also) kinds are not of great interest, since the corresponding bundles would destroy on the irregularities of bottom in real waveguides.

Let us find the conditions of the existence of WDB rays of the 1st and 2nd kinds for the partial case in which the profile of the refractive index squared is bi-linear [2]

$$n^2(z) = \begin{cases} n_0^2 + \alpha_1(z - z_0), & H \le z \le z_0 \\ n_0^2 + \alpha_2(z - z_0), & z_0 \le z \le 0. \end{cases}$$

Here z_0 is the channel axe, $n_0 \equiv n(z_0)$, $\alpha_1 > 0$, $\alpha_2 < 0$.

For such profile

$$\frac{1}{2}D(a) = \int_{z_<}^{z_0} \frac{a\,dz}{\sqrt{n_0^2+\alpha_1(z-z_0)-a^2}} + \int_{z_0}^{z_>} \frac{a\,dz}{\sqrt{n_0^2+\alpha_2(z-z_0)-a^2}} = \\ = \alpha a\sqrt{n_0^2-a^2} + a\left(\frac{\sqrt{n_0^2+\alpha_2(z_>-z_0)-a^2}}{\alpha_2} - \frac{\sqrt{n_0^2+\alpha_1(z_<-z_0)-a^2}}{\alpha_1}\right), \tag{34}$$

where $\alpha \equiv 1/\alpha_1 - 1/\alpha_2 > 0$. Note that WDB rays of the 2nd kind can occur only if $n(0) > n(H)$. On the contrary, WDB rays of the 3rd

[2] More full investigation of conditions for existing of WDB in different, really existing natural oceanic waveguides was made in work [25].

kind can occur only if $n(0) < n(H)$. Taking into account the above comment about the possibilities of realization of WDB rays of the 3rd kind we consider only the case $n(0) > n(H)$.

3.1 WDB rays of the 1st kind

For the 1st kind ray $n^2(z_<) = n^2(z_>) = a^2$, so $\max(n(0), n(H)) \leq a \leq n_S$ and we have, from (34),

$$\frac{1}{2}D(a) = \alpha a\sqrt{n_0^2 - a^2},$$
$$\frac{1}{2}\frac{dD}{da} = \alpha\frac{\left(n_0^2 - 2a^2\right)}{\sqrt{n_0^2 - a^2}}.$$

The only solution of the equation $dD/da = 0$ is $a = n_0/\sqrt{2}$. The necessary and sufficient conditions of the existence of WDB ray with this value of the parameter a are

$$\left\{\begin{array}{c} \frac{n_0}{\sqrt{2}} < n_S \Leftrightarrow c_S < \sqrt{2}c_0 \\ \frac{n_0}{\sqrt{2}} > n(0) \Leftrightarrow c(0) > \sqrt{2}c_0 \\ \frac{n_0}{\sqrt{2}} > n(H) \Leftrightarrow c(H) > \sqrt{2}c_0 \end{array}\right\}.$$

The first of these conditions holds for most natural waveguides. The next two conditions are, however, very strong and do not occur for natural media. Thus, the 1st kind of WDB rays is not typical for such kind of waveguides.[3]

3.2 WDB rays of the 2nd kind

The necessary condition for the existence of WDB ray of the 2nd kind is $n(H) \leq n(0)$. Suppose also that $n_0 < \sqrt{2}n(H)$, which always takes place for natural waveguides. Then

$$\frac{1}{2}D(a) = \alpha a\left(\sqrt{n_0^2 - a^2} - \gamma\sqrt{n^2(0) - a^2}\right),$$
$$\frac{1}{2}\frac{dD}{da} = \alpha\left(\frac{n_0^2 - 2a^2}{\sqrt{n_0^2 - a^2}} - \gamma\frac{n^2(0) - 2a^2}{\sqrt{n^2(0) - a^2}}\right),$$

where $\gamma \equiv \alpha_1/(\alpha_1 - \alpha_2)$, $0 < \gamma < 1$.

[3] Of course, it doesn't mean, that the 1st kind WDB ray is impossible for other kinds of the waveguides.

Let us prove that the derivative dD/da reverses sign in the interval $n(H) < a < n(0)$. As the derivative is continuous, it is sufficient for the existence of one or more roots of the equation $dD/da = 0$.

If $a \uparrow n(0)$, then $dD/da \uparrow +\infty$. On the other hand, for $a = n(H)$

$$\frac{1}{2}\frac{dD}{da} = \alpha(A - \gamma B),$$
$$A \equiv \frac{n_0^2 - 2n^2(H)}{\sqrt{n_0^2 - n^2(H)}} < 0, \quad B \equiv \frac{n^2(0) - 2n^2(H)}{\sqrt{n^2(0) - n^2(H)}} < 0,$$

and if γ is sufficiently small[4], then $dD/da < 0$.

Thus, we obtain the sufficient conditions of the existence of WDB rays of the 2nd kind in the form

$$\gamma < |A| / |B|,$$

or in the form

$$\begin{cases} p \equiv \gamma \dfrac{f\left(\frac{n(0)}{n(H)}\right)}{f\left(\frac{n_0}{n(H)}\right)} < 1, \\ n(H) < n(0), \end{cases} \tag{35}$$

where $f(x) \equiv \frac{2-x}{\sqrt{x-1}}$. As the simple estimations show in real waveguides, $p \simeq 0.1 \div 0.5$, so WDB rays of the 2nd kind usually exist. For example, for the analyzed in the previous section waveguide $p \simeq 0.17$. The corresponding diagram of $D(a)$ see on Fig. 5. As follows from a more full research of conditions for existence of WDB in real oceanic-type waveguides [25], the WDB of the second kind exist for broad class of oceanic waveguides. Another result consits in the high probability of existence of WDB of the first kind in asymmetrical.

4 CONCLUSION

In this work the phenomenon of multiscale coherenece of the acoustic field of a noise source in oceanic waveguides is investigated with use of the ray approach. It is shown, that multiscale coherence is connected with the existence of local extrema in the dependencies of lengths of a ray cycles on output angles. The result field can be descripted as the sum of three parts: the bundles of rays with most stable coherence, the part of the field, formed by rays with hardly distinguished cycles and quickly destroyed coherence, and the

[4] Note, that γ depends on only the ratio of gradients of α_1 and α_2. Thus, γ is small while values A and B are given.

part with intermediate coherence scales. These structures can be singled out as sets of rays with close parameters which form certain structures in space-time domains, which can be considered as non-uniform waves with inherent scales of coherences. To illustrate this multiscale coherence phenomenon, we investigated the dependencies of the characteristics of acoustic waves coherence, as functions of the coherence length of the source-radiated noise, and as of the characteristics of spatially distributed random inhomogeneities localized in oceanic waveguides. The scales of coherence of the propagating acoustic signals are estimated for typical characteristics of random inhomogeities. It is shown, that the results of the signal coherence measurement can essentially depend on the displacement of observation region, and also on the characteristics of the spatial-temporal filters used at the measurements. Increase of the frequency band of the noise radiated by the source, as well as of fluctuations of the oceanic environment, leads to destruction of coherence. The results obtained in this paper permit the estimation of the degree of coherence for different areas of oceanic waveguides.

1. From the practical point of view, the existence of bundles of rays can be interest for tomographical monitoring of of oceanic inhomogeneities [17, 24]. Conditions of existence of various types of Weakly Diverged Bundles are analysed in this work (see also [25]). They can be used to classify of the ocean hydroacoustic channels from the point of view of possibilities of formation of such structures.

2. Investigations of coherence phenomena can play an important role for the development of physical models of the WDB formation in oceanic waveguides. As an example, it may be noted the problem associated with coherent and noncoherent ray summation. According [26] the ray field can be calculated using the noncoherent summation of rays in limits of some rectangular squares. The results of coherent and noncoherent summation can strongly differ, as is illustrated, for example, by Fig. 10. The coherent interference structure image as a quasinoise structure near the oceanic waveguide axis. As follows from our research, the rule of ray summation may be different for different points of observation. Appropriate areas structures are defined by the waveguide characteristics, the spectrum parameters of the source and random inhomogeneities.

3. Partial decreasing of coherence of an illuminating field permits the reduction of the influence of speckle-noise, partially allowing opportunities for space-time filtering in tomographical schemes [16, 17]. The results obtained in this work, which concern the multiscale coherence of acoustic waves in oceanic waveguides, can be useful in choosing the schemes and algorithms for effective tomographical monitoring of the ocean. It should be mentioned, that multiscale phe-

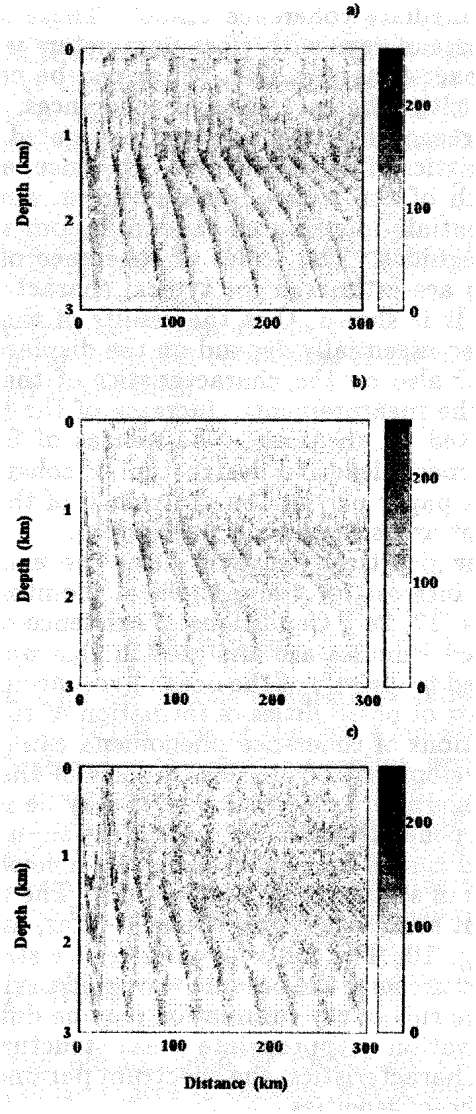

Fig. 10. Maps of the intensity in bilinear waveguide for different types of summation of the partial waves: a) noncoherent, b) partial coherent, c) coherent.

nomena arise due to the existence of smooth extrema in dispersive dependancies for partial waveguide waves.

Similar interference effects, which can be interpreted as non-uniform waves or bundles, are observed in shallow-water channels, at mode description of hydroacoustical fields [27].

4 ACKNOWLEDGMENTS

This study was supported by the Office of Naval Research and Russian Foundation of Fundamental Investigations, Grant N 96-02-18621, and Grant N 97-02-17536. The authors are most grateful to Vera Burdukovskaia for help in the preparation of the manuscript.

References

[1] *Brekhovskikh L.M. and Lysanov Yu.P.* Theoretical Fundamentals of Oceanic Acoustics. Moscow; 1982. 264 p.

[2] Sound Transmission Through a Fluctuating Ocean/ Ed. Flatte S. Cambridge Uu. Pr. Cambridge, 1979.

[3] *Sazontov A.G.* Acoustic Coherence in a Deep Random Ocean// The Formation of Acoustical Fields in Oceanic Waveguides, ed. by V.I.Talanov and V.A.Zverev, 1995, p.37–62.

[4] *Goodman J.W.* Introduction to Fourier Optics// McGraw-Hill, NY, 1968.

[5] *Roder U., Scherg C., and Brettel H.* Coherence and Noise in Ultrasonic Transmission Imaging// Acoustical Imaging, v.10, p. 131-142, 1982.

[6] *Khil'ko A.I.* Partially Coherent Image Reconstruction// Proc. of the International Symposium SPIE, Orlando, FL, 2-3 April, 1993, p.381-411.

[7] *Ikeda O. and Sato T.* Super-Resolution Imaging System Using Waves with a Limited Frequency Bandwidth// JASA, 1979, v.65, N1, p. 75-81.

[8] *Potter J.R.* Acoustic Imaging Using Ambient Noise: Some Theory and Simulation Results// JASA, 1994, v.95, p.21-33.

[9] *Buckingham M.J., Berkhout B.V., and Glegg S.A.L.* Imaging the Ocean with Ambient Noise// Nature, 1992, v.356, p.327-329.

[10] *Makris N.C., Ingenito F., and Kuperman W.A.* Detection of a Submerged Object Insonified by Surface Noise in an Ocean Waveguide// JASA, 1994, v.96, p.1703-1724.

[11] *Khil'ko A.I.* Spatial Filtering of the Partially Coherent Acoustical Images// Acoustical Imaging, 1994, v.21.

[12] *Farmer D. and Ding L.* Coherent Acoustical Radiation from Breaking Waves// JASA, 92(1) July, 1992, p.397–402.

[13] *Goriunov A.A. and Saskovetz A.V.* Inverse Scattering Problems in Acoustics// Moscow Univesity, 1989, 150p.

[14] *Urick R.J.* Principles of Underwater Sound// McGraw-Hill, NY, 1975.

[15] *Kuryanov B.F. and Vedenev A.I.* Investigation of Bottom Sediments Profiling Method in the Deep Ocean by Means of Ship Noise Analysis// Oceanology, v.34, N 4, 1994, p. 621–628.

[16] *Smirnov I.P., Khil'ko A.I., and Caruthers J.W.* Tomograhpical Reconstruction of Ocean Inhomogeneities: Part 1: Forming Partially Coherent Acoustic Wave Structures in the Ocean with Spatially Localized Noise Sources// Proc. of International Meeting OCEANS 95, San Diego, 8-13 October 1995.

[17] *Abrosimov D.I., Khil'ko A.I., and Caruthers J.W.* Tomographical Reconstruction of Oceanic Inhomogeneities: Part 2: Application of Partially Coherent Acoustic Waves Structure to Fresnel Diffraction and Differencial Tomography// Proc. of of International Meeting OCEANS 95, San Diego, 8-13 October 1995.

[18] *Smirnov I.P., Khil'ko A.I., and Zorin A.Yu.* Characteristics of Energetic Coupling of the Inhomogeneous Medium Points// Radiophysics and Qantum Electronics, 36(8), Sept., 1993, p.738–751.

[19] *Khil'ko A.I. et.al.* Space and Time Characteristics of Noise Propagation Paths in the Non-Homogeneous Media// Proc. Int. Noise and Vibration Control Conference, St. Peterburg: Interpablish LTD, 1993, v.5, p. 145–148.

[20] *Petukhov Yu.V.* A Sound Beam with Minimal Wavefront Divergence in a Stratified Ocean Wavewguide// J. of Acoustics. 1994, v..40, N 1, p.111-120.

[21] *Goncharov V.V. and Kurtepov V.M.* Formation and Propagation of Weakly Diverging Bundles of Rays in a Horizontally Inhomogeneous Ocean// J. of Acoustics. 1994, v.40, N 5, p.773-781.

[22] *Munk W.H. and Zachariasen F.* Sound Propagation through Fluctuating Stratified Ocean: Theory and Observation// J.Acoust.Soc.America 1976, vol.59, N 4, p.818-838.

[23] *Ritov S.M., Kravtzov Yu.A., and Tatarsky V.I.* Introduction to Statistical Radiophysics, Part II, Random Fields, Moscow, Nauka, 1978, 464p.

[24] *Munk W.H., Spindel R.C., Baggeroer A., and Birdsell T.G.* The Heard Island Feasibility Test// J. Acoust. Soc. Am., 1994, v.96, p.2330-2343.

[25] *Smirnov I.P., Caruthers J.W., and Khil'ko A.I.* On Justification of One Algorithm of Field Intensity Calculation (in press).

[26] *Piskarev A.L.* About Calculation of Averaging Distribution of Intensity of Sound Waves in Ocean// Akust.Zurnal, v.35, N 4, 1989, p. 724–731.

[27] *Borodina E.L., Stromkov A.A., and Khil'ko A.I.* The Dependence of Spatio–Temporal Structure of Broadband Pulses on the Sediment Layer Parameters (see this book p. 186 – 212).

[28] *Goncharov V.V., Kurtepov V.N., Zaicev V.Y., Nechaev A.G., Khil'ko A.I.* Acoustical Tomography of Ocean, IAP RAS, Nizhny Novgorod, 1997, 295p.

EXPERIMENTAL METHOD FOR DETERMINING THE SCATTERING CHARACTERISTICS OF ELONGATED OBJECTS

A.V. Lebedev, B.M. Salin

To solve problems concerned with the optimisation of sound scattering characteristics one has both to make a forecast and measure these characteristics. There has recently been considerable progress in solving the problems of sound diffraction on elastic bodies. In order to calculate the scattering properties one can use either the T-matrix method or the boundary element and finite element methods (BEM&FEM) [1, 2]. Also we should mention the approximate methods of calculation, such as the heuristic method proposed in [4] and developed in the subsequent papers by the same author [5, 6].

In hydroacoustics, there are different ways to measure scattering characteristics in the far region [7, 8]. However, two problems occur in any case.

Firstly, in the far region, when the scattering signal represents a spherical wave, it is required to detect a weak useful signal against the background of a powerful illumination signal. Using directional receiving-emitting systems, only finite attenuation of a direct signal (within the limits of 20-30 dB, as shown by the experience) can be achieved because of the presence of noises. This greatly complicates the problem of determining scattering characteristics in the region of low frequencies and in directions close to that in which a direct wave comes. The use of a pulsed sonar imposes stringent requirements on distances between the source, the scatterer and the receiver, and creates an additional reverberation noise.

Secondly, which seems to be more significant, the aquatorium, in which the measurements are made, can distort considerably the scattering characteristics owing to the waveguiding properties of sound propagation. This difficulty can, in principle, be avoided by using provisional calibration of the reservoir. The difficulties arising here are well known, and we shall not discuss them. It is important to note that the measurements of scattering characteristics in the far region place rigorous requirements on the aquatorium and measuring facilities, also requiring preliminary work and rather complicated data processing in order to detect a useful signal.

Hence, a measurement technique used in the near region seems to be preferable for determining bistatic scattering cross-sections in hydroacoustical problems. A similar procedure is used to measure the characteristics

of the weak radiation from spatially distributed partly coherent sources [9]. When solving scattering problems, in which the sources of secondary radiation are coherent, an effective algorithm can also be developed to find the scattering characteristics using near-region measurements.

Measurements in the near region of a scatterer have obvious advantages. One is the high signal-to-noise ratio, which increases the accuracy of measurement. The second is the absence of distortions due to the waveguiding property of sound propagation in the aquatorium.

Among the papers that deal with experimental methods using near-field measurements, one should mention Refs. [10, 11, 12, 13, 15, 16]. There are two methods to determine far-field characteristics using near-region measurements. One of them, developed in [10, 11], is based on integral transforms. This method is really used in this paper in application to the sound scattering problem. The second one, developed in [12, 13] [1], is connected with solving a set of linear equations and permits one to determine not only the far-field characteristics but also the primary (radiation) or secondary (scattering) source distribution. The latter method is useful under the different conditions of wave propagation. For using this method, however, one must assume that the sources are either of a monopole or dipole type [12]. Moreover, in papers [12, 13] only theoretical investigations aimed at checking errors were made.

In this paper, the method of near-field measurements of scattering characteristics applying to elongated objects is developed. This method is based on illumination of a measured object by a sequence of tone signals of discrete frequencies. Due to the high signal-to-noise ratio and the stability of a tone signal of illuminating field, small perturbation caused by the scattering object can be defined by coherent subtraction of two distributions of pressure at the array hydrophones. One of them corresponds to a record without the measured scattering object, and the other corresponds to a record with the object present. The accuracy in measurement of scattering properties are restricted by two factors. Firstly, there are systematic errors due to data processing. These errors are discussed in the first two sections. Secondly, there are random errors due to the noise in aquatorium and acoustic field fluctuations at the measuring array. These errors are estimated on the base of experimental data.

[1] Also paper [14] should be mentioned. This paper is concerned with source reconstruction using far-region measurements.

THEORY. INFINITE APERTURE OF THE RECEIVING SYSTEM

Consider the geometry of a measuring system (Fig. 1) that operates in the near region of the scatterer.

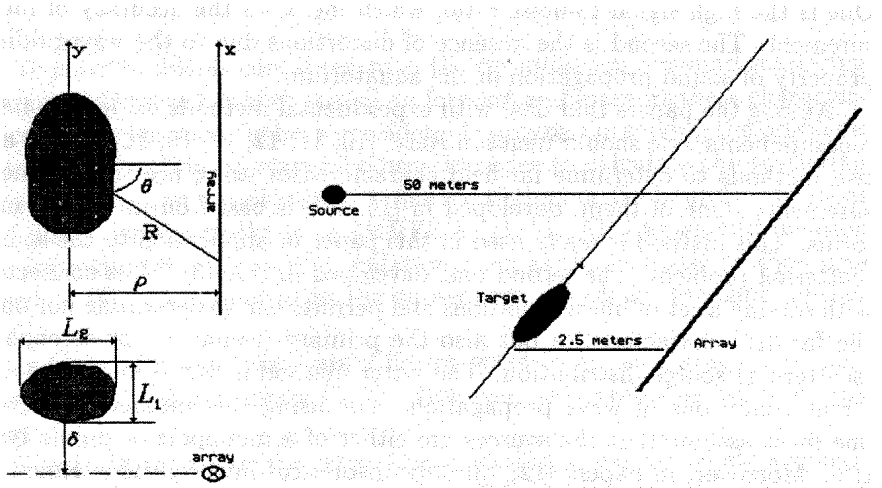

Figure 1: The geometry of the problem considered.

The field of radiation from external sources, located on an object, is determined by the Kirchhoff integral [1], which can conveniently be rewritten as

$$p(\mathbf{x}) = \int_S \left(-Q(\mathbf{y}) + D(\mathbf{y})(\mathbf{n}(\mathbf{y}), \nabla)\right) G(\mathbf{x}, \mathbf{y})\, dS_y, \qquad (1)$$

where $Q(\mathbf{y}) = \partial p(\mathbf{y})/\partial n_y$ is the density of simple external sources (distribution of the normal component of velocity), D(y)=p(y) is the density of dipole sources (distribution of pressure), $\mathbf{n}(\mathbf{y})$ is a unit vector of the external normal to the scatterer surface, $G(\mathbf{x}, \mathbf{y}) = \dfrac{\exp(ik|\mathbf{x} - \mathbf{y}|)}{4\pi|\mathbf{x} - \mathbf{y}|}$ is a Green's function of free space, $\mathbf{x}$ and $\mathbf{y}$ are vectors taken from the origin of coordinates to the point of observation and the region of source distribution over the surface S surrounding the scatterer.

Consider the cross-section of a target (Fig. 1), where L_1 is the maximum height and L_2 is the maximum width of the object. Assume that a linear array, composed of equidistant nondirected pressure receivers, is located at a distance such that L_1 is less than the dimension of the first Fresnel zone,

i.e., $L_1^2 \ll 2\pi\rho_{min}/k$, where ρ_{min} is the distance from the array axis to the object (Fig. 1), and k is the wavenumber. We also suppose that the array is located in the wave zone $k\rho_{min} \gg 1$. Then, for the field estimation, the distribution of sources over the surface S can be reduced, without loss of generality, to a respective distribution of sources localised on one side of the plane bounded by the object contour. Restrictions on thickness of the object and on changes of ρ will be shown below, when deriving the equations of scaling the array measurements for the far region. In addition, we now assume that the object has a zero thickness (L_2) and is parallel to the receiving system. In this case, the array field can be represented as a linear integral with respect to a longitudinal (parallel to the array axis) coordinate y, which is related to the scatterer by:

$$p(\rho_0, x) = L_1 \int_{-B/2}^{B/2} \left(-\tilde{Q}(y) + \tilde{D}(y)(\tilde{\mathbf{n}}, \nabla)\right) \times \\ \times \frac{\exp\left[ik\sqrt{\rho^2 + (x-y)^2}\right]}{4\pi\sqrt{\rho^2 + (x-y)^2}}\, dy, \qquad (2)$$

where $\tilde{Q}(y)$ and $\tilde{D}(y)$ are the equivalent linear densities of a simple and a dipole source. The emergence of a term L_1 in explicit form is due to the small (compared to the first Fresnel zone) vertical dimension of the object and the choice of the source distributions $\tilde{Q}(y)$, $\tilde{D}(y)\tilde{\mathbf{n}}(y)$, x and y are the projections of the vectors **x** and **y** onto the axis, along which the array and the scatterer are located, and ρ_0 is the distance between the array and the scatterer (Fig. 1).

When the point of observation is in the far region with respect to the length B of the object, at the point with coordinates (R, θ) (Fig. 1), the integral (2) can be re-written as:

$$p(R, \theta) = -L_1 \frac{\exp(ikR)}{4\pi R} \int_{-B/2}^{B/2} \left(\tilde{Q}(y) + ik\tilde{D}_1(y) + ik\tilde{D}_2(y)\right) \times \\ \times \exp(-iky\sin\theta)\, dy, \qquad (3)$$

where $\tilde{D}_1(y) = \tilde{D}(y)n_\rho$ is an equivalent linear density of the dipoles oriented along the ρ coordinate, $\tilde{D}_2 = \tilde{D}(y)n_y$ is an equivalent density of the dipoles oriented along the y coordinate, and $\tilde{D}_1^2(y) + \tilde{D}_2^2(y) = \tilde{D}^2(y)$.

Thus, for determining the radiation field in the far region using the near region measurements, it is required to find conditions under which the resultant equations will differ from (3) only in the function dependent solely

on the mutual arrangement of the object and the array, rather than on the scatterer geometry.

Expressions (3) can be related to the array field measurements by using the well-known representation of the free space Green's function [17]:

$$\frac{\exp(ik\sqrt{(\rho_0-\rho)^2+(x-y)^2})}{\sqrt{(\rho_0-\rho)^2+(x-y)^2}} =$$

$$= \frac{i}{2}\int H_0^{(1)}(\sqrt{k^2-\gamma^2}(\rho_0-\rho))\exp(i\gamma(x-y))\,d\gamma\,, \qquad (4)$$

where $H_0^{(1)}(t)$ is a zero-order Hankel function of the 1st kind.

The field at the array hydrophones, in view of (2) and (4), can be represented as a sum of three integrals differing only in the kernels:

$$p(\rho_0,x) = L_1\int_{-B/2}^{B/2}\left(-\tilde{Q}(y)+\tilde{D}_1(y)\frac{\partial}{\partial\rho}+\tilde{D}_2(y)\frac{\partial}{\partial y}\right)\times \qquad (5)$$

$$\times\ \frac{\exp(ik\sqrt{(\rho_0-\rho)^2+(x-y)^2})}{4\pi\sqrt{(\rho_0-\rho)^2+(x-y)^2}}\,dy = \frac{iL_1}{8\pi}\int_{-B/2}^{B/2}dy\int d\gamma\ \times$$

$$\times\left(-\tilde{Q}(y)H_0(\kappa\rho_0)+\tilde{D}_1H_1(\kappa\rho_0)\kappa-i\tilde{D}_2(y)H_0(\kappa\rho_0)\gamma\right)\exp(i\gamma(x-y)),$$

where $\kappa^2 = k^2-\gamma^2$.

Let us use the Fourier operator $\hat{F} = \int \exp(-ikx\sin\theta)\,dx$, acting on the left-hand side and the right-hand side of Eq. (5). In the case of an infinite array, expression (5) transforms to:

$$\hat{F}(p(\rho_0,x)) = p(\rho_0,\theta) = -\frac{iL_1H_0(k\rho_0\cos\theta)}{4}\int_{-B/2}^{B/2}\exp(-iky\sin\theta)\times$$

$$\times\left(\tilde{Q}(y)+ik\tilde{D}_2(y)\sin\theta-k\tilde{D}_1(y)\cos\theta\frac{H_1(k\rho_0\cos\theta)}{H_0(k\rho_0\cos\theta)}\right)dy. \qquad (6)$$

We assumed above that the array is in the wave region with respect to the scatterer. If an additional condition $k\rho\cos\theta \gg 1$ is satisfied, then the ratio of the zero-order and first-order Hankel functions is equal to an imaginary unity, and the relative error is equal to $i/2k\rho\cos\theta$. Therefore, the equation of scaling these measurements in the near region (relative to the length of the object) for those in the far region is written as:

$$p(R,\theta) = \frac{\hat{p}(\rho_0,\theta)\exp(ikR)}{i\pi RH_0(k\rho_0\cos\theta)}. \qquad (7)$$

Note that expression (7) is "accurate" in the case $k\rho_0 \cos\theta \gg 1$. Assuming R=1m and taking the module of this expression it is easy to find the scattering strength, a quantity which is often used in hydroacoustics:

$$\text{Scattering strength} = 20 \log |p(1,\theta)/p_0|,$$

where p_0 is the field amplitude of an incident plane wave of illumination.

Let us find the error due to the finite dimension of the object in the ρ direction (the thickness of the object) in determining the radiation (scattering) field in the far region using expression (7). For $L_2 > 0$, expression (3) will contain an integral with respect to the thickness of the object, (ρ), from $-\Delta\rho$ to $+\Delta\rho$. The term, which takes the additional phase delays into account, has the form $\exp(-ik\rho\cos\theta)$. The right-hand side of (7) is governed by a similar binary integral over the object surface with the same distribution of sources. A unique difference is that the integrand will include $H_0(k(\rho_0 - \rho)\cos\theta)/H_0(k\rho_0\cos\theta)$ instead of $\exp(-ik\rho\cos\theta)$. It is exactly the difference of the Hankel functions ratio from $\exp(ik\rho\cos\theta)$, which will define the accuracy in calculation of the far field by the near field measurements using expression (7).

Assuming that the change $\Delta\rho$ is small compared to the mean value of ρ_0 and using the asymptotic expressions for the Hankel function [18], we obtain the relative error, which mainly is due to the amplitude dependence of the Hankel function on ρ. This error amounts to $\Delta\rho/2\rho_0$. For example, in the experiment described below the value $\Delta\rho = 0.3m$, $\rho_0 = 2.5m$ and the relative error due to the finite thickness of the object will be 6 percent.

Based on expression (7) we define the scattering function in the form [1]:

$$p_s(R,\theta,\theta_0,\varphi) = p_0 f_s(\theta,\theta_0,\varphi)\frac{\exp(ikR)}{kR},$$

where $p_0(\theta_0)$ is the complex amplitude of the field of an incident (in θ_0 direction) plane wave of illumination at point (0, 0) (Fig. 1).

Using expression (7) we write down an expression for $f_s(\theta,\theta_0,\varphi)$ through the measured quantities:

$$f_s(\theta,\theta_0) = \frac{-ik\hat{p}(\rho_0,\theta)}{\pi p_0(\theta_0)H_0(k\rho_0\cos\theta)}. \qquad (8)$$

Here, the dependence on angle φ is omitted (the receiving system represents a linear array and we have a dependence $f_s(\theta)$ for constant $\varphi = \arctan(\delta/\rho_0)$ for each δ (Fig. 1).

The unknown $p_0(\theta)$ can be specified using the same receiving system in the absence of a scatterer:

$$p_0(\theta_0) = \frac{\hat{p}_0(\rho_0, \theta_0)\exp(-ik\rho_0\cos\theta_0)}{A}, \tag{9}$$

where $\hat{p}_0(\rho_0, \theta_0)$ corresponds to the maximum value of the spatial spectrum $\hat{p}_0(\rho_0, \theta)$ of the illumination field on the array in the absence of a scatterer, and A is the length of the array.

The final expression for the scattering function $f_s(\theta, \theta_0)$ has the form:

$$f_s(\theta, \theta_0) = \frac{-ikA\hat{p}(\rho_0, \theta)\exp(ik\rho_0\cos\theta)}{\pi\hat{p}_0(\rho_0, \theta_0)H_0(k\rho_0\cos\theta)}. \tag{10}$$

The scattering function can be determined as follows. In the first stage, the object under study is shifted to a maximum large distance from the array or is removed from the reservoir. This is to find the pressure distribution at the array hydrophones, $p_0(x)$ and, correspondingly, $\hat{p}_0(\rho_0, \theta_0)$ in the principal maximum direction without a scatterer. Then a scatterer is placed into a point with coordinates (0, 0). The quantity $\hat{p}(\rho, \theta)$ is defined as a Fourier integral of perturbations $p(x) - p_0(x)$.

In case $\delta = 0$, $\theta = \theta_0$, expression (10) allows the total scattering cross-section to be found. By virtue of the optical theorem [1, 2]:

$$\sigma_{tot} = \frac{4\pi}{k^2} Im(f_s(\theta \equiv \theta_0, \theta_0, \varphi = 0)). \tag{11}$$

Substituting (10) into (11) we obtain:

$$\sigma_{tot} = -\frac{4A}{k} Re \frac{\hat{p}(\rho_0, \theta_0)\exp(ik\rho_0\cos\theta_0)}{\hat{p}_0(\rho_0, \theta_0)H_0(k\rho_0\cos\theta_0)}. \tag{12}$$

Simplifications are possible for large $k\rho_0\cos(\theta_0) \gg 1$:

$$\sigma_{tot} = -4A\sqrt{\frac{\pi\rho_0\cos\theta_0}{k}} Re\left(\frac{\hat{p}(\rho_0, \theta_0)}{\hat{p}_0(\rho_0, \theta_0)}\exp(i\pi/4)\right). \tag{12'}$$

Let us check the validity of expression (12). Suppose that the scatterer represents an acoustically rigid strip. Consider a high frequency domain where $kL_1, kB \gg 1$. We use the Kirchhoff hypothesis to determine the field of the secondary sources [1]. The quantities $\tilde{Q}(y)$ and $\tilde{D}(y)$, which enter integral (2) are equal to each other:

$$\tilde{Q}(y) = 0,\ \tilde{D}(y) = -2p_0\exp(iky\sin\theta_0),\ \tilde{D}_1 = \tilde{D},\ \tilde{D}_2 = 0. \tag{13}$$

The negative sign is due to the fact that the external normal vector, $\mathbf{n}$, is opposite to the ρ axis.

Inserting (13) into expression (6) we find ($k\rho_0 \cos\theta_0 \gg 1$):

$$\hat{p}(\rho_0, \theta_0) = -p_0 k B L_1 \cos\theta_0 H_0(k\rho_0)/2,$$
$$\hat{p}_0(\rho_0, \theta_0) = p_0 A \exp(ik\rho_0 \cos\theta_0) , \qquad (14)$$

$\sigma_{tot} = 2BL_1 \cos\theta_0$. This coincides with the high-frequency asymptotic form [1].

INFLUENCE OF THE FINITE APERTURE OF THE RECEIVING SYSTEM

Above we assumed that the measuring system is infinitely long. The finiteness of the array aperture and its arrangement impose additional requirements on the measuring system.

The finiteness of the aperture of the receiving system can be represented in the form of the weight functions $S_j(y)$ and the additional phase term ($\exp(ik\Delta y \sin\theta)$ in the integral (6) (the expressions specified below can be obtained if we use a Fourier operator for finite segment [-A/2,+A/2] acting on the right-hand side of Eq.(5)):

$$\hat{p}_A(\rho_0, \theta) = -\frac{iL_1 H_0(k\rho_0 \cos\theta) \exp(ik\Delta y \sin\theta)}{4} \int_{-B/2}^{B/2}$$
$$\exp(-iky \sin\theta) \left(\tilde{Q}(y) S_0(y) + ik \sin\theta \tilde{D}_2(y) S_2(y) - \right. \qquad (15)$$
$$\left. -k \cos\theta \tilde{D}_1(y) S_1(y) \frac{H_1(k\rho_0 \cos\theta)}{H_0(k\rho_0 \cos\theta)} \right) dy ,$$

where

$$S_0(y) = \frac{kA}{2\pi H_0(k\rho_0 \cos\theta) \cos\theta} \exp(-ik(y - \Delta y)\zeta) \times$$
$$\times \int H_0(k\rho_0 \beta(\zeta)) \operatorname{sinc}(kA\zeta/2)\, d\gamma , \qquad (16a)$$

$$S_1(y) = \frac{kA}{2\pi H_1(k\rho_0 \cos\theta) \cos\theta} \exp(-ik(y - \Delta y)\zeta) \times$$
$$\times \int H_1(k\rho_0 \beta(\zeta)) \beta(\zeta) \operatorname{sinc}(kA\zeta/2)\, d\gamma , \qquad (16b)$$

$$S_2(y) = \frac{kA}{2\pi H_0(k\rho_0 \cos\theta)\sin\theta} \exp(-ik(y-\Delta y)\zeta) \times$$
$$\times \int H_0(k\rho_0\beta(\zeta))(\zeta + \sin\theta)\,\mathrm{sinc}(kA\zeta/2)\,d\gamma\,, \qquad (16c)$$

$\beta^2(\zeta) = \cos^2\theta - 2\zeta\sin\theta - \zeta^2$, $\mathrm{sinc}(t) = \sin(t)/t$, A is the length of the array, $\hat{p}_A(\rho_0, \theta)$ is the Fourier transform of the field on the array aperture, Δy, ρ_0 is the displacement of the array center with respect to the model center, and $y = 0, \rho = 0$ again correspond to the middle of the scatterer (Fig. 1).

From expression (15) it is seen that the quantity $\hat{p}_A(\rho, \theta)$ differs from $\hat{p}(\rho, \theta)$. Since individual contributions from each source are unknown, the small differences between the weight functions and their proximity to a constant on the longitudinal scale of the object are the only criteria of the accuracy in measurement.

Let us check the validity of expressions (15) and (16). Assume that $kA \to \infty$ and make use of the definition of the δ-function through a limit [18]: $\delta(x) = \lim_{\alpha\to\infty} \alpha\,\mathrm{sinc}(\alpha x)/\pi$. It is easily seen that in the first case the weight functions are equal to unity and expression (15) coincides with expression (6).

A limit transition from $\mathrm{sinc}(kA\zeta/2)$ to the δ-function is possible if the remaining quantities entering integrals (16) are slowly varying functions as to the scale of variation of the function $\mathrm{sinc}(kA\zeta/2)$, i.e., for $|\zeta| < \frac{2\pi}{kA}$. Suppose that $kA \gg 1$, $k\rho_0 \gg 1$. We make use of the high-frequency asymptotic form of the Hankel function [18]. In the estimation of integrals (16) we take only "fast" phase changes into consideration. It is readily seen that within the framework of these assumptions, the functions $S_j(y)$ are the closer to unity and expression (15) is the closer to (6) the better the conditions

$$|\rho_0 \tan\theta - \Delta y + y| \ll A/2 \;\; or \;\; y \in \rho\tan\theta - \Delta y \pm A/2\,, \qquad (17a)$$

$$\frac{2\pi\rho_0}{kA^2\cos\theta} \ll 1 \qquad (17b)$$

are satisfied.

Condition (17a) means that in the measurements the object should be in the projector zone of the array ($\rho_0 \tan\theta = -\Delta y$) and should have a length not exceeding the aperture of the measuring system [10, 11]. Actually, condition (17b) means that the geometrical acoustics approximation works well (the quantity $P = \sqrt{kA^2\cos\theta/2\pi\rho_0}$ is a Fraunhofer parameter).

Thus, when a receiving system with a finite aperture is used, conditions (17) need to be satisfied. If these conditions are met, then for determining the scattering characteristics one can use expressions (7) and (10)-(12), where the quantities calculated from measurements on a finite-size array are used as $\hat{p}(\rho,\theta)$[2] The term $\exp(ik\Delta y \sin\theta)$ should necessarily be taken into account. The final expression (7') is written as:

$$p(R,\theta) = \frac{\hat{p}_A(\rho_0,\theta)\exp(-ikR)}{i\pi RH_0(k\rho_0\cos\theta)}\exp(-ik\Delta y\sin\theta). \qquad (7')$$

In the calculation of integrals that define the weight functions it is convenient to use the algorithm of a fast Fourier transform. The results of the calculations are plotted in Fig. 2. In these calculations the quantity ρ_0 was assumed to be equal to 1/4 of the array length A. We chose two frequencies differing by one order of magnitude. The upper frequency was equal to the maximum operating frequency of a 64 element hydroacoustic array, which was used in the experiment ($max(kA) = \pi(N-1) = 63\pi$).

Figures 2a,b exhibit the results of calculations for $\theta = 0$. It is easily seen that the weight function is the closer to unity the more is the magnitude of the parameter P. That exactly P, rather than kA, is the parameter that determines the accuracy is seen from the diagrams in Figs. 2c,d, which correspond to kA=100 and $\theta = 30$, 60 degrees, respectively. For $\theta = 60$ the parameter P is almost the same as that for Fig. 2a. These diagrams are also similar in form.

Comparing the diagrams presented in Fig. 2 it should be noted that the accuracy in measurement is influenced by two facts. One is the proportional length of the scatterer and the antenna, B/A; the second is the mutual arrangement of the scatterer and the measuring system.

Measurements are not allowed for $B \geq A$. If $B/A \ll 1$, the weight functions can be replaced by calculated values for coordinates corresponding to the center of the object.

An optimal relative position depends on an angle θ, for which we restore the directivity pattern in the far region. When non-zero angles are measured, the position of the scatterer should satisfy the requirement (17a).

[2] Accurate estimation of the errors caused by the finite aperture of the measuring system requires apriori ideas concerning the distribution of sources in a longitudinal direction, the amplitude relation of the simple and each of the dipole sources, etc. For example, for a smooth distribution of sources, a small difference not directly between the weight functions but between their integrals on the object dimensions is sufficient. If the source amplitude relation is known, then the correction term in expression (15) can be specified more accurately, etc.

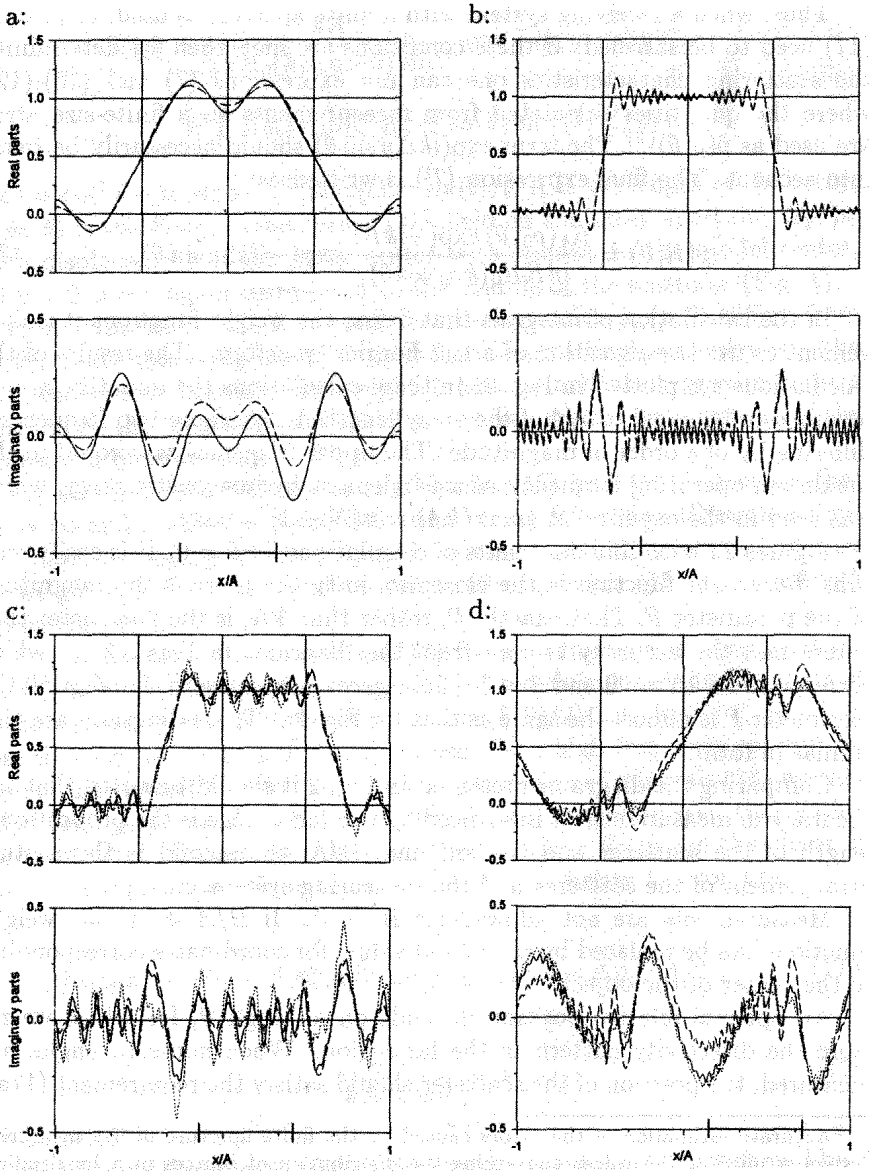

Fig. 2. Weighting functions S_j. Solid lines correspond to monopole sources, dash lines – to transversal dipole sources and dotted lines – to longitudinal dipoles. Other comments in the text.

Thus, in case kA = 100, θ= 60 (Fig. 2d) the displacement Δy, in view of $\rho/A = 0.25$, will be 0.43 A. From the diagrams presented in Fig. 2d it is seen that this displacement will correspond to a minimum error both in amplitude and in phase. For an object in a fixed position, the range of angles where $S_j \approx 1$ is determined by a simple geometrical construction of parallel straight lines through the edge of the array and one of the edges of the object.

Defining the total scattering cross-section in terms of an optical theorem imposes additional requirements on the length of the array and on the wave dimensions of the object being investigated. As is seen from the diagram shown in Fig. 2, the finite aperture of the receiving system causes an additional phase term to appear. The magnitude of the phase term depends on the position of the object inside the projector zone of the array.

The presence of this phase term leads to the fact that the true value of the scattering function will differ from the measured value by a complex term. Hence, the relative error in determining the total scattering cross-section by Eq. (12) is given by

$$\delta\sigma = \frac{Re(f_s)\sin\chi + Im(f_s)(\cos\chi - 1)}{Im(f_s)}, \qquad (18)$$

where χ is a phase term due to the limited length of the array (assuming $S_0 = S_1 = S_2 = S$, $\chi = \arctan(Im(S)/Re(S))$ and f_s means the true value of the scattering function. In the limiting case $P \to \infty$ the value χ tends to zero in inverse proportion to P.

As is seen from Eqs. (12) and (14), in the high frequency domain, where the wave dimensions of the object are large, $Re(f_s) = 0$ and the error constitutes $-2\sin^2(\chi/2)$. In the most unfavorable case, in which the Fraunhofer parameter is small (Fig. 2a), the difference between S_j can yield $\chi \approx \arctan(0.1) = 6^o$. In this case, the relative error $\delta\sigma$ will amount to -0.5 percent and cannot be taken into account in the analysis of experimental data.

In the low-frequency domain, where the wave dimensions of the object are small, $Re(f_s)$ can markedly exceed $Im(f_s)$. As an example, we consider the problem of sound scattering on an air bubble. Based on expressions given in [19], it is easy to make sure that:

$Im(f_s) \approx Re(f_s)\xi^3$, $\omega \ll \omega_0$ (the bubble behaves as an acoustically rigid body);
$Im(f_s) \approx Re(f_s)\xi$, $\omega \gg \omega_0$ (the bubble behaves as an acoustically soft body);
$Im(f_s) \gg Re(f_s)$, $\omega = \omega_0$ (the resonance).

Here, ξ is the wave dimension of the bubble (assuming $\xi \ll 1$) and ω_0 is the eigenfrequency of the bubble oscillations.

In the most unfavorable case, where $\omega \ll \omega_0$, the relative error in determining the scattering cross-section is of order $\sin\chi/\xi^3$ The minimum wave dimension, for which the relative error does not exceed 100%, is $\sqrt[3]{\sin\chi}$. Under the assumption of $k\rho_0\cos\theta \gg 1$ the field distribution in the projector zone of the array (of the S_j function) is governed by the Fresnel integrals. Analysis of the high-frequency asymptotic form of these functions [18] indicates that the value χ is of order $1/P$. Therefore, a lower limit is placed on the size of the object:

$$\frac{min(L_1, L_2, B)}{A} = \frac{1}{kA\sqrt[3]{P}}. \qquad (19)$$

At a frequency kA = 20 (Fig. 2a) we have: $min(L_1, L_2, B) = A/34$.

APPLICATION OF THE METHOD

Consider as an example the use of the method described above for the measurement of the scattering cross-section of an elastic body of complex geometry (a cylindrical shell with rigidity ribs and a large number of internal structure inhomogeneities). The length of the object was 5 m and the transverse dimensions did not exceed 0.6 m (slowly varied along the axis of the object).

In the experiment on determining the scattering cross-section the following values of the parameters were adopted:

- Distance = 2.5 m;
- Receiving array: a 64 element array of length A = 10 m;
- Depth of deployment of the array: 5 m (the total depth of the reservoir at the measurement site was 10 m).

A monopole emitter was situated 50 m from the array (Fig. 1).

Coherent accumulation of the illumination field (without the model), occurred during 20 to 40 s. The magnitude of the scattering field was defined by way of coherent deduction of the value of $p_0(x)$ from the current values of $p(x)$ when the model was situated in the projector zone of the array.

The measurements of the total scattering cross-section and the angular dependence of scattering strength are presented in the form of crests on the diagram in Fig. 3. The calculation of the total cross-section in terms of the non-resonance model proposed in [20] and based on [21], is also shown. This simple model describes the scattering of sound by an elastic cylindrical

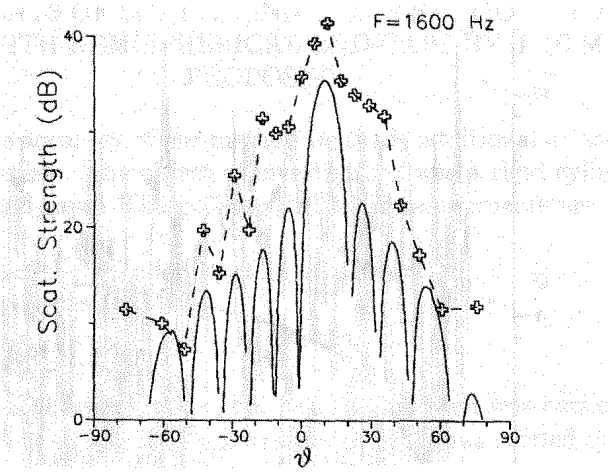

Fig. 3. Angle dependence of the scattering strength. Solid line corresponds to [20].

shell of finite length when its resonance responses are overlapped. Such a description is convenient in the analysis of general laws responsible for the formation of the radiation and scattering fields of sophisticated mechanical systems with a large number of resonances.

This part of the paper pursues the goal only to demonstrate the applicability of the method proposed. Because of that we did not try to compare measured values with accurate calculations. Moreover, such calculations are not possible because a number of internal parameters (mass and rigidity distribution) are not known. Nevertheless comparison with a simple theoretical model that predicts general dependences (the similar approach was used in Ref. 4-6) and gives clear results makes it possible to judge on the accuracy and presence of systematic mistakes. When the frequency response of a real object is observed, we must see that the measured values oscillate round the theoretical curve [20]. If regular mistakes take place, then the measured values will be strongly displaced with respect to the theoretical curve.

On the diagram in fig. 4 the frequency dependence of the total cross-section in a wide band region is shown. The measurements were made by the following way. During 6 minutes two records of a set of discrete frequencies without the object were made. Then the same records were

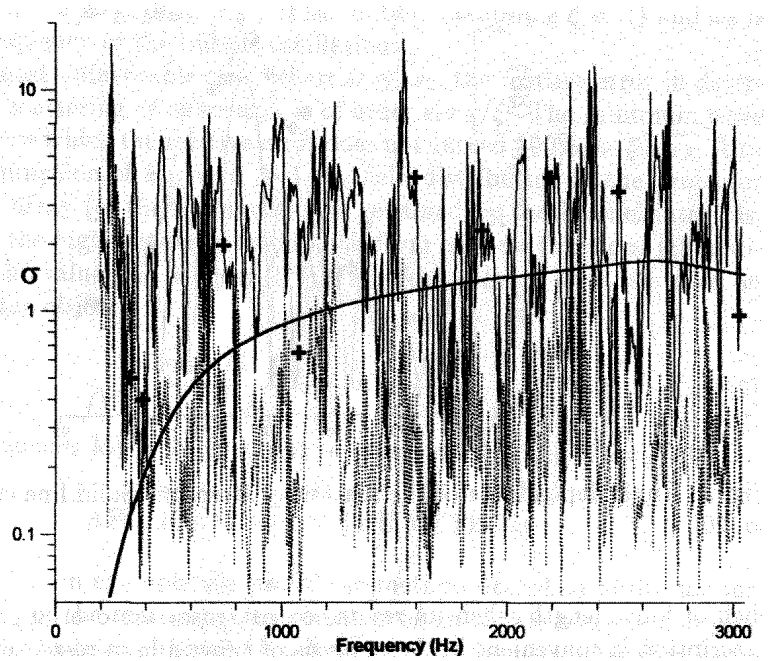

Fig. 4. Frequency dependence of the total cross-section (solid line and crosses). Dotted line depicts errors caused by fluctuations. Fat line corresponds to [20]. Discrete frequencies measurements (crosses) were made after at least 20 seconds of coherent accumulation of the illuminating field.

made when the object was placed in front of the array. Finally, the same records were repeated without the object. Such a scheme of measurement permits one to estimate the accuracy in determination of the total cross-section determination. The illumination field can be defined, using the first and the last series . Then we can find the perturbation at the array hydrophones by the method explained above and calculate the total cross-section. If any arbitrary combination of idle measurements is used, then the random errors due to the noises in the aquatorium and the instability of the illumination field can be determined. It is seen that the relative error due to the noises and instability is about 10 percent and the experimental data really oscillate about the theoretical curve.

MEASUREMENTS OF SCATTERING CROSS-SECTION OF A RIGID CYLINDER WITH HEMISPHERICAL END-CAPS BY THE METHOD PROPOSED

To define the accuracy of our method we made additional measurements in anechoic chamber. The object of investigation was a rigid cylinder with hemispherical end-caps. The geometry of the measurements are shown in fig. 5.

- The diameter of the cylinder $L_1 = L_2 = 130mm$,
- The length of it $B = 548mm$,
- $\rho_0 = 550mm$, $\rho_{min} = \rho_0 - 0.5L_1 = 495mm$,
- $A = 65 \times 15mm = 975mm$.

Frequency range was $0.2 \div 4$ kHz. An illumination was carried out by wide-band random signal. The registration of fields was carried out by two microphones: the first of them was unmovable (base channel) while the second one was moved along the array axis with the 15 mm step. Complex

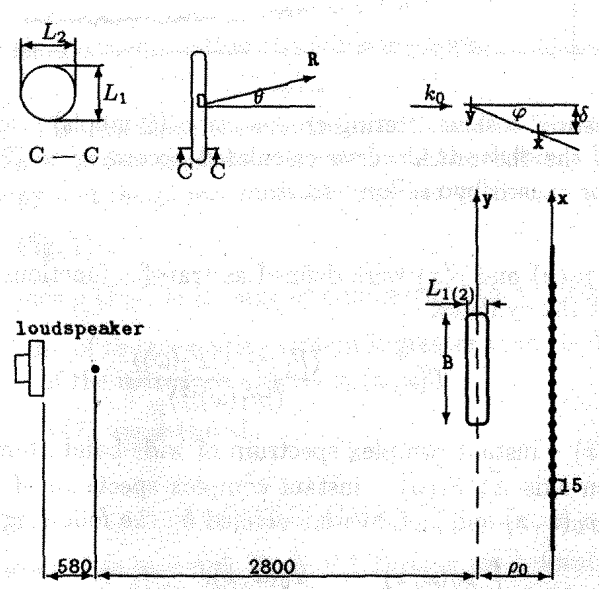

Fig. 5. The geometry of measurements in anechoic chamber.

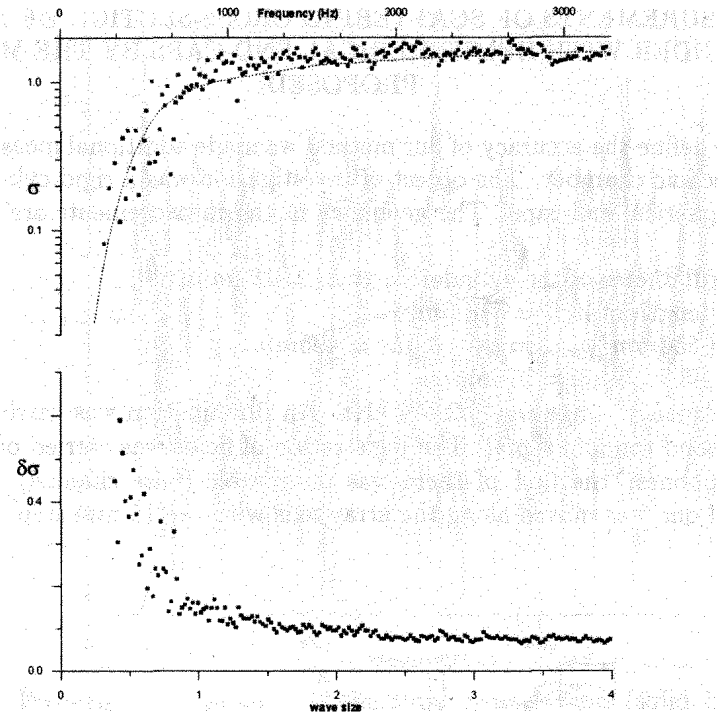

Fig. 6. Measured total scattering cross-section (symbols). Dotted line corresponds to the theoretical curve calculated according to [22]. $\delta\sigma$ is the relative error caused by random errors.

amplitudes $p_0(x)$ and $p(x)$ were defined as transfer functions $T(\omega, x)$ with and without the cylinder:

$$T(\omega, x) = \frac{\langle F_1^*(\omega, x) F_2(\omega) \rangle}{\langle |F_1(\omega)|^2 \rangle}. \tag{20}$$

Here $F_2(\omega, x)$ - instant complex spectrum of wide-band illuminating field, measured on axis $\vec{X}$; $F_1(\omega)$ - instant complex spectrum of base channel. The values $p_0(\omega, x)$ and $p(\omega, x)$ were defined by the following way:

$$\begin{cases} p_0(\omega, x) &= T_0(\omega, x), \\ p\ (\omega, x) &= T\ (\omega, x) - T_0(\omega, x). \end{cases}$$

"Measured" value of total scattering cross-section is shown in fig. 6 as symbols. In the same figure the results of calculations (according to [22])

were presented as dashed line. One can see that the measured values are in good comparison with theoretical ones. Small shift of experimental data compared to the theoretical ones at frequencies $ka \sim 1$ is caused by finiteness of aperture. Using the results of calculations one can be evident that at frequencies $ka \sim 1$: $Re(f_s) \sim Im(f_s)$. Assuming in (18) that $Re(f_s) = Im(f_s)$, and making calculations of weighting functions S_j, one could obtain $\chi \approx 0.2$ and $\sin(0.2) \approx +20\%$. Such simple estimation is very close to observed shift of experimental data. In frequency region $ka \geq 1$ uncertainties of σ_{tot} are about $\pm 10\%$ and caused by noise character of illumination.

CONCLUSIONS

We now draw conclusions. The proposed algorithm for experimental determination of the scattering cross-sections of elongated objects makes it possible to measure the scattering characteristics with a sufficiently high accuracy without using complex algorithms of data processing and without imposing rigorous requirements on the aquatorium in which the measurements are made. The proximity of the measuring system ensures a high signal-to-noise ratio and, correspondingly, high trustworthiness of the results obtained.

Finally, we should mention that the following approximations have been used:

1. L_1 (Fig. 1) is less than the dimension of the first Fresnel zone, so the measured object must be elongated and the distance between the linear array and the object must be large enough.
2. $L_2 \ll \rho$ (Fig. 1).
3. The distance ρ (Fig. 1) is large as compared with λ: $k\rho\cos\theta_0 \gg 1$.
4. The aperture of the measuring system is greater than the longitudinal dimension of the measured object.
5. Conditions (17) are satisfied.

ACKNOWLEDGMENTS

The authors would like to thank Prof. V.I.Turchin for helpful discussions, A.Ya.Balalaev and Dr. A.E.Ekimov for help in the measurements, the leading programmer A.V.Tsiberev for data acquisition and pre-processing, and A.V.Kraev for translation this text. This work was supported by the Russian Foundation for Basic Research (RFBR) grants №96-02-19460.

REFERENCES

1. *E.L.Shenderov*, Radiation and Scattering of sound [in Russian], Sudostroenie, Leningrad, 1989.

2. *V.K.Varadan and V.V.Varadan*, Acoustic, Electromagnetic and Elastic Wave Scattering: Focus on the T-Matrix Approach, Ohio State University, 1979.

3. *W.Tobocman*, Comparison of the T-Matrix and Helmholtz Integral Equation Methods for Wave Scattering Calculations // Journ. Acoust. Soc. Amer., 1985, V.77, N2, P.369-374.

4. *T.K.Stanton*, Simple Approximate Formulas for Backscattering of Sound by Spherical and Elongated Objects // Journ. Acoust. Soc. Amer., 1989, V.86, N4, P.1499-1510.

5. *D.T.DiPerna and T.K.Stanton*, Fresnel Zone Effects in the Scattering of Sound by Cylinders of Various Length // Journ. Acoust. Soc. Amer., 1991, V.90, N6, P.691-705.

6. *T.K.Stanton*, Sound Scattering by Elongated Elastic Objects. I. Means of Scattered Field // Journ. Acoust. Soc. Amer., 1992, V.92, N3, P.1641-1664. *T.K.Stanton and D.Chu*, II. Fluctuation of Scattering Field // ibid, P.1665-1678.

7. *R.J.Urick*, Principles of Underwater Sound, McGraw-Hill Book Company, 1975.

8. *D.M.Photiadis, J.A.Bucaro, B.H.Houston*, Scattering from flexural waves on a ribbed cylindrical shell // Journ. Acoust. Soc. Amer., 1994, V.96, N5, Pt.1, P.2785-2790.

9. *B.M.Salin and V.I.Turchin*, Holographic Reproduction of Wave Fields with an Arbitrary Time Dependence [in Russian] // Akust.Zh. 1992, V.38, N1, P.150-155; Sov. Phys. Acoust. 1992, V.38, N1 [in English].

10. *V.I.Turchin, N.M.Tseitlin and A.K.Chandaev*, Measurements of the Directional Diagram of an Array from Source Radiation in the Fresnel Zone by Microwave Holography and Computer Processing [in Russian], Radio-engineering and Electronics, 1973, V.18, N4, P. 725-734.

11. *V.I.Turchin and I.Sh.Fix*, Remote Measurements of the Characteristics of Moving Sources with Complex Spatio-Temporal Structure [in

Russian], In: Tomographic Methods in Physical-Technical Measurements, Moscow, 1990, Proc. Institute of Physical-Technical and Radio-Engineering Measurements, P. 159-173.

12. *G.V.Borgiotti, K.E.Jones*, The determination of the acoustic far field of a radiating body in an acoustic fluid from boundary measurements // Journ. Acoust. Soc. Amer., 1993, V.93, N5, P.2788-2797.

13. *G.V.Borgiotti, E.M.Rosen*, The determination of the far field of an acoustic radiator from sparse measurement samples in the near field // Journ. Acoust. Soc. Amer., 1992, V.92, N2, Pt.1, P.807-818.

14. *A.Sarkissian*, Reconstruction of the surface acoustic field on radiating structures // Journ. Acoust. Soc. Amer., 1992, V.92, N2, Pt.1, P.822-830.

15. *I.Sh.Fix, N.A.Sidorovskaia, V.I.Turchin*, Diagnostics of noise acoustic sources // Colloque C5, supplément an Journal de Physique IV, V. 4, mai 1994.

16. *I.Sh.Fix, N.A.Sidorovskaia, V.I.Turchin*, Reconstruction of spatial-time structure of complex acoustical sources from near-field measurements // Proc. of Third Int. Cong. on Air- and Structure-borne Sound and Vibration, June 13-15, 1994, Montreal, Canada, Vol. 1, P. 1701-1708.

17. *L.Felsen and N.Marcuvitz*, Radiation and Scattering of Waves, Prentice-Hall, Inc. Englewood Cliffs, New Jersey, 1973.

18. *G.Korn and T.Korn*, A Handbook of Mathematics [in Russian], The Nauka Publishers, Moscow, 1977.

19. *C.Clay and H.Medwin*, Acoustic Oceanography: Principles and Applications, John Willey &Sons, N-Y: 1977.

20. *A.V.Lebedev and A.L.Khil'ko*, Sound Scattering by Thin-Walled Elastic Cylinders of Finite Length // Sov. Phys. Acoust. 1992, V.38, N6, P.578-582.

21. *A.V.Lebedev*, The Asymptotic Method for Predicting Acoustic Radiation from a Cylindrical Shell of Finite Length, Journ. Acoust. Soc. Amer., 1993, V.94, N3, P.3493-3502.

22. *Junger M.C.*, Scattering by slended bodies of revolution // Journ. Acoust. Soc. Amer., 1982, V.72, P.1954-1956.

NUMERICAL AND EXPERIMENTAL STUDY OF SOUND FIELD FORMING IN SHALLOW WATER ENVIRONMENTS

M. Yu. Galaktionov, V. V. Borodin, A. V. Mamayev

INTRODUCTION

Sound field forming in shallow waters is a problem being actually of interest for applications. This work deals with numerical and experimental study of high frequency signal structure in shallow water environments by using high time resolution signals and angle resolving receiving systems.

Deterministic model of high frequency fields in the ocean waveguide is well-known [1] and is based on the geometrical (ray) approximation of the Helmholtz equation (under the supposition on linearity of the sound propagation). However it's also well-known that the deterministic model of ocean waveguide is not satisfactory in most cases. There are always hydrodynamical or temperature fluctuations in the sea water resulting as fluctuations of effective sound velocity. Since usually nothing is known about them from the deterministic point of view they need a statistical description. Also, boundaries of the waveguide (free surface and bottom) are usually rough and need a statistical description. Sound field forming in such waveguides presenting stochastic factors is a process that needs a careful theoretical and experimental studying. It shall be noticed that the factor of random boundaries may be often neglected for the deep water case, but in shallow water environments the sound field forming is strongly effected by the boundaries whose effect shall be accurately accounted.

The above mentioned random factors may be classified as "fast" and "slow" with respect to the characteristic time interval of primary signal processing (estimating of sound field parameters) in a sonar system. Usually the rough surface may be considered as "fast" factor since the characteristic correlation time interval of sea is about one second. The sound velocity fluctuations being effect of internal waves or ocean turbulence may be usually considered as "slow" for a sonar system.

In this work a general model of high frequency sound field forming in random shallow water environments is described and studied on simulated and experimental data.

1. THEORETICAL BACKGROUND

Let's consider an omnidirectional point source radiating narrow band signals ($\Delta\omega/\omega << 1$) with normalized spectrum $S_0(\omega)$. Since we deal with linear problems the general Green's function method may be used to calculate spectrum of the field created by the source:

$$p_S(\mathbf{r},\omega) = G(\mathbf{r},\mathbf{r}';\omega)S_0(\omega)\sqrt{W\rho c\gamma/4\pi}\ , \qquad (1)$$

where G(.) is the waveguide's frequency Green's function, W, γ, $\rho_{Wat}c$ are respectively the radiated acoustic power, concentration coefficient of the source array (pattern factor) and wave resistance of the medium.

In the case where there are random volume fluctuations $\mu(\mathbf{r},t)=c(\mathbf{r},t)/c_0(\mathbf{r})$ of the effective sound velocity in the waveguide ($c_0(\mathbf{r})$ is reference sound velocity field), the Green's function is also random and shall be described by statistical moments. Also, the boundaries of the waveguide (surface and bottom) may be rough and can be described only statistically. In this case the statistical description to the Green's function shall also be applied. The most interesting for applications are the two first moments: the mean ("coherent") field $\overline{G}(\mathbf{r},\mathbf{r}';\omega) = E[G(\mathbf{r},\mathbf{r}';\omega)]$ (the averaging E[.] of Green's functions of current waveguide realizations is done over the ensemble of fluctuations) and the second moment ("coherence function") $\Gamma(\mathbf{r}_1,\mathbf{r}_2,\mathbf{r}';\omega_1,\omega_2) = E[G(\mathbf{r}_1,\mathbf{r}';\omega_1)G^*(\mathbf{r}_2,\mathbf{r}';\omega_2)]$ or the local angle spectrum $N(\mathbf{e},\omega;\mathbf{R})$ related to the second moment of locally homogeneous fields:

$$\Gamma(\mathbf{r}_1,\mathbf{r}_2,\mathbf{r}';\omega,\omega) = \overline{G}(\mathbf{r}_1,\mathbf{r}';\omega)\overline{G}^*(\mathbf{r}_2,\mathbf{r}';\omega) + K(\mathbf{r}_1,\mathbf{r}_2,\mathbf{r}';\omega),$$

$$K(\mathbf{r}_1,\mathbf{r}_2,\mathbf{r}';\omega) = \oint_{\Sigma:|\mathbf{e}|=1} N(\mathbf{e},\omega;\frac{\mathbf{r}_1+\mathbf{r}_2}{2})e^{j\frac{\omega}{c}\mathbf{e}(\mathbf{r}_1-\mathbf{r}_2)}d\Omega(\mathbf{e}). \qquad (2)$$

In the most cases fluctuations μ are effect of hydrodynamic motions in the water layer (internal waves, large-scale turbulence) and of thin vertical fluctuations in the water stratification. Some spectral models of such fluctuations are well-known [2].

Deterministic model of the Green's function

The geometrical (ray tracing) approach to Green's function calculation is an effective and often used method for solving sound propagation problems as in layered as well as in irregular 2D or 3D deterministic ocean waveguides for frequency range from hundreds of Hz up to several kHz.

Under this approach the waveguide's time and frequency Green's functions are represented as a sum of quasi-plane wave fields arriving along ray paths [1]:

$$G(\mathbf{r},\mathbf{r}';\omega) = \sum_{\mu=1}^{M(\mathbf{r},\mathbf{r}')} A_\mu(\mathbf{r},\mathbf{r}';\omega)\cdot e^{i\omega t_\mu(\mathbf{r},\mathbf{r}')}, \qquad (3)$$

where $M(\mathbf{r},\mathbf{r}')$ is the total number of rays connecting the observation point $\mathbf{r}$ and the point $\mathbf{r}'$ where the incident source is located, $A_\mu(\mathbf{r},\mathbf{r}';\omega) = (f_\mu(\mathbf{r},\mathbf{r}')V_\mu(\mathbf{r},\mathbf{r}';\omega))^{1/2}/|\mathbf{x}-\mathbf{x}'|$ is amplitude of the μ-th ray path, $f_\mu(\mathbf{r},\mathbf{r}')$ is its focusing factor, the factor $V_\mu(\mathbf{r},\mathbf{r}';\omega) = |V_{Surf}(\omega)|^{2n_{\mu Surf}}|V_{Bot}(\omega)|^{2n_{\mu Bot}} \times 10^{-0,1\beta_{Wat}c\,t_\mu(\mathbf{r},\mathbf{r}')}$ is field weakening due to propagation along the μ-th ray path with $n_{\mu Surf}$ and $n_{\mu Bot}$ - numbers of reflections on ocean boundaries with reflection indexes $V_{Surf}(\omega)$, $V_{Bot}(\omega)$, β_{Wat} is *dB/km* absorption of acoustical energy in the sea water, $t_\mu(\mathbf{r},\mathbf{r}')$ is the ray's travel time.

Stochastic models of direct field fluctuations

Mostly general and frequency invariant mathematical model for the two first moments of the Green's function for the random ocean waveguide is described in [3]. The model is developed for a mean-regular stratified (layered) waveguide and takes account of the effect of multiple scattering from rough boundaries and from large-scale volume fluctuations of sound velocity. In the frame of this model, the single frequency second order moment that determines the field's space correlation and in particular its angular spectrum, satisfies to some integral equation derived in the work. The kernel and the free term of the equation describe the wave scattering from the fluctuations of sound velocity and boundaries' roughness. However, the numerical implementation of this comprehensive mathematical model is rather difficult. Hereafter, a more simple mathematical models for the two first moments of the Green's function is presented with regard to the multiple scattering from large-scale sound velocity fluctuations and to the first-order scattering from rough boundaries. The models are based on the geometric (ray) approximation applicable for high frequency sound fields. To build these more simple models, "fast" and "slow" random factors shall be considered separately.

Model of "slow" fluctuations

Let's consider first the "slow" fluctuations that are in general volume perturbations μ of sound velocity on the background of a mean sound velocity field $c_0(\mathbf{r})$. In this case current realization of the Green's function may be

presented under the ray approximation as follows:

$$G(\mathbf{r},\mathbf{r}';\omega) = \sum_{\nu=1}^{N(\mathbf{r},\mathbf{r}')} \bar{A}_\nu(\mathbf{r},\mathbf{r}';\omega) e^{j\omega\left(\bar{t}_\nu(\mathbf{r},\mathbf{r}')+\delta t_\nu(\mathbf{r},\mathbf{r}')\right)}, \qquad (4)$$

where $\bar{A}_\nu, \bar{t}_\nu$ are the mean ray amplitudes and travel times (equal to those for the reference waveguide, where $c = c_0(\mathbf{r})$) and $\delta t_\nu = t_\nu - \bar{t}_\nu$ are travel time fluctuations. So, the sound velocity perturbations are effecting only ray travel times and resume as phase perturbations defined by integrating $\mu(\mathbf{r})$ along reference ray paths $\Im_\nu$:

$$\delta t_\nu = -\int_{\Im_\nu} \mu(\mathbf{r})/c_0(\mathbf{r})\, ds \,. \qquad (5)$$

Ray amplitudes and the number of ray paths remain the same as for the reference waveguide. The well-known equation for the coherent field derives from averaging the exponent in (4):

$$\bar{G}(\mathbf{r},\mathbf{r}';\omega) = \sum_{\nu=1}^{N(\mathbf{r},\mathbf{r}')} \bar{A}_\nu(\mathbf{r},\mathbf{r}';\omega) e^{j\omega\, t_\nu(\mathbf{r},\mathbf{r}') - \frac{1}{2}\omega^2 D_{t_\nu}(\mathbf{r},\mathbf{r}')}, \qquad (6)$$

where $D_{t_\nu} = E\left[(\delta t_\nu)^2\right]$ is the variance of the travel time defined through the covariance function $K_\mu(\mathbf{r}_1,\mathbf{r}_2) = E[\mu(\mathbf{r}_2)\mu(\mathbf{r}_2)]$ by integrating along the reference ray path connecting the points $\mathbf{r}'$ and $\mathbf{r}$:

$$D_{t_\nu}(\mathbf{r},\mathbf{r}') = \int_{\Im_\nu}\int_{\Im_\nu} \frac{K_\mu(\mathbf{r}(s'),\mathbf{r}(s''))}{c_0(\mathbf{r}(s'))c_0(\mathbf{r}(s''))} ds' ds'' \approx \int_{\Im_\nu} \frac{Z_\mu(\mathbf{r}(s))}{c_0^2(\mathbf{r}(s))} ds, \quad (7)$$

where $Z_\mu(\mathbf{r}) = \int_{\Im_\nu} B_\mu(\mathbf{r}, s\mathbf{e}_\nu(s)) ds$, $\mathbf{e}_\nu(s) = d\mathbf{r}(s)/ds\big|_{\Im_\nu}$, $B_\mu(\mathbf{r},\rho) =$ $= K_\mu(\mathbf{r}+\rho/2,\mathbf{r}-\rho/2)$. The meaning of Z_ν is integral correlation interval of the field $\mu(\mathbf{r})$ along the ν-th ray path.

Thus, the effect of the scattering from large-scale fluctuations of sound velocity is manifested as additional attenuation of the coherent field in comparison with the propagation in the reference waveguide. For example in the case of scattering from fluctuations due to Harret-Munk's internal waves, RMS of ray travel times may reach units of millisecond for ranges of tens kilometers. So, in this case at frequency 1 kHz the coherent field is $\sim \exp\{-(2\pi)^2/2\} \approx \exp\{-20\} < 10^{-8}$ times weaker than the reference field.

For the coherence function (the second order moment) the following equation derives after averaging:

$$\Gamma(\mathbf{r}_1,\mathbf{r}_2,\mathbf{r}_0;\omega_1,\omega_2) = \sum_{\kappa=1}^{K(\mathbf{r}_1,\mathbf{r}_0)} \sum_{\nu=1}^{N(\mathbf{r}_2,\mathbf{r}_0)} A_\kappa(\mathbf{r}_1,\mathbf{r}_0;\omega_1) A_\nu^*(\mathbf{r}_2,\mathbf{r}_0;\omega_2) e^{j\omega_1 t_\kappa(\mathbf{r}_1,\mathbf{r}_0) - j\omega_2 t_\nu(\mathbf{r}_2,\mathbf{r}_0)} \times$$

$$\times \exp\left\{ -\frac{\omega_1^2}{2} D_{t_\kappa}(\mathbf{r}_1,\mathbf{r}_0) - \frac{\omega_2^2}{2} D_{t_\nu}(\mathbf{r}_2,\mathbf{r}_0) + \omega_1 \omega_2 R_{\kappa\nu}(\mathbf{r}_1,\mathbf{r}_2;\mathbf{r}_0) \right\}, \qquad (8)$$

where

$$R_{\kappa\nu}(\mathbf{r}_1,\mathbf{r}_2;\mathbf{r}_0) = \int_{\Delta_\kappa} \int_{\Delta_\nu} \frac{K_\mu(\mathbf{r}(s'),\mathbf{r}(s''))}{c_0(\mathbf{r}(s'))c_0(\mathbf{r}(s''))} ds' ds'' \qquad (9)$$

is the covariance of travel times for the κ-th and ν-th ray paths. Thus, the covariance function $R_{\kappa\nu}(\mathbf{r}_1,\mathbf{r}_2;\mathbf{r}_0)$ fully defines the two first moments under the geometric (ray) approximation.

If the distance between the points $\mathbf{r}_1$ and $\mathbf{r}_2$ is much more larger than the correlation interval of sound velocity fluctuations, then the correlation of travel time fluctuations is defined, firstly, by the vicinity of the source from where the contribution may be approximated as

$$\int_0^\infty \int K_\mu(\mathbf{e}_\kappa(\mathbf{r}_0)s', \mathbf{e}_\nu(\mathbf{r}_0)s'') c_0^{-2}(\mathbf{r}_0) ds' ds'' ,$$

where $\mathbf{e}_\kappa(\mathbf{r}_0)$, $\mathbf{e}_\nu(\mathbf{r}_0)$ are the unit vectors tangent to the κ-th and ν-th ray paths at the source point. This fact is evident if the observation points $\mathbf{r}_1$ and $\mathbf{r}_2$ are lying in some horizontal plane because the reference ray paths have a constant divergence in the horizontal plane, so that if they pass through volumes of medium with not correlated fluctuations after the first cycle, they do the same further more. If the observation points are lying in some vertical plane, the vicinities of intersection points $\boldsymbol{r}_q$ of reference rays should contribute also into the travel times' correlation:

$$\sum_q \int_{-\infty}^{\infty} \int K_\mu(\mathbf{e}_\kappa(\mathbf{r}_q)s', \mathbf{e}_\nu(\mathbf{r}_q)s'') c_0^{-2}(\mathbf{r}_q) ds' ds'' .$$

However, for the Harret-Munk's spectrum, as for any other one vanishing to zero when the wave number tends to zero, this integral is equal to zero.

Let it be $\mathbf{r}_1+\mathbf{r}_2 = 2\mathbf{r}$, $\rho = \mathbf{r}_1-\mathbf{r}_2$ for small separations of observation points. Let the point $\mathbf{r}$ is connected to the source point $\mathbf{r}_1$ by N ray paths in the reference medium. Let also consider such separations of observation points that are not larger than the characteristic width of reference ray beams. That means that if a reference ray connecting the points $\mathbf{r}_1$ and $\mathbf{r}$ is described by a function $\boldsymbol{r}_\nu(s)$, then the corresponding reference ray connecting the points $\mathbf{r}_0$ and $\mathbf{r}\pm\rho/2$ is described by the function $\mathbf{r}_\nu(s)\pm(\rho/2)\Lambda_\nu(s,L)$.

where $\Lambda_\nu(s,L)$ is the matrix solution of the problem

$$\mathbf{F}(s)\Lambda_\nu(s,L)=0,\ \Lambda_\nu(0,L)=0,\ \Lambda_\nu(L,L)=\mathbf{P}_\nu,\ \left[\mathbf{P}_\nu\right]^{\alpha\beta}=\delta^{\alpha\beta}-e_\nu^\alpha e_\nu^\beta,$$
$$\mathbf{F}(s)=\mathrm{diag}\left\{n^{-1}\frac{d}{ds}\left(n\frac{d}{ds}\right)+\left(\kappa^2-\frac{\partial^2\ln n}{\partial\nu^2}\right),n^{-1}\frac{d}{ds}\left(n\frac{d}{ds}\right)\right\}. \tag{10}$$

The operator $\mathbf{P}_\nu$ projects onto the subspace that is orthogonal to the tangent vector $\mathbf{e}_\nu=\{e^\alpha{}_\nu\}$ of the ν-th ray path. Under the above conditions, the covariance of travel time fluctuations along a single reference ray path is computed as follows

$$R_{\nu\nu}(\mathbf{r},\rho;\mathbf{r}_0)=D_{t_\nu}(\mathbf{r},\mathbf{r}_0)-\frac{1}{2}\frac{B_\mu(\mathbf{r},0)(\mathbf{e},\rho)^2}{c_0^2(\mathbf{r})}- \tag{11}$$
$$-\frac{1}{2}\int_0^\infty\rho_\alpha\Lambda_\nu^{\alpha\gamma}(s,L)\frac{\mu_{\gamma\delta}(s,l(s))}{c_0^2(\mathbf{r})}\Lambda_\nu^{\delta\beta}(s,L)\rho_\beta ds,$$

where $\mu_{\gamma\delta}(s,l(s))=\int_{-\infty}^{\infty}\partial^2{}_{\rho_\gamma\rho_\delta}B_\mu(u,\rho_1)\Big|_{\rho_\alpha=0}du$. The covariance for any two different reference rays can be written as

$$R_{\kappa\nu}(r,\rho;r_0)=\int_0^\infty\int\frac{K_\mu(e_\kappa(r_0)s',e_\nu(r_0)s'')}{c_0^2(r_0)}ds'ds''+\int_0^\infty\int\frac{K_\mu(e_\kappa(r)s',e_\nu(r)s'')}{c_0^2(r)}ds'ds''-$$
$$-\frac{B_\mu(\mathbf{r},0)}{4c_0^2(\mathbf{r})}\left\{(\mathbf{e}_\kappa(\mathbf{r}),\rho)(\mathbf{e}_\nu(\mathbf{r}),\rho)-(\mathbf{e}_\kappa(\mathbf{r}),\mathbf{e}_\nu(\mathbf{r}))\left[(\mathbf{e}_\kappa(\mathbf{r}),\rho)^2+(\mathbf{e}_\nu(\mathbf{r}),\rho)^2\right]\right\}+ \tag{12}$$
$$+\frac{1}{4c_0^2(\mathbf{r})}\left(\int_{-\infty}^0\int K_\mu(\mathbf{e}_\kappa(\mathbf{r})s',\mathbf{e}_\nu(\mathbf{r})s'')ds'ds''(\rho_1^\kappa+\rho_1^\nu),(\rho_1^\kappa+\rho_1^\nu)\right).$$

It follows from the equation (11) that the matrix

$$\Lambda_\nu^{\alpha\beta}(\mathbf{r},\mathbf{r}_0)=c_0^2(\mathbf{r})\int_0^\infty\Lambda_\nu^{\alpha\gamma}(s,L)\frac{\mu_{\gamma\delta}(s,l(s))}{c_0^2(\mathbf{r}(s))}\Lambda_\nu^{\delta\beta}(s,L)ds \tag{13}$$

has the meaning of covariance matrix of ray arrival angle fluctuations. In force of the space symmetry of the internal wave spectrum and thanks to the layered model for the deterministic part of the sound velocity field, this matrix is diagonal: arrival angle fluctuations in the horizontal plane are not correlated with those in the vertical plane for one ray. Fluctuations of travel time and of arrival angle are also not correlated for each ray.

In the equation (12), the two first terms describe the correlation of travel time along the κ-th and ν-th ray paths, and the last term does the same for the correlation of ray arrival angles. Correlation of arrival angles of different rays is determined only by the vicinity of the receiver, and the correlation of travel time fluctuations is determined by the vicinities of the source and the receiver (the vicinities of the intersection points of any two different reference rays do not contribute to the correlation). As the variances of ray travel time and arrival angle fluctuations should grow with the distance from the source but theirs correlation for different ray paths should not globally grow, hence they may vary from one cycle to another, the correlation coefficient decreases when the number of ray cycles grows, though the correlation coefficient for one cycle can be considerable.

The equation for statistical characteristics of arrival time and angle fluctuations can be rewritten to express them trough the spectrum of sound velocity fluctuations. Then after using the Harret-Munk's spectral model of internal waves an equation derives that allows to compute the statistical characteristics of rays (variances of travel time fluctuations and correlation functions of arrival angle fluctuations in the vertical and horizontal plane) by doing a simple integrating along ray paths. It's to note that as follows from this equation the main contribution to the correlation functions in the deep ocean case is given by ray turning points. Equations for time correlation intervals of ray travel times and of grazing arrival angles also derive.

The equation (7) for the variance of ray travel times can be simplified under the supposition that the covariance function of sound velocity fluctuations can be approximated by a gaussian function

$$K_\mu(\mathbf{r},\mathbf{r}') = D_\mu(z)\exp\left\{-\frac{1}{2}(\mathbf{r}-\mathbf{r}')\mathbf{R}_\mu^{-1}(\mathbf{r}-\mathbf{r}')\right\}, \qquad (14)$$

where $\mathbf{R}_\mu^{-1} = \mathrm{diag}\left(\rho_H^{-2}(z), \rho_H^{-2}(z), \rho_V^{-2}(z)\right)$, $\rho_H(z)$ and $\rho_V(z)$ are horizontal and vertical correlation intervals for the field μ. One integration in (7) can be done by the Laplace method and the following equation derives:

$$D_{t_\nu}(\mathbf{r},\mathbf{r}_0) = \frac{\sqrt{2\pi}}{c_\nu^2}\int_{\Im_\nu} \frac{D_\mu(z)\rho_V(z)}{\cos^2\chi\sqrt{\sin^2\chi+\varepsilon^2(z)\cos^2\chi}}ds, \qquad (15)$$

$\varepsilon(z) = \rho_V(z)/\rho_H(z)$, $c_\nu = c_0/\cos\chi_0$ (c_ν is sound velocity at the returning point of the ν-th ray path). By the same way similar equations derive for variances of fluctuations of ray arrival angles:

$$D_{\varphi_\nu}(\mathbf{r},\mathbf{r}_0) = \frac{\sqrt{2\pi}}{R^2(\mathbf{r},\mathbf{r}_0)}\int_{\Im_\nu} \frac{D_\mu(z)\varepsilon(z)R^2(\mathbf{r}(s),\mathbf{r}_0)}{\rho_H(z)\cos^2\chi\sqrt{\sin^2\chi+\varepsilon^2(z)\cos^2\chi}}ds, \qquad (16)$$

$$D_{\chi_0}(\mathbf{r},\mathbf{r}_0)=\frac{\sqrt{2\pi}}{\Delta^2(\mathbf{r},\mathbf{r}_0)}\int_{\Lambda}\frac{D_\mu(z)\varepsilon(z)\Delta^2(\mathbf{r}(s),\mathbf{r}_0)}{\rho_H(z)\cos^2\chi\left(\sin^2\chi+\varepsilon^2(z)\cos^2\chi\right)^{2/3}}ds\,, \qquad (17)$$

where $\Delta=\left(\partial R/\partial\chi_0\right)\sin\chi$. Time correlation interval of fluctuations is

$$\tau_v(\mathbf{r},\mathbf{r}_0)=\sqrt{\int_{\Lambda}\frac{\cos^{-2}\chi K_\tau(z)\rho_V(z)}{\sqrt{\sin^2\chi+\varepsilon^2(z)\cos^2\chi}}ds\Bigg/\int_{\Lambda}\frac{\cos^{-2}\chi D_\mu(z)\rho_V(z)}{\sqrt{\sin^2\chi+\varepsilon^2(z)\cos^2\chi}}ds}\,. \qquad (18)$$

In the case where sound velocity fluctuations are effect of free internal waves they are related by a simple equation:

$$\mu(\mathbf{r},t)=DN^2(z)\xi(\mathbf{r},t)\,, \qquad (19)$$

with $\xi(\mathbf{r},t)$ the function describing the field of internal waves, $N(z)$ the frequency profile of free gravitational waves: $N^2(z)=d\ln\rho_{Wat}(z)/dz$, with $\rho_{Wat}(z)$ water density at depth z. The value D depends slightly on ocean regions and on depth and is equal to $\sim 10\ sec^2/m$. For the case of ocean internal waves the parameter $\rho_H\sim 7\ km$ and the anisotropy factor $\varepsilon(z)$ depends on depth and varies usually in the range from 1/70 to 1/100.

If the Harret & Munk's spectral model is used, following expressions for functions intervening in the above equations derive:

$$D_\mu(z)=\frac{\Psi q}{\pi}\frac{N^3(z)}{\Omega_i}\,,\quad K_\tau(z)=\frac{2\Psi q^3\langle e^2\rangle}{\pi}\frac{N^4(z)}{\Omega_i^2}\,,$$
$$\rho_H(z)=\frac{1}{q\bar{e}}\sqrt{\frac{\Omega_i}{2N(z)}}\,,\quad \rho_V(z)=\frac{\Omega_i}{q\bar{e}N(z)}\,, \qquad (20)$$

where Ω_i is the Earth rotation frequency, and $\langle e^2\rangle\approx 40$, $\bar{e}=\sqrt{\langle e^2\rangle}$, $q=\pi\Omega_i\Big/\int\sqrt{N^2(z)-\Omega_i^2}dz$.

Errors due to the use of the geometrical (ray) approximation and frequency and distance ranges of its validity can be estimated. The approach does not valid in the vicinity of any focal point of the reference field (so, near field's caustics) since the denominator in the equation (17) vanishes. The estimation for the deep water case shows that, excepting this special case, the above geometrical approach is well-founded to model sound fields' fluctuations being effect of the scattering from internal waves in the ocean for sound frequencies 100 Hz and higher, and in some situations for more low frequencies. For shallow waters the question about validity is much more subtle. As to fluctuations of ray travel times, the approach should be valid above some higher frequency (about 500 Hz). As to fluctuations of ray arrival angles, the

approach ceases to be valid from ranges about one or two kilometers since the probability to be in the vicinity of some field's caustic becomes to high for any point of reception in the waveguide. Another theoretical approach shall be applied to consider fluctuations of ray arrival angles in the shallow water case.

Model of "fast" fluctuations (sea reverberation)

Let's consider now "fast" fluctuations of sound fields (reverberation) that are generally due to the scattering from waveguide's boundaries and from small scatterers in water volume. As the reverberation is effect of scattering from large number of independent roughness or scatterers it may be considered as normally time-space distributed process with zero mean value (taking into account some well-known limitations [4]). Thus, the reverberation interference on any two array's elements at points $\mathbf{r}_1$, $\mathbf{r}_2$ are fully statistically described by its space-time covariance function

$$K_{\text{Rev}}(\mathbf{r}_1,\mathbf{r}_2,t_1,t_2) = K_{\text{Rev}}(\mathbf{r},\tau;\mathbf{R},T),$$
$$\mathbf{R} = (\mathbf{r}_1+\mathbf{r}_2)/2,\ T = (t_1+t_2)/2,\ \mathbf{r} = \mathbf{r}_1-\mathbf{r}_2,\ \tau = t_1-t_2. \qquad (21)$$

Under the ray approach the first statistical moment of some sound field ("mean" field) after averaging over random scatteres is defined by the equation (3) where the coefficients of surface and bottom reflection ($V_{\text{Surf}}(\omega)$, $V_{\text{Bot}}(\omega)$) and of volume absorption (β_{Wat}) are different from the deterministic case to take into account the scattering of sound energy (coherent coefficients).

If it may be admitted that the reverberation is quasi-stationary on observation intervals (its time-space covariance functions depend slowly on the argument T) then the covariance function (21) can be expressed through a space-frequency covariance function $K_{\text{Rev}}(\mathbf{r},\omega,\mathbf{R},T)$:

$$K_{\text{Rev}}(\mathbf{r},\tau;\mathbf{R},T) = \int K_{\text{Rev}}(\mathbf{r},\omega;\mathbf{R},T)\exp\{j\omega\tau\}d\omega\ . \qquad (22)$$

Usually it may be admitted also that the reverberation is locally space homogeneous on the receiving array (its space-frequency covariance function depend slightly on the argument $\mathbf{R}$ that may be considered as phase center $\mathbf{r}_{\text{R}}$ of the receiving array). In this case the space-frequency covariance function can be expressed through the angle-frequency spectrum $N_{\text{Rev}}(\mathbf{e},\omega,\mathbf{R},T)$:

$$K_{\text{Rev}}(\mathbf{r},\omega;\mathbf{r}_{\text{R}},T) = \oint\limits_{\Sigma|\mathbf{e}|=1} N_{\text{Rev}}(\mathbf{e},\omega;\mathbf{r}_{\text{R}},T)e^{j\frac{\omega}{c}(\mathbf{e},\mathbf{r})}d\Omega(\mathbf{e})\ . \qquad (23)$$

Sea reverberation is the major source of interference for active sonar systems. As the reverberation is effect of the sound scattering from rough boundaries of the ocean (from bottom and surface) and from biological or

bubble scattering layers in the water volume, it's reasonable to distinguish surface, bottom and volume reverberation components regarding the generating mechanism.

In the general case, the reverberation noise is not a stationary process. Its variability interval is the same or some larger then the incident signal's duration if it is not larger than several seconds. Nevertheless the reverberation may be often considered as random process close to quasi-stationary processes (whose correlation coefficient depends on the time difference and the variance depends on the current time moment). In the case where the dependence of the variance versus the current time is enough "slight" it becomes allowed to consider the reverberation process as stationary. For forward scattering active sonar systems where large or even continuous signals are radiated this approach is still more right. For active systems using deterministic high time resolution probing signals the time correlation function of some reverberation process shall be considered as known since it is equal to the correlation function of the probing signal. Also, in the case where receiving arrays are smaller than sound field variability interval in the waveguide, the reverberation can be considered as homogeneous random field and described by an angle-frequency spectrum in accordance with (23).

Models for all types of reverberation – for the boundary reverberation including the surface and the bottom reverberation types as well as for the volume reverberation – are well known. As the boundary reverberation is usually the main (dominant) interference for active sonar systems (and especially for the forward-scattering sonar or the sonar with quasi-continuous radiation), we'll consider only this type of reverberation in this work. Following notations are used in the equation for the reverberation to support the previously defined notations:

$S^2(t)$ is the power shape of radiated signal,

$\mathbf{r}_R = (\mathbf{x}_R, z_R)$, $\mathbf{r}_S = (\mathbf{x}_S, z_S)$ are coordinate vectors of the receiving and source arrays' phase centers,

$\mathbf{e}_R$, $\mathbf{e}_S$ is the normalized vector defining some direction from the receiving and source arrays' phase centers,

$B_S(\mathbf{e}_S - \mathbf{e}_S^0)$ is directivity pattern of the source (on pressure), $\mathbf{e}_S^0$ is its direction of compensation,

$\mathbf{e}_\perp$ is unit vector orthogonal to the scattering boundary,

$\mathbf{e}(\mathbf{e}', \mathbf{r}, \mathbf{r}')$ is the normalized tangent vector of a ray path connecting points $\mathbf{r}'$ and $\mathbf{r}$ when considered at the point $\mathbf{r}$ and equal $\mathbf{e}'$ at the point $\mathbf{r}'$,

$t(\mathbf{e}', \mathbf{r}, \mathbf{r}')$ is propagation time for the ray path connecting the points $\mathbf{r}'$ and $\mathbf{r}$ if its tangent vector at the point $\mathbf{r}'$ is $\mathbf{e}'$,

$f_\nu(\mathbf{r},\mathbf{r}')$, $t_\nu(\mathbf{r},\mathbf{r}')$, $\mathbf{e}_\nu(\mathbf{r},\mathbf{r}')$ are focusing factor, propagation time and arrival tangent vector considered at the point $\mathbf{r}$ for the ν-th ray path connecting the points $\mathbf{r}'$ and $\mathbf{r}$,

$$V_\nu(\mathbf{r},\mathbf{r}';\omega) = |V_{Surf}(\omega)|^{2n_{\nu Surf}} |V_{Bot}(\omega)|^{2n_{\nu Bot}} \cdot 10^{-0,1\beta_{Wat} c\, t_\nu(\mathbf{r},\mathbf{r}')},$$

$\chi(\mathbf{e})$ is the grazing angle of the vector $\mathbf{e}$,

$M_I(\mathbf{e},\mathbf{e}';\omega)$ is the energetic scattering index from the direction $\mathbf{e}'$ to the direction $\mathbf{e}$ for the boundary I (the subscript I may be equal to "*Surf*" or to "*Bot*"), it depends on frequency and maybe on coordinates, but usually all boundaries are considered as homogeneous,

$\mathbf{r}^I_\eta(\mathbf{e}_R) = (\mathbf{x}^I_\eta(\mathbf{e}_R), z^I) = \mathbf{r}^I_1(\mathbf{e}_R) + (\eta - 1)CL(\mathbf{e}_R)\mathbf{e}_\parallel$ are points $(\eta = 1,2,...\infty)$, where a ray having the direction $\mathbf{e}_R$ at the reception arrives onto the boundary I, with $CL(\mathbf{e}_R)$ the length of ray cycle's horizontal projection when the ray has the direction $\mathbf{e}_R$ at the receiver, z^I - depth of the boundary and $\mathbf{e}_\parallel = \dfrac{\mathbf{e}_R - (\mathbf{e}_R,\mathbf{e}_\perp)\mathbf{e}_\perp}{\left|\mathbf{e}_R - (\mathbf{e}_R,\mathbf{e}_\perp)\mathbf{e}_\perp\right|}$; so for each η the vector $\mathbf{r}^I{}_\eta(\mathbf{e}_R)$ defines a point of sound scattering from the boundary.

Using above introduced notations and supposing that

1) space correlation intervals of rough boundary surfaces are not larger then the space interval of variability of sound field complex amplitude in the ocean,
2) boundary is quasi-horizontal and its roughness is homogeneous

following equation for the instant angle spectrum $N^I_{Rev}(\mathbf{e}_R,\omega,T)$ of the first-order scattered boundary (surface or bottom) reverberation was derived for the narrow-band pulse radiation mode:

$$N^I_{Rev}(\mathbf{e}_R,\omega,T) = \frac{W\rho c\gamma}{4\pi} \sum_{\eta=1}^{\infty} \sum_{\nu=1}^{N(\mathbf{r}^I_\eta(\mathbf{e}_R),\mathbf{r}_S)} \frac{M_I(-\mathbf{e}(\mathbf{e}_R,\mathbf{r}^I_\eta(\mathbf{e}_R),\mathbf{r}_R),\mathbf{e}_\nu(\mathbf{r}^I_\eta(\mathbf{e}_R),\mathbf{r}_S);\omega)}{\left(\mathbf{e}(\mathbf{e}_R,\mathbf{r}^I_\eta(\mathbf{e}_R),\mathbf{r}_R),\mathbf{e}_\perp\right)} \times$$

$$\times V(\mathbf{r}_R,\mathbf{r}^I_\eta(\mathbf{e}_R);\omega) f_\nu(\mathbf{r}^I_\eta(\mathbf{e}_R),\mathbf{r}_S) V_\nu(\mathbf{r}^I_\eta(\mathbf{e}_R),\mathbf{r}_S;\omega) R^{-2}(\mathbf{r}^I_\eta(\mathbf{e}_R),\mathbf{r}_S) \times$$
$$\times \mathrm{B}^2_S(\mathbf{e}_\nu(\mathbf{r}_S,\mathbf{r}^I_\eta(\mathbf{e}_R)) - \mathbf{e}^0_S) S^2(T - t(\mathbf{e}_R,\mathbf{r}^I_\eta(\mathbf{e}_R),\mathbf{r}_R) - t_\nu(\mathbf{r}^I_\eta(\mathbf{e}_R),\mathbf{r}_S)). \quad (24)$$

The equation (24) is written for a horizontally regular waveguide by it's easily generalized for some arbitrary slightly changing waveguide. It's to note that when doing calculation of boundary reverberation by (24), the signal's shape $S^2(...)$ acts as "window function" and determines on the boundary a band area of pseudo-ellipse form from where the re-

verberation is collected. The area encircles points of projections of the receiver and source position on the boundary. In the case of continuous radiation the factor $S^2(...)$ isn't zero for any argument and the area spreads on the whole boundary.

The scattering index pattern entering in the equation (24) is the major factor defining the sea reverberation. It may be calculated by using different known approximations. For the free surface (sea wind waving) the most practical is the DSM (Dual-Scale Model) [5] that uses simultaneously the approximation of the SPT (Small Perturbations Theory) and of the Kirchhoff method (tangent plane approximation). Another approximation is the SSM (Small-Slope Method) proposed by Voronovich [6] and already tested by one of the authors [7–9]. Finally, a model based on both the SSM and DSM may be proposed and seems to be a good compromise between accuracy of modeling results and requirements of computer implementation. As to the scattering from a rough bottom having random internal structure, a set of empirical and theoretical models is also available.

2. NUMERICAL IMPLEMENTATION AND MODELING

Simulations were done by using the SSS[1] software for numerical simulation of underwater sonar systems. The software is developed by the authors for computer simulations of coherent and interference components of sound fields in ocean environments and of raw signal data received by an underwater sonar based on a linear array. The sound field modeling is done by a Fortran-77 program SHELF3 realizing the above presented theoretical models: the deterministic Green's function model, the stochastic ones and interference models. The main future of the software is the ability of the ray tracing program SHELF3 to conduct simulations for irregular shallow water environments with 3D[2] bottom surfaces where bottom effects are very important and even have major effect on sound propagation and signal forming.

The both above methods (DSM and SSM) of scattering index pattern calculation for reverberation modeling are implemented in the software (a combined spectrum of waving sea surface based on the Peirson-Moskowitz spectral model is used). The shadowing effect is taken into account that decreases scattering index when one of grazing angles (of the incident or scattered wave) is lower than the RMS of roughness slope. Scattering index pattern is normalized to conserve the total acoustical energy in one act of scattering on a rough and partially absorbing surface.

---

[1] SSS – Sonar Simulation System.

[2] 3D bottom surface is some one where depth values are depending on both two horizontal coordinates.

The fluctuation modeling (the above described stochastic model of the Green's function) is done by another Fortran-77 program RASS. It's a 1D ray tracing program for 1D environments with a mean flat bottom surface and only 1D mean sound velocity profile (not varying in the horizontal plane). The program RASS calculates for some 3D grid of points in the waveguide statistical parameters of rays (variances of ray arrival angles and travel times and also time correlation interval of these fluctuations) for the case where random fluctuations of sound velocity are due to free internal waves of some spectral model (the Harret & Munk's model is actually implemented).

The software is developed for both the two computer platforms: IMB-PC compatible or SUN computers having some windows-based operation system (like Windows 3.1 or Windows-95/NT for PCs and OpenWindow for SUNs).

3. VALIDATION AND NUMERICAL INVESTIGATION

Published experimental data from the SACLANT's shallow water experiment [10] (experiment # 1) and raw signal data from a sea experiment conducted by AAI in the Barents sea in summer (experiment # 2) were used to validate the signal and fluctuation models of the SSS software and as experimental background to the numerical investigation of sound fields forming in shallow water conditions.

Experiment # 1 (Elba's shelf in Mediterranean)

This experiment was conducted by the SACLANT Center on the Elba's shelf (Italian western coast) in 1978-79. Experimental conditions described in [10] were used to do numerical modeling by the SHELF3 program. As in [10] there are no information on sea state during the experiment, it was supposed for simulations that sea states corresponded to developed wind seas for wind speeds 10 m/sec for winter propagation conditions and 8 m/sec for summer conditions. Simulated and experimental data are compared for following items:

1. Propagation losses.
2. Fluctuations of ray travel times.
3. Frequency shifts (calculated as $1/\tau$ where τ is the correlation time of ray travel time fluctuations, a parameter calculated by RASS).

Twenty five corresponding modeling tasks were formulated to validate the signal and fluctuation models by the experimental data from [10]. In general, results of propagation losses modeling (Fig. 1 – Fig. 2) show satisfactory agreement with the measured data if one takes into account the fact that the modeling results strongly depend on the bottom reflection index pattern used for it, especially for the summer conditions (with sub-bottom sound channel). Since in [10] there are no real measured data on bottom reflection index for that sea area to implement in the model, the simulation was done with some empirical model of bottom reflection. Bottom reflection index pattern corresponding to the bottom structure proposed in [10] for numerical modeling purposes was calculated and it was shown that it doesn't give a good agreement of modeling and experimental data when using the SHELF3 3D ray tracing program. Simulated data shown on the Fig. 1a prove that the real effective bottom reflection coefficient in the SACLANT's experiment is some higher than the empirical model predicts, especially for

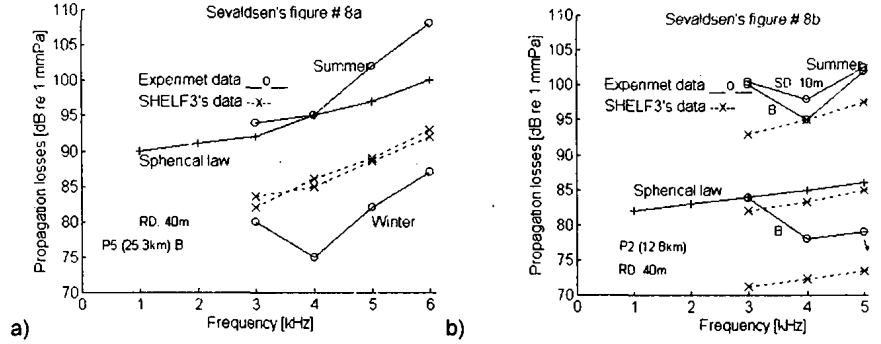

Fig. 1. Simulated and measured data on propagation losses versus frequency for the source a) P5 at 25.3 km on the bottom, b) P2 at 12.8 km on the bottom (receiver depth 40 m).

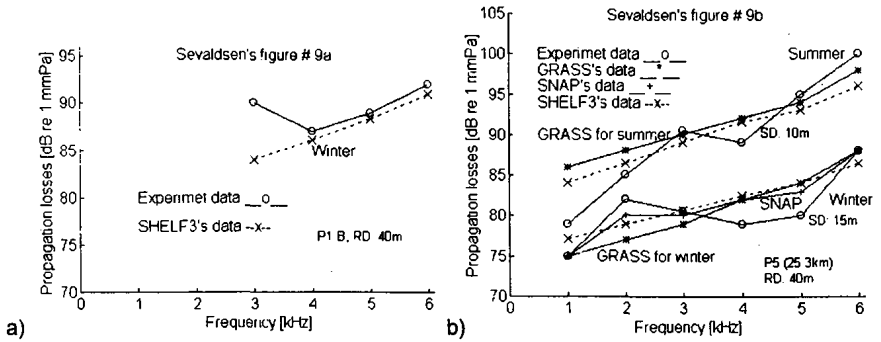

Fig. 2. Simulated and measured data on propagation losses versus frequency for the source a) P1 on the bottom, b) P5 at 25.3 km on 10 m and 15 m depth (receiver depth 40 m).

slow grazing angles. It follows from the data on the Fig. 1b since simulated and measured data differ some more for the source placed on the bottom. For the winter conditions, propagation losses are generally determined by the surface reflection index that depends on the sea surface state established by the wind speed. Simulated data prove that the wind speed during the experiment should be some lower than supposed for the numerical modeling (10 m/sec). It seems to be a rather realistic conclusion. So, by adjusting the parameter that the modeling results depend on it's possible to match better the experimental data on propagation losses.

RMS of ray delays calculated by the RASS numerical model (Fig. 3b, Fig. 4) are generally smaller than measured in the SACLANT's experiment. Simulated and experimental data agree better for summer conditions (Fig. 4b). Also, the simulated data on RMS of ray delays or on frequency shift don't manifest any frequency dependence while among the experimental data presented in [10] (Fig. 3a and Fig. 5) there are some experimental curves showing high dependence of frequency shift versus central frequency of signals. It's to note that corresponding values of frequency shift are rather high (about several deciHz).

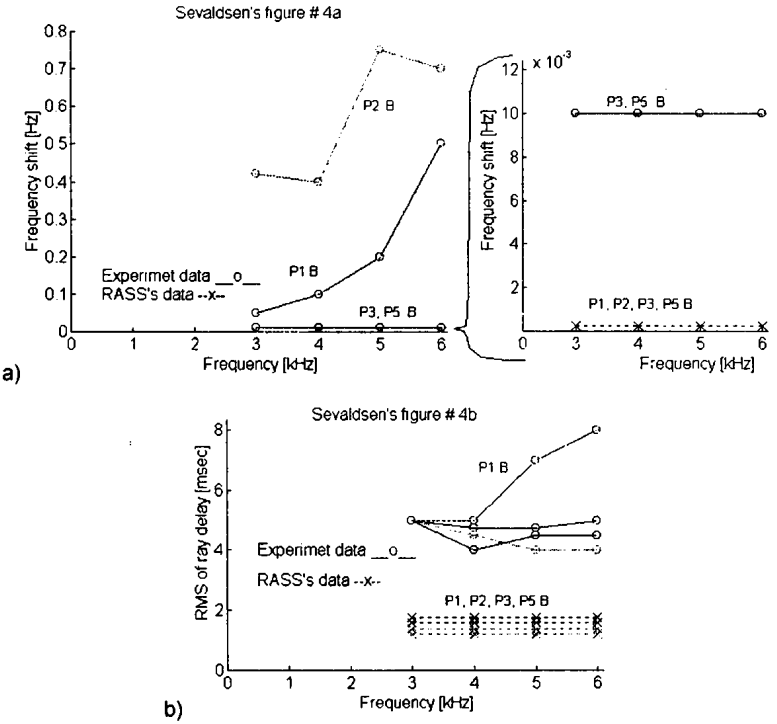

Fig. 3. Simulated and measured data on frequency shift and RMS versus frequency (winter, sources on the bottom) averaged on receiver depths 40 m and 54 m.

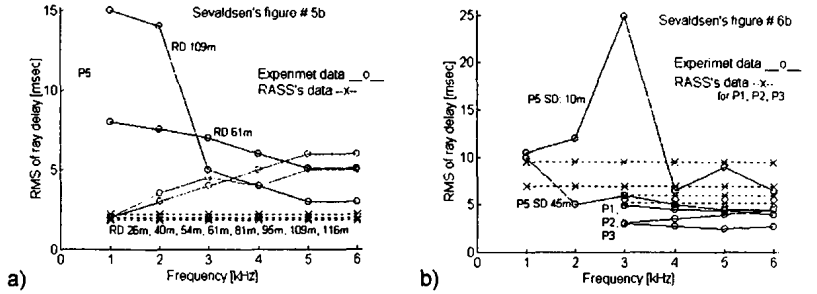

Fig. 4. Simulated and measured data on delay RMS versus frequency for a) winter, source P5 at 15 m depth, various receiver depths, b) summer, sources P1, P2, P3 on the bottom) averaged on receiver depths 40 m and 54 m.

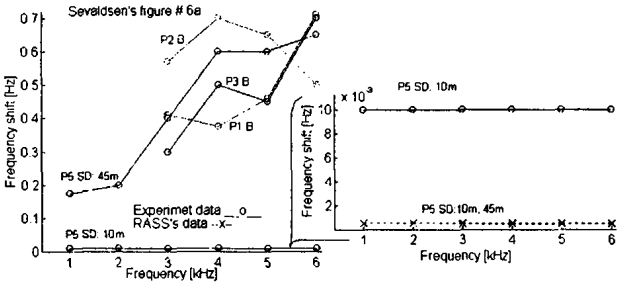

Fig. 5. Simulated and measured data on frequency shift versus frequency (summer, source at P5 on 10 m and 45 m depth) averaged on receiver depths 40 m and 54 m.

As to the disagreement between the simulated and experimental data on frequency shift, Sevaldsen himself wrote in [10] that the fast ray travel time fluctuations (that correspond to high frequency shifts) should be due to the surface scattering. Really, if it's the case, one shall observe some strong frequency dependence of frequency shift because the Raleigh parameter changes strongly with the signal's central frequency and then more of surface roughness become "of large-scale" (compared to sound wave's length) and produce their part of fluctuations. It's to note also that corresponding experimental values of frequency shift match well common value of correlation time of surface roughness (about one or several seconds) as it should be expected. So, it's the effect that is referred to the surface reverberation in the SSS software. The RASS model doesn't deal with this type of sound field fluctuations.

On the other hand, in the data from [10] (Fig. 3a, Fig. 5) there are some curves where frequency dependence of frequency shift are rather slow. It's to note that corresponding values of frequency shift are low (about 10 mHz). These frequency shifts should be corresponding to the scattering from slow fluctuations of effective sound velocity in the water like internal waves and large-scale turbulence produce. It follows from the scattering theory for such sound velocity fluctuations that resulting perturbations of ray phase parameters are well (even rigorously) described by the geometrical (ray) approach

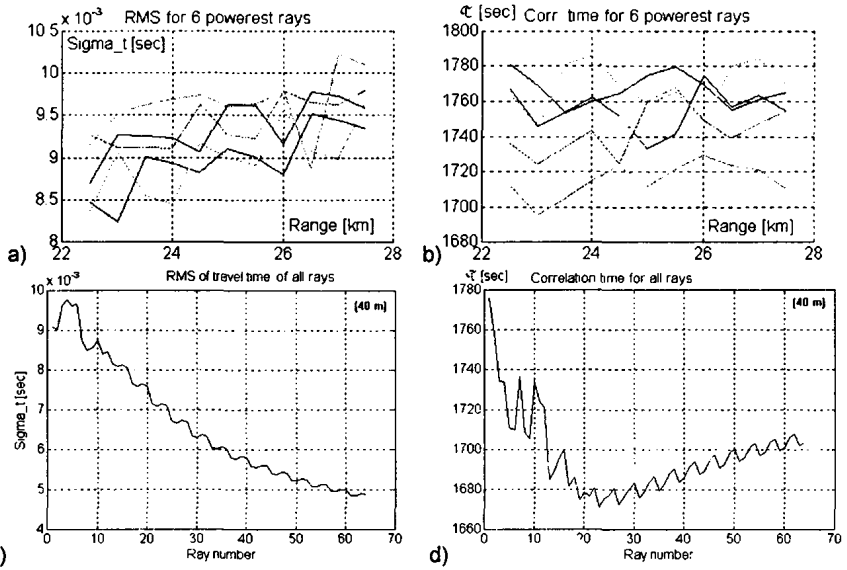

Fig. 6. Example of delay RMS and τ data simulated by RASS (summer, source at 45 m depth).

implemented in the RASS numerical model. Evidently such fluctuations shall be frequency independent since ray path are not depending on frequency. Of cause, when frequency increases, the wave length decreases and there are some more of sound velocity fluctuations in the medium volume that adds to the scattering, but these fluctuations are of very small power and one may estimate their effect as being not significant. So the data from the SACLANT's experiment match well the theoretical conclusion about frequency independence (the slow frequency dependence observed in the experimental low frequency shift data may be due to measurement errors). It's to note also that in most cases experimental delay RMS data are slow depending on frequency as it should be if delay fluctuations were due to the scattering from large-scale fluctuations of effective sound velocity in the water (the slow dependence versus frequency in the experimental RMS data for this case may be as well the effect of measurement errors). It also matches the theory. Of cause, delay RMS being effect of the surface scattering should be more strongly frequency depending, but they shall be less than 1 msec, so the measurement of corresponding fast delay fluctuations is prevented by strong delay fluctuations (about several msec) due to the scattering from large-scale volume perturbations in the sea medium.

The main reason of the disagreement of simulated and modeled values of RMS and correlation times of ray delays being effect of the scattering from low perturbations in the sea medium shall be particularities of the time-space spectrum of sound velocity fluctuations in shallow water areas. The

numerical model RASS is based on the assumption that the sound scattering is due to internal waves of the Harret & Munk's spectrum. Nevertheless real spectra of internal waves and other medium perturbations for a shallow water area may be rather different from the Harret & Munk's spectrum so that small-scale fluctuations become more powerful. Other spectra of internal waves for shallow waters exist (unpublished) and will be incorporated in the numerical model on following stage of its development.

Experiment # 2 (Barents sea, shallow water)

Experiment # 2 whose raw signal data is used to test the SSS software and to study field forming in shallow water environments was conducted by AAI in summer 1990 in the Barents sea (shallow water area) with mean bottom depth ~ 245 m. Sound velocity profile was of the bottom channel type, bottom reflection index pattern was characteristic for this sea and was defined by a table for simulations, sea state was about 2 points (low wind ~ 4 m/sec). One moving source was emitting LFM (linear frequency modulated) pulses from ~ 7.3 m depth, source's speed was ~ 12 knots (~ 6 m/sec). Source trajectory relative to the receiver, start and end moments are shown on the Fig. 7. The source has some directivity pattern, nevertheless in the case of the experiment's geometry it's sure that received signals were radiated by the main lobe of this pattern.

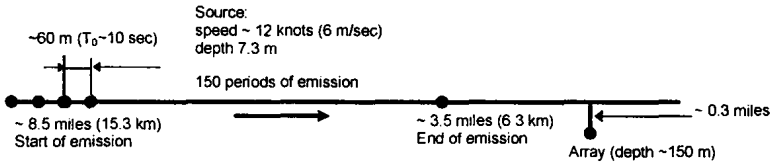

Fig. 7. Scheme of the experiment # 2 (Barents sea).

Signal parameters were following:

- LFM pulse duration ~ 0.095 sec,
- Central frequency ~ 3243 Hz,
- Deviation ~ 600 Hz,
- Signal recurrence ~ 10 sec.

Reception was by a vertical linear array of uniformly spaced 21 hydrophones (spacing 26 cm), array's phase center was at ~ 150 m depth and its drift was ~ 0.5 knot (~ 0.25 m/sec). Signals were sampled at frequency 2600 Hz. Each raw signal record corresponds to a 0.3635 sec time window and contains 1024 signal level measurements. Therefore, raw signal data for each period consists of 21•1024 float point numbers (for each sampled time moment the 21 channels were recorded quasi simultaneously). The recorded time window was chosen so that the signal pulse arrive at the beginning. To do it, time spacing between start moments of the records was calculated by the formula

$$T = T_0 [1 - v(c_{mean} \cos\chi_{mean})^{-1}] , \quad (25)$$

where T_0 is the recurrence of the signal radiation, v is the source's speed, c_{mean} is the mean sound velocity of the channel and χ_{mean} is the mean grazing angle of ray paths for this situation.

Simulation of signals received by the array have been done by the simulating part of the SSS with taking into account all parameters of the experiment. Then following processing steps were done both on experimental and simulated raw signal data:

1) For all 150 records, decision statistics of primary processing by time correlation for only one hydrophone (11th) are built to observe time evolution of correlation functions (the Doppler frequency shift about 13 Hz due to the source motion was accounted).
2) For each correlation function all correlation maximums exceeding some relative threshold are found and shown as a point. The result is shown on the Fig. 8.

It's clearly seen that the time evolution of correlation functions for the experimental data is some similar to those for simulated data. In particular, one can see the same general structure in the delay-time space due to several ray arrivals evaluating in time. The difference is that for the simulated data this evolution of arrivals has a rather regular and deterministic character: peaks are forming curved lines on the (Delay, Time) plane. It's seen in the simulated data that each peak correspond not to a solitary ray arrival but to a couple of ray arrivals since peaks have amplitudes fluctuating in time. These amplitu-

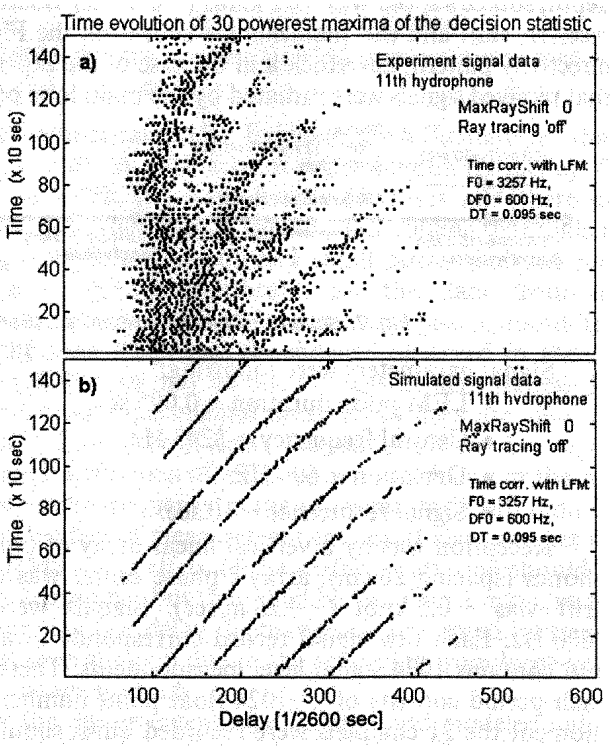

Fig. 8. Time evolution of correlation maximums for the 11th hydrophone for experiment # 2 (Barents sea): a) experiment data, b) simulated data (flat bottom).

de fluctuations are effect of the source motion since phase difference between rays in each couple is changing because of the motion. Characteristic period T_{coupl} of this time modulation of couple peaks may be estimated from the equation

$$\omega v_{source} T_{couple} (\cos\chi_1 - \cos\chi_2) / c_{mean} \sim 2\pi ,$$

from where using the value of parameters in the experiment one can estimate $T_{coupl} \sim 50$ sec. Really, it is in the range 70 - 100 sec for different rays. In the experiment data we observe also the same curves but they are like « blurred » curved structures formed by groups of maximums.

Fig. 9 shows two correlation functions of two consecutive periods. In the simulated data we see clearly well-distinguished ray arrivals. For the experimental data we have another situation where there are much more of correlation maximums and they form groups of maximums corresponding to the well-segregated maximums we observe in the simulation.

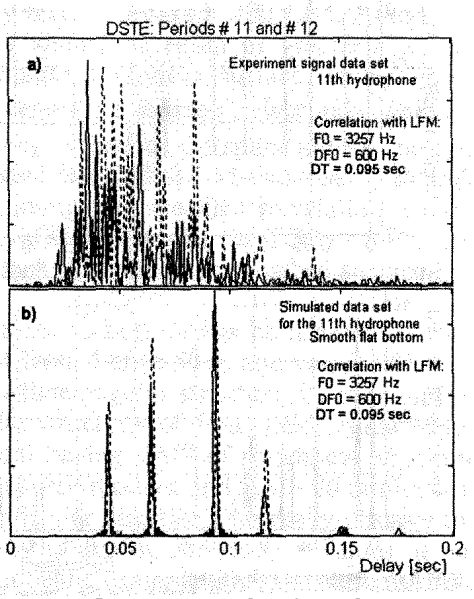

Fig. 9. Two correlation functions of two consecutive periods for the 11th hydrophone for experiment # 2 (Barents sea): a) experiment data, b) simulated data (smooth flat bottom).

It follows from theoretical estimations that this effect is due essentially to the fact that the real bottom is not flat but has some large-scale roughness. So, when a sufficiently high frequency sound field is reflected (scattered) on the bottom, there are always roughness (since the spectrum of the bottom roughness is continuous) on which the scattering resumes as specula reflection. Quantity of such roughness is determined by the ratio of the efficiently[3] sounded area to the projection of the area of the Fresnel zone of a ray path. Estimating shows that this number can be rather high for the experimental situation (the bottom in the experimental area is rather rough), so there are many ray arrivals in the reception.

[3] May be determined as area on the scattering interface from which specula reflected ray paths can arrive to the receiver. The area is mainly depending on the RMS of roughness slope and SVP.

Such a field should be statistically interpreted and considered as coherent reverberation. Really, we should consider the waveguide as random one since the bottom is not flat but rough, so when a sound source moves, bottom realizations are different for consecutive periods of signal radiation. It makes points of specula reflection moving on the bottom and makes corresponding correlation maximums fluctuating in delay and amplitude. Estimations and the experiment correlation functions (Fig. 9) show that delay fluc-

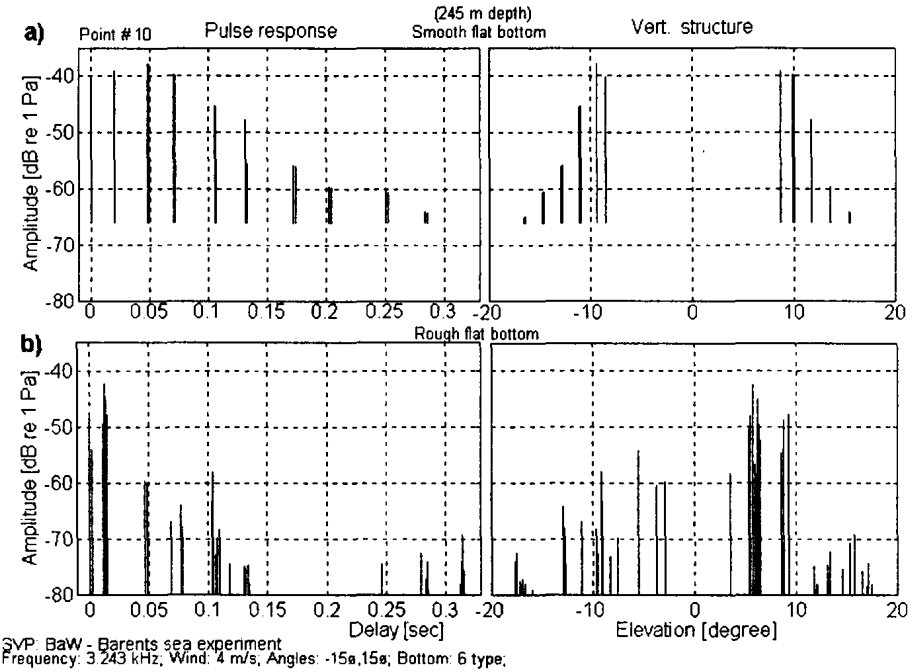

Fig. 10. Time-angle structure of the direct field for experiment # 2 (Barents sea) when simulated for a flat (a) and a rough (b) bottom (RMS of two-scale roughness height 50 m and 20 m, correlation length 2 km and 0.2 km).

tuations of the correlation maximums are small and relatively slow (they are quasi stable), but their amplitudes are fluctuating much more quickly and sharply than their delays. This effect is due essentially to the fact that all these correlation maximums are due at least to couples of rays

(as it is for the maximums of the direct signal in simulation). Some maximums may be corresponding not to couples but to couples of ray couples since the time resolution of the signal may be not sufficient to segregate maximums of these ray couples. In this case, those maximums should be some more rapidly fluctuating in amplitude. Also, the amplitude fluctuation of the maximums may be partially the effect of the motion of caustics created by the reflection from the not-flat bottom interface, but this effect should not be very significant.

To simulate this effect we should do a numerical modeling of the direct field for the experimental situation with a rough bottom surface as model of the real surface by using the 3D ray tracing program SHELF3. Roughness correlation radius for this modeling should be equal or greater than the Fresnel radius. So we have to simulate a random surface having about $N*Range/Fresnel\_radius$ points versus the source-receiver axis, where N is about 10 to well calculate the bottom surface for the spline approximation. This is done by the specially developed RANDBOT Matlab tool that adds normally distributed perturbations having user specified correlation lengths to some bottom surface stored in an ASCII file under the TOP or SURFER formats used in the SSS software. Then, it writes the perturbed surface in a file specified by user.

The direct signal modeling for a rough bottom has been done for various RMS values of roughness height from 1 m to 50 m and various correlation length to study how the signal's time-angular structure depends on this parameter. Fig. 10 shows time-angular structures of direct field simulated for a flat bottom and for a rough bottom having RMS of roughness 50 m and correlation length 2 km for the axis source-receiver and RMS 20 m and correlation length 0,2 km for the perpendicular direction. We really observe the same effect of « ray breeding » as in the experiment. So, the values of parameters having been used for this modeling example might be close to those of the real shallow water waveguide in the experiment area. We note also that the values are rather realistic.

The direct signal modeling for big number of random realizations of the bottom surface and theoretical estimations allows to conclude that the « ray breeding » is also effect of the horizontal refraction due to bottom roughness. Let's prove this sentence. As ray paths are extremal solutions of the eukonal equation (the Fermat principle), only a movement of points of specula reflection versus the normal direction to the mean (large-scale) boundary is able to give rise to a first-order change of ray travel times. In our case the flat bottom is the mean boundary and we may estimate RMS of ray travel times due to specula reflection on roughness when considering them only in the source-receiver axis as

$$\sigma_t \sim 2(N_{cycles})^{1/2}\sigma_{bot}\, \sin\chi \,/\, c_{mean}\,. \qquad (26)$$

Taken values used for the modeling, we have $\sigma_t \sim 0.010\ sec$ that matches the delay width of groups of maximums we observe in the experiment data. Now let's consider the effect of the horizontal refraction. As the RMS of roughness slope is about the ratio $\sigma_\alpha \sim \sigma_{bot} / correlation\_length$ (~ 1 degree for the modeling) and this is also an estimate for the horizontal refraction of one ray on bottom roughness, we can estimate RMS of ray travel times due to this effect as

$$\sigma_{t\alpha} \sim (N_{cycles})^{1/2} Range\ (\sigma_\alpha)^2 / c_{mean}\ , \qquad (27)$$

so the ratio of two RMS is

$$\sigma_{t\alpha} / \sigma_t \sim Range\ \sigma_{bot} / (2\ sin\chi\ correlation\_length^2)\ , \qquad (28)$$

and we have $\sigma_{t\alpha} / \sigma_t \sim 1$ for our set of values of parameters in the experiment. It shall be noticed that if RMS of roughness slope increases, the relative effect of horizontal refraction will increase also and the horizontal refraction should be taken into account more properly. To do it by making computer modeling, the source azimuth sector of calculated ray paths shall be wider than the RSM of the azimuth refraction (σ_α).

So, the direct field modeling for a flat or a rough bottom surface shows that there should be solitaire ray arrivals (for the flat bottom case) or groups of ray arrivals (for the rough bottom case) in the time-angle structure of received signals. Each group is created by some area of points of specula reflection on the bottom surface. It's to note that there should be more of such points versus the orthogonal direction than versus the source-receiver axis. It's due to the fact that the ratio of Fresnel radius for these axes is about $sin\chi \sim 0.1$, so there are more of bottom perturbations having correlation length about the smaller radius than those having length about the bigger radius. We derive from this consideration that the horizontal refraction needs to be taken into account by a correct and accurate way in computer simulations of direct signals.

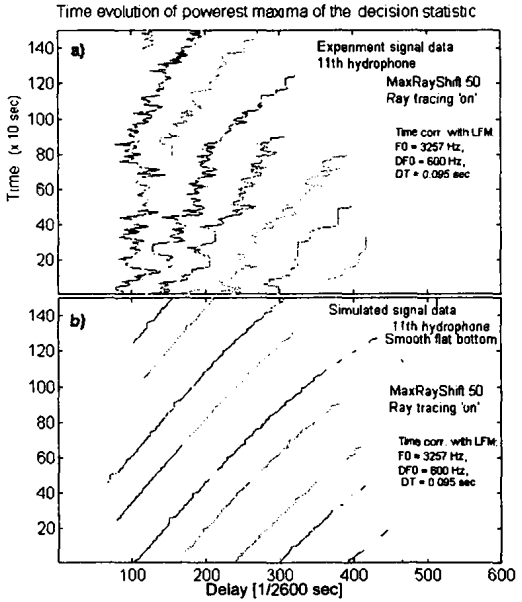

Fig. 11. Tracing of identified correlation maximums for 11th hydrophone for the experiment # 2 (Barents sea): a) experiment data, b) simulated data (smooth flat bottom).

Finally, the computer modeling provides an estimate of delays between solitaire rays or groups that is for the experimental conditions at least about 50 points of resolution (~ 17 msec) of the correlation processing. Taking into account this information, let's do the following:

3) For each period find the highest maximum in the correlation function and suppress all other maximums in the delay window ±50 resolution elements around the highest maximums. Further, find another highest maximum (amongst kept ones), do the same thing for it, and so on (peak selection with window peak suppression).
4) Do peak tracing. Result is shown on the Fig. 11.

After all this processing we find the same curves of ray arrivals as in the modeling with flat bottom, but fluctuating in delay. The ray parameters A_{ij}, τ_{ij}, may be processed to get their mean values $\langle A \rangle_{ij}$, $\langle \tau \rangle_{ij}$ and RMS (the averaging in time domain should be done for some time window) but this results isn't able to provide us a useful information about sound field stability since the fluctuations are due to the source motion and bottom roughness, as we have established above.

Also, validation of the reverberation model implemented in the SSS software was done on SNR normalized data from time correlation processing for each hydrophone channel (the normalization of correlation functions for each hydrophone is done at the primary processing output by dividing them by the noise level estimated as mean function value without account of correlation peaks higher than 0.2 of the global maximum).

It was established that when the DSM was used, simulated and experimental SNR data do not agree (compare Fig. 12 a and c). The simulated reverberation level should be suppressed by the factor ~10^3 or more to match the experiment. When the SSM is used, the comparison of modeled and experimental SNR data shows a much better agreement (see Fig. 12 b, c).

The reason of such disagreement of the DSM and experimental results is that the DSM is not valid for low grazing angles. Simulations and theoretical study show (Fig. 3) that the DSM's pattern of scattering index has always a Kirchhoff's maximum for the specula direction. When the incident angle tends to zero the slope's RMS for the Kirchhoff's lobe tends also to zero and the lobe grows to infinity. The behavior of the SSM's pattern of scattering index is very different from the DSM for slow incident grazing angles. The SSM's pattern has no maximum for the specula direction, its maximum is directed to some higher angle. The effect of such an angular pattern will be scattering of sound energy to the bottom of the waveguide where it will be absorbed. As result, the total reverberation intensity at reception shall be lower than in the case of the DSM's pattern. It shall be also noticed that the SSM's pattern for slow incident angles is rather similar to the SPT[4]'s one at

[4] SPT - Small Perturbations Theory.

scattering angles some higher than the incident one. Nevertheless the SPT's pattern is quasi zero at the vicinity of the specula direction where the SSM's pattern has some realistic level.

For high incident angles (10° and more) the SSM's and DSM's results become rather similar. The SPT gives a very high level for the angle range where it is not valid (the Raleigh parameter is more then unity).

All the above described processing of the experimental raw signal data set for shallow water propagation conditions allows us to do some very important conclusions.

I. In the presence of a rough interface in a shallow water waveguide having large-scale roughness, time structure of real high time resolution signals is composed of big number of ray arrivals. This number is about the ratio of the efficiently sounded area to the Fresnel zone area projected onto the rough interface.

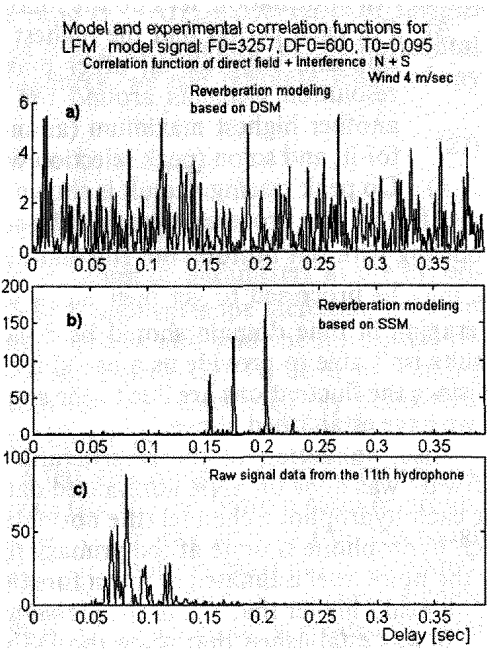

Fig. 12. Normalized correlation functions calculated on simulated (a, b) and experimental (c) raw signal data for the Barents sea summer experiment when using the Dual Scale (a) and the Small Slope (b) scattering models.

II. Accordingly to propagation conditions, ray arrivals are grouped around model ray arrivals predicted by a deterministic numerical model of sound propagation in the « mean waveguide » where the large-scale roughness of the interface is not taken into account.

III. Each group of ray arrivals is a rather stable (on delay and angle) structure (fluctuations on delay and angle for each ray in some group are small). Also, the corresponding group of correlation peaks is stable, but peak levels are usually very fluctuating if the source or the receiver moves since each peak contains in fact several ray arrivals.

IV. To predict well in modeling a signal structure (pulse response of a real ocean waveguide) for propagation conditions where the bottom effect is crucial, it is necessary to do modeling with some random realization of the rough bottom interface with roughness correlation lengths of the interface realization about characteristic lengths of projections of the Fresnel radius of

a ray path connecting the receiver and the emitter on the axis source-receiver and the orthogonal one. The effect of horizontal refraction on signal structure forming needs to be correctly taken into account. In the most cases it makes the numerical modeling unrealistic because of a high computer power (high CPU and memory consuming) needed to do it. If it's the case, one might do a modeling for interface realizations having larger correlation intervals, with doing correctly reverberation modeling. Such one will be to add in the received signal time-angle structure new ray arrivals providing signals being coherent with the direct signal. The new ray arrivals shall be distributed following some probability law that needs to be established theoretically or by numerical modeling.

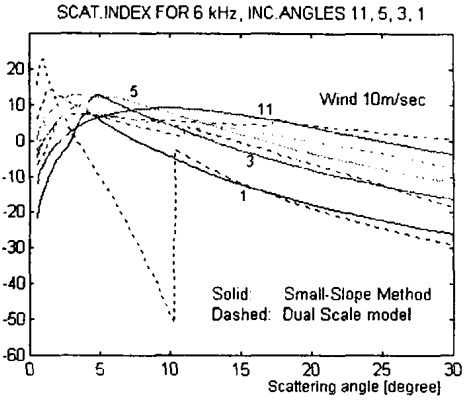

Fig. 13. Comparisons between the SSM and DSM for 6 kHz sound and wind 10 m/sec.

V. The DSM (Dual-Scale Model) is not a good tool for reverberation modeling for shallow water environments. The SSM (Small-Slope Method) provides much better and realistic scattering index pattern. A comprehensive model based on both the small-slope (for low grazing angles) and the dual-scale (for abrupt and backscattering angles) methods may be proposed as a compromise between accuracy of modeling results and requirements of computer implementation.

CONCLUSION

A software system SSS for sonar signal and processing simulation actually in development by the BUWAL Group is described in this document. Results of software testing on experimental data and raw signal data are presented. It shows a satisfactory agreement between experimental and modeling results. Important conclusions on time-angle structure of coherent signals and interference for shallow water environments are presented. Development of this software system will be continued in accordance to those conclusions to match better particularities of acoustic signals and interference forming in shallow water propagation conditions.

REFERENCES

1. Brekhovskikh L. M., Lysanov Yu. P. *Fundamentals on ocean acoustics.* Springer-Verlag, Berlin - Heidelberg - New York, 1983.
2. *Sound Transmission Through A Fluctuating Ocean* / St. M. Flatté (Editor). Cambridge Univ. Press, London - New York - Melbourne.

3. Borodin V. V., Galaktionov M. Yu. New *Mathematical Model of Sound Field Fluctuations in Shallow Water Environments with Boundary and Volume Roughness.*

4. *Akustika okeana* / Brekhovskikh L. M. (Ed.). Moscow, Nauka Editions, 1954.

5. Galaktionov M. Yu., Kopyl E. A. *Modeling of angle-frequency spectrum of sound fields scattered from sea waving surface* // Aspects Récents de l'Acoustique Sous-Marine Russe. IFREMER Editions, 1994.

6. Voronovich A. G. *On the theory of sound scattering from rough surfaces* // Sov. Phys. Acoust. V. 30 (1984), № 6, p. 747.

7. Galaktionov M. Yu. *Use of new methods for computation of scattering index of a scalar wave field on a rough surface with a complicated spectral constitution* // Phys. Acoust. V. 37 (1991), № 2, p. 270.

8. Galaktionov M. Yu., Kopyl E. A., Volkova A. V. *Comparison of the small-slope method and the dual-scale model for calculation of the ocean surface sound scattering index* // Phys. Acoust. V. 40 (1994), № 1, p. 63.

9. Galaktionov M. Yu. *Scattered Sound Angular-Frequency Spectra of The Ocean Perturbed Surface: Application and Numerical Investigation of The Small-Slope Method* // Proceedings of the 2nd European Conference on Underwater Acoustics. Copenhag, 1994.

10. Sevaldsen E. *On effect of medium fluctuations to underwater sound propagation* // Bottom-Interacting Ocean Acoustic / Edited by A. Kuperman and F. B. Jensen. Plenium Press, New York and London, 1980.

NEW MATHEMATICAL MODEL OF SOUND FIELD FLUCTUATIONS IN SHALLOW WATER ENVIRONMENTS WITH BOUNDARY AND VOLUME ROUGHNESS

V. V. Borodin, M. Yu. Galaktionov

INTRODUCTION

It's well-known that the oceanic waveguide is a complex medium where some mean sound velocity profile and boundaries determining a regular refraction are accompanied by fluctuations of sound velocity and boundary surfaces. These fluctuations shall be described only statistically since a detailed information on them is not available. Therefore acoustical fields in such a waveguide shall also be described statistically and the problem of calculating their statistical characteristics arises. The same problem may be formulated for the atmosphere acoustics and in the theory of electromagnetic wave propagation where some waveguide propagation may be available with accompanying scattering from the air turbulence and roughness of the Earth surface (relief).

Knowledge on statistical characteristics of sound fields in the ocean and the ability to do a prognostic on them are crucial for development of various hydroacoustical systems: communication and data transmission, detection, localization and classification, acoustical probing and solving inverse problems in the ocean (including the tomography), etc. The interest to statistical problems of underwater acoustics is growing because of last studying the long-range acoustical propagation for tomography mapping of the ocean and for investigation of global climatic processes. Analysis of fluctuations of parameters of received signals can bring a useful information about the origin of fluctuations, therefore inverse problems of stochastic tomography of the ocean could be formulated and solved. Thus, the theoretical development of an adequate mathematical model of sound fields for statistic waveguides is still of high practical interest.

Development of such mathematical models has already a long history [1] —[7] however almost all known models take into account only one of three major stochastic factors (surface waving, rough randomly heterogeneous bottom and volume fluctuations of effective sound velocity in the water) determining the statistics of hydroacoustical signals (an exclusion is the study [8], where both the scattering from the surface and volume fluctuations are considered but under the low-frequency approximation using the normal mode approach). That approach is sufficient for some applications, in particular for deep water propagation conditions. Nevertheless it's not usually the case for shallow waters where a simultaneous account of all above mentioned random factors should be done. Also, approximations of sound fields used to build the known models (for example the ray approximation [9], [10]) prove to be not valid or quickly losing their validity with range in shallow water propagation conditions. Another important shortcoming of the known models is the lack of ability to describe statistically fluctuations of the small-scale interference structure of sound fields. It may be a consequence of the model origin and of the used approximation for sound field description (for example, the case of the energy transport equation [5], [11], [12]) or of simplifications of the model being done to obtain a solution that could be practically used (for example the case of equations for normal modes' correlation coefficients [13]). All this is the reason to continue theoretical researches for development of mathematical models of sound fields in the random ocean that would be free of the above mentioned shortcomings.

In this work such a model is developed that is based on the rigorous wave formulation of the problem with using a minimum of physically well-founded approximations. It's done by generalizing the approach of [7] to deriving equations for statistical moments of fields in refractive waveguides for the case of two scattering boundaries and volume fluctuations of sound velocity. Particular merit of this new model is its validity for a wide range of sound frequency and various propagation conditions including the shallow water case. Another merit is the ability of the model to describe statistically fluctuations of the small-scale interference structure of sound fields.

1. FORMULATION OF THE PROBLEM

Taking into account physical aspects in science in engineer problems for which the results of this theoretical investigation should be of interest we assume for this work that volume fluctuations of properties of the ocean medium affecting the underwater sound propagation can be described as slight and slow fluctuations of the effective sound velocity $c(\mathbf{r},\varepsilon t)$ or refraction index (here ε is small parameter), so the classic Helmholtz wave equation with the operator $\Delta - c^{-2}(\mathbf{r},\varepsilon t)\partial_t^2$ is a good model of sound propagation. Since

the correlation time of sound velocity fluctuations is usually much larger than the period of sound waves, duration of emitted signals and characteristic time of primary signal processing ($\varepsilon << 1$) then the dependence of the effective sound velocity on t will be neglected in this work.

The motion of the sea surface should be taken into account when considering the sound scattering from it. In this case the sound energy is diffused not only in space but also in frequency. However the correlation time of sea waving is usually much smaller than the period of sound waves so it becomes allowed to neglect the frequency scattering effect for some applications. The account of the frequency scattering in the mathematical model of statistical characteristics of acoustical signals in the random ocean should be a topic for following theoretical researches.

Thus the mathematical formulation of the problem is following. Sound field (the Green's function) $G(\mathbf{r},\mathbf{r}_0)$ of a monochromatic point source at the point $\mathbf{r}_0$ in the ocean where the sound velocity field $c(\mathbf{r})$ ($\mathbf{r}=(\mathbf{x},z)$, $\mathbf{x}=(x,y)$) and boundaries - the free surface Σ_S (described by the function $0+\zeta_S$) and the bottom Σ_B (described by the function $H+\zeta_B$) - are random, is governed by the boundary problem:

$$\left(\Delta + \omega^2 c^{-2}(\mathbf{r})\right) G(\mathbf{r},\mathbf{r}_0) = \delta(\mathbf{r}-\mathbf{r}_0)\ , \tag{1}$$

$$\lim_{\|\mathbf{r}-\mathbf{r}_0\|\to\infty} G(\mathbf{r},\mathbf{r}_0) = 0 \ \text{ if } \ \mathrm{Im}\{c\} < 0\ , \tag{2}$$

$$G(\mathbf{r},\mathbf{r}_0)\big|_{\mathbf{r}\in\Sigma_s} = 0,\ \left[G(\mathbf{r},\mathbf{r}_0)\right]_{\mathbf{r}\in\Sigma_e} = \left[\rho^{-1}\partial_n G(\mathbf{r},\mathbf{r}_0)\right]_{\mathbf{r}\in\Sigma_a} = 0. \tag{3}$$

We will assume that the sound velocity field is distributed accordingly to the normal low with the mathematical expectation (mean value) $\mathrm{M}[c(\mathbf{r})] = c_0(z)$ depending only on depth z and with the space covariance function $\mathrm{M}\left[\tilde{c}(\mathbf{r})\tilde{c}(\mathbf{r}')\right] = K_c(\mathbf{x}-\mathbf{x}',z,z')$, $\tilde{c}(\mathbf{r}) = c(\mathbf{r}) - c_0(z)$ (so, the fluctuation field is statistically homogeneous in the horizontal plane). Let's suppose also that the mean values of boundary roughness $\zeta_S(\mathbf{x})$ and $\zeta_B(\mathbf{x})$ are constant and equal to zero: $\mathrm{M}[\zeta_I(\mathbf{x})] = 0$ and that their space covariance functions depend also only on difference of coordinate vectors: $\mathrm{M}[\zeta_I(\mathbf{x})\zeta_I(\mathbf{x}')] = K_I(\mathbf{x}-\mathbf{x}')$ (here and below the subscript I takes the meaning "S" or "B"), so that they can be expressed through spatial spectra $S_I(\kappa)$, where κ is the horizontal wave vector.

Our task consists of deriving equations for the two first moments of the sound field in this stochastic waveguide with taking into account the scattering from boundaries and volume fluctuations of effective sound velocity, and also of solving such equations.

2. OPERATOR FORMALISM AND FIELD EQUATIONS

A system of differential operator equations of first order for two operators $\mathbf{G}_+$ and $\mathbf{G}_-$ describing waves propagating "up" and "down" along the z-axis in the waveguide can be derived from the equation (1). To do it let's introduce the operator $\mathbf{K}^2(z) = \Delta_{\mathbf{x}} + \omega^2 c^{-2}(\mathbf{r})$. Then the Helmholtz equation (1) can be rewritten under the operator formalism:

$$d_z^2\mathbf{G}(z,z_0) + \mathbf{K}^2(z)\mathbf{G}(z,z_0) = \mathbf{E}\delta(z-z_0)\ , \tag{4}$$

where $\mathbf{E}$ is the unity operator in the functional space on the horizontal plane

$$(\forall\, \varphi(\mathbf{x}),\ \mathbf{E}[\varphi](\mathbf{x}) = \int \delta(\mathbf{x}-\mathbf{x}')\varphi(\mathbf{x}')d^2\mathbf{x}' = \varphi(\mathbf{x})),$$

and the operator $\mathbf{G}$ is defined on the same plane by the following way:

$$\mathbf{G}(z,z_0)[\varphi](\mathbf{x}) = \int G(\mathbf{r},\mathbf{r}_0)\varphi(\mathbf{x}_0)d^2\mathbf{x}_0.$$

Let's develop the solution of the equation (4) as a sum

$$\mathbf{G}(z,z_0) = \mathbf{G}_+(z,z_0) + \mathbf{G}_-(z,z_0)\ , \tag{5}$$

with the condition

$$d_z\mathbf{G}(z,z_0) = i\mathbf{K}(z)\big(\mathbf{G}_+(z,z_0) - \mathbf{G}_-(z,z_0)\big)\ , \tag{6}$$

to do uniform development. The condition (6) signifies that the operators $\mathbf{G}_+$ and $\mathbf{G}_-$ describe waves propagating "up" and "down" along the z-axis. Using (5), (6) in (4) and the notation $\mathbf{K}'(z) = d_z\mathbf{K}$, we derive a system of linear differential equations of first order for $\mathbf{G}_+$ and $\mathbf{G}_-$ for all $z \neq z_0$:

$$\begin{cases} d_z\mathbf{G}_+(z,z_0) = \left[i\mathbf{K}(z) - \mathbf{K}^{-1}(z)\mathbf{K}'(z)/2\right]\mathbf{G}_+(z,z_0) + \mathbf{K}^{-1}(z)\mathbf{K}'(z)\mathbf{G}_-(z,z_0)/2 \\ d_z\mathbf{G}_-(z,z_0) = \mathbf{K}^{-1}(z)\mathbf{K}'(z)\mathbf{G}_+(z,z_0)/2 - \left[i\mathbf{K}(z) + \mathbf{K}^{-1}(z)\mathbf{K}'(z)/2\right]\mathbf{G}_-(z,z_0) \end{cases}. \tag{7}$$

Following equations for jumps of operators $\mathbf{G}_+$ and $\mathbf{G}_-$ derive from the continuity of the Green's function and from the unity jump of its derivative for $z = z_0$:

$$\left[\mathbf{G}_+\right]_{z=z_0} = \mathbf{K}^{-1}(z_0)/2i,\ \left[\mathbf{G}_-\right]_{z=z_0} = -\mathbf{K}^{-1}(z_0)/2i\,. \tag{8}$$

By introducing vectors $|\mathbf{G}\rangle = \left(\mathbf{G}_+, \mathbf{G}_-\right)^T$, $|\mathbf{n}\rangle = \left(\mathbf{E}, -\mathbf{E}\right)^T$ and the operator matrix $\mathbf{L}$ composed of operator coefficients of the system (7) we rewrite the equations (7) and (8) as

$$d_z|\mathbf{G}\rangle = \mathbf{L}|\mathbf{G}\rangle,\ z \neq z_0\ , \tag{7'}$$

$$\left[\!\left[\mathbf{G}\right\rangle\right]_{z=z_0} = \mathbf{K}^{-1}(z_0)|\mathbf{n}\rangle/2i\ . \tag{8'}$$

The system (7) and jump condition (8) shall be completed by boundary conditions for $z = 0$ and $z = H$ to have a unique solution. They can be formulated if we assume that such operators $\mathbf{U}_S$ and $\mathbf{U}_B$ exist that

$$\begin{aligned} &\mathbf{G}_+(z,z_0) - \mathbf{U}_S\mathbf{G}_-(z,z_0)\big|_{z=0} = 0, \\ &\mathbf{G}_-(z,z_0) - \mathbf{U}_B\mathbf{G}_+(z,z_0)\big|_{z=H} = 0. \end{aligned} \tag{9}$$

So-defined operators $\mathbf{U}_S$ and $\mathbf{U}_B$ describe the scattering from waveguides boundaries (free surface and bottom) in the homogeneous medium (where sound speed is constant and equal to its value near the corresponding boundary).

Let $\mathbf{U}(z,z_1)$ is an operator matrix $\mathbf{U}(z,z_1) = \begin{bmatrix} \mathbf{U}_{++}(z,z_1) & \mathbf{U}_{+-}(z,z_1) \\ \mathbf{U}_{-+}(z,z_1) & \mathbf{U}_{--}(z,z_1) \end{bmatrix}$ satisfying (7) and the initial condition $\mathbf{U}(z_1,z_1) = \mathbf{E}$. By using it, the boundary conditions and the jump conditions at the source following equations for the operators $\mathbf{G}_+(z_1,z_0)$ and $\mathbf{G}_-(z_1,z_0)$ at any depth z_1 can be derived. Let's consider $z_1 > z_0$ for simplification (the opposite case is considered by the same way). It's to notice that the solution $\mathbf{U}(z,z_1)$ has the following property:

$$\mathbf{U}(z,z_1) = \mathbf{U}(z,z')\mathbf{U}(z',z_1)\ . \tag{10}$$

It follows from the meaning of elements of the matrix $\mathbf{U}(z,z_1)$ and from the boundary condition for $z = H$ that the operators $\mathbf{G}_+(z_1,z_0)$ and $\mathbf{G}_-(z_1,z_0)$ are related by the equation

$$\begin{aligned} &\mathbf{U}_B\left[\mathbf{U}_{++}(H,z_1)\mathbf{G}_+(z_1,z_0) + \mathbf{U}_{+-}(H,z_1)\mathbf{G}_-(z_1,z_0)\right] - \\ &-\left[\mathbf{U}_{-+}(H,z_1)\mathbf{G}_+(z_1,z_0) + \mathbf{U}_{--}(H,z_1)\mathbf{G}_-(z_1,z_0)\right] = 0, \end{aligned}$$

from where we derive

$$\mathbf{G}_-(z_1,z_0) = \mathbf{U}_\cup(z_1,z_1)\mathbf{G}_+(z_1,z_0)\ , \tag{11}$$

where $\mathbf{U}_\cup(z_1,z_1) = \left[\mathbf{U}_{--}(H,z_1) - \mathbf{U}_B\mathbf{U}_{+-}(H,z_1)\right]^{-1}\left[\mathbf{U}_B\mathbf{U}_{++}(H,z_1) - \mathbf{U}_{-+}(H,z_1)\right]$.

To satisfy the boundary condition for $z = 0$ it's necessary to use first the jump condition (8). By using (8'), the matrix $\mathbf{U}$ and its property (10) we get

$$\left|\mathbf{G}(z_0+0,z_0)\right\rangle = \mathbf{U}(z_0,z_1)\left|\mathbf{G}(z_1,z_0)\right\rangle\ , \tag{12}$$

$$\left|\mathbf{G}(z_0-0,z_0)\right\rangle = \mathbf{K}^{-1}(z_0)|\mathbf{n}\rangle/2i + \mathbf{U}(z_0,z_1)\left|\mathbf{G}(z_1,z_0)\right\rangle\ , \tag{13}$$

$$\left|\mathbf{G}(0,z_0)\right\rangle = \mathbf{U}(0,z_0)\mathbf{K}^{-1}(z_0)|\mathbf{n}\rangle/2i + \mathbf{U}(0,z_1)\left|\mathbf{G}(z_1,z_0)\right\rangle\ . \tag{14}$$

From (14), from the definition of $\mathbf{U}$ and from the boundary condition (9) on the surface we derive:

$$\begin{aligned}&\left(\mathbf{U}_{++}(0,z_1)\mathbf{G}_{+}(z_1,z_0)+\mathbf{U}_{+-}(0,z_1)\mathbf{G}_{-}(z_1,z_0)\right)-\\&-\mathbf{U}_S\left(\mathbf{U}_{-+}(0,z_1)\mathbf{G}_{+}(z_1,z_0)+\mathbf{U}_{--}(0,z_1)\mathbf{G}_{-}(z_1,z_0)\right)=\\&=\left[\left(\mathbf{U}_{++}(0,z_0)+\mathbf{U}_{+-}(0,z_0)\right)-\mathbf{U}_S\left(\mathbf{U}_{-+}(0,z_0)-\mathbf{U}_{--}(0,z_0)\right)\right]\mathbf{K}^{-1}(z_0)/2i.\end{aligned} \tag{15}$$

By introducing operators

$$U_{\cap}(z_1,z_1)=\left[U_{++}(0,z_1)-U_S U_{-+}(0,z_1)\right]^{-1}\left[U_S U_{--}(0,z_1)-U_{+-}(0,z_1)\right]\ , \tag{16}$$

$$U_{dd}(z_1,z_0)=\left[U_{++}(0,z_1)-U_S U_{-+}(0,z_1)\right]^{-1}\left[U_{++}(0,z_0)+U_S U_{-+}(0,z_0)\right], \tag{17}$$

$$U_{du}(z_1,z_0)=\left[U_{++}(0,z_1)-U_S U_{-+}(0,z_1)\right]^{-1}\left[U_S U_{--}(0,z_0)-U_{+-}(0,z_0)\right]\ . \tag{18}$$

we derive the second equation connecting $\mathbf{G}_{+}(z_1,z_0)$ and $\mathbf{G}_{-}(z_1,z_0)$:

$$G_{+}(z_1,z_0)=U_{\cap}(z_1,z_1)G_{-}(z_1,z_0)+\left[U_{dd}(z_1,z_0)+U_{du}(z_1,z_0)\right]K^{-1}(z_0)/2i\ . \tag{19}$$

By expressing the operators $\mathbf{G}_{+}(z_1,z_0)$ and $\mathbf{G}_{-}(z_1,z_0)$ from (11) and (19) we get resulting equation for them:

$$\begin{cases}\mathbf{G}_{+}(z_1,z_0)=\mathbf{U}_{\cap}(z_1,z_1)\mathbf{U}_{\cup}(z_1,z_1)\mathbf{G}_{+}(z_1,z_0)+\left[\mathbf{U}_{dd}(z_1,z_0)+\mathbf{U}_{du}(z_1,z_0)\right]\mathbf{K}^{-1}(z_0)/2i\\ \mathbf{G}_{-}(z_1,z_0)=\mathbf{U}_{\cup}(z_1,z_1)\mathbf{U}_{\cap}(z_1,z_1)\mathbf{G}_{-}(z_1,z_0)+\left[\mathbf{U}_{ud}(z_1,z_0)+\mathbf{U}_{uu}(z_1,z_0)\right]\mathbf{K}^{-1}(z_0)/2i\end{cases}, \tag{20}$$

where operators $\mathbf{U}_{ud}$ and $\mathbf{U}_{uu}$ are calculated by the same way as $\mathbf{U}_{dd}$ and $\mathbf{U}_{du}$:

$$U_{uu}(z_1,z_0)=\left[U_{--}(0,z_1)-U_B U_{+-}(0,z_1)\right]^{-1}\left[U_{--}(0,z_0)+U_B U_{+-}(0,z_0)\right]\ , \tag{18'}$$

$$U_{ud}(z_1,z_0)=\left[U_{--}(0,z_1)-U_B U_{+-}(0,z_1)\right]^{-1}\left[U_B U_{++}(0,z_0)-U_{-+}(0,z_0)\right]\ . \tag{19'}$$

System (20) can be rewritten under the matrix form:

$$\left(\mathbf{E}-\mathbf{A}\right)\left|\mathbf{G}(z_1,z_0)\right\rangle=\left|\mathbf{F}\right\rangle,\ \mathbf{A}=\begin{bmatrix}\mathbf{U}_{\cap}(z_1,z_1)\mathbf{U}_{\cup}(z_1,z_1) & \mathbf{0}\\ \mathbf{0} & \mathbf{U}_{\cup}(z_1,z_1)\mathbf{U}_{\cap}(z_1,z_1)\end{bmatrix}, \tag{20'}$$

$$\left|\mathbf{F}\right\rangle=\left(\left[\mathbf{U}_{dd}(z_1,z_0)+\mathbf{U}_{du}(z_1,z_0)\right]\mathbf{K}^{-1}(z_0)/2i\quad\left[\mathbf{U}_{ud}(z_1,z_0)+\mathbf{U}_{uu}(z_1,z_0)\right]\mathbf{K}^{-1}(z_0)/2i\right)^{T}.$$

In the system (20):

the operator $\mathbf{U}_{\cap}(z_1,z_1)$ describes the wave propagation from the depth z_1 to the surface, scattering from it and following propagation to the depth z_1;

the operator $\mathbf{U}_{\cup}(z_1,z_1)$ describes the propagation from the depth z_1 to the bottom, scattering from it and following propagation to the depth z_1;

the operator $\mathbf{U}_{dd}(z_1,z_0)$ describes the propagation from the source depth to the depth z_1;

the operator $\mathbf{U}_{du}(z_1,z_0)$ describes the propagation from the source to the surface, scattering from it and following propagation to the depth z_1;

the operator $\mathbf{U}_{ud}(z_1,z_0)$ describes the propagation from the source to the bottom, scattering from it and following propagation to the depth z_1;

operator $\mathbf{U}_{uu}(z_1,z_0)$ describes the propagation from the source to the surface, scattering from it, propagation from the surface to the bottom, scattering from the bottom and finally the propagation from the bottom to the depth z_1.

(Note: the term "propagation" in this context means the propagation under the refraction defined by the mean sound velocity profile and the scattering from volume fluctuations in the medium).

Equations (20) for a 3D random ocean are operator homologue of the classic functional equations for space spectra of a sound field in a layered waveguide [9]. Operators $\mathbf{U}_{\cap}$ and $\mathbf{U}_{\cup}$ are homologues of the coefficients of reflection from waveguide's parts lying "up" and "down" the depth z_1. Operators $\mathbf{U}_{\alpha\beta}$, with α and β equal to "*d*" or "*u*" are homologues to the four quasi plane waves going from the receiver "up" (the second subscript "*u*") and "down" (the second subscript "*d*") and coming to the receiver from the "up" (the first subscript "*u*") and "down" (the first subscript "*d*") directions.

Approximation of forward scattering

If the backscattering from volume fluctuations is not significant and can be neglected then the non-diagonal terms in the system (7) shall be avoid and the matrix $\mathbf{U}(z,z_1)$ becomes diagonal. Therefore the equations for the operators $\mathbf{U}_{\alpha\beta}$, are simplified:

$$
\begin{aligned}
&\mathbf{U}_{\cap}(z_1,z_1)=\mathbf{U}_{++}(z_1,0)\mathbf{U}_S\mathbf{U}_{--}(0,z_1),\\
&\mathbf{U}_{\cup}(z_1,z_1)=\mathbf{U}_{--}(z_1,H)\mathbf{U}_B\mathbf{U}_{++}(H,z_1),\\
&\mathbf{U}_{dd}(z_1,z_0)=\mathbf{U}_{++}(z_1,z_0),\\
&\mathbf{U}_{du}(z_1,z_0)=\mathbf{U}_{++}(z_1,0)\mathbf{U}_S\mathbf{U}_{--}(0,z_0),\\
&\mathbf{U}_{ud}(z_1,z_0)=\mathbf{U}_{--}(z_1,H)\mathbf{U}_B\mathbf{U}_{++}(H,z_0),\\
&\mathbf{U}_{uu}(z_1,z_0)=\mathbf{U}_{--}(z_1,H)\mathbf{U}_B\mathbf{U}_{++}(H,0)\mathbf{U}_S\mathbf{U}_{--}(0,z_0).
\end{aligned}
\tag{21}
$$

Under this approximation the above described physical sense of the operators $\mathbf{U}_{\alpha\beta}$ becomes more clear and evident for the intuition.

We have to notice that if the approximated equations (21) are used then not only the backscattering from volume fluctuations is neglected but also the back refraction of waves at the turning points. Therefore the equations (21) shall be used with precaution: if a wave does not reach a boundary and is refracted in the opposite direction then the operators $\mathbf{U}_S$ and $\mathbf{U}_B$ describing the scattering from the surface and the bottom shall be substituted in (21) by operators of wave reflection at the turning points. To formalize it the operators $\mathbf{U}_S$ and $\mathbf{U}_B$ shall have a block structure where some blocks are to describe the scattering and others - to describe the reflection from the turning points.

3. EUQATIONS FOR THE TWO FIRST MOMENTS

In this section equations for the two first statistical moments of operators $\mathbf{G}_+$ and $\mathbf{G}_-$ will be derived by algebraic methods of the stochastic theory of perturbations [14]. Equation for the first moment $\overline{\mathbf{X}}$ of the solution of some stochastic operator equation $(\mathbf{E}-\mathbf{A})\mathbf{X}=\mathbf{F}$, where $\mathbf{A}$ and $\mathbf{F}$ are random operators, is

$$
(\mathbf{E}-\mathbf{D})\overline{\mathbf{X}}=\mathbf{C} \tag{22}
$$

(the Dyson equation), where $\mathbf{D}=\overline{\mathbf{A}}$ and $\mathbf{C}=\overline{\mathbf{F}}$ under the first order approximation with respect to RMS of randomness. If $\overline{\mathbf{A}}=0$ (as it is for the case of scattering from volume fluctuations) then $\mathbf{D}=\overline{\mathbf{A}^2}$. For the second moment $\overline{\mathbf{X}\otimes\mathbf{X}^+}$ (the sign "$\otimes$" means the tensor product of operators, the superscript "+" is used for the Hermitian conjugate) the equation is:

$$
\left[(\mathbf{E}-\mathbf{D})\otimes(\mathbf{E}-\mathbf{D})^+-\mathbf{B}\right]\overline{\mathbf{X}\otimes\mathbf{X}^+}=\overline{\mathbf{F}\otimes\mathbf{F}^+} \tag{23}
$$

(the Bethe-Salpeter equation) where $\mathbf{B}=\overline{\tilde{\mathbf{A}}\otimes\tilde{\mathbf{A}}^+}$, $\tilde{\mathbf{A}}=\mathbf{A}-\overline{\mathbf{A}}$ under the first order approximation with respect to RMS of randomness.

For our case of the operator stochastic equations (20) the Dyson and Bethe-Salpeter equations for $\mathbf{G}_+$ and $\mathbf{G}_-$ are

$$\begin{cases} \overline{\mathbf{G}_+(z,z_0)} = \overline{\mathbf{U}_\cap(z,z)\mathbf{U}_\cup(z,z)}\cdot\overline{\mathbf{G}_+(z,z_0)} + \overline{\left[\mathbf{U}_{dd}(z,z_0)+\mathbf{U}_{du}(z,z_0)\right]\mathbf{K}^{-1}(z_0)/2i} \\ \overline{\mathbf{G}_-(z,z_0)} = \overline{\mathbf{U}_\cup(z,z)\mathbf{U}_\cap(z,z)}\cdot\overline{\mathbf{G}_-(z,z_0)} + \overline{\left[\mathbf{U}_{ud}(z,z_0)+\mathbf{U}_{uu}(z,z_0)\right]\mathbf{K}^{-1}(z_0)/2i} \end{cases} \quad (22')$$

and

$$\begin{cases} \left[\left(\mathbf{E}-\overline{\mathbf{U}_\cap\mathbf{U}_\cup}\right)\otimes\left(\mathbf{E}-\overline{\mathbf{U}_\cap\mathbf{U}_\cup}\right)^+ - \overline{\left(\mathbf{U}_\cap\mathbf{U}_\cup-\overline{\mathbf{U}_\cap\mathbf{U}_\cup}\right)\otimes\left(\mathbf{U}_\cap\mathbf{U}_\cup-\overline{\mathbf{U}_\cap\mathbf{U}_\cup}\right)^+}\right]\times \\ \qquad \times\overline{\mathbf{G}_+\otimes\mathbf{G}_+^+} = \overline{\left(\left(\mathbf{U}_{dd}+\mathbf{U}_{du}\right)\mathbf{K}^{-1}/2i\right)\otimes\left(\left(\mathbf{U}_{dd}+\mathbf{U}_{du}\right)\mathbf{K}^{-1}/2i\right)^+} \\ \left[\left(\mathbf{E}-\overline{\mathbf{U}_\cup\mathbf{U}_\cap}\right)\otimes\left(\mathbf{E}-\overline{\mathbf{U}_\cup\mathbf{U}_\cap}\right)^+ - \overline{\left(\mathbf{U}_\cup\mathbf{U}_\cap-\overline{\mathbf{U}_\cup\mathbf{U}_\cap}\right)\otimes\left(\mathbf{U}_\cup\mathbf{U}_\cap-\overline{\mathbf{U}_\cup\mathbf{U}_\cap}\right)^+}\right]\times \\ \qquad \times\overline{\mathbf{G}_-\otimes\mathbf{G}_-^+} = \overline{\left(\left(\mathbf{U}_{ud}+\mathbf{U}_{uu}\right)\mathbf{K}^{-1}/2i\right)\otimes\left(\left(\mathbf{U}_{ud}+\mathbf{U}_{uu}\right)\mathbf{K}^{-1}/2i\right)^+} \end{cases} \quad (23')$$

(equations for the cross-moments $\overline{\mathbf{G}_+\otimes\mathbf{G}_-^+}$ are not shown here but they can be easily derived from the general matrix equation (23) for seconds moments and from the matrix formulation (20') of our stochastic operator equations).

Now Dyson equations for horizontal spectra $\overline{G}_A$ of kernels of operators $\overline{\mathbf{G}}_A$, with A = "+", "–", will be derived from the equations (22') by using the approximation (21) of *forward scattering*.

First, when equations for kernels or their spectra are derived from some operator equations an operator product corresponds to a convolution of kernels or of spectra. Second, because of the horizontal homogeneity of all random factors in the waveguide all second moments of kernels of all operators entering in the equations (22') and (23') contain δ-functions of differences of horizontal wave vectors, therefore the equations are simplified and their solutions also contain the same δ-functions. Let's denote U_I, I = "S", "B" kernels of the operators $\mathbf{U}_I$ describing the scattering from boundaries, $U_{\alpha\beta}$, α,β = "+", "–" kernels of the operators $\mathbf{U}_{\alpha\beta}$ describing the propagation and scattering from volume fluctuations and

$$\begin{aligned} U_V(z,z) &= U_{++}(z,0)*U_{--}(0,z)*U_{--}(z,H)*U_{++}(H,z) = \\ &= U_{++}(z,0)*U_{--}(0,H)*U_{++}(H,z) \end{aligned} \quad (24)$$

kernel of the operator describing the propagation and scattering in the waveguide without scattering from the boundaries (the convolution is calculated through the variable on which the operators act). Notice that the kernels U with different subscripts have the meaning of scattering amplitudes for stochastic surfaces or for a water layer with volume fluctuations.

So, because of the horizontal statistical homogeneity of the waveguide the coefficients and the right part of the equation (22') are proportional to $\delta(\kappa-\kappa_0)$:

$$\begin{cases} \overline{U}_I(\kappa-\kappa_0)=\delta(\kappa-\kappa_0)\overline{U}_I(\kappa_0),\ I=S,B \\ \overline{U}_{\alpha\beta}(z,z_0,\kappa-\kappa_0)=\delta(\kappa-\kappa_0)\overline{U}_{\alpha\beta}(z,z_0,\kappa_0),\ \alpha,\beta="+","-". \end{cases} \tag{25}$$

If the development

$$\overline{U}_V(z,z)=\overline{U}_{++}(z,0)*\overline{U}_{--}(0,H)*\overline{U}_{++}(H,z) \tag{26}$$

is valid then

$$\overline{G}_A(z,z_0,\kappa,\kappa_0)=\delta(\kappa-\kappa_0)\overline{G}_A(z,z_0,\kappa_0),\ A="+","-" . \tag{27}$$

Notice that the equation (26) defines some approximation under which the correlation of volume fluctuations for different parts of one ray cycle is neglected. It's evident that in the case of fluctuations being enough large-scale in the horizontal plane this approximation does not allow to take into account the correlation of fields being scattered on different ascending or descending parts of a ray cycle.

Thus, taking into account that all scattering factors (boundary and volume) are statistically independents from each other following scalar equations for the mean field derive from (22'):

$$\begin{cases} \overline{G}_+(z,z_0,\kappa_0)=\overline{U}_c(\kappa_0)\overline{G}_+(z,z_0,\kappa_0)+ \\ \qquad +\dfrac{\overline{U}_{++}(z,z_0,\kappa_0)+\overline{U}_S(\kappa_0)\overline{U}_{+-}(z,z_0,\kappa_0)}{2i\sqrt{\kappa_v(z,\kappa_0)\kappa_v(z_0,\kappa_0)}}, \\ \overline{G}_-(z,z_0,\kappa_0)=\overline{U}_c(\kappa_0)\overline{G}_-(z,z_0,\kappa_0)+ \\ \qquad +\dfrac{\overline{U}_{-+}(z,z_0,\kappa_0)\overline{U}_B(\kappa_0)+\overline{U}_{--}(z,z_0,\kappa_0)\overline{U}_B(\kappa_0)\overline{U}_S(\kappa_0)}{2i\sqrt{\kappa_v(z,\kappa_0)\kappa_v(z_0,\kappa_0)}}, \end{cases}$$

where $\overline{U}_c(\kappa)=\overline{U}_V(z,z,\kappa)\overline{U}_S(\kappa)\overline{U}_B(\kappa)$, $\kappa_v(z,\kappa)=\sqrt{k_0^2(z)-\kappa^2}$ is vertical wave number, $k_0(z)=\omega/c_0(z)$. The equations are valid under the *forward scattering approximation* and the *approximation (26)*. Solving them we obtain:

$$\begin{cases} \overline{G}_+(z,z_0,\kappa_0)=\dfrac{\overline{U}_{++}(z,z_0,\kappa_0)+\overline{U}_S(\kappa_0)\overline{U}_{+-}(z,z_0,\kappa_0)}{2i\left(1-\overline{U}_c(\kappa_0)\right)\sqrt{\kappa_v(z,\kappa_0)\kappa_v(z_0,\kappa_0)}}, \\ \overline{G}_-(z,z_0,\kappa_0)=\dfrac{\overline{U}_{-+}(z,z_0,\kappa_0)\overline{U}_B(\kappa_0)+\overline{U}_{--}(z,z_0,\kappa_0)\overline{U}_B(\kappa_0)\overline{U}_S(\kappa_0)}{2i\left(1-\overline{U}_c(\kappa_0)\right)\sqrt{\kappa_v(z,\kappa_0)\kappa_v(z_0,\kappa_0)}}. \end{cases} \tag{28}$$

Now a system of equations for second moments of horizontal spectra of operators that derives from the operator Bethe-Salpeter equations (23') will be presented. The equations are valid under the same approximations: *of forward scattering* and *(26)*. It's evident that the coefficients and right parts of equations (23') and their solutions shall depend on four wave vectors: on κ_0 and λ_0 that specify the directions of two incident quasi-plane waves and on κ and λ that specify two directions of scattering. However because of the same horizontal statistical homogeneity of the waveguide the coefficients, right parts and solutions of (23) are proportional to $\delta(\kappa-\lambda-\kappa_0+\lambda_0)$, therefore the solution depends really only on three arguments. After introducing new vectors

$$\xi = \frac{\kappa+\lambda}{2},\ \zeta = \kappa-\lambda,\ \xi_0 = \frac{\kappa_0+\lambda_0}{2},\ \zeta_0 = \kappa_0-\lambda_0\ ,$$

the solution will be proportional to $\delta(\zeta-\zeta_0)$. Let's introduce also

$$\overline{G_A(z,z_0,\kappa,\kappa_0)G_A^+(z,z_0,\lambda,\lambda_0)} = I_A(z,z_0;\xi,\xi_0,\zeta)\delta(\zeta-\zeta_0)\ , \qquad (29)$$

where A = "+", "–", and following notations:

$$\begin{cases} \tilde{M}_{cd}(z,z;\xi,\xi_0,\zeta) = \overline{\left(U_\cap U_\cup - \overline{U_\cap U_\cup}\right)\otimes\left(U_\cup^+ U_\cap^+ - \overline{U_\cup^+ U_\cap^+}\right)}(z,z;\xi,\xi_0,\zeta), \\ \tilde{M}_{cu}(z,z;\xi,\xi_0,\zeta) = \overline{\left(U_\cup U_\cap - \overline{U_\cup U_\cap}\right)\otimes\left(U_\cap^+ U_\cup^+ - \overline{U_\cap^+ U_\cup^+}\right)}(z,z;\xi,\xi_0,\zeta), \\ M_{\alpha\beta}(z,z_0;\xi,\xi_0,\zeta) = \overline{U_{\alpha\beta}(z,z_0)\otimes U_{\alpha\beta}^+(z,z_0)},\ \alpha,\beta = \text{"u","d"}. \end{cases} \qquad (30)$$

Using it we derive following equations for I_A from Bethe-Salpeter equations (23'):

$$\begin{aligned} &\left(1-\overline{U}_c(\xi+\zeta/2)\right)\left(1-\overline{U}_c(\xi-\zeta/2)\right)^* I_A(z,z_0;\xi,\xi_0,\zeta) - \\ &-\int \tilde{M}_{c\alpha}(\xi,\xi',\zeta) I_A(z,z_0;\xi',\xi_0,\zeta)d^2\xi' = \\ &= \frac{M_\alpha(z,z_0;\xi,\xi_0,\zeta) + M_{\alpha\beta}(z,z_0;\xi,\xi_0,\zeta)}{4\kappa_v(z_0,\xi_0)\kappa_v(z,\xi_0)},\ \alpha\neq\beta. \end{aligned} \qquad (31)$$

Under the *forward scattering approximation* by using (21) we derive:

$$\begin{aligned} &\tilde{M}_{cd}(z) = U_V(z,0)*U_S*U_V(0,H)*U_B*U_V(H,z), \\ &\tilde{M}_{cu}(z) = U_V(z,H)*U_B*U_V(H,0)*U_S*U_V(0,z), \\ &\tilde{M}_{du}(z,z_0) = U_V(z,0)*U_S*U_V(0,z_0), \\ &\tilde{M}_{ud}(z,z_0) = U_V(z,H)*U_B*U_V(H,z_0). \end{aligned} \qquad (32)$$

If it is allowed to neglect correlation effects in sound fields for any two

points horizontally spaced by more than on ray cycle length then following simplified form of the equations (31) derives:

$$I_A(z,z_0;\xi,\xi_0,\zeta) - \int \overline{M}_{c\alpha}(\xi,\xi',\zeta) I_A(z,z_0;\xi',\xi_0,\zeta) d^2\xi' = \\ = \frac{M_\alpha(z,z_0;\xi,\xi_0,\zeta) + M_{\alpha\beta}(z,z_0;\xi,\xi_0,\zeta)}{4\kappa_\nu(z_0,\xi_0)\kappa_\nu(z,\xi_0)}, \quad \alpha \neq \beta, \tag{33}$$

where

$$\overline{M}_{cd}(z,z;\xi,\xi_0,\zeta) = \overline{\left(U_\cap U_\cup\right) \otimes \left(U_\cup^+ U_\cap^+\right)}(z,z;\xi,\xi_0,\zeta), \tag{34}$$

$$\overline{M}_{cu}(z,z;\xi,\xi_0,\zeta) = \overline{\left(U_\cup U_\cap\right) \otimes \left(U_\cap^+ U_\cup^+\right)}(z,z;\xi,\xi_0,\zeta).$$

By calculating the inverse Fourier transform with respect to ζ we obtain equations for the wave spectra $I_A(z,z_0;\xi,\xi_0,\mathbf{x})$:

$$I_A(z,z_0,\mathbf{x};\xi,\xi_0) - \int \overline{M}_{c\alpha}(\xi,\xi',\mathbf{x}) * I_A(z,z_0,\mathbf{x};\xi',\xi_0) d^2\xi' = \\ = \frac{M_\alpha(z,z_0,\mathbf{x};\xi,\xi_0) + M_{\alpha\beta}(z,z_0,\mathbf{x};\xi,\xi_0)}{4\kappa_\nu(z_0,\xi_0)\kappa_\nu(z,\xi_0)}, \quad \alpha \neq \beta, \tag{35}$$

where the convolution $*$ is done on the variable $\mathbf{x}$.

4. CALCULATION OF MOMENTS OF SCATTERING AMPLITUDES

Let's calculate kernels and right parts of the equations (26) and (31), (33).

The boundary scattering is described by the second moments of kernels U_l that have the meaning of scattering amplitudes. Several methods of modeling them for rough surfaces such as the sea waving surface or the rough bottom for underwater sounds. We have no possibility to discuss those methods in this work but should notice that the most adequate to the physical phenomenon and to requirements of computer implementation is now the combined model of scattering index proposed in [15] and based on the straight calculation of the Kirchhoff's integral of the *small-slope method* around the specula direction and on the use of the resonance scattering index of the *dual-scale model* for other directions (see references in [15]).

Also, a rather big number of scattering models for the sea bottom are known (see for example Ivakin's works) including models accounting the bottom roughness and a stochastically heterogeneous structure of bottom sediments or the presence of compact scatterers. In this research domain both the two groups of results of the theory of scattering from rough surfaces and from volume fluctuations in stratified media are applied. Notice that as it

bed is necessary for adequate modeling of the bottom reflection and scattering only for low frequencies where the sound is yet able to penetrate considerably the sediment.

Thus we may consider for our problem that some models of boundary scattering are known and may be used to calculate the second moments of the scattering amplitudes U_j that are entering in the equations (26), (31), (33). In this section only moments of forward scattering amplitudes from a stratified layer with fluctuations of sound velocity are calculated.

To do it let's write equations for the horizontal spectra of kernels of the operators $\mathbf{U}_{dd}$ and $\mathbf{U}_{uu}$ that derive from the equations (7) under the approximations of *forward scattering* and *of first order with respect to* μ :

$$\begin{cases} d_z U_{dd}(z,z_0,\kappa,\kappa_0) = \left[i\kappa_v(z,\kappa) - \kappa_v^{-1}(z,\kappa)\kappa_v'(z,\kappa)/2\right] U_{dd}(z,z_0,\kappa,\kappa_0) - \\ \qquad - \int \frac{2i\omega^2 \mu(z,\kappa-\kappa') U_{dd}(z,z_0,\kappa',\kappa_0)}{c_0^2(z)\left(\kappa_v(z,\kappa)+\kappa_v(z,\kappa')\right)} d^2\kappa' \\ d_z U_{uu}(z,z_0,\kappa,\kappa_0) = \left[-i\kappa_v(z,\kappa) - \kappa_v^{-1}(z,\kappa)\kappa_v'(z,\kappa)/2\right] U_{uu}(z,z_0,\kappa,\kappa_0) + \\ \qquad + \int \frac{2i\omega^2 \mu(z,\kappa-\kappa') U_{uu}(z,z_0,\kappa',\kappa_0)}{c_0^2(z)\left(\kappa_v(z,\kappa)+\kappa_v(z,\kappa')\right)} d^2\kappa' \end{cases} \tag{36}$$

$$U_{dd}(z_0,z_0,\kappa,\kappa_0) = \delta(\kappa-\kappa_0), \quad U_{uu}(z_0,z_0,\kappa,\kappa_0) = \delta(\kappa-\kappa_0),$$

where $\mu(z,\kappa)$ is the horizontal Fourier image of the fluctuation field $\mu(\mathbf{x},z)$. Here and below we avoid the subscript 1 for simplification. Notice that the kernels U_{dd} and U_{uu} have the meaning of forward scattering amplitudes of the waveguide describing the scattering from sound velocity fluctuations. Then solutions for the amplitudes will be obtained from the above equations.

Approximation of phase screen

In this work we will consider the scattering only from that part of the spectrum of the field $\mu(\mathbf{r})$ of sound velocity fluctuations that corresponds to relatively "large-scale" volume heterogeneity like vortices, internal waves, fine structure of sound velocity stratification, large-scale ocean turbulence since that's those fluctuations in the ocean that are the most powerful (for them $\sqrt{\overline{\mu^2}} \approx 10^{-2} \div 10^{-3}$). The fact to be of "large scale" means that the characteristic horizontal and vertical scales of the above mentioned heterogeneity types are much larger than the sound wave length. Usually this is true for sound of hundreds of Hertz and higher in the ocean. On the formal way it means that the function $\mu(z,\kappa)$ is not zero only for a narrow interval of κ

around $\kappa = 0$. Using this we can solve approximately the equations (24) by applying the so-called *phase screen method* [4].

Let's obtain the solution for the scattering amplitude U_{dd} that we note as U in this section (the solution for U_{uu} is derived by the same manner). To do it we express

$$U(z,z_0,\kappa,\kappa_0) = U_0(z,z_0,\kappa)\cdot U_1(z,z_0,\kappa,\kappa_0)\ , \tag{37}$$

where $U_0(z,z_0,\kappa) = \sqrt{\frac{\kappa_\nu(z_0,\kappa_0)}{\kappa_\nu(z,\kappa)}}\exp\left\{i\int_{z_0}^{z}\kappa_\nu(z',\kappa)dz'\right\}$. The equation

$$d_z U_1(z,z_0,\kappa,\kappa_0) = \int\frac{2i\omega^2\mu(z,\kappa-\kappa')}{c_0^2(z)\left(\kappa_\nu(z,\kappa)+\kappa_\nu(z,\kappa')\right)}\sqrt{\frac{\kappa_\nu(z,\kappa)}{\kappa_\nu(z,\kappa')}}\times$$
$$\times\exp\left\{i\int_{z_0}^{z}\left(\kappa_\nu(z',\kappa')-\kappa_\nu(z',\kappa)\right)dz'\right\}U_1(z,z_0,\kappa',\kappa_0)d^2\kappa' \tag{38}$$

and the initial condition for it $U_1(z,z_0,\kappa,\kappa_0)=\delta(\kappa-\kappa_0)$ derives for $U_1(z,z_0,\kappa,\kappa_0)$.

For large-scale fluctuations the number $\kappa_\nu(z,\kappa)$ is slightly changing when κ is changing on the support of μ (in the area where $\mu(z,\kappa)$ is not equal to zero). Let's neglect this slight changing in the amplitude terms of the kernel of the equation (38) but respect the linear term of this changing in the phase terms. As result we deduce:

$$d_z U_1(z,z_0,\kappa,\kappa_0) = -\frac{i\omega^2}{c_0^2(z)\kappa_\nu(z,\kappa_0)}\int\mu(z,\kappa-\kappa')e^{i\left(\mathbf{d}(z,z_0,\kappa),\kappa-\kappa'\right)}U_1(z,z_0,\kappa',\kappa_0)d^2\kappa' \tag{39}$$

with $\mathbf{d}(z,z_0,\kappa) = -\partial_\kappa\int_{z_0}^{z}\kappa_\nu(z',\kappa)dz'$

If the vector $\mathbf{d}(z,z_0,\kappa)$ is also slightly changing when κ is from the support of μ then the kernel of the equation (39) depends only on the difference $\kappa-\kappa'$ and therefore this equation can be made diagonal by the Fourier transform with respect to κ:

$$d_z U_1(z,z_0,\delta,\kappa_0) = -\frac{i\omega^2}{c_0^2(z)\kappa_\nu(z,\kappa_0)}\mu(z,\delta+\mathbf{d}(z,z_0,\kappa_0))U_1(z,z_0,\delta,\kappa_0)\ , \tag{40}$$

where δ is the dual vector to κ. Solving this equation with respect to the initial condition $U_1(z_0,z_0,\delta,\kappa_0) = \exp\{i(\delta,\kappa_0)\}$ and then doing the inverse Fourier transform with respect to δ we get a solution for the scattering amplitude corresponding to the *phase screen method*:

$$U_{dd}(z,z_0,\kappa,\kappa_0)=\sqrt{\frac{\kappa_v(z_0,\kappa_0)}{\kappa_v(z,\kappa)}}\exp\left\{i\int_{z_0}^{z}\kappa_v(z',\kappa)dz'\right\}\times$$
$$\times\frac{1}{4\pi^2}\int d^2\delta\exp\left\{-i(\kappa-\kappa_0,\delta)-i\int_{z_0}^{z}k_0(z')\mu(z',\delta+\mathbf{d}(z',z_0,\kappa))ds(z')\right\}. \quad (41)$$

Notice that the length of the vector $\mathbf{d}$ is equal to the horizontal length of the ray corresponding to the wave vector κ that goes from the depth z_0 to the depth z and that $ds(z')=\dfrac{\kappa_0(z')}{\kappa_v(z',\kappa_0)}dz'$ is the differential of the ray length. The meaning of the solution (34) is following: the difference of the scattering amplitude for a medium with sound velocity fluctuations from that for a medium without fluctuations is the additional phase term $\int_{z_0}^{z}k_0(z')\mu(z',\delta+\mathbf{d}(z',z_0,\kappa))ds(z')$ calculated as integral of the fluctuating field μ along the reference ray path.

Boundaries of validity of the *phase screen method* for a mean-stratified medium are determined by the condition that the vector $\mathbf{d}$ is slightly changing on κ from the area $|\Delta\kappa|<\kappa_m$, with $\kappa_m=2\pi/\rho_h$ the maximum horizontal wave number of fluctuations, ρ_h their correlation length in the horizontal plane. Mathematical formulation of this condition is:

$$\left|\mathbf{d}(z,z_0,\kappa_0+\Delta\kappa)-\mathbf{d}(z,z_0,\kappa_0)\right|<\rho_h,\ \forall\Delta\kappa:\ |\Delta\kappa|<\frac{2\pi}{\rho_h}. \quad (42)$$

The difference in (42) may be developed as the Teylor series. Taking only the linear term we can rewrite the condition (42) as

$$\left\|\mathbf{F}(z,z_0,\kappa_0)\right\|<\frac{\rho_h^2}{\pi},\ \text{where}\ \mathbf{F}(z,z_0,\kappa)=-\frac{\partial^2}{\partial\kappa^2}\int_{z_0}^{z}\kappa_v(z',\kappa)dz' \quad (43)$$

and elements of the matrix $\mathbf{F}$ are expressed through the transversal and longitudinal horizontal divergence of ray beams corresponding to the wave vector κ. Speaking the physical language this condition means that the horizontal Fresnel zone of rays has to be smaller than the horizontal correlation length of fluctuations.

Let's calculate now the two first moments of the scattering amplitude $U(z,z_0,\kappa,\kappa_0)$ under the common supposition [10] that the field μ is gaussian. For the first moment we obtain the well-known result [7]

$$\overline{U}(z,z_0,\kappa,\kappa_0)=\delta(\kappa-\kappa_0)\exp\left\{-\frac{1}{2}\omega^2 D_t(z,z_0,\kappa_0)\right\}, \quad (44)$$

where $D_t(z,z_0,\kappa_0) = \int_{z_0}^{z} L_\mu(z',\mathbf{e}(z',\kappa_0),0)c^{-2}(z')ds(z')$ and

$L_\mu(z,\mathbf{e},\delta) = \int_{-\infty}^{+\infty} K_\mu(z,\mathbf{e}t+\delta)dt$. The vector $\mathbf{e}(z,\kappa_0)$ is tangent to the ray defined by the wave vector κ_0 at the point z.

Calculating the second moment of the amplitude $U(z,z_0,\kappa,\kappa_0)$ we obtain:

$$\overline{U(z,z_0,\kappa,\kappa_0)U^*(z,z_0,\lambda,\lambda_0)} = M(z,z_0;\xi,\xi_0,\zeta)\delta(\zeta-\zeta_0),$$
$$M(z,z_0;\xi,\xi_0,\zeta) = \overline{U}(z,z_0;\xi+\zeta/2)\overline{U}^*(z,z_0;\xi-\zeta/2)\delta(\xi-\xi_0)+ , \qquad (45)$$
$$+ \tilde{M}(z,z_0;\xi,\xi_0,\zeta),$$

where

$$\tilde{M}(z,z_0;\xi,\xi_0,\zeta) = \sqrt{\frac{k_v(z_0,\xi+\zeta/2)k_v(z_0,\xi-\zeta/2)}{k_v(z,\xi+\zeta/2)k_v(z,\xi-\zeta/2)}} \times$$
$$\times \exp\left\{ i\int_{z_0}^{z}\left(k_v(z',\xi+\zeta/2)-k_v(z',\xi-\zeta/2)\right)dz' - \right.$$
$$\left. -\frac{1}{2}\int_{z_0}^{z} k_0^2(z')L_\mu(z',\xi+\zeta/2)ds(z') - \frac{1}{2}\int_{z_0}^{z} k_0^2(z')L_\mu(z',\xi-\zeta/2)ds(z')\right\} \times$$
$$\times \frac{1}{4\pi^2}\int d^2\delta\left[\exp\left\{-i\left(\xi-\xi_0,\delta\right)+\int_{z_0}^{z}\int_{z_0}^{z} k_0(z')k_0(z'')ds(z')ds(z'')\times\right.\right. \qquad (46)$$
$$\left.\left.\times K_\mu(z',z'',\delta+\mathbf{d}(z',z_0,\xi+\zeta/2)-\mathbf{d}(z'',z_0,\xi-\zeta/2))\right\}-1\right].$$

After calculating the Fourier image of $\tilde{M}(z,z_0;\xi,\xi_0,\zeta)$ with respect to ζ we have the kernel $\tilde{M}(z,z_0,\mathbf{x};\xi,\xi_0)$ of the integral equation (35).

Before calculating the integral from (46) we should notice that $L_\mu(z,\mathbf{e},0) \propto \overline{\mu^2} l_\mu$, where l_μ is the integral correlation interval of sound velocity fluctuations along the ray path. So far as powerful ray paths in the ocean have slight grazing angles then $l_\mu \propto \rho_h$, where ρ_h is the horizontal correlation interval of fluctuations being about one or more kilometers for such heterogeneity like internal waves, fine structure of water stratification. Distance per cycle coming by some ray in layers where fluctuations are powerful is also about one kilometers or more. Thus, for frequencies higher than 100 Hz and for $\overline{\mu^2} \geq 10^{-6}$ or higher a big parameter $k_0^2\overline{\mu^2}l_\mu l_h >>$ arises in the exponent. It allows to calculate the integral with respect to δ in (46) by the Laplace method and the integral with respect to ζ - by the

constant phase method. Such an approach corresponds to the *geometrical optics approximation*. To do it we develop the function $L_\mu(z,\mathbf{e},\delta)$ as Teylor series with respect to δ up to the second order term. The first order term from this development vanishes since the function L_μ has a maximum for $\delta = 0$.

When calculating the integral on ζ we use the fact that the function $\int_{z_0}^{z}\left(\mathrm{k}_\nu(z',\xi+\zeta/2)-\mathrm{k}_\nu(z',\xi-\zeta/2)\right)dz'$ is anti-symmetric, therefore the second order term in the Teylor series vanishes. Thus the standard method of constant phase can not be applied for the point $\zeta = 0$ and we have to take into account the third order term with respect to ζ in the Teylor development of the integral term

$$\int_{z_0}^{z}\int_{z_0}^{z} k_0(z')k_0(z'')K_\mu(z',z'',\delta+\mathbf{d}(z',z_0,\xi+\zeta/2)-\mathbf{d}(z'',z_0,\xi-\zeta/2))ds(z')ds(z'').$$

Points of constant phase are solutions of the equation

$$\mathrm{r} = \frac{1}{2}\left(\mathrm{d}(\mathrm{z},\mathrm{z}_0,\xi+\zeta/2)+\mathrm{d}(\mathrm{z},\mathrm{z}_0,\xi-\zeta/2)\right). \tag{47}$$

It follows from the symmetry of this equation that if some ζ is a solution then $-\zeta$ is too. The matrix of second order derivatives of the phase with respect to ζ is

$$\frac{1}{4}\left(\mathrm{F}(\mathrm{z},\mathrm{z}_0,\xi+\zeta/2)-\mathrm{F}(\mathrm{z},\mathrm{z}_0,\xi-\zeta/2)\right). \tag{48}$$

Let's denote

$$\mathbf{I}_\mu(z,\mathbf{e}) = \frac{\partial^2}{\partial\delta^2}L_\mu(z,\mathbf{e},\delta)\Big|_{\delta=0} \tag{49}$$

and introduce matrices

$$\Gamma_0(z,z_0,\xi_0) = \int_{z_0}^{z} k_0^2(z')\mathbf{I}_\mu(z,\mathbf{e}(z',\xi_0))ds(z'),$$

$$\Gamma_1(z,z_0,\xi_0) = \int_{z_0}^{z} k_0^2(z')\mathbf{I}_\mu(z',\xi_0)\mathbf{F}(z',z_0,\xi_0)ds(z'),$$

$$\Gamma_2(z,z_0,\xi_0) = \int_{z_0}^{z} k_0^2(z')\mathbf{F}^T(z',z_0,\xi_0)\mathbf{I}_\mu(z',\xi_0)\mathbf{F}(z',z_0,\xi_0)ds(z'),$$

$$\Gamma_{\chi}(z,z_0,\xi,\zeta) = \int_{z_0}^{z}\int_{z_0}^{z} k_0(z')k_0(z'')ds(z')ds(z'') \times$$
$$\times \frac{\partial^2}{\partial\delta^2} K_{\mu}(z',z'',\delta+\mathbf{d}(z',z_0,\xi+\zeta/2)-\mathbf{d}(z'',z_0,\xi-\zeta/2))\Big|_{\delta=0} \qquad (50)$$

and the value $\rho(z,z_0,\xi,\zeta)$ =

$$= \int_{z_0}^{z}\int_{z_0}^{z} k_0(z')k_0(z'')K_{\mu}(z',z'',\mathbf{d}(z',z_0,\xi+\zeta/2)-\mathbf{d}(z'',z_0,\xi-\zeta/2))ds(z')ds(z'').$$

By using these notations we derive following expression for the kernel

$$M(z,z_0;\xi,\xi_0,r) = \left[\left|\bar{U}_{\nu}(\xi)\right|^2 \delta(\xi-\xi_0)\delta(r-d(z,z_0,\xi)) + \frac{\exp\left\{-\frac{1}{2}\left\langle\Gamma^{-1}l,l\right\rangle\right\}}{\sqrt{\det\{2\pi\Gamma\}}}\right] \frac{k_{\nu}(z_0,\xi)}{k_{\nu}(z,\xi)} +$$

$$+\sum_{\nu>0} \frac{\cos\left[(\xi_0,\mathbf{r}) + \int_{z_0}^{z}\left(k_{\nu}(z',\xi+\zeta_{\nu}/2)-k_{\nu}(z',\xi-\zeta_{\nu}/2)\right)dz'\right]}{\sqrt{\det\left\{\frac{1}{4}\left(\mathbf{F}(z,z_0,\xi+\zeta_{\nu}/2)-\mathbf{F}(z,z_0,\xi-\zeta_{\nu}/2)\right)\right\}}} \times$$

$$\times \exp\left\{-\frac{\omega^2}{2}\left[D_l(z,z_0,\xi+\zeta_{\nu}/2)+D_l(z,z_0,\xi-\zeta_{\nu}/2)\right]\right\} \times \qquad (51)$$

$$\times \sqrt{\frac{k_{\nu}(z_0,\xi+\zeta_{\nu}/2)k_{\nu}(z_0,\xi-\zeta_{\nu}/2)}{k_{\nu}(z,\xi+\zeta_{\nu}/2)k_{\nu}(z,\xi-\zeta_{\nu}/2)}} \times$$

$$\times \left[\delta(\xi-\xi_0)+\exp\{\rho(z,z_0,\xi,\zeta_{\nu})\}\frac{\exp\left\{-\frac{1}{2}\left\langle\Gamma_{\chi}^{-1}(\xi-\xi_0),(\xi-\xi_0)\right\rangle\right\}}{\sqrt{\det\{2\pi\Gamma\}}}\right],$$

where $\mathbf{l}$ is a 4D vector $\mathbf{l} = \{\xi-\xi_0, \mathbf{x}-\mathbf{d}(z,z_0,\xi_0)\}$ and the matrix $\Gamma(z,z_0,\xi_0)$ has a block structure

$$\Gamma(z,z_0,\xi_0) = \begin{bmatrix} \Gamma_0 & \Gamma_1 \\ \Gamma_1 & \Gamma_2 \end{bmatrix}.$$

Follows a consideration of the obtained solution that contains two terms.

The first term describes the energy structure of the forward scattering amplitude of a waveguide layer. It is determined by the coherent component being proportional to losses $\left|\bar{U}_{\nu}(\xi)\right|^2$ per ray cycle and also by the

distribution of energy of the scattered field. The space distribution of the coherent field is described by the product of δ-functions versus the horizontal coordinates and wave vectors. It means that the energy of the coherent field is determined only by reference rays and that the angle spectrum of the field is transferred from the depth z_0 to the depth z without distortion. The space distribution of the scattered field is described by a gaussian function that characterizes fluctuations of perturbed rays in the vicinity of reference rays and fluctuations of wave vectors of the perturbed rays around the wave vectors of the reference rays. Notice that the ray's and wave vector's fluctuations are statistically related (the matrix Γ_1 is not zero).

The second term in (51) describes the small-scale interference structure of the scattering amplitude being effect of the multi-ray structure of sound fields developed practically for any propagation conditions in the ocean. This term consists of two parts. The first part characterizes the interference structure of the coherent field. It is determined by the phase difference of two coming rays and by appropriated ray amplitudes of the coherent field. The second part describes statistically the interference structure of the scattered field. It is characterized by some slighter weakening than that of the coherent field and its angle spectrum is also a gaussian function. It's to notice that the angle scattering for a couple of rays is smaller than for each ray itself. The reason of it is in the fact that angle fluctuations for each ray are accumulated along the hole ray path but angle fluctuations for a couple of rays are accumulated only in the vicinities of the source, receiver and crossroads points.

5. SOLUTION FOR THE MEAN FIELD

It follows from (44) that the mean field is governed by the Snell-Descartes low for the reference medium (this is described by the factor $\delta(\kappa-\kappa_0)$). It is determined by the horizontal homogeneity of the problem. This property of the mean field is not related to the use of the *phase screen method*: if we had solved the problem without using it the mean field should also have that property, the difference would manifesting only in the corresponding solution for $U(z,z_0,\kappa_0)$. The value $D_t(z,z_0,\kappa_0)$ has a clear physical sense - it's dispersion of fluctuations of propagation time for the ray path specified by the wave vector κ_0 when it goes from the depth z_0 to the depth z. Thus the mean field's structure is the same as for the reference waveguide and differs from it only by the presence of coefficients of coherent reflection for the sea surface and bottom and by an additional attenuation because of the scattering from fluctuations of sound velocity, where the attenuation is determined by the dispersion of fluctuations of ray travel times. If we do the horizontal inverse Fourier transform and then calculate the integral by the constant phase method the ray representation of the mean field is derived:

$$\overline{G}(\mathbf{r},\mathbf{r}_0)=\sum_{\mu=1}^{M}A_\mu(\mathbf{r},\mathbf{r}_0)\exp\left\{i\omega t_\mu(\mathbf{r},\mathbf{r}_0)-\frac{1}{2}\omega^2 D_{t_\mu}(\mathbf{r},\mathbf{r}_0)\right\}U_S^{n_\mu}U_B^{m_\mu}, \qquad (52)$$

where M is number of rays connecting points $\mathbf{r}$ and $\mathbf{r}_0$, the powers n_μ and m_μ are equal to numbers of ray arrivals on the surface and the bottom of the ocean, A_μ and t_μ are ray amplitudes and travel times (all these parameters are calculated for the mean waveguide), D_{t_μ} is the dispersion of fluctuations of ray travel times.

6. SOLUTION FOR THE SECOND MOMENT

It was shown above that the kernel of the integral equation for the second moment of the scattering amplitude is composed of two terms: the first one describes the energy space distribution of the second moment and the second one describes its interference structure. If the second term is neglected the rest will provide a model that corresponds to the energy description of sound fields and therefore to the classic radiation transport theory. Notice that it is possible to transform the standard differential equations of the radiation transport theory to the form of the above derived integral equations. The question about when the interference effects may be neglected we keep still open. But we note that the integral equations derived in this work under the energy approach (when the interference effect is neglected) seem to be better than the differential equations of radiation transport because the numerical algorithm to solve our equations should be more convenient for computer realization. Really, a numerical solving of the differential equations of the radiation transport theory needs that some strict limitations on the step of integration shall be respected. On the contrary the equation (35) binds the second moment of the scattering amplitude for two points spaced by the horizontal ray cycle length. Therefore the grid in distance to solve numerically the equation (35) for some waveguide may be equal to the minimal horizontal ray cycle length for the environment. The equations derived under the energy approach correspond to the classic radiation transport theory with account of the use of the *phase screen method.*

To see more clearly the structure of solutions of the equations (35) let's consider only water ray paths to do not account of the boundary scattering. Furthermore let's assume for simplification that fluctuations of ray travel times per cycle are so powerful that it is reasonable to neglect the coherent field $\left|\overline{U}_c(\xi_0)\right|^2$. In this case an iterative procedure may be used to find the solution as a Neumann series:

$$I_A(z,z_0,\mathbf{x};\xi,\xi_0)=\sum_{n=0}^{\infty}\overline{M}_{c\alpha}(\xi,\xi',\mathbf{x})*_{..n}..*\,\overline{M}_{c\alpha}(\xi',\xi'',\mathbf{x})* \\ *\frac{M_\alpha(z,z_0,\mathbf{x};\xi'',\xi_0)+M_{\alpha\beta}(z,z_0,\mathbf{x};\xi'',\xi_0)}{4\kappa_\nu(z_0,\xi_0)\kappa_\nu(z,\xi_0)},\ \alpha\neq\beta. \tag{53}$$

So far as the kernels M are gaussian functions for our case and a convolution of two gaussian functions is also a gaussian function then the obtained Neumann series is a sum of gaussian functions. Therefore the structure of wave spectra of the scattered field is a sum of gaussian functions each of which is concentrated around the corresponding ray for the reference medium. It means that the mean vector of those gaussian functions is the vector $\{\xi_0,\mathbf{d}(z,z_0,\xi_0)\}$, where ξ_0 is the wave vector of the reference ray, $\mathbf{d}(z,z_0,\xi_0)$ is the horizontal vector connecting the source point and the point where the reference ray comes to the depth z. The matrix $\Gamma(z,z_0,\xi_0)$ determines fluctuations of the wave vector around the reference vector and fluctuations of the ray path in the vicinity of the reference one. The upper diagonal block in the matrix Γ determines fluctuations of the wave vector, the downside diagonal block determines ray path fluctuations and the non-diagonal block describes statistical correlation between the wave vector fluctuations and the ray path fluctuations. Thus the matrix Γ is accumulated along each reference ray, therefore fluctuations grow when the distance from the source is growing, hence maybe it is not a monotone process.

If $\mathbf{d}$ depends slightly on ξ_0 for the characteristic variability scale of Γ_0 then it follows from (53) that the solution for the second moment of the field becomes

$$I_A(z,z_0,\mathbf{x};\xi,\xi_0)=\frac{\exp\left\{-\frac{1}{2}\left\langle\Gamma_{\mathbf{x}}^{-1}(z,z_0,\xi_0)\mathbf{l}_{\mathbf{x}},\mathbf{l}_{\mathbf{x}}\right\rangle\right\}}{\sqrt{\det\left\{2\pi\Gamma_{\mathbf{x}}(z,z_0,\xi_0)\right\}}}, \tag{54}$$

where $\Gamma_{\mathbf{x}}$ and $\mathbf{l}_{\mathbf{x}}$ are calculated as sum of per cycle values Γ and $\mathbf{l}$ along reference ray paths connecting the source and receiving points (the sum is calculated on the total number of cycles and on final ray arcs).

To obtain the wave spectrum of a point source the expression (54) has to be integrated on ξ_0:

$$I_A(z,z_0,\mathbf{x};\xi)=\int d^2\xi_0\,\frac{\exp\left\{-\frac{1}{2}\left\langle\Gamma_{\mathbf{x}}^{-1}(z,z_0,\xi_0)\mathbf{l}_{\mathbf{x}},\mathbf{l}_{\mathbf{x}}\right\rangle\right\}}{\sqrt{\det\left\{2\pi\Gamma_{\mathbf{x}}(z,z_0,\xi_0)\right\}}}. \tag{55}$$

If nevertheless the value $\mathbf{d}$ versus ξ_0 is changing considerably on the characteristic variability scale of Γ_0 then it becomes necessary to calculate carefully the convolutions of gaussian functions when calculating the solution as a Neumann series (53).

7. ON THE VALIDITY OF OBTAINED EQUATIONS AND SOLUTIONS

The *phase screen method* was used above to calculate the forward scattering amplitude for volume fluctuations. The calculation of the integral in (46) by the Laplace method corresponds to the *geometrical optics approximation*. Therefore the equation (35) with the kernel (51) describes well the angle distribution of the total field in the case where the geometrical approximation is valid for one ray cycle. On the contrary, the solution (54) is valid in the case where the geometrical approximation is valid for the total ray's length between the source and the receiver. To obtain a more rigorous solution being valid for distances where the geometrical approach is not applicable it is necessary to calculate "truly" the terms of the Neumann series that is the iterative solution of the equation (35). So-obtained solutions describe already the micro-multi-ray phenomenon. Really, not only the direct ray paths coming to some point contribute to the second moment but also other rays coming in some vicinity of this point. This vicinity is defined by fluctuations of those ray paths. So, if the point is lying in some vicinity of a caustic of the reference field and is in the shadow zone for some reference ray family and if fluctuations of ray paths from this family are enough strong to cover the observation point then this ray family contributes to the second moment of the scattered field. Thus, virtual rays arise in this point that don't come to it in the reference waveguide.

Notice that equations (33) and (35) were derived only with the use of the *forward scattering approximation* and of the *approximation* (26). Therefore they are valid also for the low frequency case and for small-scale fluctuations when the *phase screen method* can not be applied. If it's the case we should try other approximations than the *phase screen method* to describe the sound scattering per ray cycle and to calculate the kernels of the equations. We notice that even under the *phase screen approach* the above derived mathematical model is able to describe statistically fluctuations of the interference structure of sound fields. It means that the model describes the correlation of signals coming to the receiver along different rays. It's done by means of the second term of the kernel (51).

8. ON STRUCTURE OF ALGORITHMS FOR NUMERICAL IMPLEMENTATION OF THE MODEL

Algorithm for numerical solution of the equation (35) in the presence of only volume fluctuations is very simple. It is based on to the algorithm of ray path calculation for a regular layered waveguide. It consists of following steps:

- calculation of ray paths going from the source for some grid of vertical directions,
- calculation of ranges $\mathbf{d}(z,z_0,\xi_0)$ where the ray paths come to some given receiving depth,
- calculation of the matrix $\Gamma(z,z_0,\xi_0)$,
- calculation of $\Gamma_{\mathbf{x}}$ and $\mathbf{I}_{\mathbf{x}}$ and application of () or "truly" calculation of the convolutions of the Neumann series () and summation of them.

Account of the boundary scattering from the waving sea surface and rough and statistically heterogeneous bottom does not change the above algorithm but asks to calculate convolutions of second moments of scattering amplitudes of volume fluctuations with those of boundaries. Nevertheless for the high frequency and small-slope roughness case where the second moments of scattering amplitudes may be approximated by gaussian lobes the account of the boundary scattering resumes as adding to the upper non-diagonal block of the matrix Γ some matrices that characterizes the angle width of the lobes in the vertical and horizontal planes. There are no changes for other topics of the numerical algorithm.

Notice that the above designed numerical solving algorithm is to obtain solution of the equation (35) for the angle spectrum of the total field. So this equation provides a field characteristic whose physical sense is more clear for intuition and corresponds to the notion of ray intensity used in the classic radiation transport theory 5]. However there is another way to calculate the second statistical moment of the field that is based on the equation (33) if the kernel describing the volume scattering is a "narrow" function versus ξ. In this case all functions entering in (33) depend practically only on the difference $\xi-\xi_0$, so the equation (33) may be solved by the Fourier transform with respect to ξ:

$$I_A(z,z_0,\mathbf{x};\zeta)=\frac{M_\alpha(z,z_0,\mathbf{x};\zeta)+M_{\alpha\beta}(z,z_0,\mathbf{x};\zeta)}{4\kappa_v(z_0,\xi_0)\kappa_v(z,\xi_0)\left(1-\overline{M}_{\alpha\alpha}(\mathbf{x},\zeta)\right)},\ \alpha\neq\beta\ , \quad (56)$$

where $I_A(z,z_0,\mathbf{x},\zeta)$ is the Fourier image of the covariance function of the field with respect to the difference of coordinate vectors:

$$I_A(z,z_0,\mathbf{x};\zeta)=\frac{1}{(2\pi)^2}\int K_A(z,z_0,\mathbf{x},\delta)\exp\left\{-i(\zeta,\delta)\right\}d^2\delta\ . \quad (57)$$

Thus the covariance function is calculated by the inverse Fourier transform with respect to ζ:

$$K_A(z,z_0,x,\delta)=\int\frac{M_\alpha(z,z_0,x;\zeta)+M_{\alpha\beta}(z,z_0,x;\zeta)}{4\kappa_v(z_0,\xi_0)\kappa_v(z,\xi_0)\left(1-\overline{M}_{\alpha\alpha}(x,\zeta)\right)}\exp\left\{i(\zeta,\delta)\right\}d^2\zeta,\quad \alpha\neq\beta. \quad (58)$$

Numerical algorithm corresponding to the above described solution for the covariance function is following:

- calculation of Fourier images of the kernels M of various subscripts,
- application of (56),
- calculation of the inverse Fourier transform (58) with respect to ζ.

Under the phase screen approximation the Fourier image of the kernel $\tilde{M}$ can be easily calculated from (46):

$$\tilde{M}(z,z_0,\mathbf{x};\zeta)=\sqrt{\frac{k_v(z_0,\xi+\zeta/2)k_v(z_0,\xi-\zeta/2)}{k_v(z,\xi+\zeta/2)k_v(z,\xi-\zeta/2)}}\times$$

$$\times\exp\left\{i\int_{z_0}^{z}\left(k_v(z',\xi+\zeta/2)-k_v(z',\xi-\zeta/2)\right)dz'-\right.$$

$$\left.-\frac{1}{2}\int_{z_0}^{z}k_0^2(z')L_\mu(z',\xi+\zeta/2)ds(z')-\frac{1}{2}\int_{z_0}^{z}k_0^2(z')L_\mu(z',\xi-\zeta/2)ds(z')\right\}\times$$

$$\times\left[\exp\left\{\int_{z_0}^{z}\int_{z_0}^{z}k_0(z')k_0(z'')ds(z')ds(z'')\times\right.\right.$$

$$\left.\left.\times K_\mu(z',z'',\mathbf{x}+\mathbf{d}(z',z_0,\xi+\zeta/2)-\mathbf{d}(z'',z_0,\xi-\zeta/2))\right\}-1.\right. \tag{59}$$

CONCLUSION

The problem of deriving equations for the two first moments of sound fields in the random ocean waveguide with simultaneous account of the scattering from rough boundaries and fluctuations of sound velocity in the volume is considered and solved in this paper. Main moments of the work and obtained results are listed below:

- An operator formalism is used to formulated the mathematical problem and to derive main equations (section 1).
- General equations are derived that describe the two first moments of the field (section 2).
- Forward scattering amplitude for a mean-stratified layer with fluctuations of sound velocity is calculated by using the *phase screen method* and the *geometrical optics approximation* (section 3).
- Structure of solutions of the equations for the mean field and the second moment using the *geometrical optics approximation* is described (sections 4 and 5).
- Validity boundaries of the derived equations and their solutions are discussed (sections 3 and 6).
- Algorithms for numerical implementation of the developed mathematical model are described and discussed (section 7).

ACKNOWLEDGMENT

This research was supported by the French company Thomson-Sintra.ASM.

REFERENCES

1. Kravtsov Yu. A., Rytov S. M., Tatarskiy V. I. *Introduction to statistical radiophysics. Part 2: Random fields.* Moscow, Nauka Editions, 1978.
2. Kliatskin V. I. *Stochastic equations and waves in randomly heterogeneous media.* Moscow, Nauka Editions, 1980.
3. Tatarskiy V. I. *Wave propagation in turbulent atmosphere.* Moscow, Nauka Editions, 1967.
4. Tchernov L. A. Waves in randomly heterogeneous media. Moscow, Nauka Editions, 1975.
5. Ishimaru A. *Wave Propagation and Scattering in Random Media*, Academic Press, New York – San Francisco – London, 1978.
6. Koler V., Papanikolau D. K. Wave propagation in random ocean // Keller D. B., Papadakis D. S. (Ed.), *Wave Propagation and Underwater Acoustics*, Springer-Verlag, Berlin – Heidelberg – New York, 1980.
7. Borodin V. V. On equations for the two first moments of sound field in a layered waveguide with a rough boundary // *Sov. Physics Acoust.* V. 33 (1987), № 4, p. 588.
8. Moiseev A. A. *On calculation of some statistical characteristics of sound fields in the randomly heterogeneous ocean.* Ph. D. thesis, Moscow Institute of Physics and Technology, Moscow, 1984.
9. Brekhovskikh L. A., Lysanov Yu. P. *Fundamentals on Ocean Acoustics.* Springer-Verlag, Berlin – Heidelberg – New York, 1983.
10. *Sound Transmission Through A Fluctuating Ocean* / Flatté S. M. (Ed.). Cambridge University Press, Cambridge - London - New York - Melbourne 1979.
11. Lurton X. Application de la modélisation géométrique de la propagation acoustique sous-marine en petits fonds et hautes fréquences // 12ème Colloque GRETSI, 1989.
12. Smith P. W. 1) The averaged impulse response of a shallow-water channel // *J. Acoust. Soc. Amer.* V. 50 (1971), p. 332; 2) Averaged sound transmission in range-dependent channels // *J. Acoust. Soc. Amer.* V. 55 (1974), p. 1197.
13. Artelnyi V. V., Didenkulov N. N., Rayevskiy M A. Low-frequency noise field in the ocean in the presence of seas // *Sov. Physics Acoust.* V. 34 (1988), № 6, p. 972.
14. Apresian L. A. Methods of statistical theory of perturbations // *Universities' News, Radiophysics.* V. 17 (1974), № 2, p.165.
15. Galaktionov M. Yu., Borodin V. V., Mamayev A. V. Numerical and Experimental Study of Sound Field Forming in Shallow Water Environments.
16. Volovov V. I., Efimov A. V., Ivakin A. N. Secondary radiation of a spherical sound wave by a continuosly layered bottom // *Sov. Physics Acoust.* V. 31 (1985), № 5, p. 591.

COHERENT STRUCTURE OF BROADBAND PULSE SIGNALS IN THE SHALLOW SEA

E.L. Borodina, A.A. Stromkov and A.I. Khil'ko

INTRODUCTION

Various techniques of acoustical monitoring and communication in shallow regions of the World ocean require understanding of the coherent properties of broadband pulse structure. Formation of these structures is caused by an interference of partial waves (i.e. normal modes). With receding from the source the broadband coherent structures are substantially transformed due to inter- and intramode dispersion (a difference between mode frequency dependencies during propagation). In common, an increase of pulse duration and special dependencies of a number of interacting modes and mode velocities from a waveguide structure at various frequencies produce rather complex space - time structures [1–3]. At low frequencies in the shallow sea the Rayleigh and Stoneley - Scholte waves significantly contribute into a total field formed by a few modes [4–8]. With growth of frequency the number of interacting modes increases; besides, some waveguide modes may have close or multiple wave numbers, under the certain conditions it can cause the formation of non-stationary beams, just as it occurs in deep-water waveguides [9–12].

The interference effects in oceanic waveguides appreciably depend on a coherence of modes, that, in turn, is defined by an influence of random inhomogeneities and an attenuation in bottom. For example, in deep waveguides at small distances the interference structure of the broadband pulse is formed mostly by a refraction duct; and in shallow waveguides the influence of bottom composition and attenuation is defining. Thus, the correct modeling of broadband space - time structures in shallow waveguides requires to account at least the phenomena of: the transformation of the interference structure during propagation along the waveguide, the influence of the bottom attenuation and the scattering of modes by random inhomogeneities.

The study of an influence of a bottom structure on acoustical signal propagation [13, 16] shows, that a part of modes interacts with sediment layers at resonance that yields an increased attenuation in a bottom and deformations of the broadband interference structure. Note, that just these resonant modes can give the information about the layered bottom structure. The scattering by random inhomogeneities also causes a transformation of the signal spectrum [17–20]: the most powerful part of spectrum shifts to higher frequencies, where

attenuation in the bottom is largest. So that, due to the scattering a part of modes forming the multi - mode interference structure disappear [10, 19, 20].

The present paper is devoted to an investigation of the influence of sediment layers on the space - time coherent structure of broadband pulses. The formation of unsteady in time beams caused by an interference of waveguide modes in a wide frequency region is considered. An influence of variations in acoustical parameters on a shape of wide - band acoustical pulses is investigated. The conditions of a constructive interference of modes are analyzed.

1. MODELING THE BROADBAND PULSE PROPAGATION IN THE SHALLOW SEA

1.1. Acoustic field structure in the shallow waveguide

For the modeling of the real conditions of propagation we have taken the composition of two fluid layers and the elastic half-space [21]. All media are supposed to be iso-velocity, here c_w, c_s, c_b are respectively the water, the sediment and the bottom sound speeds, v_b the shear speed; with constant densities ρ_w, ρ_s, ρ_b, respectively. A cylindrical-polar coordinate system is introduced having $z-$axis pointed upward, and an origin at the water surface. A point source is assumed to be disposed in the water layer of the thickness H at the depth z_s; h is the thickness of the sediment layer. In the foregoing formulation, we use the potential approach [2]

$$\left[\Delta - \frac{1}{c^2}\frac{\partial^2}{\partial t^2}\right]\varphi(r,\theta,z,t) = -\frac{2}{r}\delta(z-z_s)\delta(r), \qquad c = \{c_w, c_s, c_b\}\ , \quad (1)$$

$$\left[\Delta - \frac{1}{v_b^2}\frac{\partial^2}{\partial t^2}\right]\psi(r,\theta,z,t) = 0\ , \qquad c_b = \sqrt{\frac{\lambda+2\mu}{\rho_b}}, \quad v_b = \sqrt{\frac{\mu}{\rho_b}}\ ,$$

where φ is the scalar particle displacement potential of compression waves, $\vec{\psi} = (0, \psi, 0)$ the vector potential describing the rotational component of motion, the scalar ψ is a function of r and z only, λ, μ the Lame parameters.

Assuming the normal-mode propagating model for a monotone oscillation of a frequency f consider the solution as a result of the Fourier-Bessel decomposition by plane waves

$$\varphi(r,z,t) = \int_0^\infty J_0(\xi r)\varphi(\xi,z)\xi d\xi\, e^{-i\omega t}\ , \quad (2)$$

$$\psi(r,z,t) = \int_0^\infty J_0(\xi r)\psi(\xi,z)\xi d\xi\, e^{-i\omega t} \ ,$$

where $J_0(\cdot)$ is zeroth order Bessel function, $\omega = 2\pi f$.

We now seek the boundary conditions, and begin with writing the displacement $\vec{u}$ and the pressure p in the general form

$$\vec{u} = \nabla\varphi + \nabla \times \vec{\psi} \qquad p = -\rho c^2 \nabla \cdot \vec{u} \ . \tag{3}$$

Hence the equations for the pressure at the boundaries of the water layer give

$$\varphi|_{z=0} = 0, \quad \rho_w \varphi|_{z=H_s^+} = \rho_s \varphi|_{z=H_s^-} \ , \tag{4}$$

where $H_w = -H$ is the depth of the lower water layer boundary, $H_w^+ = H_w + 0$, $H_w^- = H_w - 0$. The condition of continuity of the normal displacement at the boundaries of the sediment layer is

$$\left.\frac{\partial\varphi}{\partial z}\right|_{z=H_w^+} = \left.\frac{\partial\varphi}{\partial z}\right|_{z=H_w^-} , \quad \left.\frac{\partial\varphi}{\partial z}\right|_{z=H_s^+} = \left.\frac{\partial\varphi}{\partial z} + \frac{1}{r}\frac{\partial}{\partial r}\left(r\frac{\partial\psi}{\partial r}\right)\right|_{z=H_s^-} , \tag{5}$$

where $H_s = -(H+h)$ is the depth of the lower sediment layer boundary, $H_s^+ = H_s + 0$, $H_s^- = H_s - 0$. The condition of continuity of the normal stress is

$$\rho_s c_s^2 \Delta\varphi\big|_{z=H_s^+} = \lambda\Delta\varphi + 2\mu\frac{\partial}{\partial z}\left(\frac{\partial\varphi}{\partial z} + \Delta\psi - \frac{\partial^2\psi}{\partial z^2}\right)\Big|_{z=H_s^-} , \tag{6}$$

the condition of zero shear stress gives

$$2\frac{\partial\varphi}{\partial z} + \Delta\psi - 2\left.\frac{\partial^2\psi}{\partial z^2}\right|_{z=H_s^-} = 0 \ . \tag{7}$$

The field $\varphi(r,z)$ in a water layer satisfying the inhomogeneous Helmholtz equation (1) and boundary conditions (4)–(7) can be expressed in the form

$$\varphi(r,z,t) = -e^{-i\omega t}\int_{-\infty}^{\infty} \frac{F((z_s+H)\phi_1/H)}{F(\phi_1)}\frac{\sin(z_s\phi_1/H)}{\sqrt{k^2-\xi^2}} H_0^{(1)}(\xi r)\xi d\xi \ , \tag{8}$$

$$F(\phi) = \frac{S\sqrt{d^2v^2-1}}{\sqrt{v^2-1}}\sin\phi[P\cos\phi_2 - Q\sin\phi_2] + \cos\phi[P\sin\phi_2 + Q\cos\phi_2] \ ,$$

$$Q = \frac{S}{R}\frac{1}{(av)^4}\frac{\sqrt{d^2v^2-1}}{av}\left[(b^2v^2-2)^2 - 4\sqrt{a-b^2v^2}\sqrt{1-a^2v^2}\right] \ ,$$

$$P = \left(\frac{b}{a}\right)^4 \frac{\sqrt{1-a^2v^2}}{av} , \quad \phi_1 = kz\frac{\sqrt{v^2-1}}{v} , \quad \phi_2 = kh\frac{\sqrt{d^2v^2-1}}{v} ,$$

$$R = \frac{\rho_w}{\rho_b} , \quad S = \frac{\rho_w}{\rho_s} , \quad a = \frac{c_w}{c_b} , \quad b = \frac{c_w}{v_b} , \quad d = \frac{c_w}{c_s} ,$$

$$v = \frac{v_{ph}}{c_w} , \quad k = \frac{\omega}{c_w} , \quad \xi = \frac{k}{v} ,$$

where $H_0^{(1)}$ is the zero-th order Hankel function and $z_s \leq z$. The expression for the case $z_s \geq z$ can be obtained from (8) by the replacement $z_s \rightleftharpoons z$. Then use of the standard procedure of integration of analytical functions over the closed contour in the upper half-space of the complex ξ–plane [1, 2]. Thus, the expression (8) can be divided into two parts: a sum of residues and a result of integration by branch cuts. As in the investigated frequency region a value of the last component is negligible, the acoustic potential field can be presented in a normal-mode form:

$$\varphi(r,z,t) = \sqrt{\frac{8\pi}{kr}} e^{-i\pi/4 - i\omega t} \sum_{n=0}^{N} \frac{\sqrt{v_n} F((z_s+H)\phi_1/H)\sin(z\phi_1/H)}{\sqrt{v_n^2-1}\,[\partial F(\phi_1)/\partial\xi]\,|_{v_n}} , \quad (9)$$

here $z_s \leq z$, v_n is the phase velocity associated with n-th mode, $n = 0 \ldots N$, satisfying the corresponding dispersion relation

$$F(\phi_1) = 0 . \quad (10)$$

For the considered relation between sound velocities $c_w < v_b$ and $c_s < v_b$ in absence of the attenuation wavenumbers of propagating modes lie on the real axis, i.e. $\Im\xi_n = 0$ when $\xi \geq \omega/v_b$. So that, the condition $v_n = v_b$ substituted into (10) gives the expression for critical frequencies f_n^c corresponding an origin of a mode with number n

$$\tan\phi_w = -\Omega_1 \left(1 + \frac{(1+\Omega_2^2)\tan\phi_s}{\Omega_2(1-\Omega_2\tan\phi_s)}\right) , \quad (11)$$

$$\phi_w = kH\sqrt{1-b^2} , \quad \phi_s = kh\sqrt{d^2-b^2} ,$$

$$\Omega_1 = \frac{\sqrt{1-b^2}}{R\sqrt{b^2-a^2}} , \quad \Omega_2 = \frac{S\sqrt{d^2-b^2}}{R\sqrt{b^2-a^2}} .$$

The numerical estimation of (11) shows, that when the relation $c_w < c_s < v_b < c_b$ takes place, mode critical frequencies decrease with growth of the sediment thickness.

As it was mentioned above, interactions with the sediment layer result in an appreciable attenuation of resonant modes in corresponding frequency regions [13]; moreover, these modes are characterized by a substantial intra-mode dispersion, so that propagated signals are distributed over a large interval of delays. However, restrict the discussion to a simple model in form of linear dependence of attenuation factor in the water layer: $\beta_n = \beta_{0n} f$. The value β_{0n} is also proportional to a mode number. Numerical simulations for $\beta_{0n} = 5.10^{-7} \ldots 1.10^{-5}$ dB/(m.Hz) shown the coincidence with experimental results at small values of β_{0n}.

It should be mentioned, that more correct model of attenuation in fluid media [16] gives a linear dependence only for zero-mode. Frequency dependencies of other modes correspond the group velocity curves, with maximums at the ranges where each mode is resonant to the sediment layer.

1.2. Influence of the sediment layer parameters on the mode dispersion

Modeling a seafloor by uniform half-space defines a shape of the group velocity frequency curve with a single minimum, so-called the Airy phase [1, 3]. An account of a bottom stratification transforms this dependency.

The influence of the layer is evidently seen in the Figs. 1,2 showing the frequency dependencies of phase v_{ph} and group v_g velocities for parameters: $c_w = 1.45\ 10^3$ m/s, $c_s = 1.58\ 10^3$ m/s, $v_b = 1.70\ 10^3$ m/s, $c_b = 2.70\ 10^3$ m/s, $\rho_w = 1.0\ 10^3$ kg/m^3, $\rho_s = 1.5\ 10^3$ kg/m^3, $\rho_b = 2.0\ 10^3$ kg/m^3, $H = 300$ m, $h = 30$ m and $h = 50$ m.

First of all, the slow fundamental mode is clearly resolved having a constant velocity in all the frequency region above 10 Hz. An account of stratification results in additional spatial resonances. Conditionally it is possible to separate at least three space scales: the thickness of water column, the thickness of sediments and the total thickness of two liquid layers, which define peculiarities of dispersion curves. The mode critical frequencies are defined, in general, by the total thickness. An increase of the sediment thickness leads to decrease of mode critical frequencies: in the considered case the number of propagating modes is $65, 72, 79$ for $h = 0, 50, 100$ m, respectively.

In the set of waveguiding modes it is possible to find a number of modes (of small numbers) with frequency dependencies similar to ones for the Pekeris waveguide [1,3]. In another words, these modes do not experience an influence of the deposit layer. A number of such modes increases with reduction of its thickness (Figs.1-3).

Since some numbers the shape of dispersion curves changes qualitatively: frequency intervals appear where velocities increase. Such

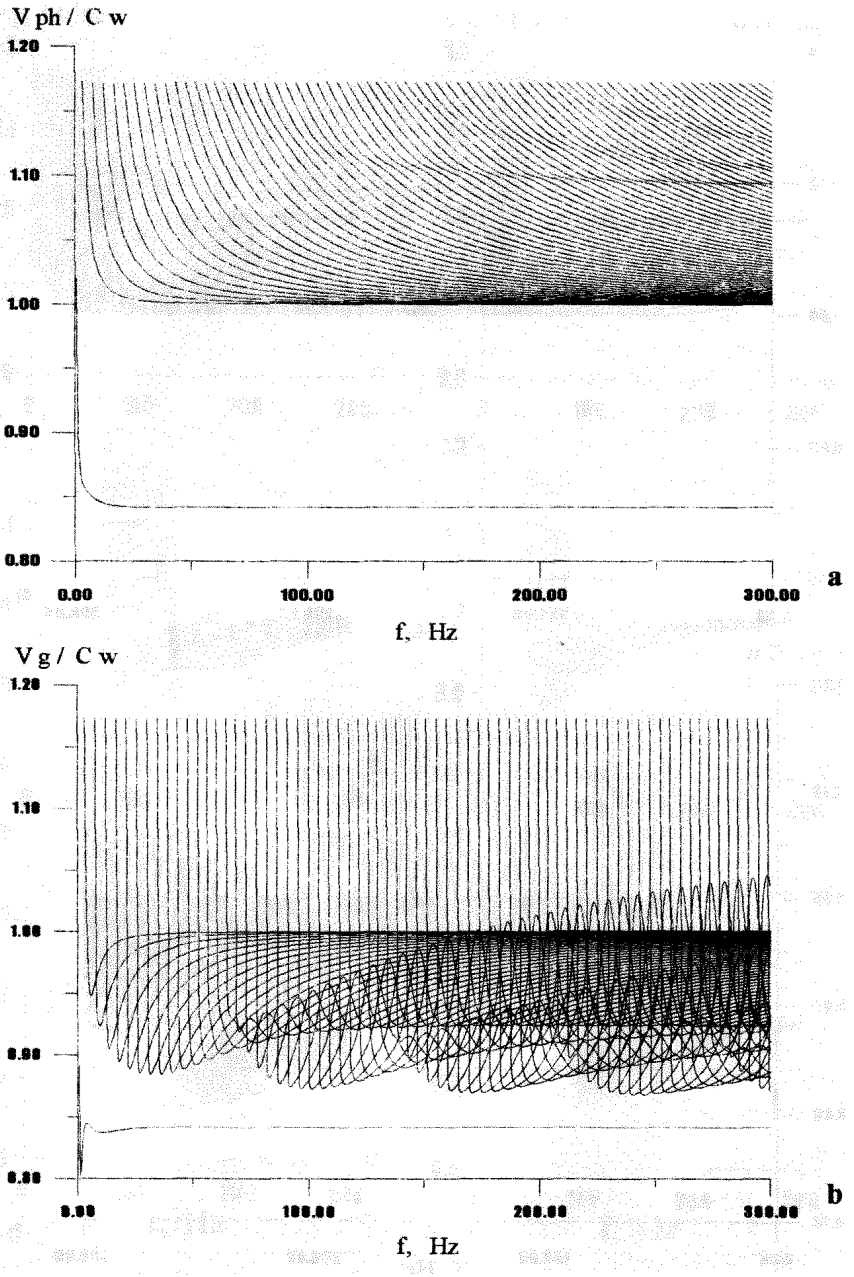

Fig. 1. Phase (a) and group (b) velocities vs frequency for the thickness $h = 30$ m.

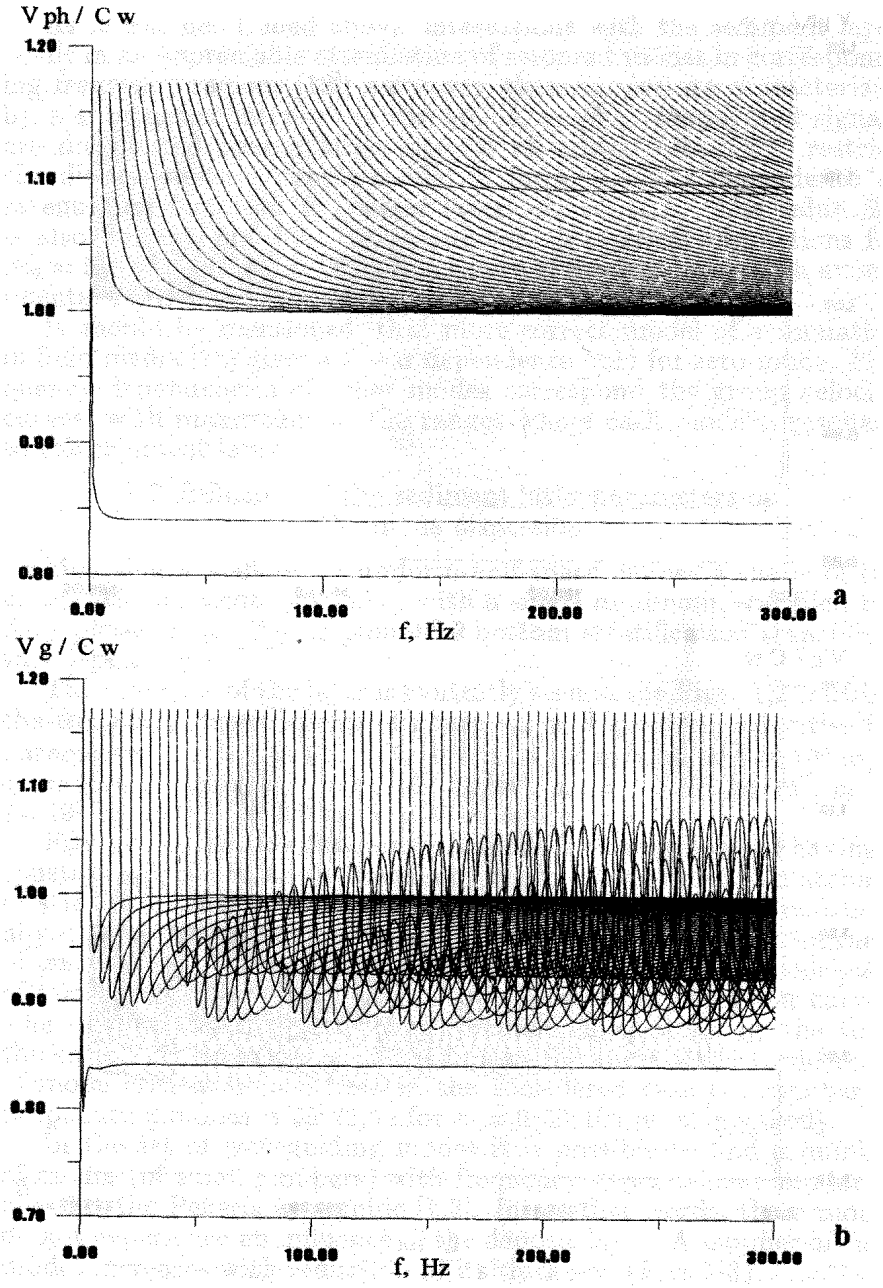

Fig. 2. Phase (a) and group (b) velocities vs frequency for the thickness $h = 50$ m.

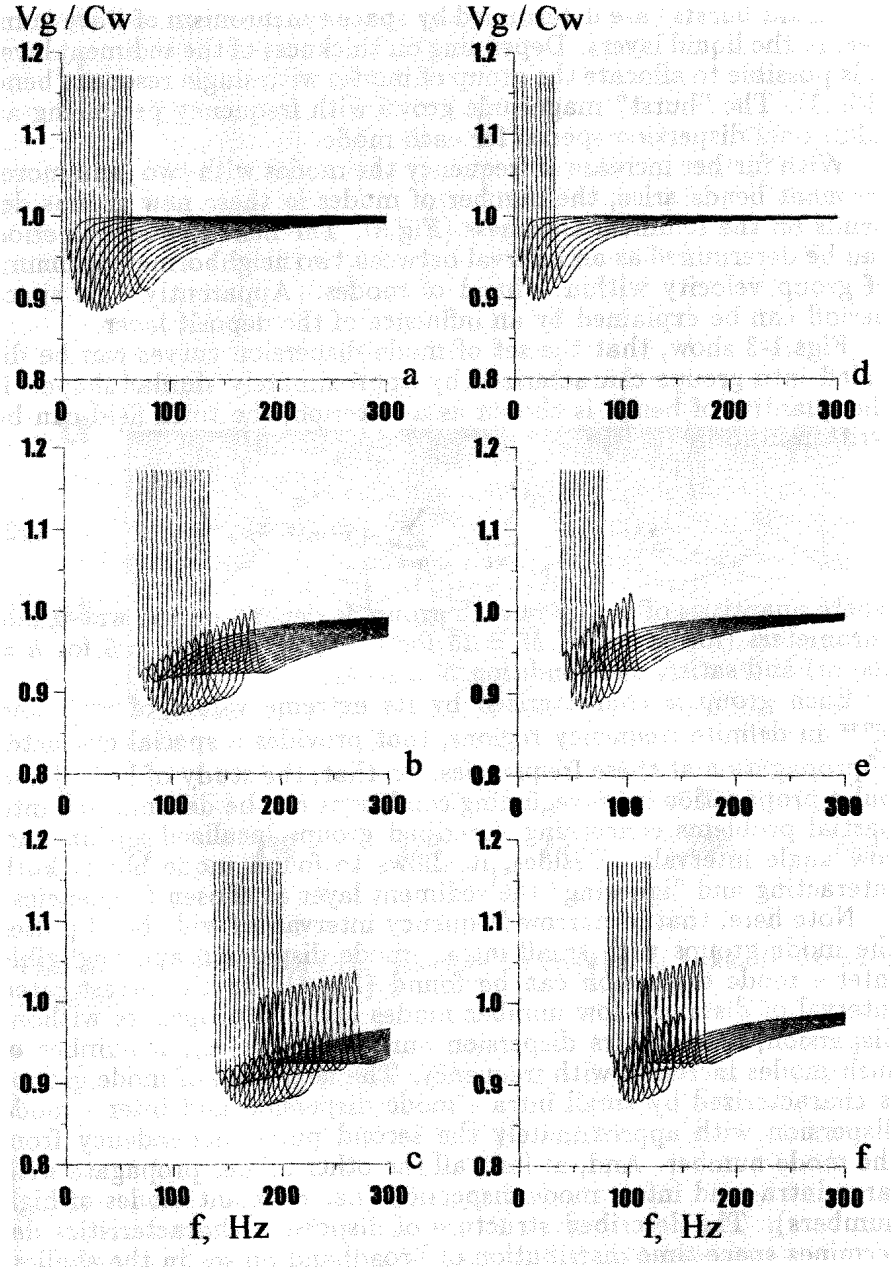

Fig. 3. Groups of modes with characteristic shape of frequency dependencies for the sediment layer thickness $h = 30$ m (a, b, c) and $h = 50$ m (d, e, f).

"resonant bursts" are determined by space synchronism of wave numbers in the liquid layers. Depending on thickness of the sediment layer it is possible to allocate the group of modes with single resonant bend (Fig.3). The "burst" magnitude grows with frequency producing an additional dispersion special for each mode.

With further increase of frequency the modes with two (and more) resonant bends arise; the number of modes in these new groups depends on the sediment thickness (Fig.3). The next frequency period can be determined as an interval between two neighboring minimums of group velocity within a band of modes. Apparently, this space period can be explained by an influence of the deposit layer.

Figs.1-3 show, that the set of mode dispersion curves can be divided into groups characterized by approximately similar shape. If the quantity of bends is chosen as a criterion, the total field can be written in form

$$\varphi(r,z) = \sum_{l=1}^{L(H,h,..} \sum_{m=1}^{M(H,h,..} \varphi_{lm}(r,z) \ , \qquad (12)$$

where quantities of modes in each group M depend on the waveguide parameters (for example, $M = 15$ for $h = 30$ m and $M = 5$ for $h = 100$ m) and satisfy the condition $N = L \cdot M$.

Each group is characterized by its extreme values of v_g^{min} and v_g^{max} in definite frequency regions, that provides a special character of propagation at these frequencies. So that, the study of broadband pulse propagation in waveguiding conditions can be decomposed into partial problems concerning described groups localized within narrow angle intervals. Besides, it allows to found mode bands both interacting and "ignoring" the sediment layer at chosen frequencies.

Note here, that in narrow frequency intervals of wide band pulses the mode groups with small intra - mode dispersion and negligible inter - mode dispersion can be found (Fig.4). In the investigated interval of distances low number modes actually propagate without dispersion, since theirs dispersion curves tend to c_w; a number of such modes increases with frequency. The next kind of mode groups is characterized by small intra - mode dispersion and inter - mode dispersion with approximately the second power dependency from the mode number. And, at last, all the other modes propagate with large intra- and inter- mode dispersion (i.e. resonant modes of high numbers). The described structure of dispersion characteristics determines space-time distribution of broadband pulses in the shallow sea.

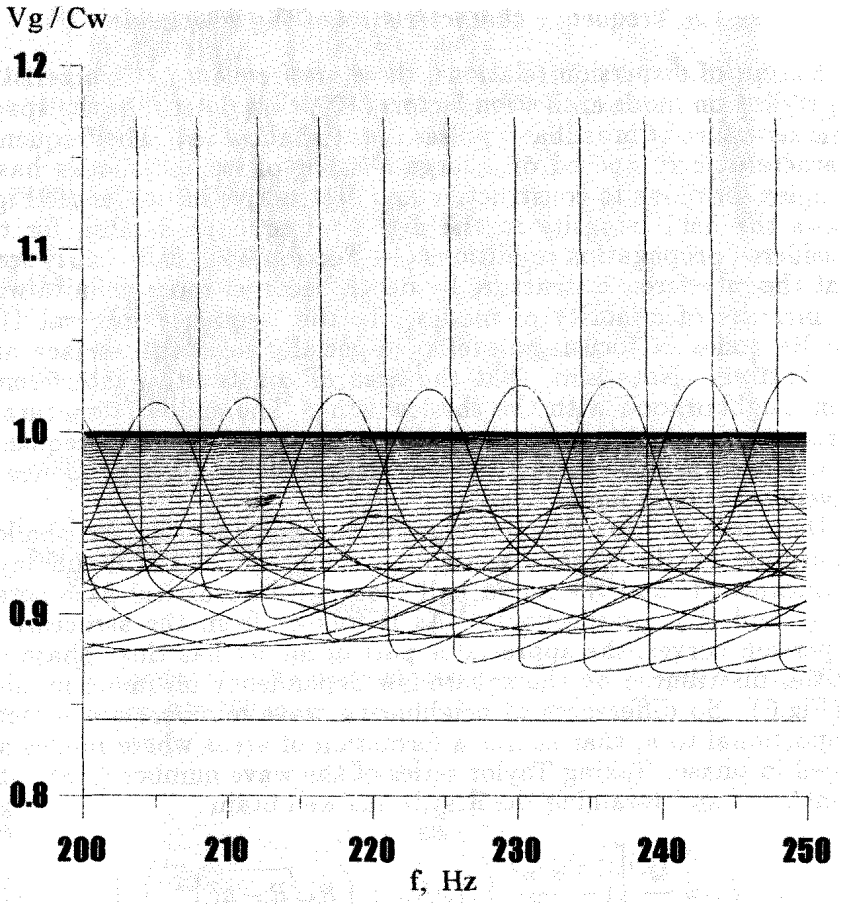

Fig. 4. Distribution of group velocities for propagating modes in the narrow frequency band.

1.3. Frequency characteristics of the waveguide

Except of dispersion relations, there are frequency characteristics depending on mode excitation factors (10), that determine the space-time structure of broadband pulses in the shallow sea. The frequency characteristic composed of a large number of excited modes has a complex form due to constructive and destructive interference. Fig.5 shows the field intensity in the depth - frequency domain for the considered propagation conditions (see Section 2.2). It is clearly seen, that the interference structure by depth becomes more definite with an increase of quantity of modes. In the frequency interval 110–120 Hz zones of focusing develop, especially near the surface and the bottom. Note also, that the area of constructive interference is in neighborhood with the shadow zone. The similar structure is observed also in frequency interval of 220–240 Hz. The frequency period of focusing is expected to be determined by a dependence of wavenumber on a mode number.

Demonstrate this effect using the simple model of the shallow waveguide — the Pekeris waveguide composed of the liquid layer of thickness H and the liquid half-space with acoustical parameters c_w, ρ_w and c_b^l, ρ_b, respectively. As it follows from the structure of dispersion curves, the appreciable part of modes has close phase velocities distributed by the square-law dependency on mode number n (Fig.6). So differences of neighboring wave numbers are directly proportional to n, that causes a formation of areas where modes are added in phase. Taking Taylor series of the wave number ξ_n about a point ω/c_w and retaining the first terms we obtain

$$\xi_n \approx \frac{\omega}{c_w}\left[1 - \frac{\pi^2 n^2}{2}\left(H\omega/c_w + \left(R\sqrt{R-a_l^2}\right)^{-1}\right)^2\right], \qquad (13)$$

where $a_l = c_w/c_b^l$. And the condition of constructive interference of two next modes is

$$r(\xi_{n-1} - \xi_n) = \frac{r\omega}{c_w}\frac{\pi^2(2n-1)}{\left(H\omega/c_w + \left(R\sqrt{R-a_l^2}\right)^{-1}\right)^2} = 2\pi m\ , \qquad (14)$$

where $m = 0, 1, 2\ldots$ This condition allows to determine frequencies at which modes appear in phase at the fixed distance $r = r_f$.

As waveguide modes are known to be quasi- periodic in depth, the relation (14) accounting $z-$ dependence defines also focusings by depth. For fixed r_f and various numbers m the focusings arise with

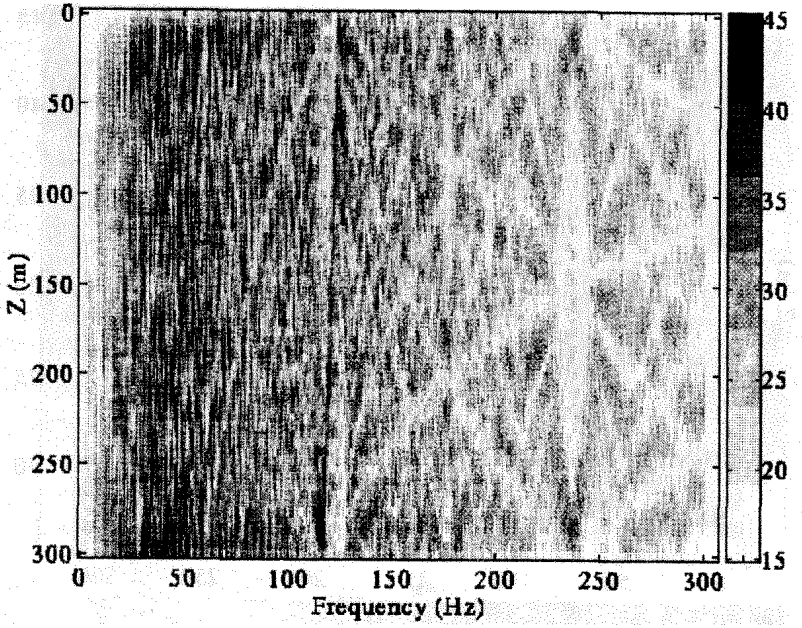

Fig. 5. The amplitude - frequency characteristic for the waveguide with the sediment thickness $h = 100$ m.

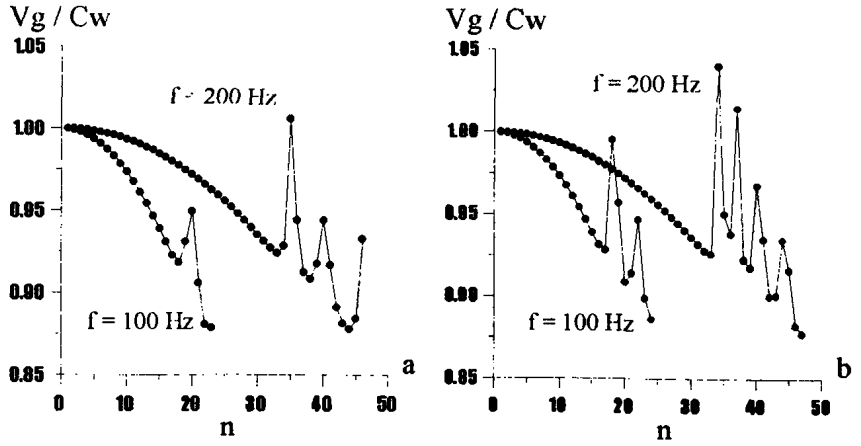

Fig. 6. Group velocities vs mode number for sediment layer thickness $h = 30$ m (a) and $h = 50$ m (b) for $f = 100$ Hz and 200 Hz.

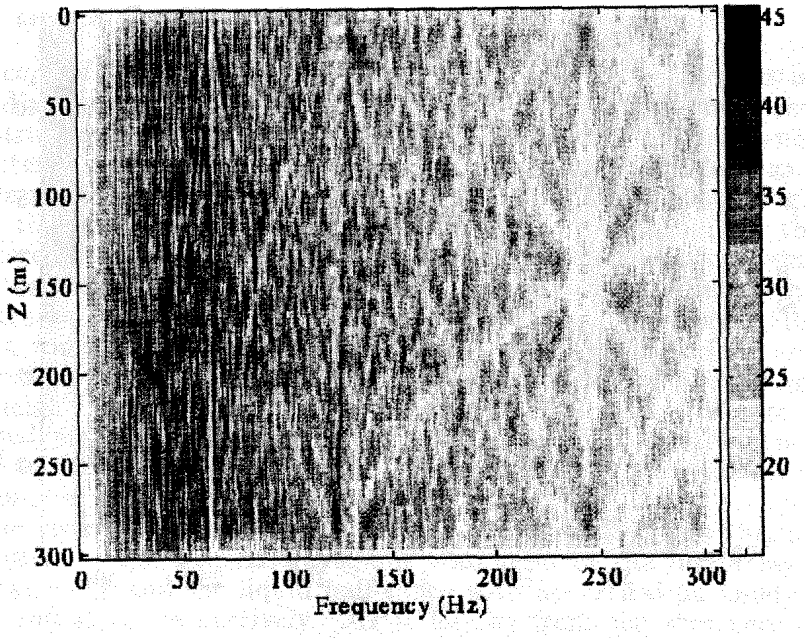

Fig. 7. The amplitude - frequency characteristic for the Pekeris waveguide.

equal frequency intervals (Figs.5,7). Note, that the approximate conditions (13) and (14) are satisfied only for modes with sound velocities rather close to c_w.

The coherent structure of pulse signals is formed mainly by these modes with low numbers and weak attenuation. Some small differences from square law cause spreading of areas of constructive interference expanding with an increase of distance r and multiplicity of focusing m. The width of focusing zone (in a frequency - depth domain) is determined by a difference of the wave number distribution from square low and can be derived analytically retaining second - power terms in Taylor decomposition. At the same time, numerical simulations indicate the reduction of the focusing properties of shallow waveguides with complication of the bottom structure (Figs.5,7).

A part of modes does not couple in focusing formation, namely, normal modes arising in the considered frequency interval and modes effectively interacting with the deposit layer (Fig.4). The contribution of these modes in focusing formation depends on relation between the distance and the sediment thickness.

As it was described above, the total field in the waveguide with layered bottom can be separated into mode groups characterized by specific dispersion curves and also by frequency characteristics. Fig.8.

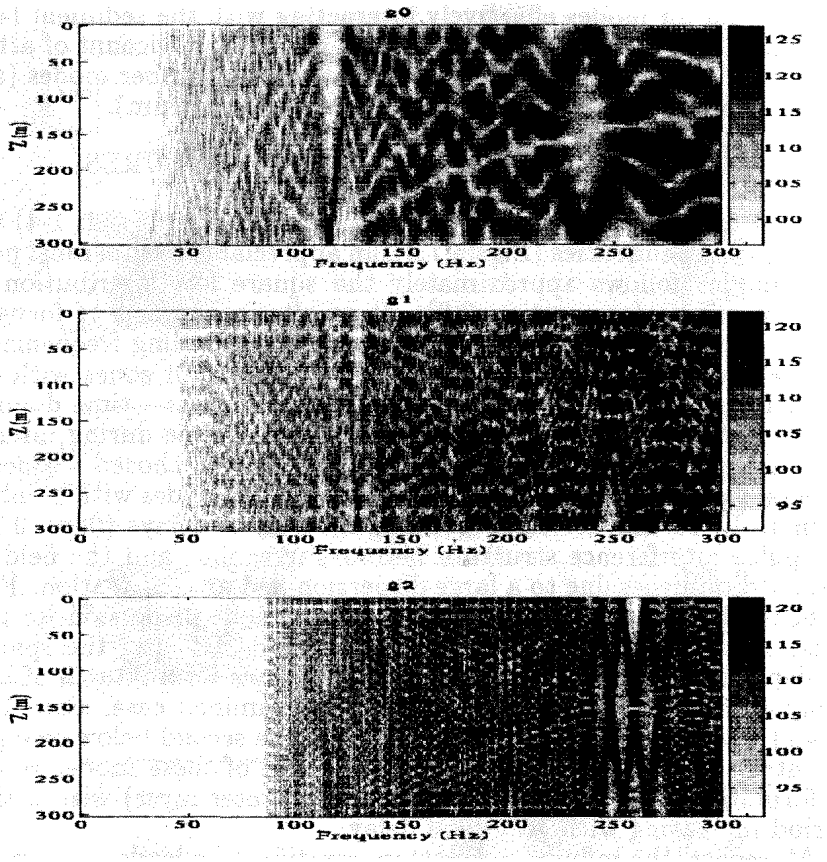

Fig. 8. The amplitude - frequency characteristics of mode groups for the sediment thickness $h = 50$ m.

shows the frequency characteristics of three first groups (g_0, g_1, g_2) for the sediment thickness $h = 50$ m (corresponding Fig.3.(d,e,f)). The strongest focusings are formed mostly by modes with numbers from first to sixteenth practically ignoring the deposit layer.

Other modes of higher numbers interacting with the deposit layer form theirs own zones of constructive interference, but field amplitudes in these areas are much weaker (it is not clear from Fig.8, since each frame is normalized independently).

An account of bottom attenuation for the waveguide model composed of liquid media [13] have shown agreement between attenuation and group velocity frequency curves. Reasoning similarly, with allowance for elasticity of substrate we can conclude about the increased

attenuation for modes effectively interacting with the sediment layer in corresponding frequency intervals. In general, an account of attenuation results in a substantial decrease of high - number modes (and suppression of high frequency part of a signal spectrum).

2. COHERENT SPACE - TIME STRUCTURES

As it follows from the analysis of dispersion curves (Figs.1-4) and frequency dependencies (Figs.5,7,8), an appreciable part of most powerful modes follows approximately the square low distribution by mode numbers (see section 2.2). It results in forming of focusing zones at various distances and depths at corresponding frequencies.

For wide - band signals it results in formation of zones with elevated intensity presented in form of a beam in space - time domain. Fig.9 shows the development of the beam with time during interaction of first two tens of waveguide modes. In the chosen frequency interval the sediment layer influences only on the modes with numbers from 15 to 20. In the corresponding interval of delays (0.6...0.7 s) the pulse interference structure becomes irregular, and the field intensity diminishes due to a large dispersion and an attenuation. First eight modes experience, mostly, the inter - mode dispersion, so that adjacent mode pulses do not overlap in time. Besides, the spacing by depth of the interference structure decreases with growth of time delay. Since some mode number (in the examined case, since 10th mode), each mode pulse begins to lap over the second below owing to an intra - mode dispersion. The interference of these modes results in formation of beams (taking up a whole water layer) with a time period increasing with growth of delay.

Moreover, the influence of bottom stratification leads to asymmetry in the interference pattern formed by low number modes, that is seen from transformation of the pulse structure with increase of the sediment thickness $h = 10,\ 70,\ 100$ m shown in Fig.10. A rather fast destruction of mode pulses is caused, in particular, by modes with resonant bends (Figs.1-4). The power of these modes is uniformly distributed over the wide interval of delays, so that some blanks or distortions of the intensity pattern at the appropriate intervals are brought about by mode destruction. Note, that these components probably contain an information on characteristics of sediment layer. For example, in a wide frequency band (to 300 Hz) the mode group with one resonant bend (see b, e in Fig.3 and g_1 in Fig.8) forms corresponding parts of the total pulse at various instants of time, that is indicated in Fig.11 for $h = 30,\ 60,\ 100$ m.

The discussed behavior of the interference pattern can be used for diagnostics of sedimentary bottom. Numerous calculations of the

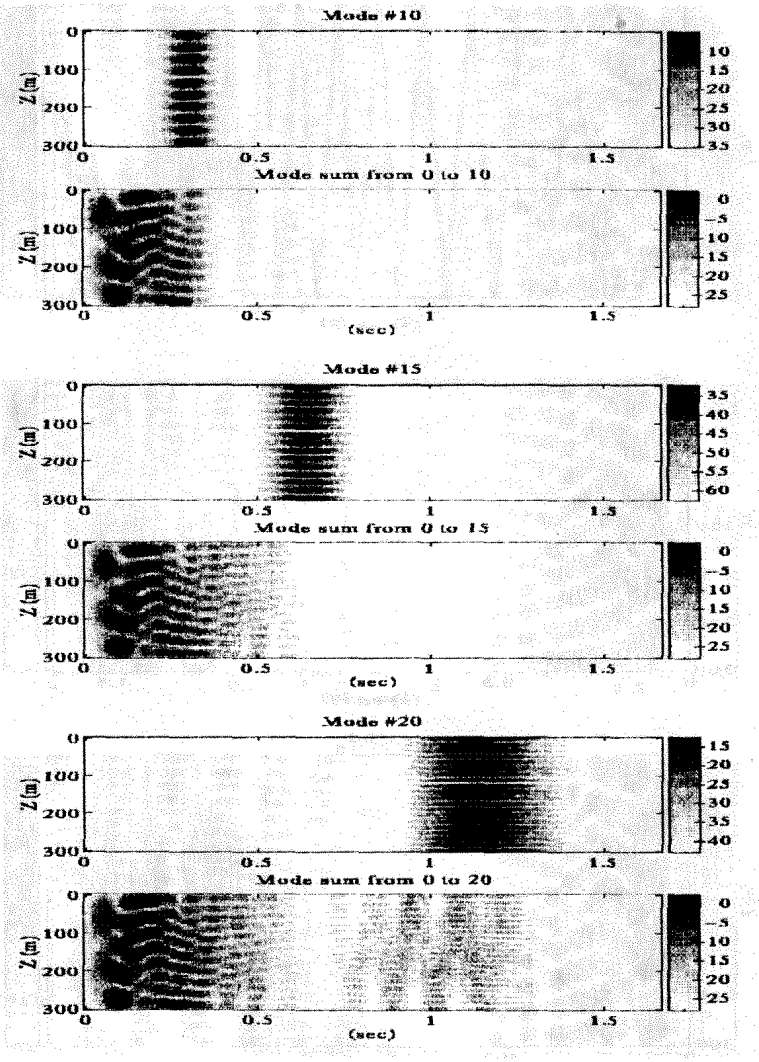

Fig. 9. Formation of the beam in space - time domain for the narrow frequency band and the sediment thickness 50 m.

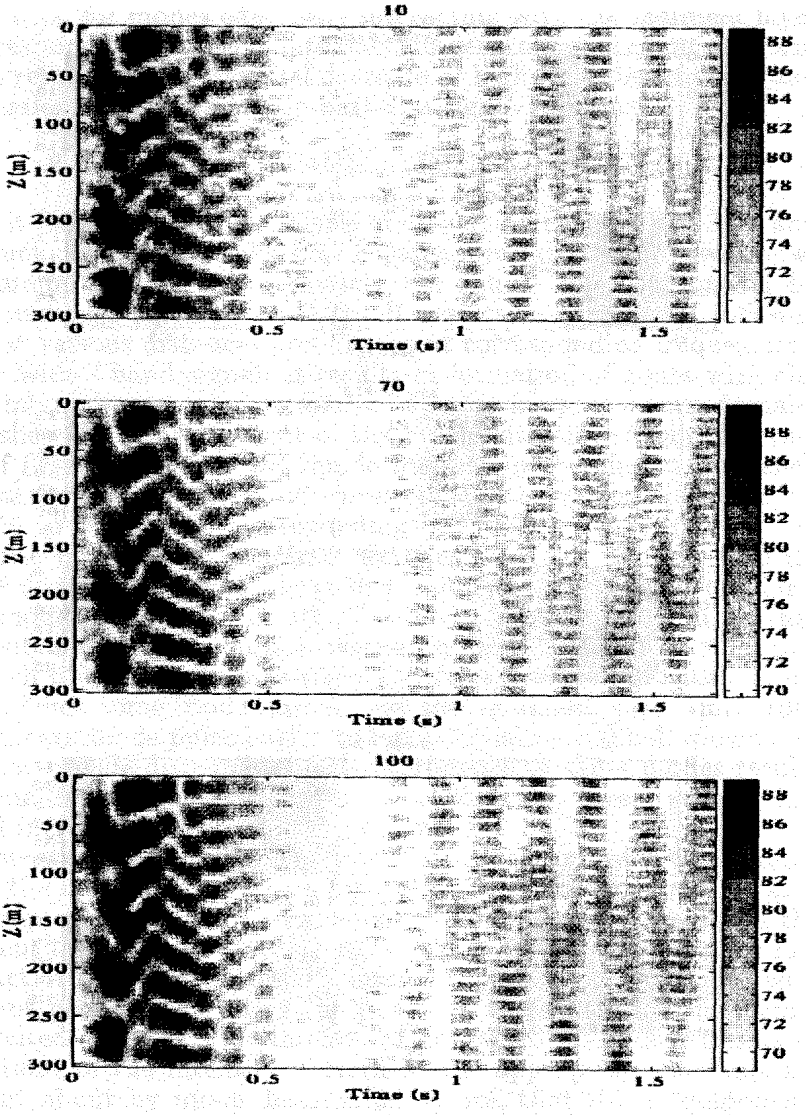

Fig. 10. The deformation of beam with growth of sediment thickness: $h = 10$ m (a), 70 m (b), 100 m (c).

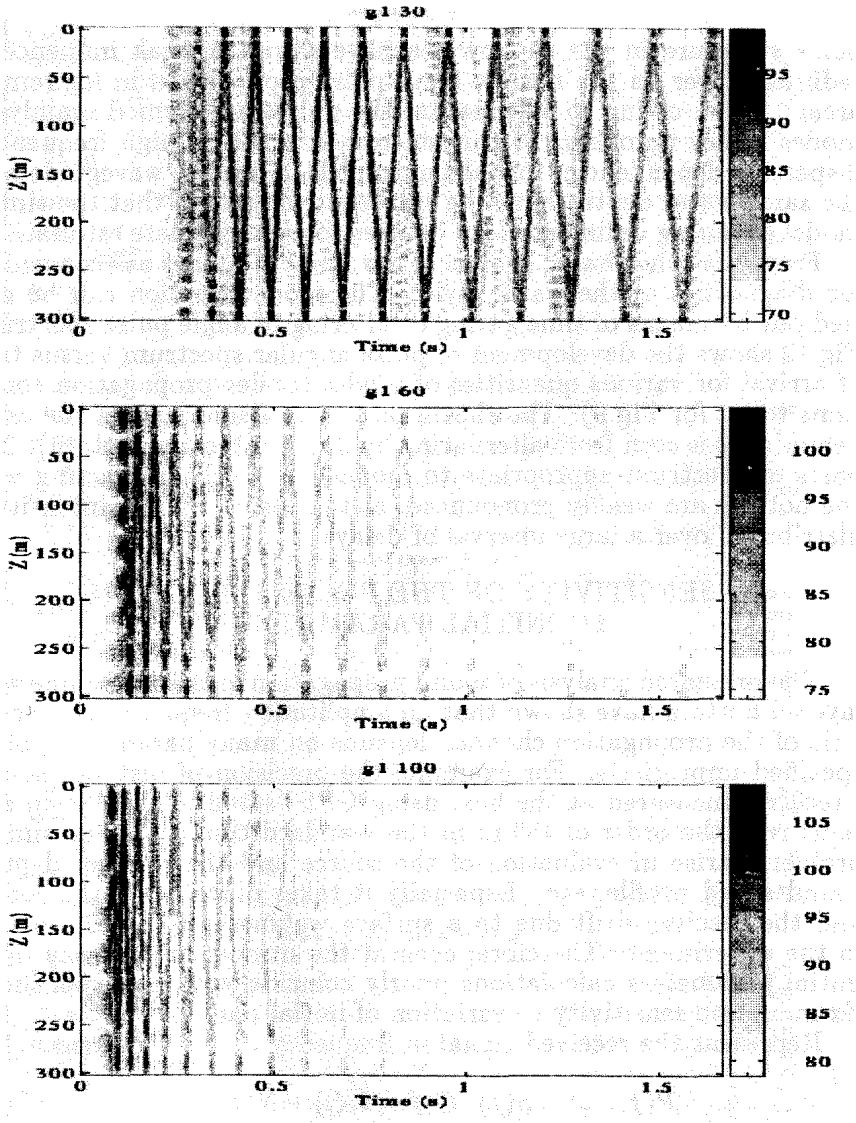

Fig. 11. Pulse bands formed by a group of resonant modes for sediment thickness: $h = 30$ m (a), 60 m (b), 100 m (c).

pulse structure in the shallow sea have shown a weak influence of sediment layer on the narrow band pulse propagation in far remote areas. Then, owing to attenuation the pulses are formed mainly by modes of low numbers. Within narrow intervals of high frequencies dispersion dependencies for various models of shallow waveguide with the same water depths have the similar structure, so that the simple model (ignoring sediments) can be used for approximate estimations.

From the other hand, groups of low number modes are convenient for diagnostics of the water layer. The mode selection can be carried out by means of time gating or filtering of angle pulse spectrum. Fig.12 shows the development of pulse angular spectrum versus time of arrival for various quantities of modes (under propagation conditions taken for Fig.9). The shown pulse has a structure of the angle beam (as it is seen from alternating by depth intensity pattern). The parts of spectrum appropriate to modes effectively interacting with the bottom are weakly pronounced, as the corresponding intensity is distributed over a large interval of delays.

3. SENSITIVITY OF THE PULSE STRUCTURE TO INITIAL PARAMETERS

The presented analysis of sound propagation in the waveguide with layered bottom have shown that an amplitude - frequency characteristic of the propagation channel depends on many parameters, often specified unprecisely. For example, the precision of distance source - receiver measured at the best using GPS (satellite navigation system) is in the order of 150 m in the standard condition The similar problems arise in evaluation of the source and the receiver depths, sound speed profile, etc. Especially it takes place when the source and the receiver drift due to a surface waviness, as usually occurs in the experiment. Therefore, even at the utmost in accuracy of all initial parameters calculations poorly coincide with an experiment. Examine the sensitivity to variation of initial parameters.

Represent the received signal in frequency domain in form

$$P(f,r,z) = S(f) \cdot G(f,r,z,\zeta_j) + N(f,r,z)\ , \qquad (15)$$

where $S(f)$ is the spectrum of the incident signal, $N(f,r,z)$ the noise spectrum, $G(f,r,z,\zeta_j)$ the Green function, $\zeta_j,\ j = 1 \ldots J$ the vector of parameters characterizing the propagation channel.

Actually, the argument (f,r,z) represents a finite set of M independent measurement positions in space and time domain. Designate these points by the discrete variable x_i and obtain the expression for propagating signal $Y(x_i,\zeta_n) = S(f) \cdot G(x_i,\zeta_n)$.

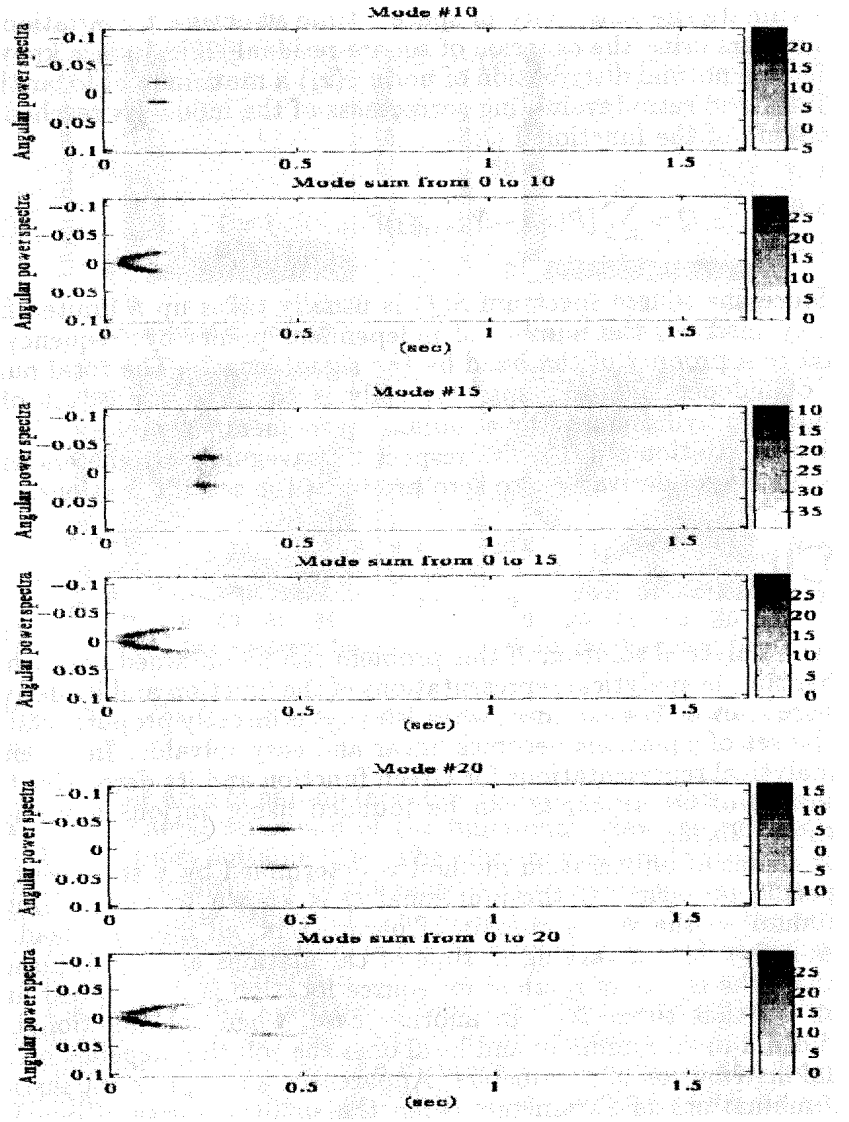

Fig. 12. The angular pulse spectra vs the time of arrival.

Estimate the sensitivity of space - time structure to variation of parameters using the criterion of square residual [22]. As it is known, under the normal distribution of noise $n(x_i)$ a maximum of logarithm of likelihood ratio (evaluating correctness of the model) is reached at minimum of the functional Q:

$$Q = \sum_{i}^{M} [P(x_i) - Y(x_i, \zeta_j)]^2 \ , \qquad j = 1 \ldots J \ . \tag{16}$$

Since the source spectrum $S(f)$ is usually takes up a limited frequency interval, the number of independent points by frequency is equal to a product of the band by the signal length. The total number of independent points M typically is equal to a product of a quantity of hydrophones by a number of frequency samples.

Differentiation of (16) with respect to waveguide parameters with an equating of derivatives to zero produces the set of equations:

$$\sum_{i}^{M} \left[P(x_i) \frac{\partial Y(x_i, \zeta_j)}{\partial \zeta_j} \right] = \sum_{i}^{M} \left[Y(x_i, \zeta_j) \frac{\partial Y(x_i, \zeta_j)}{\partial \zeta_j} \right] \ , \qquad j = 1 \ldots J \ . \tag{17}$$

An analytical solution of this problem can be obtained only when rather simple analytical representations of the function and its derivative are known. For example, when $Y(x_i, \zeta_j)$ is directly proportional to ζ_j, the set of equations becomes linear and easy solvable. In absence of analytical representations for Green function and its derivative the minimum of functional Q can be founded using various numerical methods [22,23].

A choice of an iteration method is determined by a statement of a specific problem. If the functional Q is known to have a single minimum on the whole domain of parameters, all methods lead to an unique solution varying in time of calculations and an accuracy. So that, the choice of method for source location is determined first of all by that time [24]. In another case, when the functional Q has both a main minimum and local ones the solution depends on an initial distribution of parameters. Apparently, a complete exhaustion of combinations of parameters (even the small quantity of ones) is often impossible. To facilitate the search of solution combinations of various methods can be applied (Monte - Carlo, gradient descent, Newton methods, etc.) [22–24].

An existence of any priory information substantially promotes the solving limiting a range of the initial parameters. In the considered case the peculiarities of forming focusings, beams, shadow zones bound the area of parameters. If there is an opportunity to evaluate

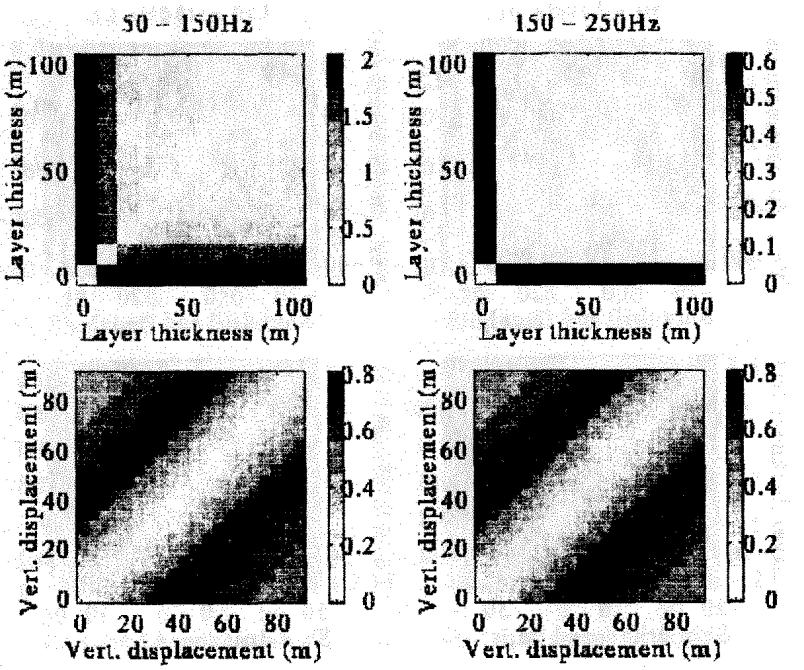

Fig. 13. The functional Q in sediment thickness - vertical displacement domain.

priory some area of parameters close to desired solution and including a single general minimum of the functional, Newton method seems to be the most suitable [24]. The efficiency of application of similar methods is determined by the sensitivity of solution to an accuracy of initial parameter definition. The easiest way to evaluate the sensitivity is to analyze derivatives of the functional Q by each of parameters close to its main minimum.

Fig.13 presents matrixes of functional Q depending on the sediment thickness h and the vertical displacement z for the waveguide of thickness $H = 300$ m, the distance $r = 90$ km, in the frequency intervals 50–150 Hz and 150–250 Hz with sampling of 0.6 Hz and the vertical array of 64 equidistant receivers. Fig.14 shows values of Q depending on ship drift speed u in $z - u$ and $h - u$ domains. It is seen from Fig.13, that notwithstanding that the diagonal of the matrix has a deep minimum for all h, the functional has a higher sensitivity to change of sediment thickness h at small ones (10–30 m) and at high frequencies. An existence of additional minimums at the distribution of Q by source and receiver depths allows to bound theirs precise by value of 10–15 m.

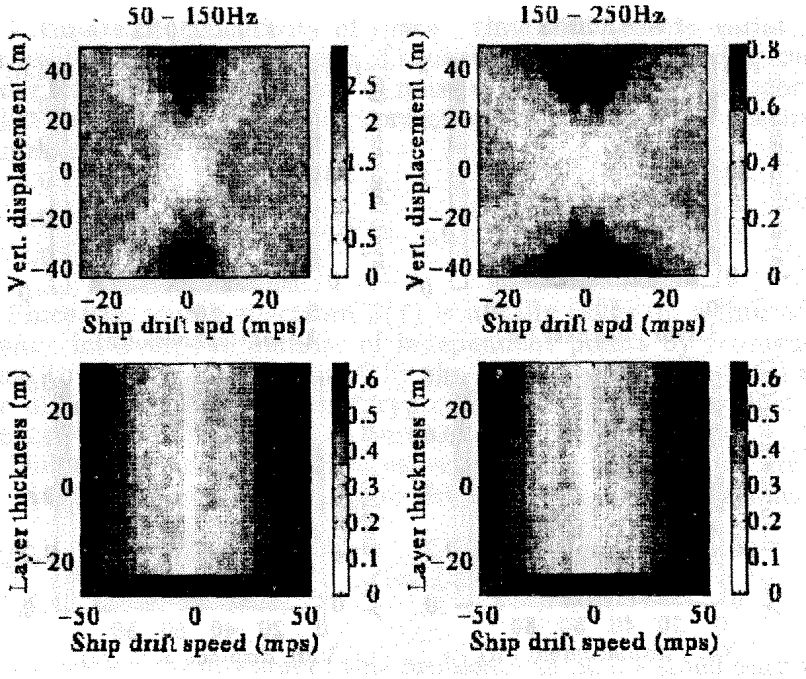

Fig. 14. The functional Q in vertical displacement - ship drift speed and sediment thickness - ship drift speed domains.

An influence of source and receiver drift appears insignificant and can be neglected.

Fig.14 shows the behavior of functional Q about the main minimum depending on various pairs of parameters. It enables to determine the allowable accuracy of priory evaluation of parameters at which the solution converges to the true one.

Under experimental conditions a random interference is expected to moderate the sensitivity of the signal structure to initial parameters. In Fig.15 the same dependencies are shown including an interfering noise. Here the signal/noise ratio is -6 dB. Under such conditions the amplitude - frequency characteristic looks irregular, but the functional has a distinct minimum coinciding with the true distribution of parameters.

CONCLUSIONS

In the paper the peculiarities of formation of space - time pulse structure were considered for shallow sea conditions. The rather simple model of layered bottom including a liquid deposit layer was used. The main attention was given to study of forming of focusings and

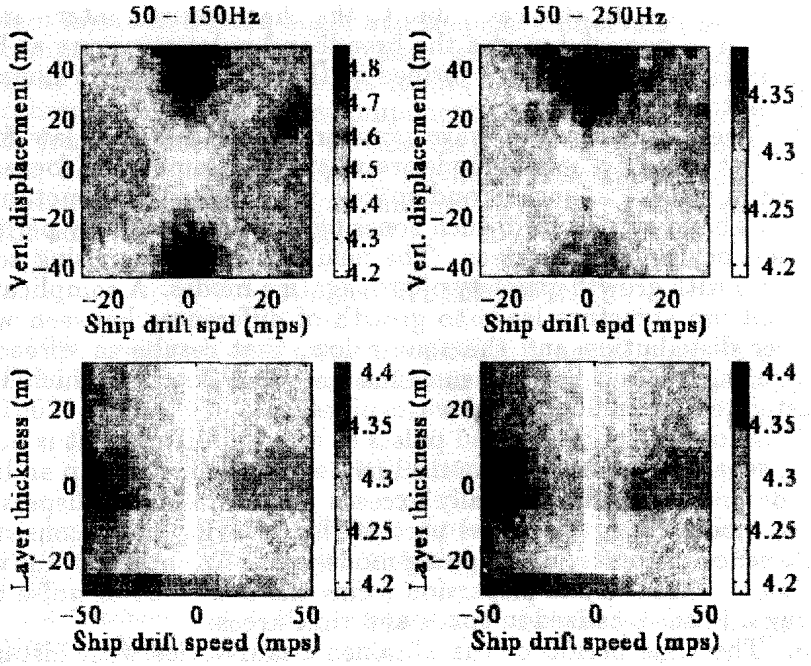

Fig. 15. The functional Q in vertical displacement - ship drift speed and sediment thickness - ship drift speed domains in presence of noise.

beams due to the constructive interference during multi - mode propagation, and also the analysis of influence of deposit layer parameters on the pulse structure.

The main results can be formulated:

1. The set of normal modes in the shallow layered waveguide can be divided into groups characterized by the specific shape of dispersion curve with inherent number of resonant bends. Quantity of modes in each group decreases, and number of groups increases with growth of sediment layer thickness. Dispersion dependencies within each group are identical in topology. This circumstance simplifies an interpretation of broadband signal propagation in the shallow sea.

2. In forming of broadband pulses at high frequencies (when a few tens of normal modes are excited) modes with large numbers can contribute insignificantly into the total field. It is caused, probably, by: 1) an intra - mode dispersion, when the energy of high modes is distributed within intervals of angles and delays substantially exceeding the corresponding intervals for low number modes; 2) the relatively large attenuation of high modes. So the total field is formed mainly by low number modes with appropriate resonant bends arising at

low frequencies. In this case, due to the characteristic inter - mode dispersion of powerful modes the broadband pulse structure at high frequencies is similar to one formed in the waveguide with homogeneous bottom.

3. The distribution of wave numbers close to square law for a significant part of powerful modes results in development of focusings of field in space - frequency and space - time domains. Monotone or narrow - band signals form such zones of increased intensity periodic in frequency and space areas. The field intensity in focusing zones increases with growth quantity of propagating modes. A complication of a bottom structure leads to growth of differences between wave number distribution and the square low, that results in spreading of focusing zones. Such phenomena are close to that which were investigated for radiophysical waveguides [24].

4. In forming of broadband pulses at selected distances it is possible to separate two sets of powerful modes: in the first group an inter - mode dispersion substantially exceeds an intra - mode dispersion. These modes form the initial part of the resulting pulse consisting of sequence of weakly overlapping mode pulses. Another group with dominant intra - mode dispersion forms the next part of pulse producing a beam localized in space and time areas.

5. The time period of the obtained beam varies with distance. The time dependence of propagating pulse at the selected depth can be divided into three intervals of time delays: the first group is a result of interference of mode pulses with low numbers, the next group corresponds the separate pulses, and the last part is formed by interfering long - drawn modes of high numbers. During propagation the pulse expands by time delay axis, and since some distances the third forming group of modes becomes dominant.

6. The analysis of sensitivity of coherent broadband interference structure to variations of waveguide parameters and geometry of the problem have shown, that a number of initial parameters (for example, a source depth and a sediment layer thickness) appear to be dependent ones. Another parameters are orthogonal. In other words, for correct estimations, for example, of the sediment thickness it is necessary to determine the source depth with enough precision. Numerical evaluations of the functional Q in the area close to a main minimum allow to determine the examined sensitivity and, also, the possible resolution in solving of the inverse problem and the range of coherence of pulse signals at varying initial parameters.

7. Study of dependence of wide-band pulse structure on the sediment layer parameters, have shown that a part of modes with low numbers propagate ignoring the bottom stratification (forming so-called water component of pulse). Other modes interacting with bot-

tom layers in certain angle and frequency intervals form the bottom component of a pulse. Because within the set of modes, forming these pulse components the modes parameters differ only slightly, coherence in these pulse components is maintained for propagation to long distances. Due to this they after a corresponding filtering can be used, respectively, for further tomography reconstruction of water column and bottom parameters in the shallow sea as well as for acoustical imaging [25].

ACKNOWLEDGMENTS

This research was carried out with financial support of Russian Foundation for Fundamental Research (Projects 97-02-17536, 96-02-18621 and 97-05-65657).

REFERENCES

1. *Pekeris K.L.* The theory of propagation of sound of explosion in shallow water// Propagation of sound in ocean. Moscow: Nauka, 1951. p.48–156.

2. *Brekhovskikh L.M.* Propagation of waves in layered environments// Moscow: Nauka. 1973.

3. *Tolstoy I. and Kley K.S.* Acoustics of the ocean. Moscow: Mir, 1969.

4. *Lobanov V.N., Petukhov Y.V.* Features of space - frequency distribution of broadband sound intensity in the shallow oceanic waveguide// Nizhny Novgorod: IAP RAS, Preprint N 321. 1991. 49p.

5. *Grudskii S.M., Grudskaia O.N., et al.* Distribution of sound in simple hydroacoustical waveguides with liquid and elastic bottom// Moscow: IGP RAS, 1989. N 7. 31p.

6. *Borodina E.L., Shirokov V.N. and Khil'ko A.I.* Formation of acoustical fields by leak modes and shear and side waves// The formation of acoustical fields in oceanic waveguides/ Ed. by V.I. Talanov. Nizhny Novgorod: IAP RAS, 1995. p.23–37.

7. *Ellis D.D., Chapman D.M.F.* A simple shallow water propagation model including shear wave effects// JASA 1985 v.78, N6. p.2087–2099.

8. *Borodina E.L., Petukhov Yu.V.* Restoration of the bottom characteristics by the interference structure of the wide - band sound// Acoustics Letters, 1996. N8. p.159–162.

9. *Werby M., et al.* Broad-Band pulse signals and the characterization of challow water oceanic properties, "in Proc. of the SPIE Conf., pp97-108, April 1995.

10. *Smirnov I.P., Caruthers J.W., Khil'ko A.I.* Multi scale coherence of noise acoustical source field in randomly inhomogeneous ocean// (see pres. collect.).

11. *Abrosimov D.I. and Petukhov Y.I.* Influence of diffractive effects on forming of weakly diverged acoustical bundles in underwater sound channel// Nizhny Novgorod: IAP RAS, Preprint N 389. 1996. 20p.

12. *Goncharov V.V., Kurtepov V.M.* On formation and propagation of weakly diverged bundles of rays in horizontally - inhomogeneous ocean// Akust. zhurn., 1994. N 5.

13. *Ageeva N.S., Krupin V.D.* Behavior of the frequency characteristics of modes in shallow water at varying of speed of longitudinal waves in sediment layer and of sound speed profile in water layer// Akust. zhurn., 1984. v.30. N 5. p.577-584.

14. *Hastrup O.F.* Anomalies of losses at reflection of modes near to small grazing angles and their influence on propagation in shallow water// Acoustics of bottom of ocean/ Ed. W. Kuperman and F. Ensen. Moscow: Mir, 1982. p.105–119.

15. *Belov A.I.* On influence of shear waves in sediment layer on acoustical field in shallow water// Proc. XI All - Union Acoustic Conf./ Section D. Moscow: AKIN, 1991. p.79-82.

16. *Ageeva N.S., Krupin V.D.* The influence of the sediment layer on frequency characteristics in the shallow sea// Akust. zhurn., 1983. v.29, N 6. p.721–727.

17. *Karetnikova I.R., Nechaev A.G., Khil'ko A.I.* Features diagnostics varying in time random inhomogeneities of waveguides via complex pulse signals// Izv. Vuz., Radiophysica, 1990. v.13, N 12. p.1370–1378.

18. *Gorsky S.M., Zverev V.A., Khil'ko A.I.* Features of diffraction of acoustic waves by spatially - localized inhomogeneities in oceanic waveguides// Formation of acoustic fields in oceanic waveguides// Ed. by V.A. Zverev. Nizhny Novgorod: IAP RAS, 1991. p.82–115.

19. *Vdovicheva N.K., Sazontov A.G., Khil'ko A.I.* Diffraction of acoustical fields by body displaced in randomly inhomogeneous oceanic waveguide// Nizhny Novgorod: IAP RAS, Preprint N 393. 1996. 30 p.

20. *Sazontov A.G. and Farfel B.A.* Calculation of a degree of coherence and form of acoustic pulse signals in oceanic waveguide with rough surface// Akust. zhurn., 1995. v.41. p.128–133.

21. *Hamilton E.L.* Geoacoustic modelling of the sea floor// JASA, 1988. v.68, N5. p.1313–1340.

22. Statistical methods for computers// Ed. by Enslein K., Relston A., Wilf H.S. Moscow: Nauka, 1986.

23. *Mignerey P.C. and Finette S.* Multichannel deconvolution of an acoustic transient in an oceanic waveguide//JASA, 1992. v.92(1), N7.

24. *Rivlin L.A., Shil'diaev V.S.* Poliharmonical waveguides for coherent light, Izv. Vuz., Radiophysica. v.11, N4, pp.572–578, 1995.

25. *Sidorovskaia N.A., Khil'ko A.I.* Partially-coherent acoustical images in layered refractive waveguides, Izv. Vuz., Radiophysica, v.38, N1–2, pp.127-133, 1995.

USING REGULARITIES IN THE BEHAVIOR OF A TWO-FREQUENCY CORRELATION FUNCTION OF ACOUSTIC FIELD IN MONITORING OF OCEANIC INHOMOGENEITIES

A. A. Pokrovsky

The recent years witnessed intensive development of various methods of oceanic inhomogeneity reconstruction in the interests of World ocean assimilation. The key role is played by acoustic methods, since acoustic oscillations are best suited to transfer information in a water medium.

On of the most difficult problems in acoustic monitoring of oceanic inhomogeneities is that of extracting inhomogeneity-scattered signals and estimating their parameters against the background of intermode interference and acoustic field fluctuations due to the broad spectrum of background inhomogeneities of the medium.

Generally, these factors are alleviated by spatio-temporal filtration procedures requiring, as a rule, use of extended vertical and horizontal antennas and complex illumination signals in combination with consistent signal processing [1].

In this paper we consider a simple tomographic scheme which uses an acoustic path between the spaced emitter and receiver. We estimate the possibilities of using such a scheme to extract and estimate signals scattered by oceanic inhomogeneities against the background of a fluctuating direct illumination field by exploiting the properties of an interfrequency acoustic field correlation function in a waveguide with random inhomogeneities.

In [2], theory is developed to describe sound field characteristics in the fluctuating ocean for a canonic ocean model and Harret–Munk internal wave spectrum. Expressions are obtained for the interfrequency correlation in terms of diffraction parameter Λ and inhomogeneity parameter Φ. It is shown that the coherence band depends on the variability scale of the structural phase function and the space correlation interval of sound speed fluctuation. In the ocean model adopted there, the "distance–frequency" plane is divided into domains corresponding to various sound propagation modes on account of internal wave scattering. In the domain of nonsaturated fluctuations, the signal is the sum of signals arriving along many perturbed paths, and each signal satisfies the applicability conditions of geometric approximation. For each perturbed path, the normalized

coherence function can be written as

$$\langle \Psi(f_1) \cdot \Psi^*(f_2) \rangle \;=\; \exp\left[-\frac{1}{2} \left(\frac{\Delta f}{f} \right)^2 \Phi^2 \right], \qquad (1)$$

where f_1 and f_2 are frequencies of the emitted signals; $\Delta f = f_1 - f_2$, $f = \frac{f_1+f_2}{2}$; $\Psi(\vec{x}, t, f)$ is the normalized complex amplitude of the random field; Φ is the inhomogeneity parameter of the medium, which represents a root-mean-square signal phase fluctuation at the reception point in geometric-optics approximation.

It is demonstrated that the coherence bandwidth of the signal arriving at the reception point along one deterministic beam can be calculated by the approximate expression

$$\Delta f_k \;\simeq\; f \left(\pi^2/6 \right) \left(l_v / L_v \right)^2 \left[\Lambda \Phi^2 \ln \Phi \right]^{-1} \;, \qquad (2)$$

where l_v is the variation scale of the structural phase function, L_v is the space correlation interval of sound speed fluctuation, and Λ is a diffraction parameter describing the influence of sould speed fluctuation on diffraction effects.

For beams which do not contact the ocean bottom and surface and for typical dispersion of relative sound speed fluctuations $\langle \mu_0^2 \rangle = 2.5 \cdot 10^{-7}$ the estimates of Δf_k are about a few tens of hertz if distances are about a few tens of kilometers and f is on the order of a few hundreds of hertz.

Assume that against the background of the afore-mentioned direct field fluctuations we must extract perturbations caused by inhomogeneities of a different nature, for example, by a fish school, a vortex or similar irregularities which can be written approximately as a set of randomly arranged point scatterers. Then, using the known expression for the normalized correlation function of the scattered field $\rho(\Delta f)$, when the scatterers are randomly arranged over a circle of diameter $\frac{cT}{2}$, we find [3]

$$\rho(\Delta f) \;=\; J_0(\Delta f \cdot T) \,, \qquad (3)$$

where c is the speed of sound, and $J_0(\delta f \cdot T)$ is a zeroth-order Bessel function.

For this model, the expression for the scattered field coherence band can be written as

$$\Delta f_k \;\leq \frac{1}{\pi T} \cdot \qquad (4)$$

It follows from (4) that the interfrequency coherence band is a few hertz when the scatterers region is as long as a few hundreds of meters.

Thus, for appropriate relationships between the parameters of the problem, the interfrequency correlation intervals between fluctuations caused by background inhomogeneities exceed considerably the correlation intervals between the scattered field fluctuations caused by inhomogeneities of a different nature, for example, by a scatterer field. Therefore, by analysis of the behavior of the interfrequency correlation function of the received signals, we can, in principle, record the occurrence of a scatterer cloud on the emitter–receiver path. Basically, the estimate of Δf_k makes it possible to evaluate the spatial length of the scatterers cloud on the basis of expression (4): the smaller Δf_k, the longer the scatterer domain on the emitter–receiver path.

We now consider the factors influencing the possibility to record other than background inhomogeneities on the emitter-receiver path. Let us analyze first a simple case in which a single acoustic beam connects the emitter and the receiver and the beam passes through a scatterer cloud leading to additional (with respect to background) discorrelation of envelope signals at frequencies f_1 and f_2. We shall designate the interfrequency correlation factor of the envelopes at frequencies f_1 and f_2 by r'_{12} in the presence and by r''_{12} in the absence of a scatterer cloud. The nonzero value of r''_{12} is due to background inhomogeneities on the emitter–receiver path.

Consider a simple scheme of received signal processing, which is based on the deduction of the signal envelope at frequency f_2 from the signal envelope at frequency f_1 and the subsequent analysis of the difference. We finally arrive at

$$S_{\text{output}} = \overline{[a_{f_1} + n_{f_1} - a_{f_2} - N_{f_2}]^2}, \qquad (5)$$

where $a_{f_1}(t)$ and $a_{f_2}(t)$ are the envelopes of the illumination signals, and $n_{f_1}(t)$ and $n_{f_2}(t)$ are the additive noise envelopes at frequencies f_1 and f_2, respectively. The overbar means temporal averaging.

In the ideal case of a deterministic channel,

$$S_{\text{output}} = \overline{n_{f_1}^2} + \overline{n_{f_2}^2}$$

under the assumption of complete correlation between envelopes at frequencies f_1 and f_2. In the other limiting case of complete discorrelation due to inhomogeneities, we have

$$S_{\text{output}} = \overline{a_{f_1}^2} + \overline{a_{f_2}^2} + \overline{n_{f_1}^2} + \overline{n_{f_2}^2}.$$

Thus, as a criterion of inhomogeneity occurrence on the emitter–receiver path we can use the increase in dispersion of the output processing effect due to disturbance of correlation between illumination signal envelopes at frequencies f_1 and f_2.

The factors impeding observation of inhomogeneities include, firstly, the incomplete correlation between illumination signal envelopes at the carrier frequencies due to background inhomogeneities and, secondly, their incomplete discorrelation in the presence of the observed inhomogeneities.

In this situation, the signal-to noise ratio at the output of the signal processing scheme can be represented as

$$S/N = \frac{\overline{[a_{f_1}(t) - a_{f_2}(t)]_I^2}}{\overline{[A_{f_1}(t) + n_{f_1}(t) - a_{f_2}(t) - n_{f_2}(t)]_{II}^2}}. \qquad (6)$$

The designation $[\ldots]_I$ means that we consider the realization when the observed scatterer cloud is on the emitter–receiver path, and $[\ldots]_{II}$ means that we consider the time interval before the occurrence of the inhomogeneity cloud.

Assuming that $\overline{a_{f_1}^2} = \overline{a_{f_2}^2} = \sigma_{s'}^2$ and $\overline{n_{f_1}^2} = \overline{n_{f_2}^2} = \sigma_n^2$ the expression (6) takes the form

$$S/N = \frac{\sigma_{s'}^2}{\sigma_n^2} \frac{(1 - r'_{12})_I}{1 + \frac{\sigma_{s'}^2}{\sigma_n^2}(1 - r''_{12})_{II}}. \qquad (7)$$

In the more general case of a multibeam channel, a situation is possible where the beams which did and the beams which did not pass through the scatterer cloud cannot be received separately. In this case, the signal at the receiver is the sum of perturbed and unperturbed beams, and the beams which did not pass through the perturbed area introduce additional noise. It can be easily seen that the signal-to-noise ratio can be written as

$$S/N = \frac{\sigma_{s'}^2(1 - r'_{12})_I}{\sigma_n^2 \left[1 + \frac{\sigma_{s''}^2}{\sigma_n^2}(1 - r''_{12})\right]_{II}}, \qquad (8)$$

where $\sigma_{s''}^2$ is the total dispersion of all the beam envelopes at the reception point. In deriving (8), it was assumed for simplicity that

the interfrequency correlation is the same and is equal to r''_{12} for all the received beams. From expression (8), we can estimate the conditions under which we can watch inhomogeneities along multibeam paths by using interfrequency correlation laws for illumination signals. The calculation (fig. 1) show typical dependences of S/N on the parameters of the problem (1: $\frac{\sigma^2_{s'}}{\sigma^2_n} = \frac{\sigma^2_{s''}}{\sigma^2_n} = 10$, $r''_{12} = 1$; 2: $\frac{\sigma^2_{s'}}{\sigma^2_n} = \frac{\sigma^2_{s''}}{\sigma^2_n} = 10$, $r''_{12} = 0,9$; 3: $\frac{\sigma^2_{s'}}{\sigma^2_n} = 0,1 \cdot \frac{\sigma^2_{s''}}{\sigma^2_n} = 10$, $r''_{12} = 0,95$; 4: $\frac{\sigma^2_{s'}}{\sigma^2_n} = 0,5 \cdot \frac{\sigma^2_{s''}}{\sigma^2_n} = 10$, $r''_{12} = 0,9$; 5: $\frac{\sigma^2_{s'}}{\sigma^2_n} = 0,5 \cdot \frac{\sigma^2_{s''}}{\sigma^2_n} = 100$, $r''_{12} = 0,9$). The analysis of (8) shows that the signal-to-noise ratio increases with a decrease in r'_{12}, the correlation of envelope signals at frequencies f_1 and f_2, which passed through the scatterer cloud, an increase in r''_{12}, the interfrequency correlation of envelope signals entering the receiver in the absence of the observed scatterer cloud, and a decrease in the number of beams which arrive at the receiver without transmission through the scatterer area.

To ensure high efficiency of this method of watching oceanic inhomogeneities with use of acoustic paths, we must have a model of a random acoustic signal in the area of interest and a description of the inhomogeneities to be observed in terms of interfrequency correlation functions. A combination of all this will make it possible to determine the optimal parameters of the acoustic path, including the distance between the emitter and the receiver, the depth of their submergence, the radiated frequency, and the directivity characteristics.

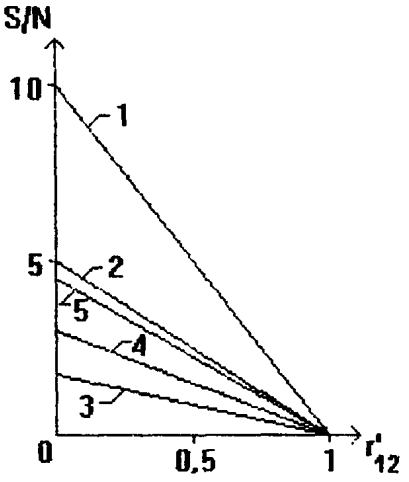

Fig. 1. Typical dependences of S/N on the parameters of the problem.

References

[1] *Gorsky S.M., Zverev V.A., and Khil'ko A.I.* Features of Acoustic Field Diffraction by Spatially Localized Inhomogeneities in Oceanic Waveguides, in: "Acoustic Field Generation in an Oceanic Waveguide" (collected papers), IAP RAS Press, Nizhny Novgorod (1991).

[2] *Flatte S., ed.* Sound Propagation in Fluctuating Ocean, Mir, Moscow (1982).

[3] *Shirman Ya.D., ed.* Theoretical Principles of Radar, Sovetskoye Radio, Moscow (1978).

PROPAGATION OF LOW-FREQUENCY SOUND IN A HYDROACOUSTIC WAVEGUIDE WITH SURFACE COVERED BY A NON-CONTINUOUS ICE LAYER

S.M. Grudskiĭ, A.I. Khilko , S.S. Mikhalkovich

The present paper is devoted to the problem of sound propagation in a stratified waveguide which is a non-homogeneous liquid layer overlaying multi-layered liquid-elastic bottom. The surface of waveguide is covered by thin (in comparison with length of an acsoutic wave) homogeneous ice layer with polynia of finite width.

Influence of the polynia to characteristics of an acoustic field is investigated. The main asymptotic terms of elements of reflection and transmission matrices by a small parameter ε are obtained, where ε characterises thickness of ice. These formulas are uniform on parameter L, where L specifies polynia width. The similar formulas for a finite width ice-floe laying on a liquid layer are given. In this case influence of attenuation in the ice on the diagonal members of the transmission matrix is analysed. We note that the used approach can be generalized to a case of a finite number of ice-floes.

INTRODUCTION

The study of sound propagation in the world ocean regions covered by ice during an essential part of a year is an urgent problem. Its meaning increases in connection with the plans of realizing a wide-scale hydroacoustic experiments in the region of Arctic ocean with the purpose to research the global rise in temperature on the globe. Note that if we take into account all real properties of ice (the bottom edge indenting, nonhomogeneities on a route, presence of a snow cover, icebergs and etc.) the problem of sound propagation is very complicated and its complete solution is apparently impossible at present.

In this paper we investigate an influence of polynia in an ice surface to a hydroacoustic field peculiarities. The similar analysis is also made in a case of a finite width ice-floe laying on a water surface. In this case ice is simulated by a homogeneous elastic layer of constant thickness (acoustic characteristics of this layer are described in details in [1], for example). The stratified hydroacoustic waveguide is supposed to be two-dimensional and consists of a non-homogeneous liquid layer laying on multi-layered liquid-elastic bottom (see figure 1).

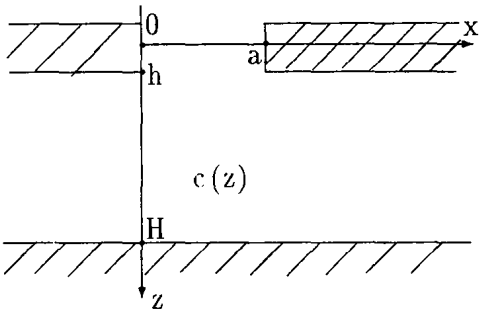

Fig. 1. Model of the waveguide.

Despite comparative simplicity of this model the authors consider that its research allows to describe peculiarities of an acoustic field structure in a case of low frequency sound, when wave length $\lambda \gg h$, where h is a thickness of an underwater part of ice.

For the problem solution a Wiener–Hopf method [2]–[4] is applied. To this end the ice layer is replaced by equivalent (see section 1) in some sense condition on a surface $z = 0$ (surface of thawing ice). This condition looks like the equation of convolution

$$\begin{cases} p(x,0) + \frac{1}{2\pi} \int\limits_{\mathbf{R}\setminus(0,a)} F(x-s)\frac{\partial p}{\partial z}(s,0)ds = 0, & x \in \mathbf{R}, \\ p(x,0) = 0, & x \in (0,a), \end{cases} \tag{1}$$

where $p(x,z)$ is a complex amplitude of sound pressure and $F(x)$ is a function taking into account acoustic parameters of ice. The ice in this case is "defreezed" in the sense that the original waveguide is replaced by a waveguide completely filled by a liquid at $z \in (0,H)$.

Problem with a condition (1) can be easily reduced to the equation of convolution on a finite interval ([3]–[4]) or, in Fourier images, to so-called ([1], ch.5) modified Wiener-Hopf equation.

To solve this equation we use a method of matrix Riemann boundary problem ([4] - [7]). It allows to construct asymptotic formulas to solve a problem of surging on edge $x = 0$ mode and to obtain effective formulas for elements of reflection and transmission matrices. These asymptotic formulas are uniform on parameter a. So, the results of the present paper are applicable in a case of a great distance between ice fields (hundred and thousand kilometers).

In the first section of paper we explain how to proceed to a condition (1) on "equivalent" surface of thawing ice $z = 0$. The same approach and its asymptotical aspects on $h \to 0$ were developed in [8] in the case of a solid ice layer.

In the second section we solve a surging mode problem by reduction to the modified Wiener–Hopf equation, then we built asymptotic on $h \to 0$ solution and explain its uniformity on parameter a.

In the third section we present qualitative and numerical research of the obtained formulas. In conclusion we mark that the given technique is suitable for a case of finite number of ice–floes and ice–holes on a surface. Certainly, the offered technique allows to analyse a field of a point monochromatic source and also to consider more complicated sources.

1. THE REPLACEMENT OF AN ELASTIC LAYER, SIMULATING ICE, BY EQUIVALENT CONDITION ON A SURFACE OF "DEFREEZED" ICE

Consider a problem of waveguide covered by a solid homogeneous ice layer with thickness d. Suppose that the water layer has constant density ϱ_0 and ice layer has constant density ϱ_{ice}. Choose an origin of z coordinate at a level of "defreezed" ice, so that low edge of ice will be at level $z = h$, where $h = \frac{\varrho_{\text{ice}}}{\varrho_0} d$, and upper one will be at level $z = h - d$.

Let $p(x, z)$ be a complex amplitude of sound pressure in a water layer $z \in (h, H)$. Then the process of sound propagation at $z \in (h, H)$ is described, as well known ([9]), by Helmholtz equation

$$\frac{\partial^2 p}{\partial x^2}(x, z) + \frac{\partial^2 p}{\partial z^2}(x, z) + k_0^2 n^2(z) p(x, z) = 0, \quad z \in (h, H), \tag{2}$$

where $k_0 = \omega / c_0$ is a wave number, c_0 is a certain typical value of sound velocity, $\omega = 2\pi f$ is the cyclic frequency, f is the frequency in hertzes, $n(z) = c_0 / c(z)$ is the index of refraction of the water layer, $c(z)$ iz the profile of the sound velocity.

In the elastic layer $z \in (h - d, h)$ propagation of sound is described by classical system of Lame equations. We will not write out these equations and say about conditions on interface between the elastic layer and liquid (see, for example, [9], [10]). Further note that using the Fourier transformation (in dimensionless form)

$$\Psi(\mu, z) = \int_{-\infty}^{\infty} p(x, z) \exp(i k_0 \mu x) dx, \quad \mu \in \mathbf{R}, \tag{3}$$

and taking into account the interface conditions we can replace the elastic layer by an equivalent ([9]) impedance condition on the lower surface of ice $z = h$:

$$\Psi(\mu, h) + \frac{f(\mu)}{k_0} \cdot \frac{\partial \Psi}{\partial z}(\mu, h) = 0, \tag{4}$$

where the function $f(\mu)$ is given below ([8]):

$$f(\mu) = -\frac{\varrho_{ice}}{\varrho_0} \frac{a\frac{\sin(k_0\eta d)}{\eta}\frac{\sin(k_0\zeta d)}{\zeta} + 2b\frac{1-\cos(k_0\eta d)\cos(k_0\zeta d)}{\eta^2+\zeta^2}}{n_2^4\left(p\cos(k_0\eta d)\frac{\sin(k_0\zeta d)}{\zeta} + d\cos(k_0\zeta d)\frac{\sin(k_0\eta d)}{\eta}\right)}, \tag{5}$$

where

$$\eta^2 = n_1^2 - \mu^2, \quad \zeta^2 = n_2^2 - \mu^2, \quad p = (2\mu^2 - n_2^2)^2,$$
$$a = 16\mu^4\eta^2\zeta^2 + p^2, \quad b = 4\mu^2 p(\eta^2 + \zeta^2), \quad d = 4\mu^2\eta^2,$$
$$n_1 = \frac{c_0}{c_1}, \quad n_2 = \frac{c_0}{c_2},$$

c_1, c_2 are velocities of longitudinal and transversal sound waves in ice.

Our goal is by "defreezing" ice and by replacing it at $z \in (0, h)$ by a homogeneous water layer with density ϱ_0 and sound velocity c_0 to pick up function $f_0(\mu)$ so that an impedance condition at a level of thawing ice $z = 0$, equivalent to a condition (4), will look like

$$\Psi(\mu, 0) + \frac{f_0(\mu)}{k_0} \cdot \frac{\partial\Psi}{\partial z}(\mu, 0) = 0. \tag{6}$$

Note for this purpose that $p(x, z)$ in a formed layer of water $z \in (0, h)$ satisfies the equation

$$\frac{\partial^2 p}{\partial x^2}(x, z) + \frac{\partial^2 p}{\partial z^2}(x, z) + k_0^2 p(x, z) = 0.$$

By acting on this equation the Fourier transformation (3) we have

$$\frac{\partial^2\Psi}{\partial z^2}(\mu, z) + k_0^2(1 - \mu^2)\Psi(\mu, z) = 0, \quad z \in (0, h).$$

The general solution of the above second order differential equation has a form

$$\Psi(\mu, z) = A(\mu)\sin(\gamma(\mu)k_0 z) + B(\mu)\cos(\gamma(\mu)k_0 z), \quad z \in (0, h),$$

where $A(\mu)$, $B(\mu)$ are coefficients dependent on μ, $\gamma(\mu) = \sqrt{1 - \mu^2}$.

From (4) and (6) we have:

$$f_0(\mu) = -k_0\frac{\Psi(\mu, 0)}{\Psi_z(\mu, 0)} = -\frac{1}{\gamma(\mu)} \cdot \frac{\mathrm{tg}(k_0\gamma(\mu)h) + f(\mu)\gamma(\mu)}{f(\mu)\gamma(\mu)\mathrm{tg}(k_0\gamma(\mu)h) - 1}. \tag{7}$$

Let $\varepsilon = k_0 h$ be a parameter characterizing thickness of ice. Simple asymptotic analysis gives the formulas

$$\left.\begin{aligned} f(\mu) &= -\varepsilon + L(\mu)\varepsilon^3 + O(\varepsilon^5), \\ f_0(\mu) &= \varepsilon^3\left(\tfrac{1-\mu^2}{3} + L(\mu)\right) + O(\varepsilon^5), \end{aligned}\right\} \tag{8}$$

where

$$L(\mu) = -\frac{4\mu^4\left(1-\frac{n_1^2}{n_2^2}\right)(\mu^2-n_2^2)+n_1^2\mu^2(n_1^2-2n_2^2)+n_2^4n_1^2}{3\left(\frac{\varrho_{ice}}{\varrho_0}\right)^2[n_2^4+4\mu^2(n_1^2-n_2^2)]}. \qquad (9)$$

Note also that as far as the functions f and f_0 are odd on parameter ε, the expansion in the formulas (8) is conducted by odd ε powers.

Acting on (6) by the inverse Fourier transformation and taking into account that product in this case transforms into a convolution, we obtain:

$$p(x,0)+\frac{1}{2\pi k_0}\int_{\mathbf{R}} F_0(x-s)\frac{\partial p}{\partial z}(s,0)ds=0, \quad x\in\mathbf{R}, \qquad (10)$$

where the function $F_0(x)$ is the inverce Fourier transformation of function $f_0(\mu)$.

Thus, the condition (10) is equivalently replaces a layer of homogeneous ice in the sense that the solution of an original problem with an elastic layer and solution of a problem with a condition (10) coincide at $z \geq h$.

Now return to a problem with polynia (figure 1). Let by analogy with (6) the following condition is realized:

$$\Pi_0(\mu,0)+\frac{f_0(\mu)}{k_0}\cdot\frac{\partial\Pi_0}{\partial z}(\mu,0)=0, \qquad (11)$$

where $\Pi_0(\mu,z)=\left(\int_{-\infty}^{0}+\int_a^{+\infty}\right)(p(x,z)\exp(ik_0\mu x)dx)$. Acting on (11) by the reverse Fourier transformation and taking into account that product transforms into a convolution, we obtain:

$$\begin{aligned}&\tfrac{k_0}{2\pi}\int_{\mathbf{R}}\Pi_0(\mu,0)e^{-ik_0\mu x}\,d\mu+\\&\quad+\tfrac{1}{2\pi}\int_{\mathbf{R}\setminus(0,a)}F_0(x-s)\tfrac{\partial p}{\partial s}(s,0)\,ds=0, \quad x\in\mathbf{R},\end{aligned} \qquad (12)$$

Taking into account the condition on a free surface

$$p(x,0)=0, \quad x\in(0,a), \qquad (13)$$

one can obtain from (12) the equality

$$p(x,0)+\frac{1}{2\pi k_0}\int_{\mathbf{R}\setminus(0,a)}F_0(x-s)\frac{\partial p}{\partial z}(s,0)ds=0, \quad x\in\mathbf{R},$$

which, according to (13), decomposes on two equalities

$$p(x,0)+\frac{1}{2\pi k_0}\int_{\mathbf{R}\setminus(0,a)}F_0(x-s)\frac{\partial p}{\partial z}(s,0)ds=0,\quad x\in\mathbf{R}\setminus(0,a),\tag{14}$$

$$\int_{\mathbf{R}\setminus(0,a)}F_0(x-s)\frac{\partial p}{\partial z}(s,0)ds=0,\quad x\in(0,a).\tag{15}$$

In contrast to a problem without polynia the problem with conditions (13)–(15) is equivalent to the original problem with polynia only in asymptotic sense (at $\varepsilon\to 0$). In the present work we are not stopped on a rigorous proof of this statement.

2. THE PROBLEM OF SURGING MODE

Consider a problem of sound propagation in stratified waveguide with conditions (13)–(15) at a level $z=0$. The liquid layer $z\in(0,H)$ is supposed to be stratified and nonhomogeneous so that the complex amplitude of sound pressure $p(x,z)$ at $z\in(0,H)$ satisfies the equation

$$\frac{\partial^2 p}{\partial x^2}(x,z)+\frac{\partial^2 p}{\partial z^2}(x,z)+k_0^2n^2(z)p(x,z)=0,\tag{16}$$

where $n(z)\equiv 1$ at $z\in(0,h)$. Sound pressure $p(x,z)$ satisfies at a level $z=0$ the conditions (13)–(15) and at a level $z=H$ the standard impedance condition, caused by set of a liquid and elastic layers in bottom. In Fourier images this condition has a form

$$\frac{\partial\Psi}{\partial z}(\mu,H)+k_0q(\mu)\Psi(\mu,H)=0.\tag{17}$$

After the Fourier transformation (3) the Helmholtz equation takes on a form

$$\frac{\partial^2\Psi}{\partial z^2}(\mu,z)+k_0^2(n^2(z)-\mu^2)\Psi(\mu,z)=0.\tag{18}$$

We shall consider two spectral problems:

$$\begin{cases}(18),\\(17),\\\Psi(\mu,0)=0,\end{cases}\tag{19}$$

and

$$\begin{cases}(18),\\(17),\\\Psi(\mu,0)+\frac{f_0(\mu)}{k_0}\cdot\frac{\partial\Psi}{\partial z}(\mu,0)=0,\end{cases}\tag{20}$$

and denote as $(k_0^2\mu_s^2, \varphi_s(z))$ and $(k_0^2\mu_{s,\varepsilon}^2, \varphi_{s,\varepsilon}(z))$ eigenvalues and eigenfunctions of the problems (19) and (20) respectively. Suppose also that eigenfunctions $\varphi_s(z)$ and $\varphi_{s,\varepsilon}(z)$ satisfy the conditions $\int_0^H |\varphi_s(z)|^2\,dz = 1$ and $\int_0^H |\varphi_{s,\varepsilon}(z)|^2\,dz = 1$.

Let $n > 0$ modes be guided in waveguides without and with ice. Let also the j–th mode $(j \le n)$ over-runs on an edge $x = 0$:

$$\varphi_{j,\varepsilon}(x, z) = \varphi_{j,\varepsilon}(z)\exp(ik_0\mu_{j,\varepsilon}x).$$

Denote the perturbated field by $\varphi(x, z)$, so that

$$p(x, z) = \varphi(x, z) + \varphi_{j,\varepsilon}(x, z).$$

For selection the physically correct solution we shall require that $\varphi(x, z)$ satisfied to a principle of limiting absorption.

We shall denote through $\Phi(\mu, z)$ the dimensionless Fourier transformation of function $\varphi(x, z)$:

$$\Phi(\mu, z) = \int_{-\infty}^{+\infty} \varphi(x, z)e^{ik_0\mu x}dx = \Phi_0(\mu, z) + \int_0^a \varphi(x, z)e^{ik_0\mu x}dx,$$

where

$$\Phi_0(\mu, z) = \left(\int_{-\infty}^{0} + \int_a^{+\infty}\right)(\varphi(x, z)\exp(ik_0\mu x)dx).$$

Taking into account that $\varphi(x, z) = p(x, z) - \varphi_{j,\varepsilon}(x, z)$ and conditions (14), (15), one can obtain:

$$\begin{cases} \varphi(x, 0) = -\varphi_{j,\varepsilon}(0)e^{ik_0\mu_{j,\varepsilon}x}, & x \in (0, a); \\ \varphi(x, 0) + \dfrac{1}{2\pi k_0}\displaystyle\int_{\mathbf{R}\setminus(0,a)} F_0(x - s)\frac{\partial\varphi}{\partial z}(s, 0)ds = \\ = -(\varphi_{j,\varepsilon}(0)e^{ik_0\mu_{j,\varepsilon}x} + \dfrac{\varphi'_{j,\varepsilon}(0)}{2\pi k_0}\times \\ \quad \times \displaystyle\int_{\mathbf{R}\setminus(0,a)} F_0(x - s)e^{ik_0\mu_{j,\varepsilon}s}ds), & x \in \mathbf{R}\setminus(0, a); \\ \dfrac{1}{2\pi k_0}\displaystyle\int_{\mathbf{R}\setminus(0,a)} F_0(x - s)\frac{\partial\varphi}{\partial z}(s, 0)ds = \\ = -\dfrac{\varphi'_{j,\varepsilon}(0)}{2\pi k_0}\displaystyle\int_{\mathbf{R}\setminus(0,a)} F_0(x - s)e^{ik_0\mu_{j,\varepsilon}s}ds, & x \in (0, a). \end{cases}$$

Acting by the Fourier transformation to each equality, we have

$$\Phi_0(\mu, 0) + \frac{f_0(\mu)}{k_0}\cdot\frac{\partial\Phi_0}{\partial z}(\mu, 0) = -[\varphi_{j,\varepsilon}(0)\mathcal{F}(\chi_{\mathbf{R}\setminus(0,a)}(x)e^{ik_0\mu_{j,\varepsilon}x}) +$$

$$+\varphi'_{j,\varepsilon}(0)\frac{f_0(\mu)}{k_0}\mathcal{F}(\chi_{\mathbf{R}\setminus(0,a)}(x)e^{ik_0\mu_{j,\varepsilon}x})] =$$

$$= -\left[\varphi_{j,\varepsilon}(0) + \frac{f_0(\mu)}{k_0}\varphi'_{j,\varepsilon}(0)\right][\mathcal{F}(e^{ik_0\mu_{j,\varepsilon}x} - \mathcal{F}(\chi_{(0,a)}(x)e^{ik_0\mu_{j,\varepsilon}x})],$$

where $\chi_{\mathbf{A}}$ is a characteristic function of set A, $\mathcal{F}(\varphi)$ is a Fourier transformation of function φ.

Taking into account that the the eigenfunction of a problem (20) satisfies the equality

$$\varphi_{j,\varepsilon}(0) + \frac{f_0(\mu_{j,\varepsilon})}{k_0}\varphi'_{j,\varepsilon}(0) = 0,$$

we have

$$\Phi_0(\mu, 0) + \frac{f_0(\mu)}{k_0} \cdot \frac{\partial\Phi_0}{\partial z}(\mu, 0) =$$

$$= -\frac{\varphi'_{j,\varepsilon}(0)}{k_0}[f_0(\mu) - f_0(\mu_{j,\varepsilon})] \cdot [\frac{1}{k_0}\delta(\mu + \mu_{j,\varepsilon}) - g(\mu)],$$

where

$$G(\mu) = \frac{\exp(iL(\mu + \mu_{j,\varepsilon})) - 1}{ik_0(\mu + \mu_{j,\varepsilon})},$$

$L = ka$, and $\delta(\mu)$ is the Dirac delta–function.

As far as $f_0(-\mu_{j,\varepsilon}) - f_0(\mu_{j,\varepsilon}) = 0$, we have

$$[F_0(\mu) - f_0(\mu_{j,\varepsilon})]\delta(\mu + \mu_{j,\varepsilon}) \equiv 0.$$

Thus, we finally obtain:

$$\Phi_0(\mu, 0) + \frac{f_0(\mu)}{k_0} \cdot \frac{\partial\Phi_0}{\partial z}(\mu, 0) = \frac{\varphi'_{j,\varepsilon}(0)}{k_0}[f_0(\mu) - f_0(\mu_{j,\varepsilon})]g(\mu). \qquad (21)$$

Let $\Psi(\mu, z)$ be throughout below in a paper the function satisfying only the conditions (18), (17), and also to the condition $\int_0^H |\Psi(\mu, z)|^2\, dz = 1$. Then $\Phi(\mu, z)$ has a form

$$\Phi(\mu, z) = A(\mu)\Psi(\mu, z) \qquad (22)$$

with some unknown function $A(\mu)$. Differentiating this equality with respect to z and assuming $z = 0$, we have:

$$A(\mu)\Psi(\mu, 0) = \Phi(\mu, 0) = \Phi_0(\mu, 0) + \int_0^a \varphi(x, 0)\exp(ik_0\mu x)dx, \qquad (23)$$

$$A(\mu)\frac{\partial\Psi(\mu,0)}{\partial z} = \frac{\partial\Phi}{\partial z}(\mu,0) = \frac{\partial\Phi_0}{\partial z}(\mu,0) + \int_0^a \frac{\partial\varphi}{\partial z}(x,0)\exp(ik_0\mu x)dx. \quad (24)$$

Excluding from (23)–(24) $A(\mu)$, we shall obtain

$$\Phi_0(\mu,0) - \int_0^a \varphi_{j,\varepsilon}(x,0)\exp(ik_0\mu x)dx = \\ = \frac{\Psi(\mu,0)}{\frac{\partial\Psi}{\partial z}(\mu,0)}\left[\frac{\partial\Phi_0}{\partial z}(\mu,0) + \int_0^a \frac{\partial\varphi}{\partial z}(x,0)\exp(ik_0\mu x)dx\right], \quad (25)$$

where

$$\int_0^a \varphi_{j,\varepsilon}(x,0)e^{ik_0\mu x}\,dx = \varphi_{j,\varepsilon}(0)\int_0^a e^{ik_0(\mu-\mu_{j,\varepsilon})x}\,dx = \varphi_{j,\varepsilon}(0)g(\mu).$$

Define the following notation:

$$\begin{aligned} X^+_{j,L}(\mu) &= \int_0^a \frac{\partial\varphi}{\partial z}(x,0)e^{ik_0\mu x}dx + \varphi'_{j,\varepsilon}(0)g(\mu); \\ X^-(\mu) &= \int_\infty^0 \frac{\partial\varphi}{\partial z}(x,0)e^{ik_0\mu x}dx; \\ e^{iL\mu}X^+(\mu) &= \int_a^{+\infty} \frac{\partial\varphi}{\partial z}(x,0)e^{ik_0\mu x}dx. \end{aligned}$$

Taking into account a condition (21), rewrite the equation (25) as follows:

$$(X^-(\mu) + \exp(iL\mu)X^+(\mu))\left(\frac{\Psi(\mu,0)}{\frac{\partial\Psi}{\partial z}(\mu,0)} + \frac{f_0(\mu)}{k_0}\right) + \\ + \frac{\Psi(\mu,0)}{\frac{\partial\Psi}{\partial z}(\mu,0)}\left(X^+_{j,L}(\mu) - \varphi'_{j,\varepsilon}(0)g(\mu)\right) = \\ = -\varphi_{j,\varepsilon}(0)g(\mu) + \varphi'_{j,\varepsilon}(0)\frac{f_0(\mu) - f_0(\mu_{j,\varepsilon})}{k_0}g(\mu) = \\ = \varphi'_{j,\varepsilon}(0)\frac{f_0(\mu)}{k_0}g(\mu) = -\varphi_{j,\varepsilon}(0)\frac{f_0(\mu)}{f_0(\mu_{j,\varepsilon})}g(\mu)$$

or, after transformations,

$$\exp(iL\mu)X^+(\mu) + X^-(\mu) + G(\mu)X^+_{j,L}(\mu) = -\frac{k_0\varphi_{j,\varepsilon}(0)}{f_0(\mu_{j,\varepsilon})}g(\mu), \quad (26)$$

where

$$G(\mu) = \frac{\Psi(\mu,0)}{\Psi(\mu,0) + \frac{f_0(\mu)}{k_0}\cdot\frac{\partial\Psi}{\partial z}(\mu,0)}. \quad (27)$$

Thus, the originalal acoustic problem is reduced to the modified Wiener-Hopf equation (26)–(27). This problem has the symbol $G(\mu)$ with zeroes and poles on a real axis (more precisely, near a real axis, because of the principle of limiting absorption). Really, the definition of μ_s, $\mu_{s,\varepsilon}$ and $\Psi(\mu, z)$ gives us

$$\begin{cases} \Psi(\mu_s, 0) = 0; \\ \Psi(\mu_{s,\varepsilon}, 0) + \dfrac{f_0(\mu_{s,\varepsilon})}{k_0} \cdot \dfrac{\partial \Psi}{\partial z}(\mu_{s,\varepsilon}, 0) = 0, \end{cases} \tag{28}$$

where the first equality (28) represents the dispersion equation of a problem (19), and the second one – of a problem (20). Note also that as far as $f_0(\mu) = O(\varepsilon^3)$, we have $\mu_{s,\varepsilon} - \mu_s = O(\varepsilon^3)$.

Reduce a problem (26)–(27) to a problem with a symbol without singularities on a real axis. To this end represent $G(\mu)$ in the form

$$G(\mu) = \Pi(\mu)(1 + \varepsilon^3 K_\varepsilon(\mu)), \tag{29}$$

where

$$\Pi(\mu) = \prod_{s=1}^{n} \frac{\mu^2 - \mu_s^2}{\mu^2 - \mu_{s,\varepsilon}^2},$$

and the function $K_\varepsilon(\mu)$ has not neither zero nor poles on a real axis.

Defining the notation

$$f_{j,L}(\mu) = \exp(iL(\mu + \mu_{j,\varepsilon})) - 1;$$

$$f_L(\mu, \mu_0) = \frac{\exp(iL\mu) - \exp(iL\mu_0)}{\mu - \mu_0};$$

$$a_{\pm s} = \operatorname{Res}\left(\frac{\Pi^{-1}(\mu)}{\mu + \mu_{j,\varepsilon}}\right)\Big|_{\mu = \pm\mu_s},$$

one can see that

$$\frac{\Pi^{-1}(\mu)}{\mu + \mu_{j,\varepsilon}} = \sum_{s=1}^{n} \left(\frac{a_s}{\mu - \mu_s} + \frac{a_{-s}}{\mu + \mu_s}\right)$$

and

$$G(\mu) = \frac{f_{j,L}(\mu)}{ik_0(\mu + \mu_{j,\varepsilon})}.$$

Multiplying (26) on $\Pi^{-1}(\mu)$ and taking into account the last equality, we shall obtain

$$e^{iL\mu} X^+(\mu)\Pi^{-1}(\mu) + X^-(\mu)\Pi^{-1}(\mu) + (1 + \varepsilon^3 K_\varepsilon(\mu)) X_{j,L}^+(\mu) = \\ = -\frac{\varphi_{j,\varepsilon}(0)}{if_0(\mu_{j,\varepsilon})} f_{j,L}(\mu) \left[\sum_{s=1}^{n} \left(\frac{a_s}{\mu - \mu_s} + \frac{a_{-s}}{\mu + \mu_s}\right)\right]. \tag{30}$$

Let $C_{j,L}(\mu)$ be the right part of (30) and $a_{\pm s,\varepsilon}$ be the expression $-\frac{\varphi_{j,\varepsilon}(0)}{if_0(\mu_{j,\varepsilon})}a_{\pm s}$. Coefficient $C_{j,L}(\mu)$ may be represented in the following form:

$$C_{j,L}(\mu) = \sum_{s=1}^{n} a_{s,\varepsilon}\frac{f_{j,L}(\mu) - f_{j,L}(\mu_s)}{\mu - \mu_s} + \sum_{s=1}^{n} a_{s,\varepsilon}\frac{f_{j,L}(\mu_s)}{\mu - \mu_s} +$$

$$+ \sum_{s=1}^{n} a_{-s,\varepsilon}\frac{e^{iL(\mu+\mu_s)} - 1}{\mu + \mu_s} + e^{iL\mu}\sum_{s=1}^{n} a_{-s,\varepsilon}\frac{e^{iL\mu_{j,\varepsilon}} - e^{iL\mu_s}}{\mu + \mu_s}.$$

Transfer second and fourth terms to the left part (30) and introduce new unknown functions:

$$\begin{cases} \Phi^+(\mu) = X^+(\mu)\Pi^{-1}(\mu) - \sum\limits_{s=1}^{n}\dfrac{x_s}{\mu - \mu_s} - \\ \qquad - \sum\limits_{s=1}^{n}\dfrac{(a_{-s,\varepsilon}f_{j,L}(-\mu_s) - x_{-s})\exp(iL\mu_s)}{\mu + \mu_s}, \\ \Phi^-(\mu) = X^-(\mu)\Pi^{-1}(\mu) - \\ \qquad - \sum\limits_{s=1}^{n}\dfrac{x_{-s}}{\mu + \mu_s} - \sum\limits_{s=1}^{n}\dfrac{a_{s,\varepsilon}f_{j,L}(\mu_s) - x_s\exp(iL\mu_s)}{\mu - \mu_s}, \end{cases} \tag{31}$$

where unknown constants $x_{\pm s}$ depend on ε and are chosen so that the functions $\Phi^{\pm}(\mu)$ have no poles in points $\mu = \pm\mu_s$. In the terms of functions $\Phi^+(\mu)$, $\Phi^-(\mu)$ the equation (30) will be written as:

$$\exp(iL\mu)\Phi^+(\mu) + \Phi^-(\mu) + (1 + \varepsilon^3 K_\varepsilon(\mu))X^+_{j,L}(\mu) =$$
$$= \sum_{s=1}^{n}(a_{s,\varepsilon}e^{iL\mu_{j,\varepsilon}} - x_s)f_L(\mu,\mu_s) + \sum_{s=1}^{n}(a_{-s,\varepsilon} + x_{-s})e^{iL\mu_s}f_L(\mu,-\mu_s) \tag{32}$$

In contrast to the equation (26), the obtained modified Wiener-Hopf equation has a symbol, not containing zeros and poles on a real axis. Solving it, applying the reverse Fourier transformation to $\Phi(\mu, z)$ and taking into account (22), we have:

$$\varphi(x,z) = \frac{k_0}{2\pi}\int_{-\infty}^{\infty} A(\mu)\Psi(\mu,z)\exp(-ik_0\mu x)d\mu.$$

From (23) and (26) we shall find $A(\mu)$:

$$A(\mu) = \frac{(f_0(\mu)/k_0)X^+_{j,L}(\mu)}{\Psi(\mu,0) + (f_0(\mu)/k_0)\frac{\partial\Psi}{\partial z}(\mu,0)}.$$

Let $\Theta(\mu)$ be a denominator of the fraction above, so we have:

$$\varphi(x,z)=\frac{1}{2\pi}\int_{-\infty}^{\infty}\frac{f_0(\mu)X_{j,L}(\mu)\Psi(\mu,z)}{\Theta(\mu)}\exp(-ik_0\mu x)d\mu. \qquad (33)$$

Using a standard technique [9], deform an integration contour into a complex plane. Taking into account residues in points $\mu=-\mu_{s,\varepsilon}$ and the fact that $\Psi(\mu_{s,\varepsilon},z)=\varphi_{s,\varepsilon}(z)$, neglecting the integrals decreasing at $|x|\to\infty$, we shall obtain the following representation of a field outside of an interval $(0,a)$ as a sum of guided normal modes:

$$\varphi(x,z)\approx\begin{cases} i\sum\limits_{s=1}^{n}\frac{f_0(\mu_{s,\varepsilon})X_{j,L}(\mu_{s,\varepsilon})}{\Theta_\mu(\mu_{s,\varepsilon})}\varphi_{j,\varepsilon}(z)e^{-ik_0\mu_{s,\varepsilon}x}, x<0; \\ i\sum\limits_{s=1}^{n}\frac{f_0(-\mu_{s,\varepsilon})X_{j,L}(-\mu_{s,\varepsilon})}{\Theta_\mu(\mu_{s,\varepsilon})}\varphi_{j,\varepsilon}(z)e^{ik_0\mu_{s,\varepsilon}x}, x>a. \end{cases} \qquad (34)$$

Similarly one can obtain the representation of a field at $x\in(0,a)$. Note that the given method allows also to obtain formulas for integral terms (lateral waves).

Let

$$\begin{cases} A_{tr}=\left\{\frac{if_0(\mu_{s,\varepsilon})X_{j,L}(-\mu_{l,\varepsilon})}{\Theta_\mu(\mu_{l,\varepsilon})}+\delta_{l,j}\right\}_{l,j=1}^{n}; \\ A_{ref}=\left\{\frac{if_0(-\mu_{s,\varepsilon})X_{j,L}(\mu_{l,\varepsilon})}{\Theta_\mu(\mu_{l,\varepsilon})}\right\}_{l,j=1}^{n}, \end{cases} \qquad (35)$$

be the transmission and reflection matrices accordingly, where $\delta_{l,j}$ is the Kronecker symbol.

Below we shall find the asymptotics of coefficients of matrices A_{tr} and A_{ref} at $\varepsilon\to 0$. For this purpose we need a number of auxiliary asymptotic formulas.

a) An asymptotics of $\mu_{s,\varepsilon}$.

Taking into account (8), (28), one can easy to obtain an asymptotics of $\mu_{s,\varepsilon}$:

$$\mu_{s,\varepsilon}=\mu_s+c_{1,s}\varepsilon^3+c_{2,s}\varepsilon^4+c_{3,s}\varepsilon^5+c_{4,s}\varepsilon^6+O(\varepsilon^7), \qquad (36)$$

where

$$\begin{cases} c_{1,s}=-\frac{L_1(\mu_s)}{k_0}\cdot\frac{\Psi_z(\mu_s,0)}{\Psi_\mu(\mu_s,0)}; \\ c_{2,s}\equiv 0; \\ c_{3,s}=-\frac{L_2(\mu_s)}{k_0}\cdot\frac{\Psi_z(\mu_s,0)}{\Psi_\mu(\mu_s,0)}; \\ c_{4,s}=-\frac{c_{1,s}}{\Psi_\mu(\mu_s,0)}\left[\Psi_{\mu\mu}(\mu_s,0)\frac{c_{1,s}}{2}+\right. \\ \qquad \left.\frac{L_1'(\mu_s)}{k_0}\Psi_z(\mu_s,0)+\frac{L_1(\mu_s)}{k_0}\Psi_{z\mu}(\mu_s,0)\right], \end{cases} \qquad (37)$$

$L_1(\mu)$ and $L_2(\mu)$ are the coefficients of asymptotics

$$F_0(\mu) = L_1(\mu)\varepsilon^3 + L_2(\mu)\varepsilon^5 + O(\varepsilon^7),$$

taking place in accord with (8) and oddity of f_0 on ε.

b) An asymptotics of $a_{\pm s}$.

By definition $a_{\pm s} = \operatorname{Res}\left(\frac{\Pi^{-1}(\mu)}{\mu+\mu_{j,\varepsilon}}\right)\Big|_{\mu=\pm\mu_s}$, and from (36) one can deduce the following asymptotic formulas:

$$\begin{cases} a_{-j} = 1 + \left(\frac{c_{1,j}}{2\mu_j} - 2\sum\limits_{s=1,s\neq j}^{n} \frac{c_{1,s}\mu_s}{\mu_j^2-\mu_s^2}\right)\varepsilon^3 + O(\varepsilon^5); \\ a_l = -\frac{c_{1,l}\varepsilon^3}{\mu_l+\mu_j} + O(\varepsilon^5); \qquad 1 \le l \le n; \\ a_{-l} = -\frac{c_{1,l}\varepsilon^3}{\mu_l-\mu_j} + O(\varepsilon^5); \qquad l \neq j, \quad 1 \le l \le n. \end{cases} \tag{38}$$

c) An asymptotics of $x_{\pm s}$.

Let $\Phi_s^{\pm}(\mu)$ and $\Phi_{-s}^{\pm}(\mu)$ be plus and minus components of the solution of (32) with the right part $f_L(\mu,\mu_s)$ and $\exp(iL\mu_s)f_L(\mu,-\mu_s)$ accordingly, and $\Phi_0^{\pm}(\mu)$ be plus and minus components of the solution of (32) with the right part

$$\sum_{s=1}^{n} a_{s,\varepsilon}e^{iL\mu_{j,\varepsilon}}f_L(\mu,\mu_s) + \sum_{s=1}^{n} a_{-s,\varepsilon}e^{iL\mu_s}f_L(\mu,-\mu_s).$$

From (31) one can obtain formulas for $X^+(\mu)$ and $X^-(\mu)$:

$$\begin{cases} X^+(\mu) = \Pi(\mu)\left[-\sum\limits_{s=1}^{n} x_s\Phi_s^+(\mu) + \sum\limits_{s=1}^{n} x_{-s}\Phi_{-s}^+(\mu) + \Phi_0^+(\mu) + \right. \\ \qquad \left. + \sum\limits_{s=1}^{n} \frac{x_s}{\mu-\mu_s} + \sum\limits_{s=1}^{n} \frac{(a_{-s,\varepsilon}f_{j,L}(-\mu_s)-x_{-s})e^{iL\mu_s}}{\mu+\mu_s}\right]; \\ X^-(\mu) = \Pi(\mu)\left[-\sum\limits_{s=1}^{n} x_s\Phi_s^-(\mu) + \sum\limits_{s=1}^{n} x_{-s}\Phi_{-s}^-(\mu) + \Phi_0^-(\mu) + \right. \\ \qquad \left. + \sum\limits_{s=1}^{n} \frac{x_{-s}}{\mu+\mu_s} + \sum\limits_{s=1}^{n} \frac{a_{s,\varepsilon}f_{j,L}(\mu_s)-x_s e^{iL\mu_s}}{\mu-\mu_s}\right]. \end{cases} \tag{39}$$

Taking into account that these functions can't have poles in points $\mu_{l,\varepsilon}$ and $-\mu_{l,\varepsilon}$ accordingly, we shall obtain the system of linear equations of $2n \times 2n$ order for the determination of the numbers x_s

and x_{-s}:

$$\begin{cases} \sum\limits_{s=1}^{n} x_s \left(-\frac{1}{\mu_{l,\varepsilon}-\mu_s}+\Phi_s^+(\mu_{l,\varepsilon})\right)+\sum\limits_{s=1}^{n} x_{-s}\left(\frac{\exp(iL\mu_s)}{\mu_{l,\varepsilon}+\mu_s}-\Phi_{-s}^+(\mu_{l,\varepsilon})\right)= \\ =\Phi_0^+(\mu_{l,\varepsilon})+\sum\limits_{s=1}^{n} a_{-s,\varepsilon}\frac{f_{j,L}(-\mu_s)\exp(iL\mu_s)}{\mu_{l,\varepsilon}+\mu_s}; \qquad 1\le l\le n; \\ \sum\limits_{s=1}^{n} x_s\left(-\frac{\exp(iL\mu_s)}{\mu_{l,\varepsilon}+\mu_s}+\Phi_s^-(-\mu_{l,\varepsilon})\right)+\sum\limits_{s=1}^{n} x_{-s}\left(\frac{1}{\mu_{l,\varepsilon}-\mu_s}-\Phi_{-s}^-(-\mu_{l,\varepsilon})\right)= \\ =\Phi_0^-(-\mu_{l,\varepsilon})-\sum\limits_{s=1}^{n} a_{s,\varepsilon}\frac{f_{j,L}(\mu_s)}{\mu_{l,\varepsilon}+\mu_s}; \qquad 1\le l\le n. \end{cases} \tag{40}$$

In [5]–[7] in a case of symbol $G(\mu)$ growing at infinity the uniform on L asymptotic estimates were obtained for the soluion of a problem (32):

$$|\Phi_{\pm s}^{\pm}(\mu)|\le c\cdot\varepsilon^3\ln\varepsilon^{-1}.$$

In the present work the function $G(\mu)$, defined by (27), is bounded at $\mu\to\infty$. Therefore it is possible to show that

$$\begin{cases} |\Phi_{\pm s}^{\pm}(\pm\mu_{l,\varepsilon})|\le c\cdot\varepsilon^3, \\ |\Phi_0^{\pm}(\pm\mu_{l,\varepsilon})|\le c\cdot\varepsilon^3, \end{cases} \tag{41}$$

where the constant c does not depend on L.

From (41) and (36) one can obtain that the system (40) has a prevailling main diagonal. Therefore an asymptotics of its solution looks like:

$$\begin{cases} X_l=c_{1,l}\varepsilon^3\dfrac{\varphi_{j,\varepsilon}(0)}{if_0(\mu_{j,\varepsilon})}\cdot\dfrac{\exp(iL\mu_{j,\varepsilon})-\exp(iL\mu_j)}{\mu_l+\mu_j}+O(\varepsilon^5); \\ X_{-l}=O(\varepsilon^5). \end{cases} \tag{42}$$

d) An asymptotics of $\varphi_{j,\varepsilon}(0)$.

$$\varphi_{j,\varepsilon}(0)=\Psi_\mu(\mu_j,0)c_{1,j}\varepsilon^3\left[1+\frac{c_{3,j}}{c_{1,j}}\varepsilon^2+\frac{c_{4,j}}{c_{1,j}}\varepsilon^3+\frac{\Psi_{\mu\mu}(\mu_j,0)}{\Psi_\mu(\mu_j,0)}\frac{c_{1,j}\varepsilon^3}{2}\right]+O(\varepsilon^7). \tag{43}$$

e) An asymptotics of $\Theta_\mu(\mu_{j,\delta})$.

$$\Theta_\mu(\mu_{j,\varepsilon})=\Psi_\mu(\mu_j,0)\left(1+\left(\frac{c_{1,j}}{2}\cdot\frac{\Psi_{\mu\mu}(\mu_j,0)}{\Psi_\mu(\mu_j,0)}-\frac{c_{4,j}}{c_{1,j}}\right)\right)\varepsilon^3+O(\varepsilon^5). \tag{44}$$

Pass now directly to the solving of (32). Let $H_{j,L}(\mu)$ be the right part of (32). Formally applying a perturbation method and taking into account that $H_{j,L}(\mu)$ is the Fourier transformation of function with support on $[0, a]$, we have:

$$\begin{cases} X^+_{j,L}(\mu) = H_{j,L}(\mu) + O(\varepsilon^3); \\ \Phi^+(\mu), \Phi^-(\mu) = O(\varepsilon^3). \end{cases} \tag{45}$$

However, the equalities (45) are not uniform on L because the function $H_{j,L}(\mu)$ at $L \to \infty$ tends to infinity in points $\mu = \mu_{\pm s}$.

Now consider an auxiliary problem:

$$e^{iL\mu}\Phi^+(\mu) + (1 + \varepsilon^3 K_\varepsilon(\mu))X^+_L(\mu) + \Phi^-(\mu) = f_L(\mu, \mu_0), \quad \mu_0 \in \mathbf{R}. \tag{46}$$

To achieve uniformity of the main asymptotic term of the solution (46) on $L \gg 1$, we shall find it as follows:

$$\Phi^\pm_0(\mu) \equiv 0, \quad X^+_{L,0}(\mu) = d_\varepsilon f_L(\mu, \mu_0).$$

Then we have the following problem for a difference of asymptotic and exact solutions:

$$\exp(iL\mu)(\Phi^+(\mu) - \Phi^+_0)(\mu) + (\Phi^-(\mu) - \Phi^-_0(\mu)) + (1 + \varepsilon^3 K_\varepsilon(\mu)) \times \\ \times (X^+_L(\mu) - X^+_{L,0}(\mu)) = f_L(\mu, \mu_0)[(1 + \varepsilon^3 K_\varepsilon(\mu))d_\varepsilon - 1]. \tag{47}$$

Choose d_ε so that the expression in square brackets in the right part of the equation above vanished at $\mu = \mu_0$:

$$d_\varepsilon = \frac{1}{1 + \varepsilon^3 K_\varepsilon(\mu_0)}.$$

Taking into account the boundness of $K_\varepsilon(\mu)$, one can easily show that in this case the norm of the right part of (47) is bounded in $L_2(\mathbf{R})$ by $c \cdot \varepsilon^3$, where the constant $c > 0$ is independent from L and ε.

Thus, the principal asymptotic term of the solution component $X^+_{j,L}$ looks like

$$X^+_{j,L}(\mu) \approx \sum_{s=1}^{n} d_{s,\varepsilon}(a_{s,\varepsilon} \exp(iL\mu_{j,\varepsilon}) - x_s) f_L(\mu, \mu_s) + \\ + \sum_{s=1}^{n} d_{-s,\varepsilon}(a_{-s,\varepsilon} + x_{-s}) \exp(iL\mu_s) f_L(\mu, -\mu_s) \tag{48}$$

where $d_{\pm s,\varepsilon} = 1/(1 + \varepsilon^3 K_\varepsilon(\mu_s))$ (note that $d_{-s,\varepsilon} = d_{s,\varepsilon}$) and asymptotic formulas (48) are uniform on $L \gg 1$.

f) An asymptotics of $d_{s,\varepsilon}$.

It is obvious that $d_{s,\varepsilon} \sim 1$, $s = 1, \ldots, n$. The coefficient $d_{j,\varepsilon}$ requires more exact representation.

$$d_{j,\varepsilon} = (1 + \varepsilon^3 K_\varepsilon(\mu_j))^{-1} = (\Pi^{-1}(\mu)G(\mu))^{-1}\big|_{\mu=\mu_j};$$

$$d_{j,\varepsilon} = 1 + \varepsilon^3 \left[2 \sum_{s=1, s\neq j}^{n} \frac{c_{1,s}\mu_s}{\mu_j^2 - \mu_s^2} - \frac{c_{4,j}}{c_{1,j}} - \frac{c_{1,j}}{2\mu_j} \right] + O(\varepsilon^4). \qquad (49)$$

Find an asymptotics of $X^+_{j,L}(-\mu_{j,\varepsilon})$:

$$X^+_{j,L}(-\mu_{j,\varepsilon}) \approx \sum_{s=1}^{n} d_{s,\varepsilon}(a_{s,\varepsilon} \exp(iL\mu_{j,\varepsilon}) - x_s) f_L(-\mu_{j,\varepsilon}, \mu_s) +$$

$$+ \sum_{s=1}^{n} d_{s,\varepsilon}(a_{-s,\varepsilon} + x_{-s}) \exp(iL\mu_s) f_L(-\mu_{j,\varepsilon}, -\mu_s)$$

Taking into account (37), (38), (39), (42), (43) and (49), we shall obtain

$$\begin{aligned} X^+_{j,L}(-\mu_{j,\varepsilon}) &\approx d_{j,\varepsilon} a_{-j,\varepsilon} \exp(iL\mu_j) f_L(-\mu_{j,\varepsilon}, -\mu_j) \approx \\ &\approx \left(1 + \varepsilon^3 \left[2 \sum_{s=1, s\neq j}^{n} \frac{c_{1,s}\mu_s}{\mu_j^2 - \mu_s^2} - \frac{c_{4,j}}{c_{1,j}} - \frac{c_{1,j}}{2\mu_j} \right] \right) \times \\ &\times \left(1 + \varepsilon^3 \left[\frac{c_{1,j}}{2\mu_j} - 2 \sum_{s=1, s\neq j}^{n} \frac{c_{1,s}\mu_s}{\mu_j^2 - \mu_s^2} \right] \right) \times \\ &\times \left(-\frac{\varphi_{j,\varepsilon}(0)}{i f_0(\mu_{j,\varepsilon})} \right) \exp(iL\mu_j) \frac{\exp(-iL\mu_{j,\varepsilon}) - \exp(-iL\mu_j)}{\mu_j - \mu_{j,\varepsilon}} \approx \\ &\approx \frac{\Psi_\mu(\mu_j, 0)}{i f_0(\mu_{j,\varepsilon})} \left[1 - \frac{c_{4,j}}{c_{1,j}} \varepsilon^3 + \frac{\Psi_{\mu\mu}(\mu_j, 0)}{\Psi_\mu(\mu_j, 0)} \cdot \frac{c_{1,j}\varepsilon^3}{2} \right] [e^{iL(\mu_j - \mu_{j,\varepsilon})} - 1]. \end{aligned}$$

Taking into account (44), find now the asymptotics of $[A_{tr}]_{j,j}$:

$$[A_{tr}]_{j,j} = \frac{i f_0(\mu_{j,\varepsilon}) X^+_{j,L}(-\mu_{j,\varepsilon})}{\Theta_\mu(\mu_{j,\varepsilon})} + 1 \approx$$

$$\approx \frac{f_0(\mu_{j,\varepsilon})}{f_0(\mu_{j,\varepsilon})} \cdot \frac{\Psi_\mu(\mu_j, 0) \left[1 + \frac{\Psi_{\mu\mu}(\mu_j,0)}{\Psi_\mu(\mu_j,0)} \cdot \frac{c_{1,j}\varepsilon^3}{2} - \frac{c_{4,j}}{c_{1,j}} \varepsilon^3 \right]}{\Psi_\mu(\mu_j, 0) \left[1 + \frac{\Psi_{\mu\mu}(\mu_j,0)}{\Psi_\mu(\mu_j,0)} \cdot \frac{c_{1,j}\varepsilon^3}{2} - \frac{c_{4,j}}{c_{1,j}} \varepsilon^3 \right]} \times$$

$$\times[\exp(iL(\mu_j - \mu_{j,\varepsilon})) - 1] + 1 \approx \exp(iL(\mu_j - \mu_{j,\varepsilon})).$$

Thus, we have:

$$[A_{tr}]_{j,j} = \exp(iL(\mu_j - \mu_{j,\varepsilon})) + o(\varepsilon^3). \tag{50}$$

The main terms of asymptotics of $[A_{tr}]_{j,l}$, $l \neq j$, and $[A_{ref}]_{j,l}$ have been obtained similarly:

$$[A_{tr}]_{j,l} \approx -\varepsilon^3 \frac{\Psi_z(\mu_j, 0)}{k_0 \Psi_\mu(\mu_l, 0)} \cdot \frac{L_1(\mu_l) e^{-iL\mu_{l,\varepsilon}}}{\mu_l - \mu_j} \left[e^{iL\mu_l} - e^{iL\mu_j}\right], l \neq j; \tag{51}$$

$$[A_{ref}]_{j,l} \approx -\varepsilon^3 \frac{\Psi_z(\mu_j, 0)}{k_0 \Psi_\mu(\mu_l, 0)} \cdot \frac{L_1(\mu_l)}{\mu_l + \mu_j} \left[e^{iL(\mu_j + \mu_l)} - 1\right]. \tag{52}$$

Note that the formulas (50) – (52) are uniform on parameter $L \gg 1$. Pay attention also to the fact that the term of ε^3 order is absent in (50) (as far as in the case of a constant impedance $f_0(\mu) = \text{const}$ of works [5] - [7]). The exact analysis based on the formulas (41) shows that in (50) $o(\varepsilon^3) = O(\varepsilon^5)$.

Remark 0.1 *The problem with ice-floe of finite width* a *laying on a water surface can be solved in the same way. Making the similar calculations, it is easy to obtain that in the final formulas for coefficients of transmission and reflection matrices* μ_j *and* $\mu_{j,\varepsilon}$ *changes places. So, for diagonal terms of a transmission matrix we have*

$$[A_{tr}]_{j,j} = \exp(iL(\mu_{j,\varepsilon} - \mu_j)) + o(\varepsilon^3). \tag{53}$$

Remark 0.2 *If the system of several polynias with widths* $a_1, \ldots, a_m$ $(m > 1)$ *is considered, the transmission and reflection matrices for the whole system are obviously the same as the product of transmission and reflection matrices of each polynia separately. Hence, the diagonal elements of a transmission matrix for system with* m *polynias looks like:*

$$[A_{tr}^{(m)}]_{j,j} \approx \exp\left(ik_0 \sum_{s=1}^{n} a_s(\mu_j - \mu_{j,\varepsilon})\right). \tag{54}$$

Apparently the given formula is uniform on m *and* $L = k_0 \sum_{s=1}^{m} a_s$ *that makes its attractive for use in a considered problem.*

The similar formula takes place for system of m *ice-floes.*

3. THE ANALYSIS OF COEFFICIENTS OF TRANSMISSION AND REFLECTION MATRICES

As follows from (50), the elements of reflection matrix and also non–diagonal elements of transmission matrix have the order $O(\varepsilon^3)$. The diagonal elements of $[A_{tr}]_{j,j}$ have the order $O(1)$ and

$$\begin{cases} [A_{tr}]_{j,j} \approx 1 \quad \text{if} \quad \left| L - \frac{2\pi s}{|\mu_j - \mu_{j,\epsilon}|} \right| \varepsilon^3 \ll 1, s \in \mathbf{N}; \\ [A_{tr}]_{j,j} \approx -1 \quad \text{if} \quad \left| L - \frac{\pi(2s-1)}{|\mu_j - \mu_{j,\epsilon}|} \right| \varepsilon^3 \ll 1, s \in \mathbf{N}. \end{cases} \tag{55}$$

Thus, in the first case (particularly at $L\varepsilon^3 \ll 1$) the influence of the polynia to a transmitted field is negligible, in second one (particularly at $L \approx \pi/|\mu_j - \mu_{j,\epsilon}|$) it is maximal.

To obtain quantitative estimates we spent the numerical research of relation between the first "critical" size of the polynia $a_1^j = \frac{\lambda}{2|\mu_j - \mu_{j,\epsilon}|}$, when $[A_{tr}]_{j,j} \approx -1$, from frequency and thickness of ice (here λ is a wave length). Model of "liquid homogeneous layer on liquid homogeneous half-space" with parameters $H = 200\ m$, $c_{liq} = 1500\ mps$, $\varrho_0 = 1\ g/sm^3$, $\varrho_{bot} = 1.4\ g/cm^3$, $c_{bot} = 2000\ mps$, $c_1 = 3500\ mps$, $c_2 = 1800\ mps$, $\varrho_{ice} = 0.9\ g/cm^3$ was considered. The calculations were realised by means of the program developed by authors of [8] for the solution of dispersial equation of stratified model mentioned above.

The results of calculations at thickness of ice $d = 10\ m$ are illustrated on fig. 2.

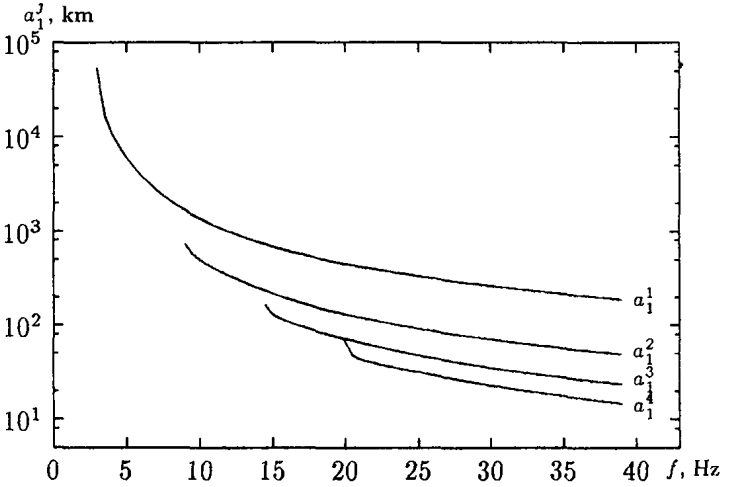

Fig. 2. Dependence of the first polynia "critical" size from frequency for various modes.

The calculations show that in the shallow sea ($H = 200\ m$) the first "critical" length of the polynia a_1^j is great (at frequency 40 Hz it equals $\sim 15 - 200\ kms$ depending on mode number) and with increase of number j of surging mode a_1^j is decreased.

4. INFLUENCE OF ABSORPTION IN ICE ON AN ACOUSTIC FIELD

The following group of calculations is devoted to investigation the influence of absorption in ice on attenuation of an acoustic field. The absorption in ice is taken into account as the small image additives $i\delta_1$ and $i\delta_2$ to n_1 and n_2 accordingly ($\delta_1 > 0$, $\delta_2 > 0$). For quantitative estimates the waveguide with the parameters same as in the previous section was chosen, with point monochromatic source located on depth 100 m. As a measure of attenuation of sound pressure on distance R from a source we consider the difference of average values of fields (taken in Db) without the polynia (p_{av}) and with it (p_{av}^{pol}), averaged by the rectangle $0 \le z \le H$, $R - r \le x \le R + r$ ($r \sim 2 - 5$ km, $R > a$).

In calculation shown on fig. 3 the length of polynia varies from 1000 up to 5000 km; the frequency f of a point source equals 11 Hz (two-moded waveguide), thickness of ice $d = 10\ m$ and distance $R = 5100\ km$. The specific position of the polynia between a source and receiver does not play a role. Here one can see a few calculations with various δ_1 and δ_2 satisfying the equality $\delta_1^2 + \delta_2^2 = 0.05^2$.

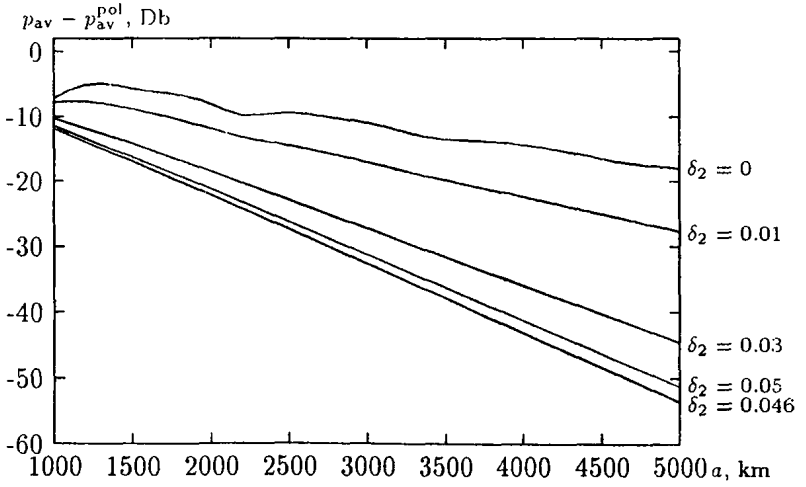

Fig. 3. Dependence of field attenuation from ice-floe length.

In calculation shown on fig. 4 frequency varies; thickness of ice $d = 10\ m$, distance $R = 1100\ km$; coeffitients of absorption $\delta_1 = 0.02$, $\delta_2 = 0.046$ satisfy the equality $\delta_1^2 + \delta_2^2 = 0.05^2$ and the attenuation is maximum (bottom diagram). For comparison similar calculation (top diagram) at absence of absorption in ice ($\delta_1 = \delta_2 = 0$) is given.

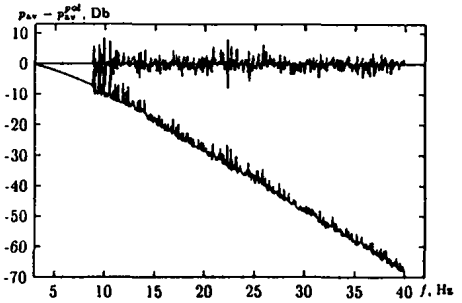

Fig. 4. Dependence of attenuation of a field from frequency.

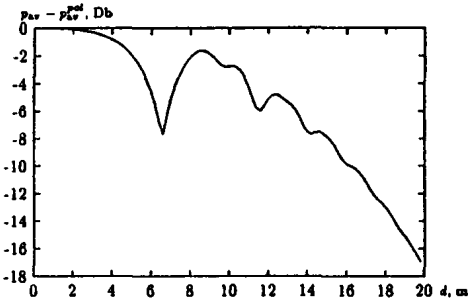

Fig. 5. Dependence of field attenuation from ice thickness. $\delta_2 = 0.01$.

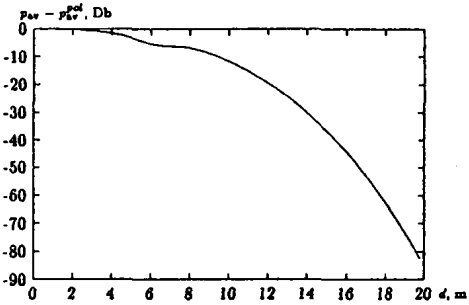

Fig. 6. Dependence of field attenuation from ice thickness. $\delta_2 = 0.05$.

Here the conversion from one–mode to two–mode waveguide ($f \sim 8.5\ Hz$) is clearly seen. After this convertion both curves begin to oscillate with amplitude $\sim 3 - 8\ Db$, and the bottom curve decreases with an average gradient $\sim 2\ Db$ on $1\ Hz$.

At last, in calculations shown on figures 5 and 6. thickness of ice varies; the other parameters are the following: $R = 1100\ km$, $f = 11\ Hz$ (two-mode waveguide), $\delta_1 = 0$. The calculations differ only by value of δ_2.

As we can see from the diagrams, difference of fields with and without polinia decreases with growth of ice thickness and absorption in ice. The increase of ice thickness also causes the oscillations on the diagrams with amplitude $\sim 4 - 8\ Db$, which become the more imperceptible, the greater is absorption in an ice layer.

This study was supported by RFFI, Grant N 95-01-01285a.

References

[1] *Bogorodskii V.V., Gavrilo V.P.* Ice. Physical properties. Modern methods of gliaciologia. M., Gidrometeoizdat, 1980.

[2] *Nobl B.* The Wiener-Hopf method. London-New York-Paris-Los Angeles, Pergamon Press, 1958.

[3] *Vorovich I.I., Babeshko V.A.* Dynamic mixed problems of the theory of elasticity for some non-classic areas. M., Nauka, 1976.

[4] *Babeshko V.A.* A method of generalized factirization. M., Nauka, 1984.

[5] *Grudskii S.M.* The equation of convolution on a finite interval with small parameter at a growing part of a symbol. DAN SSSR, 1989, Vol.309, N 5, p.1040–1043.

[6] *Grudskii S.M.* The equation of convolution on a finite interval with small parameter at a growing part of a symbol. Izv. VUZov, Mathematica, 1990, N 7, p.7–17.

[7] *Grudskii S.M., Doctorskaya L.D.* On one asymptotic method of the solution of convolution equation on a finite interval. In: Differential, integral equations and complex analysis. Elista, 1993, p.10–24.

[8] *Kovalev A.N., Rivelis E.A., Edelstein S.L.* Influence of parameters of hydroacoustic waveguide on the attenuation coefficients of modes. Akusticheskii zhurnal, 1987, Vol.33, N 1, p.132–134.

[9] *Brehovskih L.M.* Waves in layered fluids. M., Nauka, 1973.

[10] *Isakovich M.A.* General acoustics. M., Nauka, 1973.

DIFFRACTION OF ACOUSTIC WAVES BY SPATIALLY-LOCALIZED INHOMOGENEITIES IN HORIZONTALLY-INHOMOGENEOUS SHALLOW WATER OCEANIC WAVEGUIDES

A.I. Belov and A.I. Khil'ko

INTRODUCTION

Various kinds of spatially-localized and randomly distributed inhomogeneities situated in shallow water oceanic waveguides can be interesting as the objects for acoustical tomography reconstruction [1,2].

Very often the direct illuminating signal mask in essential degree the acoustical signal diffracted by inhomogeneities basically at small angles [3-5]. Efficiency of scattering signal resolutiuon can be associated with both the features of forming of multi mode acoustical field in complex structure shallow water waveguide [5-7] and the coherence of diffracted acoustical signals [8,9]. In particular, in a number of papers [1-4,10,11] the possibilities of filtering by means of mode shadow zones (formed by the use both the vertically distributed receiving and radiated array and pulse signals) were considered. In [2,5,12] the opportunities of use of natural mode shadow zones for measuring of diffracted acoustical signals were mentioned, where the observation region can be located in shadow zone in relation to direct illuminating acoustical field. It was supposed in this case, that inhomogeneities cause of the illumination of natural shadow zones. The possibilities of an additive elimination of direct illuminating field were analyzed [5,13] in the scheme, where the diffracted field was measured in mode shadow zones which were formed in shelf regions of shallow water waveguides. In this case, it is possible to speak about "megaphone" effect. A combination of the "megaphone" structure of a waveguide bottom profile and the characteristic sound velocity profile in the shallow sea form the depth-dependent distribution of intensity of illuminating acoustical field. The shadow zones arize under the surface or near the bottom, if the acoustical source is located in shallow area of shelf [5]. Researches of opportunities for diffracted acoustical fields measurements can be associated with the availability of megaphone's effect for tomographical reconstruction of the inhomogeneities characteristics, located in narrow oceanic straits, where the tomographical monitoring, for example, "of hydrophysical weather" can be especially urgent. In this connection, there is the requirement in more detailed research of features of diffraction of acoustical waves in shallow water oceanic waveguides with significant

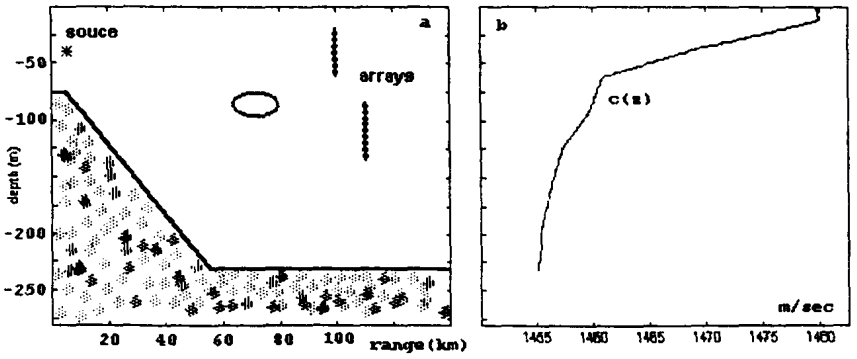

Fig. 1. Geometry of problem and structure of shallow water waveguide ($z_0 = 10\ m$) (a) and sound speed profile (b).

horizontal variability of depth. Such investigation can be useful for estimation of the formed shadow zone depths, as well as of the degree of theirs illumination by diffracted signals for various waveguide parameters, location of scatterers and observation regions.

According to this, the purpose of the present research is the study of structure of natural shadow zones, in particular, the efficiency of illumination of such zones, formed in shallow water waveguides with megaphone form, due to diffraction of acoustical waves by spatially-localized inhomogeneities taking into account the optimization of measuring scheme for tomographical monitoring in shallow water straits.

1. MEGAPHONE ILLUMINATION IN SHELF ZONE OF SHALLOW WATER WAVEGUIDE

As it is known [13], in relatively deep-water parts of shelf regions the localized by depth field is formed, if a source is situated in shallow water region (fig. 1). Physically, the structure of the bottom reminds the megaphone. Combination with refractive hydroacoustic waveguides can cause the localization of the acoustical field with depth. In shallow water regions the under - surface or near - bottom waveguides are observed very often (fig. 1) with the structure depending on seasonal conditions. As measurements show, because of an influence of seasonal conditions an acoustic field can be much more weak at under surface or near bottom parts of the waveguide.

Let us estimate the depth of these shadow zones and also other features of illumination field structure for the case, when the shelf bottom structure is simulated by the law, shown on fig. 1a, and for typical under - surface or near - bottom waveguide dependencies

of a sound velocity vs depth (fig. 1b). We shall consider bottom consisting from absorbing liquid layer of deposits and elastic half-space with absorption.

We shall formulate the problem of field calculation for submitted above model of shallow water waveguide non-uniform in horizontal domain as follows: the water layer by thickness $h_0(z)$, where $r = \{x, y = 0\}$, z - the waveguide depth, $c(z,r)$ two-dimensional distribution of sound speed, and ρ_0 density, – is situated on the system of m liquid layers with given acoustical parameters: $h_l(r)$,$\rho_l(z,r)$ and $c_l(z,r), l = 1,\ldots m$, where h_l – thickness of a l-th layer. The system of layers is placed on the elastic half-space with $\rho_L(r)$, $c_L(r)$ $c_T(r)$.

We shall look a field in water layer in an adiabatic approach by the use of cross sections method [14]:

$$p(z,r) = \sqrt{\frac{2\pi}{r}}\, e^{i\frac{\pi}{4}} \sum_{n=1}^{N} \varphi_n(z_0,0)\,\varphi_n(z,r) \exp\left[i\int_0^r æ_n(\tau)\,d\tau\right] æ_n^{-\frac{1}{2}}(r), \tag{1}$$

where $æ_n(r)$ and $\varphi_n(z,r)$, accordingly, eigenfunctions and normalized eigennumbers of a following boundary problem:

$$\begin{cases} \varphi''_{zz}(z,r) + \left[K^2(z,r) - æ^2(r)\right]\varphi(z,r) = 0, \\ \varphi(0) = \left[\varphi'_z(z,r) + g(æ)\,\varphi(z,r)\right]\Big|_{z=H(r)} = 0, \end{cases} \tag{2}$$

$K(z,r) = \frac{\omega}{c(z,r)}$, $H(r) = \sum_{i=0}^{m} h_i(r)$, $g(æ) = \frac{\rho_m}{\rho_L}\left[æ^2(r) - K_L^2(r)\right]^{1/2}$.

The solution of the problem can be found separating of the waveguide into the set of layers, in which $K^2(z,r)$ can be approximated as

$$K_p^2(z,r) = K^2(z_p,r) + \alpha_p(r)\left[z - z_p(r)\right],$$

where $z_p(r)$– border between layers $p-1$ and p. In layer the solution of the system (2) can be presented as

$$\varphi_p(z,r) = a_p(r)\,Ai(t) + b_p(r)\,Bi(t),$$

where Ai and Bi - Airy-function [14], $t = -\alpha_p^{-\frac{2}{3}}(r)\left[K_p^2(z,r) - æ^2(r)\right]$. Factors $a_p(r)$ and $b_p(r)$ are derived from the discontinuity condition of $\rho\varphi(z,r)$ and $\varphi_z(z,r)$ recalculating the layers from the top using boundary conditions. The solution $\varphi_n(z,r)$, satisfying to bottom boundary condition, is normalized by value

$$N = \left[\int_0^\infty \rho\varphi^2(z,r)\,dz\right]^{1/2}.$$

Final solution functions $æ_n(r)$ and $\varphi_n(z,r)$ can be presented as the linear interpolation in given waveguide sections.

The account of sediment layers and elastic half-space attenuation is important for estimation of the shadow zones illumination efficiency. In this case it is necessary to consider, that $K(z,r) = \frac{\omega}{c(z,r)} + i\beta(z,r)$. An image part of eigennumbers $\mu_n(r)$ can be calculated by the perturbation method [15,16]:

$$\mu_n(r) = æ_n^{-1}(r) \int_0^\infty \rho\beta(z,r) \frac{\omega}{c(z,r)} \varphi_n^2(z,r)\, dz \ , \qquad (3)$$

where $\mu_n(r)$ is taken into account only in the exponential factor, which basically determins losses of the acoustical field. We shall consider the simplified numerical model, accounting generally the typical conditions, observed in shallow water shelf zones. Let parameters of model, submitted on fig. 1a,b accept the following significances: $h_1 = 50$ m, is the layer of sediment with following parameters: $\{\rho_1, c_1\}$ from $\{1.5; (1456.8 + i*0.028)\}$ to $\{2; (1600 + i*0.049)\}$ respectively and elastic bottom with $\rho_L = 2.2$, $c_L = (2300 + i*0.03)$ and $c_T = (450 + i*0.049)$.

We research space distribution of acoustical field intensity in the case, when the acoustical source with frequencies $f = 100$ and 500 Hz is located in shallow water region of shelf waveguide on the depth $z_i = 10$ m, in condition of near bottom waveguide. The structure of a field intensity is shown on fig. 2,3. It can be seen, that in both cases it is possible to note formation of a deep shadow zone in under water part of waveguide. The depth of a shadow zone is in limits $50 \div 80$ dB on depths up to 20 m. Formation of such weak illuminated area arises due to effective excitation of near bottom waveguide by megaphone part of waveguide. In high frequency region the indicated effect is expressed brighter due to greater localization of waveguide modes more close to the axis of the refractive near bottom channel. Marked field distribution by depth, in principle, permits to judge about potential possibilities for tomographical monitoring of oceanic inhomogeneities in the shelf zone. In respect to a weak illumination in under surface area the tomographical reconstruction of surface inhomogeneities practically will be impossible. In the other hand, the near bottom inhomogeneitieslocated will be well illuminated. For under surface propagation the situation will be contrary.

Except of the shadow zone forming, the another important effect can be noted - the beam forming as the kind of narrow quasi - periodical space structure, which is characterized by increased intensity appropriate to areas the illumination field. The indicated

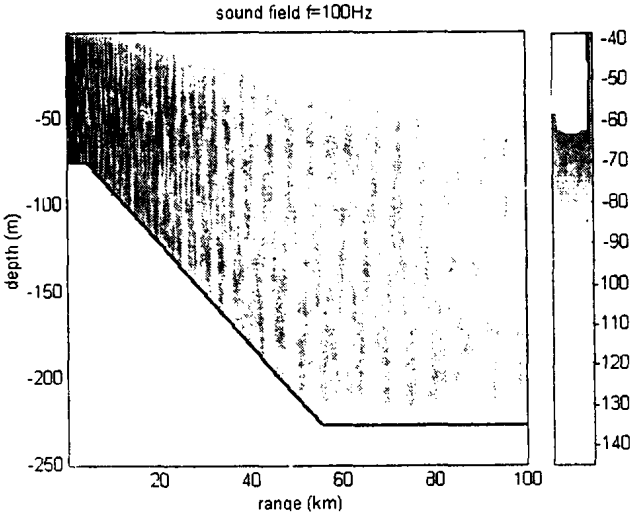

Fig. 2. Distribution of level of incident illuminating field for frequency 100 Hz

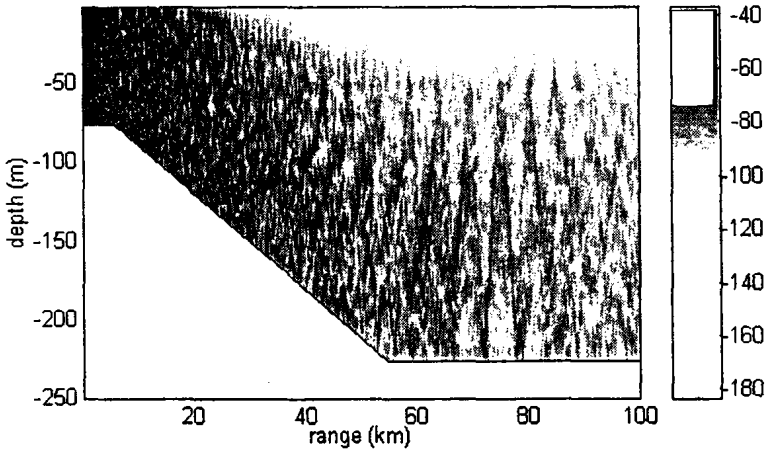

Fig. 3. Distribution of level of illuminating field for frequency 500 Hz.

phenomenon - occurrence of a weakly diverging bundles in refractive oceanic waveguides was observed experimentally and was explained by existence of the smoothed local extremums in dependencies of rays cycles on output angles [17-19]. The similar phenomenon in shallow water channels, in particular, the arising of the field focusing due to constructive mode interference, can be explained by affinity of dependencies of wave numbers from number of modes to square-law [20]. In considered case the effect of the beam arising in the field interference structure is connected with multiplicity of mode numbers. Brightly the beam structure is displayed in forward part of deep-water section of investigated waveguide in distances interval $60 < r < 90$ km, at once for an equivalent megaphone type source of illumination (it is possible to use such terminology only admitting some share of reserve). The multiplicity conditions are satisfied only approximately, therefore the bundles interference structure begins to be destroyed with increase of distance. On higher frequencies of similar structures are destroyed with growth of distance faster, though in the region of their forming they are expressed more brightly.

From the point of view of optimization of illumination in the acoustical tomography schemes the bundle formation is of great interest, so as the field can be $10 - 15$ dB more in these areas. The field coherence in these areas is also higher [17-19]. Actually, it is possible to interpret the areas of beam formation as field focusing areas. The analysis of theirs structure is important in the problems of shadow zones formation and illumination of them in presence of oceanic inhomogeneities. As it is shown in [17-19], the beam structure can depend on the source depth as well as the sound speed profile, thus, it is possible to speak about scanning by a bundles, for example, changing the acoustical source depth. We shall note, that at rather slow change of the waveguide properties on the horizontal domain the bundles can exist undergoing the smooth changes [17].

Arising of the shadow zones and the focusing areas is the feature of formation of the acoustical field in shallow water shelf. In this connection, the field structure in rather narrow straits can be possibly presented as the system of two megaphone zones, directed on each other. In these conditions it is also possible to assume about an availability of shadow zones near the bottom or under the surface of waveguide, and also the essential non-uniformity of the acoustical field distribution because of the arising of focusing areas.

2. INHOMOGENEITIES MODEL

Oceanic inhomogeneities can cause the illumination of shadow zones, due to transformation of acoustical energy to high mode

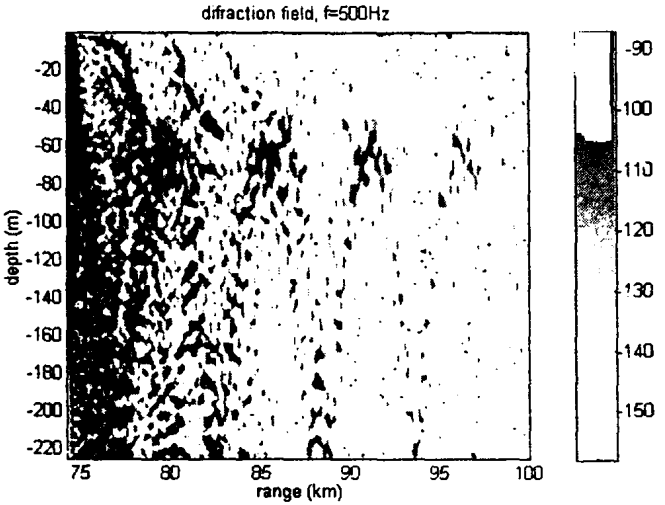

Fig. 4. Space structure of diffracted acoustical field for $f = 500Hz$ (inhomogeneity was located in point: $x_\Sigma = 72$ km, $z_\Sigma = 69.5$ m.)

number area of the mode spectrum due to diffraction. As researchs of features of diffraction of the acoustical field by inhomogeneities in layered waveguides [1-4,21-23] show, the illumination of shadow zones can be carried out by spatially-localized as well as randomly-distributed inhomogeneities. Besides, the characteristic scales and variations of acoustic parameters satisfy conditions, defined by inter mode dispersion structure for a non-uniform waveguide in field of inhomogeneities location.

For simplicity we shall consider features of illumination of the mode shadow zones on example spatially-localized inhomogeneities, associated with the fish shoals [24]. We shall consider, the sizes of shoal equal 10^2 m in horizontal and 15 m in vertical domains. The influence of a plenty fish bubbles permits to consider shoal as some impedance body. Features of acoustic fields diffraction by impedance bodies with relatively large wave sizes allow to analyze in Kirchhoff approach [21,23]. The major part of incident acoustic energy will be scattering under small angles, so that illumination efficiency high wave number range of the mode spectrum will be defined basically by vertical structure of inhomogeneities. At the same time, the intensity of illumination will be depended also from its horizontal sizes.

For calculation of diffraction field we shall replace inhomogeneity by the set of secondary sources, located in limits of shadow making equivalence screen with available complex amplitude depended from

incident field, which have the phases changed on $\frac{\pi}{2}$ relatively the phase of incident waves [21,23]. Then, using representation (1) for the diffraction field, we shall receive the following expression:

$$P_s(z', r') = -\sum_{n,m}^{N,M} \varphi_n(z_0, s')\,\varphi_m(z', r') \times \times \frac{\exp\left[i\text{æ}_n(s')\right]\exp\left[i\text{æ}_m(r')\right]e^{-i\frac{\pi}{2}}}{(\text{æ}_n(s')s')^{1/2}(\text{æ}_n(r')r')^{1/2}} S_{nm}, \tag{4}$$

where $s' = \left(x_\Sigma^2 + y_0^2\right)^{1/2}$, $r' = \left((a - x_\Sigma)^2 + y^2\right)^{1/2}$, $\text{æ}_n(s') = \int_0^{s'} \text{æ}_n(\tau)\,d\tau$, a - distance between source and field observation field, The index $m(M)$ concerns the diffraction modes, x_Σ, y_Σ, z_Σ - coordinates of center of inhomogeneity. Efficiency of exchange by energy between the incident and the diffracted modes is defined by a scattering matrix S_{nm}, which in our model can be submitted in kind of integral:

$$S_{nm} = i\text{æ}_n(s') \int_{-\infty}^{\infty}\int_{-\infty}^{\infty} \sigma(\zeta, \eta)\,\varphi_n(\zeta + z_\Sigma, s')\,\varphi_m(\zeta + z_\Sigma, r') \times \times \exp\left(i\left(\text{æ}_n(s')\frac{y_0}{s'} + \text{æ}_m(r')\frac{y'}{r'}\right)\right) d\eta d\zeta, \tag{5}$$

where $\sigma(\zeta, \eta)$ -- area, limited by shadow line.

As against the case of horizontally uniform waveguide, in (5) matrix $S_{nm} = S_{nm}(r_\Sigma)$ - is function of inhomogeneity location relatively source and receiver, because the structure of eigen functions and wave numbers are various in various parts of waveguide.

Due to losses of acoustical field in shallow water part of investigated waveguide, as well as in the field of coastal wedge in deep-water part of waveguide field of illumination is formed, the main energy of which consists of some set of low numbers waveguide modes. In essence, the mode shadow area is formed [1-4]. Defined by scattering matrix structure (5) the width of the mode spectrum of diffracted field is increased with relative reduction of the characteristic sizes of inhomogeneities $\sigma(\zeta, \eta)$ along coordinates ζ. From (5) it follows, that factor of modes transformation S_{nm} is increased for depths and locations concerning source, receiver and waveguide inhomogeneities, at which appropriate eigen functions accept the maximum values. Taking into account that diffracted field is defined as the sum of interference waveguide modes (4), it is possible to assert, that the maximum of perturbation in unperturbed field will be formed, if localized inhomogeneities is in area of focusing maximum of the illuminating field (in our case it is a bundle, formed in the beginning of a deep-water waveguide part).

Simultaneously, the receiving system should be in the shadow field of direct illumination signal. For considered waveguide this area is formed in under surface region of waveguide. It is necessary to note, that the secondary source of the diffracted signal is in uniform deep water part of waveguide. They excite the modes in this waveguide just as they are excited by the extended array with distribution of secondary sources on in limits of array which determined by incident field. Thus in this waveguide the space structure of acoustical field is formed, having its own system of focusing as in kind of the bundles, and in kind of local zones of increased intensity of diffracted field (4). As the analysis of space structures of diffracted field and form of the angular spectrum of its vertical sections show (fig. 4), the significant part of diffracted field near inhomogeneities is scattered under large angles, transforming in modes with high numbers. In agreement with the used shallow-water waveguide model, high numbers modes have rather large attenuation, so that their contribution in diffracted field decreases with increase of distance quickly. Modes of lower numbers form zones of increased intensity of diffracted field with space period about five kilometers.

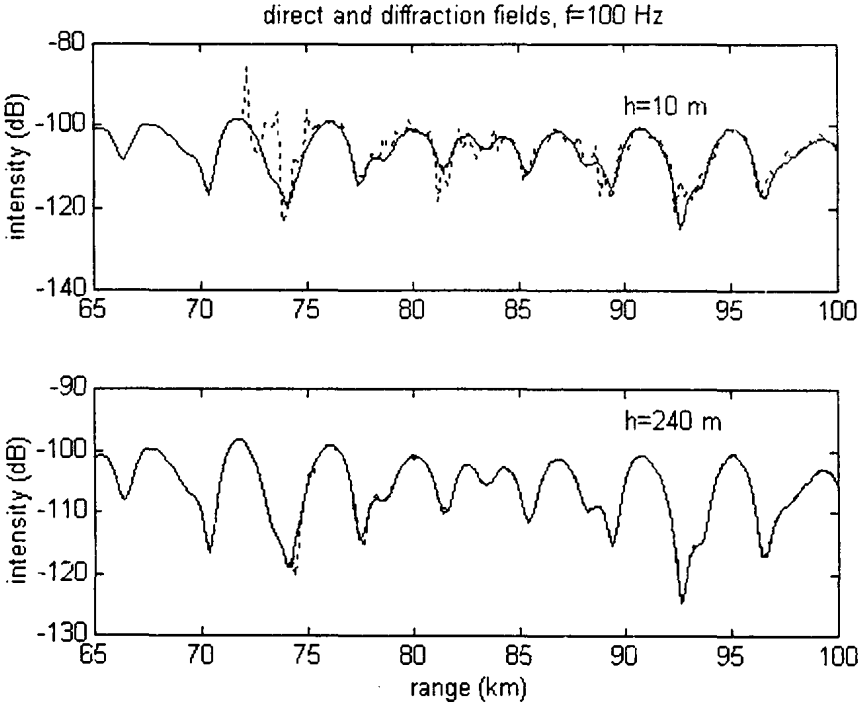

Fig. 5. Perturbed (dashed line) and unpertubed field outside ($h = 240\ m$) and inside ($h = 10\ m$) shadow zone, for $f = 100 Hz$.

3. ILLUMINATION OF SHADOW ZONES

As already was specified, efficiency of shadow zones illumination due to diffraction on oceanic inhomogeneities can be important by optimization of an scheme dislocation of elements of tomographical monitoring system. We shall consider a situation more detailed, when effect shadow zones illumination in investigated waveguide will be maximal. So we shall locate an inhomogeneity in maximum illuminated area , associated with focusing zone of incident field, on depth 69.5 m and on distance from source on 72 km. Fig. 5,6 indicates horizontal sections of a level of perturbed fields at various frequencies outside and in a shadow zone. It can be seen (Fig. 5), that the perturbation in shadow zone can be reached in some places of values up to $30 \div 40$ dB relatively to unperturbed signal. On the average, these perturbations have the level of order 15 dB at frequency 500 Hz. In low-frequency range the shadow zone illumination efficiency is much less (fig. 6). In spite of the fact, that on small distances from inhomogeneities the perturbations can reach 15 dB, as a whole, they quickly fall down because rather fast attenuations of modes with high numbers, which form of diffracted field. It is interesting to note, that an inhomogeneity is plased in area between interference maxima of the bundle, a illumination level practically not varies (fig.7). It is explained by that a zone of weak illumination between interference bursts in bundle is formed also due to the destructive interference of all illuminating modes. Due to transformation of mode spectrum, which is described by matrix S_{nm}, diffractive modes change phases and the illuminating signal in shadow zone can be rather more.

On the basis of indicated and other results of investigation, it is possible to make a conclusion that in considered (typical for real conditions) shallow water waveguide the tomographical reconstruction of spatially-localized inhomogeneities will be more effective, if the receiving systems are placed in mode shadow zones [1-4]. In case of near bottom waveguide propagation, similar shadow zone is limited by depths up to 50 m and distances from source since 60 km. In other practical case of under surface waveguides, the similar situation is observed, however the mode shadow zone is formed already near to bottom. All conclusions, which can be made relatively near bottom waveguide it is possible to apply and to case of under surface waveguide. It can be noted, that other competing sources of shadow zone illumination can be randomly distributed oceanic inhomogeneities. As well as in case spatially-localized inhomogeneities, the efficiency of shadow zone illumination will be defined by scattering matrix $\tilde{S}_{nm}$, which now is random [1-4]. Such matrix depends on the inhomogeneities type, for example, wind

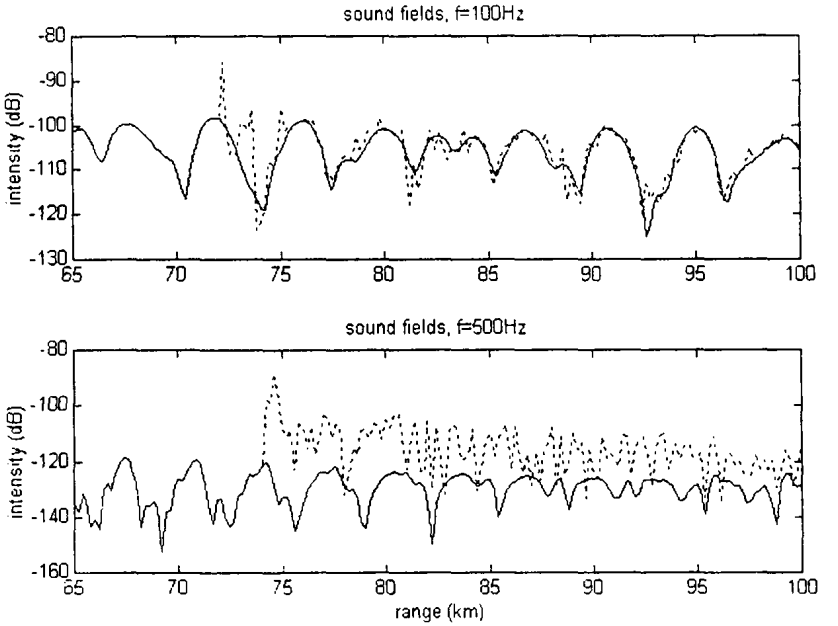

Fig. 6. Pertubations (dashed line) inside shadow zone for $f = 100$ and $500 Hz$.

waves, bottom inhomogeneities, turbulence pulsations of a sound speed in water column and other. For considered in this research waveguide the influence of wind waves will be insignificant, because all surface inhomogeneities are poorly illuminated by the incident field. Main source of random reverberation in shadow zone in this case can be volume and bottom inhomogeneities. The case with under surface waveguide was considered in [5] theoretically and experimentally, where the more essential source reverberation noise was the wind waves. Despite simplification of used in [5] model, it is possible to understand. that shadow zones illumination due to wind waves can be of the order of $5 \div 10$ dB.

The effect of the suppression of a direct signal can be increased by use of the vertical receiving arrays for additional filtering in space domain. The opportunity of such filtering can be evaluated by analysis of structure of space spectrum for arrays with different lengths, diplaced in different depths and different distances relatively of inhomogeneity. On fig. 8 angular spectra of direct illumination and diffractive signal at frequency 500 Hz are shown, when the array is placed at shadow mode zone. This distributions show, that an angular spectrum of the direct signal in whole is more narrow in relation to the spectrum of diffracted signal. This circumstance permits some additional possibilities for suppression of the direct

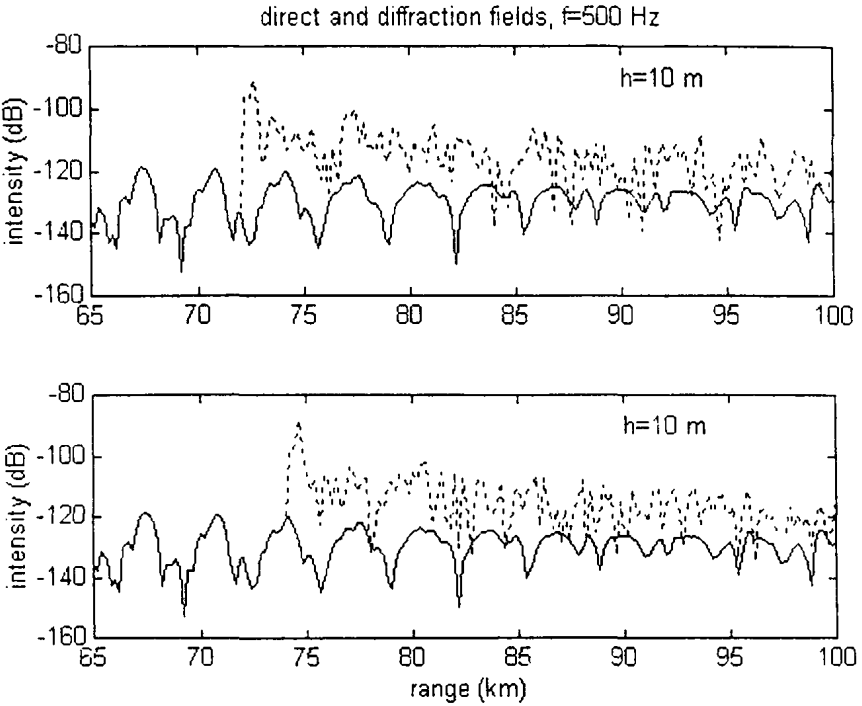

Fig. 7. Perturbations for various displacements of inhomogeneities ($f = 500 Hz$).

signal in order to $5 \div 10$ dB. It is interesting to note, that the angular spectrum of diffractive signal has quasi periodical space structure, so that on appropriate distances from inhomogeneity the spectrum tends to high frequencies and a filtering of direct signal can be more effective. As it was shown numerically, if the array is placed outside of shadow zone, the level of direct signal in high-frequency region of spectrum grows and measurements of diffracted signals are hindered.

CONCLUSION

In this work the possibilities of use of natural mode shadow zones, arising in horizontally non-uniform shallow water oceanic waveguide, are investigated analytically and numerically concerning an increase of signal measurement efficiency in schemes of acoustic tomography in the ocean.

The following results can be formulated:

1. In horizontally non-uniform shallow water waveguides, which often can be seen in shelf regions of ocean, where the acoustical source of illumination is located in shallow water part of waveguide, the deep

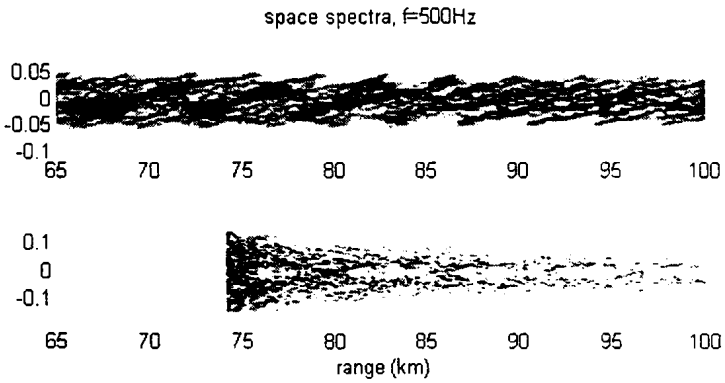

Fig.8. Angle spectrum of incident (the upper distribution) and diffracted (the low distribution) fields for frequency 500 Hz.

mode shadow zones – up to 30 – 40 dB – are formed in regions close to surface (for near-bottom channels) or close to bottom (for under-surface propagation). Moreover, due to the constructive interference of waveguide modes in deep-water part of shelf waveguide the system of focusing zones is formed in the form of bundles with the intensity contrast of the order 10 dB. As it is shown in [20], it is possible to explain the occurrence of bundles by features of mode spectrum of the deep part of shelf waveguide.

2. Diffracted field is characterized by the set of focusings, which can be seen as bundles, that it is well visible from an angular spectrum of vertical arrays (fig. 8). For chosen characteristics of inhomogeneities the essential part of diffractive field is transform to high mode numbers region of mode spectrum. By virtue of dependence of the scattering matrix from structure of horizontally non-uniform waveguide in the field of location of inhomogeneities, the structure of diffracted field depends significantly from horizontal displacement of inhomogeneities.

3. Efficiency of mode shadow zone illumination is analyzed depending on diffraction of incident acoustical field by spatially-localized inhomogeneities. Perturbation in shadow zone reaches on the average $10 \div 15$ dB (close to an inhomogeneity it can be up to 30 dB) at frequency 500 Hz. In the low frequencies region ($\sim$ 100 Hz) this effect also is observed, however its value is less. The indicated phenomenon can be interesting in differential tomography of oceanic inhomogeneities, which is based on selection of mode pulses [1-4]. According to this approach, illumination field was carried out by excitation of selected waveguide modes by vertically developed

radiated arrays. In work [5] opportunities of use of natural shadow zones in real waveguides were discussed for realizations of principles of differential tomography without the use of the radiating arrays. The obtained in the present research estimations of the field perturbation values in mode shadow zones in shelf regions permit to estimate the efficiency of the direct illuminating field suppression in respect to application them in tomographical monitoring of ocean in narrow straits.

4. It is possible to expect the suppression of direct illuminating signal on $30 \div 40$ dB due to angular filtering of diffracted field by vertically developed arrays displaced in shadow mode zones.

Summarizing received results, it is possible to make a conclusion about an opportunity of optimization of receiving and radiating elements displacement in tomographical monitoring of straits. It is seen, that in the near bottom or in under surface areas the mode shadow zones can be formed in relatively deep-water part of waveguide. Theirs structure is connected with the change of hydrological condition which lead to change of the sound speed profile. Hence, inhomogeneities in under - surface or in near - bottom areas can not be reconstructed tomographically, if they are not illuminated by the incident acoustical field.

As is known, in the differential tomography approach it is necessary to suppress the direct illuminating field considered as a noise [1-5]. From this point of view, the displacement of receiving arrays in the shadow zones can be considered as the optimum, because the noise background there can be formed, mainly, due to scattering by randomly-distributed oceanic inhomogeneities, such as volume inhomogeneities and, accordingly, surface or bottom ones.

This work was supported by RFFI (grant N 97-02-17536).

References

[1] Goncharov V.V., Zaicev V.Y. at all, Acoustic Tomography of Ocean, Nizhny Novgorod: IAP RAS, 1997, 256p.

[2] Nechaev A.G. and Khil'ko A.I. Reconstruction of Inhomogeneities of Ocean Along Acoustic Path by a Method of Differential Diagnostics. Preprint IAP RAS, N 178, Nizhny Novgorod, 1987, 23p.

[3] Nechaev A.G. and Khil'ko A.I. Differential Diagnostics of Random Inhomogeneities of Ocean. Akust. Zurn., 1988, V. 34, N 2, pp. 285-289.

[4] Nechaev A.G. and Khil'ko A.I. Reconstruction of local characteristics of distributed Along Acoustic Path Oceanic Inhomogeneities, Acust. Zurn., 1988, V.34, N 4, pp. 694-699.

[5] Borodina E.L. at all, Opportunities of shadow Methods for Study of Diffracted Sound Fields in Waveguides, in book: The Forming of Acoustic Fields in Oceanic Waveguides, Nizhny Novgorod: IAP RAS 1991, pp. 174-200.

[6] Borodina E.L. at all, Reconstruction of the Images of Noise Sources in Inhomogeneous Environments by Use of a Dark Field Method, in Proc. of the First Session of RAS, Moscow: AKIN, 1992, pp.19-22.

[7] Zorin A.Y., Smirnov I.P., Khil'ko A.I. About the Choice of Parameters for Systems of Acoustic Imaging, in book: The Forming of Acoustic Fields in Oceanic Waveguides. Reconstruction of Inhomogeneities, Nizhny Novgorod: IAP RAS 1994, pp. 214-247.

[8] Khil'ko A.I., Sazontov A.G., Vdovicheva N.K. Diffraction of Acoustic field by scatterer in a random oceanic waveguide, Akust. Zurn. 1998, V. 44, N 1, pp. 49-59.

[9] Khil'ko A.I., Sazontov A.G., Vdovicheva N.K. Diffraction of Acoustic waves by an object in a random oceanic waveguide. This book pp. 48–70.

[10] Gorskaia N.V. at all, Research of Possibilities for Use of Frequency-Modulated Waves for Study of Scattering in Non-Uniform Waveguides, Aust. Zurn., 1991, V. 37, N 5, pp. 914-921.

[11] Karetnikova I.R., Nechaev A.G., Khil'ko A.I. The Features of Diagnostics of Waveguide Random Inhomogeneities Changing in Time by Using Complex Pulse Signals. Izv. Vuz. - Radiofizika, 1990, V. 13, N 12, pp.1370-1378.

[12] Khil'ko A.I. and Shirokov V.N. The Use of Mode Shadows at Acoustic Tomography of Ice in Shallow Water Waveguides, Proc. of the 5 All-Union Symposiums on Computing Tomography, Moscow: NPO VNIIFTRI, 1991, pp.217-218.

[13] Lazarev B.A. and Petukhov Y.V. Interference Structure of a Broadband Sound in Horizontally Non-Uniform Waveguide, Acust. Zurn., 1988, V. 34, N 3, pp. 533-555.

[14] Brekhovskhikh A.M. Waves in Layered Environments, Moscow: Science, 1973, 344p.

[15] Boyles A.C. Acoustic waveguides. Applications to oceanic science. N.Y.: Wiley, 1984.

[16] Belov A.I. A method of numerical Calculation of Sound Fields in Waveguide with Absorbing Bottom. Sudostr. Prom. Ser. Acustika, 1989, N 4, pp. 30-36.

[17] Goncharov V.V. and Kurtepov B.M. Formation and Distribution of Weakly Diverging Bundles in Horizontally Inhomogeneous Ocean, Akust. Zurn, 1994, V. 40, N 5, pp. 773-781.

[18] Petukhov Y.V. A Sound Beam with Minimum Diverging of Front in Stratified Oceanic Waveguide, Akust. Zurn., 1994, V. 40, N 1, pp. 111-120.

[19] Smirnov I.P., Caruthers J.W. and Khil'ko A.I. Multiscale Coherence of the Acoustic Field of a Noise Source in Randomly Inhomogeneous ocean. In this book, pp. 71–113.

[20] Borodina E.L., Stromkov A.A. and Khil'ko A.I. Coherent Structure of Broadband Pulse signals in the Shallow Sea. In this book, pp. 186–212.

[21] Gorsky S.M., Zverev V.A. and Khil'ko A.I. Features of Diffraction of Acoustic fields by Spatially-Localized Inhomogeneities in Oceanic Waveguides in book: The Forming of Acoustic Fields in Oceanic Waveguides, Nizhny Novgorod: IAP RAS 1991, pp. 82-114.

[22] Kravtsov Y.A., Kuzkin V.M. and Petnikov V.G. The Approach to Problem about Diffraction of Waves in Multi Mode Waveguides with Slowly Changed Parameters, Izv. Vuz. Radiofika, 1983, V. 26, N 4, pp. 440-446.

[23] Eliseevnin V.A. and Tuzilkin Y.I. Diffraction of Sound Fields by Rectangular Vertical Screen in Waveguide, Akust. Zurn., 1995, V. 41, N 2, pp. 249-253.

[24] Smirnov I.P., Caruthers J.W. and Khil'ko A.I. Tomographical Reconstruction of Oceanic Inhomogeneities: Part 1–Forming Partially Coherent Acoustic Wave Structures in the Ocean with Spatially Localized Noise Sources, Proc. of OCEANIC'S, San Diego, 1995.

THE FORMATION OF ACOUSTICAL FIELDS IN OCEANIC WAVEGUIDES

COHERENCE PHENOMENA

Collected scientific papers

Responsible for the issue
A. I. Khil'ko

Институт прикладной физики РАН
ЛР 040880
Подписано к печати 30.12.97 г.
Усл. печ. л. 16,25. Уч.-изд. л. 15,5. Заказ № 111. Тираж 300 экз.

Printed by a stencil dublicator
in the Institute of Applied Physics RAS,
603600, Nizhny Novgorog, Uljanov Street, 46

E. Yu. Gorodetskaya (NN University), A. I. Malekhanov, A. G. Sazontov, V. I. Talanov (IAP RAS), and N. K. Vdovicheva (IMS RAS). **Acoustic coherence in a deep water: effects on array signal processing.**

Recent results on combined consideration of the sound wavefield coherence and array signal processing in long-range deep-water environments are presented. A distinctive feature of this study is incorporating realistic calculations of the signal MCF of space to predict the coherence effects on the array beampattern and gain for several types of processors, optimal ones included.

A. I. Khil'ko, A. G.Sazontov (IAP RAS), and N. K.Vdovicheva (IMS RAS). **Diffraction of acoustic waves by an object in a random oceanic waveguide.**

Statistical problem of short wave diffraction of partially-coherent multimode acoustic field by a scattering object in a deep-water oceanic waveguide is considered. The method presented is based on the combined use of the Kirchhoff approximation and the small angle radiation transport equation for the second moment of the medium Green's function. The general expressions for the energy and correlation characteristics of a diffracted signal in the farfield have been derived. The multiple volume scattering effects on the target strength have been also estimated.

I. P. Smirnov (NN University), J. W. Caruthers (NRL) and A. I. Khil'ko (IAP RAS). **Multiscale coherence of the acoustic field of a noise source in randomly inhomogeneous ocean.**

The space distribution of coherence of sound fields in refractive oceanic waveguides with randomly distributed volume inhomogeneities for noise acoustical sources was investigated. Conditions for bundles of rays existing, which arise due to interference of rays with close parameters were formulated, as well as their coherence were studied. The possibilities of their application for diffracted fields measurements were discussed.

A. V. Lebedev and B. M. Salin (IAP RAS). **Experimental Method for Determining the Scattering Characteristics of Elongated Objects.**

The scattering characteristics of elongated objects were investigated by measuring of acoustical scattering signals in lake. The influence of noise and environment random perturbations on result of measurements were experimentally studied.

M. Yu. Galaktionov, V. V. Borodin, A. V. Mamayev (AKIN). **Numerical and experimental study of sound field forming in shallow water environments.**

Investigation of sound field forming in shallow water areas is made based on simulated and experimental data. A software set for numerical modeling of sound fields, raw signal data and sonar signal processing is presented. Simulated and experimental data are studied and processed and main particularities of sound field forming in shallow waters are established.

V. V. Borodin, M. Yu. Galaktionov (AKIN). **New mathematical model of sound field fluctuations in shallow water environments with boundary and volume roughness.**

New equations for the two first moments of sound fields in random mean-layered waveguides are derived to describe simultaneously the scattering from rough boundaries and volume fluctuations of sound velocity. The model is valid for a large interval of sound frequency and various environments including the shallow water case. The phase screen method is used to calculate the scattering amplitude that describes the propagation through a water layer with large-scale volume fluctuations. Its statistical moments are calculated that are entering as kernel and right part in the integral equations for the two first statistical moments of sound fields. Structure of solutions of these equations is described when various approximations are used. It is shown that these solutions can describe the micro-multi-ray phenomenon and the correlation of scattered fields propagating along different ray paths. Appropriate algorithms for numerical implementation of this comprehensive theoretical model are proposed and discussed. The algorithm to compute the angle spectrum of the field proves to be analogue to the ray paths calculation in a layered waveguide.

E. L. Borodina, A. A. Stromkov and A. I. Khil'ko (IAP RAS). **Coherent structure of broadband pulse signals in the shallow sea.**

The paper deals with the investigation of the influence of sediment layers on the space - time coherent structure of broadband pulses. The formation of unsteady in time beams caused by an interference of waveguide modes in a wide frequency region is considered. An influence of variations in acoustical parameters on a shape of wide - band acoustical pulses is investigated. The conditions of a constructive interference of modes are analyzed.

A. A. Pokrovsky. **Using regularities in the behavior of a two-frequency correlation function of acoustic field in monitoring of oceanic inhomogeneities.**

In this paper a simple tomographic scheme which uses an acoustic path between the spaced emitter and receiver is considered. The possibilities of using such a scheme to extract and estimate signals scattered by oceanic inhomogeneities against the background of a fluctuating direct illumination field by exploiting the properties of an interfrequency acoustic field correlation function in a waveguide with random inhomogeneities are estimated.

S. M. Grudskii (RnD University), A. I. Khil'ko (IAP RAS), S. S. Mikhalkovich (RnD University). **Propagation of low-frequency sound in a hydroacoustic waveguide with surface covered with a non-continuous ice layer.**

The present paper deals with the problem of sound propagation in a stratified waveguide which is an inhomogeneous liquid layer overlaying a multi-layered liquid-elastic bottom. The surface of the waveguide is covered with a thin (in comparison with length of an acoustic wave) homogeneous ice layer with polynia of finite width. Influence of the polynia on characteristics of an acoustic field is investigated. The main asymptotic terms of elements of reflection and transmission matrices are obtained by a small parameter, where the small parameter characterises thickness of ice. These formulas are uniform in parameter L, where L specifies polynia width. The similar formulas for a finite width ice-floe lying on a liquid layer are given. In this case influence of attenuation in the ice on the diagonal members of the transmission matrix is analysed. We note that the used approach can be generalized to a case of a finite number of ice-floes.

A. I. Belov (SF AKIN) and A. I. Khil'ko (IAP RAS). **Diffraction of acoustic waves by spatially-localized inhomogeneities in horizontally-inhomogeneous shallow water oceanic waveguides.**

The purpose of this research is the study of the structure of natural shadow zones, in particular, the efficiency of illumination of such zones, formed in shallow water waveguides with megaphone form, due to diffraction of acoustical waves by spatially-localized inhomogeneities taking into account the optimization of measuring scheme for tomographical monitoring in shallow water straits.